Studies on Invadolysin – a novel metalloprotease localizing to lipid droplets

Ching-Wen Chang

A Thesis Submitted for the Degree of Doctor of Philosophy

The University of Edinburgh

2009

Declaration

I hereby declare that this thesis has been composed by myself, describe my own work and has not been submitted in any other application for a high degree.

Ching-Wen Chang

August 2009

Acknowledgements

I would like to sincerely thank my supervisor Prof. Margarete Heck. She gave me a great opportunity to study in Edinburgh. Thanks for her guidance, advice, encouragement and patience that make the last three years an enjoyable experience.

I am grateful to those people whom I work with during this time, for providing me good suggestions and for helping my academic writing in the thesis. Many thanks to Dr. Sharron Vass for providing me many technical assistance; Dr. Neville Cobbe for answering my countless questions; Dr. Francesca Di Cara for giving me good suggestions and always encouraging me. Many thanks also go to Edward Duca and Ekin Bolukbasi for their great support during these years. In addition I would like to thank previous members in the Heck lab, Dr. Bryce Nelson, Dr. Bin Yu, Dr. Kate Marshall and Dr. Shubha Gururaja Rao for their company. Also thanks to Dr. Eric Schirmer, Dr. Paddy Hadoke, Dr. Nik Morton and Dr. Sari Pennings for giving me advice; Dr. Christina Esteves for help with adipogenesis experiment. Especially thank to Chiu-Ju Hung for always inspiring me. Many thanks to all of the friends inside and outside CVS for the great time we had together.

Earnestly, I would like to dedicate this thesis to my parents and my husband, Chen-Yen, who always gives me endless support and is always there for me.

Contents

Contents **1**
LIST OF FIGURES **5**
LIST OF TABLES **8**
LIST OF TABLES **8**
List of Abbreviations **9**
List of Abbreviations **9**
Abstract **11**
Chapter 1: Introduction **13**
1.1 Background of Invadolysin (IX-14) 13
Why study Invadolysin? 13
The IX-14 gene encodes a novel metalloprotease 14
The localization of invadolysin (IX-14) 20
Other phenotypes described in INV mutants 23
1.2 Zinc metalloproteases 24
Overview of zinc metalloproteases 24
MMPs & ADAMs 29
Leishmanolysin 30
1.3 Lipid droplets 32
Structure of LDs 32
Lipid droplet formation 33
The protein composition of LDs 35
Functions of LDs 39
1.4 Adipocyte differentiation 41
Models of adipocyte differentiation 41
Transcriptional control of adipocyte differentiation 43
Signaling pathways in adipogenesis 44
1.5 Insulin signaling pathway 48
Overview of insulin signaling pathway 48
Insulin/TOR signaling components in lipid metabolic control 51
Insulin/TOR signaling components in glucose homeostic control 53
Insulin/TOR signaling pathway in growth control 54
1.6 Aims of the PhD. project 55
Chapter 2: Materials and Methods **57**
2.1 Preparation of competent cells for heat shock transformation 57

2.2 Ligation and transformation 57
2.3 Plasmid DNA extraction and agarose gel electrophoresis 58
2.4 BigDye Terminator sequencing 59
2.5 Polymerase Chain Reaction 60
2.6 DNA Purification 60
2.6.1 DNA purification from agarose gels 60
2.6.2 Purification of DNA from PCR reactions 61
2.7 Oligonucleotide annealing for cloning 61
2.8 Total RNA extraction 61
2.9 RT-PCR reactions 62
2.9.1 One-step RT-PCR 62
2.9.2 Two-step RT-PCR 63
2.10 Quantification of mRNA using real-time PCR 65
2.11 Preparation of protein extract 66
2.11.1 Preparation of protein extracts from cell lines 66
2.11.2 Preparation of protein extracts from larvae 67
2.11.3 Preparation of protein extracts from the fat body of *Drosophila* 67
2.12 Electrophoresis of protein samples 68
2.13 Transfer of SDS-PAGE gels to nitrocellulose membrane and immunobloting 69
2.14 Stripping nitrocellulose membranes 71
2.15 Coomassie Brilliant Blue staining of polyacrylamide gels 71
2.16 Fusion of INV fragments with GST tag 71
2.17 Expression and purification of recombinant proteins 72
2.17.1 Overexpression and purification of GST-tagged fusion proteins 72
2.17.2 Overexpression and purification of His-tagged fusion proteins 73
2.18 *In vitro* kinase assay 74
2.19 Detection of protease activity by zymography 75
2.20 Cell culture 75
2.21 Adipocyte differentiation 76
2.22 Construction of invadolysin vectors for transfection into mammalian cells 77
2.23 Transfection of mammalian cells 79
2.23.1 Transfection by electroporation 79
2.23.2 Transfection by lipofectamine 2000 79
2.24 Immunofluorescence of human cultured cells 80
2.25 Immunoprecipitation 82
Chapter 3: Identification of molecules which regulate the localization of invadolysin to lipid droplets 83

3.1 Introduction 83
3.2 Results 84
3.2.1 INV localizes to LDs 84
3.2.2 Caveolin co-localized with INV in the presence of Brefeldin A 86
3.2.3 Time course for the recruitment of INV to LDs 91
3.2.4 The targeting of INV to LDs is independent of newly synthesized INV 99
3.2.6 Protein kinase C is required for the localization of INV to newly synthesized LDs 101
3.2.7 Extracellular signal-related kinase 2 (ERK2) does not affect re-localization of INV to LDs after starvation/re-feeding 107
3.2.8 Invadolysin is a substrate of protein kinase C 110
3.3 Discussion 112
Chapter 4: Studying invadolysin expression during adipocyte differentiation 117
4.1 Introduction 117
4.2 Results 118
4.2.1 Invadolysin localized to lipid droplets in mouse 3T3-L1 fibroblast cells 118
4.2.2 The localization of invadolysin during adipocyte differentiation 118
4.2.4 Invadolysin protein levels are increased during adipocyte differentiation 127
4.2.5 Inhibition of adipocyte differentiation by PKC and PI3K inhibitors diminished the expression of invadolysin 129
4.2.6 Phospho-Akt levels are decreased when PKC activity is inhibited 135
4.3 Discussion 137
Chapter 5: Characterization of the InR/PI3K/Akt signaling pathway in Invadolysin mutant larvae 140
5.1 Introduction 140
5.2 Results 142
5.2.1 Levels of Phospho-dAkt are decreased in *INV*^{4Y7} mutant larvae 142
5.2.2 INV affects the activity of Akt downstream effectors, d4E-BP and S6K1 142
5.2.3 Perilipin homolog Lsd2 is decreased in *INV*^{4Y7} mutant larvae 144
5.3 Discussion 149
Chapter 6: Tagging invadolysin for studies of localization 152
6.1 Introduction 152
6.2 Results 152
6.2.1 Ectopic expression of GFP-tagged invadolysin in HeLa cells 152
6.2.2 INV.v1-GFP is degraded through the proteasomal pathway 153
6.2.3 Positioning tags in region 2 of invadolysin 159
6.2.4 The localization of INV with GFP, SSBP and HA tag in region 2 of INV 162

6.2.5 Inserting the tag in invadolysin in other positions 167
6.2.6 Region 2 tags in INV.v1 localized to mitochondria 171
6.2.7 Detection of expression of INV with region 2 tags by immunoblotting 171
6.3 Discussion 175
Chapter 7: Protease activity of invadolysin 179
7.1 Introduction 179
7.2 Results 179
7.2.1 Production and purification of recombinant INV from bacteria 179
7.2.2 Detection of invadolysin enzymatic activity by zymography 185
7.2.3 Purification and zymography of INV expressed in HeLa cells 187
7.3 Discussion 192
Chapter 8: Discussion 194
To LD or not to LD: that is the question 194
INV in adipocyte differentiation 199
INV and insulin signaling pathway 204
References 209

LIST OF FIGURES

Figure 1.1 Molecular characterization of Drosophila IX-14 gene. 15
Figure 1.2 The phenotype observed in l(3)IX-14 mutants. 16
Figure 1.3 T-COFFEE alignments of IX-14 homologues and the structure analysis based on Leishmanolysin. 18
Figure 1.4 IX-14 (invadolysin) variants in Drosophila and human. 19
Figure 1.5 The localization of IX-14/INV in HeLa cells and macrophages. 21
Figure 1.6 INV mutants embryos have a germ cell migration defect. 25
Figure 1.7 Categorization of zinc metalloproteases. 27
Figure 1.8 Secondary structure of a typical metzincin (A) and leishmanolysin (B). 28
Figure 1.9 The mechanism of cysteine switch. 31
Figure 1.10 Models of lipid droplet formation. 34
Figure 1.11 Extracellular signaling in adipogenesis. 45
Figure 1.12 An overview of the insulin signaling pathway. 49
Figure 3.1 Invadolysin is localized on the surface of lipid droplets. 85
Figure 3.2A Oleic acid treatment increases the size of invadolysin rings. 87
Figure 3.2B Oleic acid treatment increases the size of invadolysin rings. 88
Figure 3.3 Caveolin co-localized with INV in the presence of Brefeldin A. 90
Figure 3.4 Both INV and caveolin bind with LDs in the presence of Brefeldin A. 92
Figure 3.5A Time course of invadolysin localization in human A375 cells loaded with oleic acid. 94
Figure 3.5B Time course of invadolysin localization in human A375 cells loaded with oleic acid. 95
Figure 3.6A Invadolysin is recruited to newly formed lipid droplets. 96
Figure 3.6B Time course of invadolysin localization in human A375 cells loaded with oleic acid. 97
Figure 3.6C The BODIPY positive cells were increased by re-feeding the cells with OA/FBS medium after overnight starvation. 98
Figure 3.7 Targeting of INV to LDs is independent of newly synthesized INV. 100
Figure 3.8 Src kinase inhibitor may not affect the re-localization of INV. 102
Figure 3.9A Recruitment of INV to some newly formed LDs was inhibited by Ro31-8220 treatment. 104
Figure 3.9B INV formed as aggregates in the cytoplasm after Ro31-8220 treatment. 105
Figure 3.10 Re-localization of INV to lipid droplets after removal of PKC inhibitor. 106
Figure 3.11 PKC inhibitors, Gö6979 and GF109203 treatment may not change the localization of INV to lipid droplets in A375 cells. 108
Figure 3.12 ERK inhibitors treatment may not affect the localization of INV. 109

Figure 3.13 INV is a substrate of protein kinase C. 111
Figure 4.1 The localization of invadolysin in mouse 3T3-L1 fibroblast cells. 119
Figure 4.2 Determination of invadolysin localization during adipocyte differentiation. 121
Figure 4.3 The localization of perilipin during adipocyte differentiation. 122
Figure 4.4 Comparison of the localization of invadolysin and perilipin in adipocyte. 123
Figure 4.5 Levels of Invadolysin mRNA increase during adipocyte differentiation. 125
Figure 4.6 INV mRNA increases significantly during adipocyte differentiation. 126
Figure 4.7 Expression of INV and perilipin is increased during adipogenesis. 128
Figure 4.8 The mRNA levels of INV and perilipin were decreased with inhibition of PKC... 131
Figure 4.9 Protein levels of invadolysin and perilipin were decreased in the presence of PKC inhibitor. 132
Figure 4.10 The mRNA levels of INV and perilipin were decreased with the treatment of PI3K inhibitor, LY294002. 133
Figure 4.11 Protein levels of invadolysin and perilipin were decreased in the presence of PI3K inhibitor, LY294002. 134
Figure 4.12 Levels of Phospho-Akt are decreased in the presence of PKC and PI3K inhibitors. 136
Figure 5.1 The phosphorylation level of dAkt is decreased in the *INV*^{4Y7} mutant. 143
Figure 5.2 The expression of d4E-BP was elevated in *INV* ^{4Y7} mutant. 145
Figure 5.3 The phosphorylation level of p70S6 kinase is decreased in *INV*^{4Y7} mutant. 146
Figure 5.4 The level of Lsd2 protein is decreased in *INV*^{4Y7} mutant. 148
Figure 5.5 INV mutant exhibits impaired insulin signaling. 150
Figure 6.1 Cloning full length invadolysin variants into pEGFP-N1 mammalian transfection vector. 154
Figure 6.2 The localization of A) GFP, B) INV.v1:GFP, C) INV.v1∆37:GFP and D) INV.v2:GFP in HeLa cells. 155
Figure 6.3 Detection of the expression of INV GFP-fusion proteins by immunoblotting. 156
Figure 6.4 INV.v1:GFP fusion protein was degraded in proteasomes after transfection. 158
Figure 6.5 The degradation of INV.v1:GFP fusion protein is MG132 dose dependent. 160
Figure 6.6 Insertion of GFP, SSBP and HA tags into region 2 of invadolysin. 161
Figure 6.7 The localization of pEdG-v1Δ37:GFP in HeLa cells. 163
Figure 6.8 The localization of pEdG-v1:SSBP in HeLa cells. 165
Figure 6.9 The localization of pEdG-v1Δ37:SSBP in HeLa cells. 166
Figure 6.10 The localization of pEdG-v1:SSBP and endogenous INV in HeLa cells. 168
Figure 6.11 The localization of pEdG-v1:HA in HeLa cells. 169
Figure 6.12 The localization of pEdG-v1:HA[HIII] in HeLa cells. 170
Figure 6.13 Ectopically expressed of SSBP and HA tagged Invadolysin localized with

mitochondria..... 172
Figure 6.14 Detection of INV fused with GFP, SSBP and HA tags by immunoblotting..... 174
Figure 7.1 Schematic of human invadolysin fragments fused to the GST tag protein..... 181
Figure 7.2 Expression of INV recombinant proteins in E. coli BL21 cells..... 183
Figure 7.3 Elution of INV recombinant proteins by reduced glutathione. 184
Figure 7.4 Detection of protease activity by zymography. 186
Figure 7.5 Immunoprecipitation and zymography of INV expressed in HeLa cells. 189
Figure 8.1 The localization mechanism of INV under starvation/re-feeding condition..... 200
Figure 8.2 INV may regulate insulin signaling and mediate adipogenesis. 207

LIST OF TABLES

Table 1.1 The proteomic analysis on lipid droplets 38
Table 2.1 Bacterial strain information 57
Table 2.2 Primers used for sequencing reactions to check constructs in Chapter 6 and 7 ... 59
Table 2.3 Primers used for the RT-PCR reactions 64
Table 2.4 Primers and probes for qPCR used in Chapter 4 65
Table 2.5 *Drosophila* Stocks 68
Table 2.6 The list of the primary and secondary antibodies 69
Table 2.7 Different portions of invadolysin constructs and the corresponding primers 72
Table 2.8 The inhibitors used in Chapters 3 & 4 76
Table 2.9 The constructs and primers used for cloning of INV fragments in Chapter 6 77
Table 2.10 The fluorescent dyes, primary and secondary antibodies used for this study 81
Table 7.1 Conditions tested for developing protease activity for INV 191

List of Abbreviations

4E-BP	the eukaryotic initiation factor 4E (eIF4E) binding protein
ADAM	A Disintegrin and Metalloprotease
ADRP	Adipose differentiation related protein
ALD1	Associated with LD protein1
ap2	Adipocyte protein 2
APMA	Aminophenylmercuric acetate
ApoB	Apolipoprotein B
ATGL	Adipose triglyceride lipase
BFA	Brefeldin A
CDS	Chanarin-Dorfman syndrome
C/EBP	CCAAT enhancer binding proteins
CREB	Cyclic AMP response element-binding protein
CGI-58	Comparative Gene Identification-58
CxB	cholera toxin B
Dex	dexamethasone
DILPs	Drosophila insulin-like peptide
ECM	Extracellular matrix
ERK2	Extracellular signal-regulated kinase
ERAD	ER-associated degradation
FIT	Fat-inducing transcript
FOXO	Forkhead box, subgroup O
GLUT4	Glucose transporter 4
GPI	Glycosylphosphatidylinositol
IBMX	3-isobutyl-1-methylxantin
InR	Insulin receptor
INV/ IX-14	invadolysin
INV.v1	invadolysin variant 1+37 aa
INV.v1△37	iInvadolysin variant 1△37 aa
INV.v2	invadolysin variant 2+37 aa
INV.v2△37	invadolysin variant 2△37 aa
KLF	krüppel-like family
LD	lipid droplet
LSD1	Lipid storage droplet 1
LSD2	Lipid storage droplet 2 (perilipin homologue in *Drosophila*)
LSDP5/OXPAT	Lipid storage droplet protein 5

MEF	Mouse embryonic fibroblast
MLDP/PAT1	Myocardial lipid droplet protein
MMP	Matrix metalloprotease
OA	Oleic acid
PI3K	phosphatidylinositol-3-OH kinase
PGCs	Primordial germ cells
PPARγ	Peroxisome proliferators activated receptor γ
PLD1	Phospholipase D1
Pten	phosphatase and tensin homolog
rp49	Ribosomal protein 49
SBP	Strepavidin binding protein
SSBP	S tag (RNaseS S peptide from a.a 1-15)+SBP
SREBP1c	Sterol regulatory element binding protein
SPG20	Spastic paraplegia 20, spartin
TIP47	Tail Interacting protein of 47 kDa
TOR	Target of rapamycin
TSC	tuberous sclerosis complex

Abstract

Invadolysin (INV) is a member of the M8 family of metzincin metalloproteases. The gene was discovered in the Heck laboratory. Based on studies in *Drosophila*, INV is important for mitotic progression, nuclear envelope protein dynamics, and germ cell migration. INV-like immunoreactivity has shown its association with lipid droplets (LDs), which are intracellular organelles for lipid and protein storage. INV is the first metalloprotease found on LDs. Thus, INV's role and LD-associated pathways are the puzzles we would like to investigate.

The formation of LDs is dependent on the nutritional status of cells and starvation can disrupt the generation of LDs. Based on this concept, I established a starvation / re-feeding system. When nutrition is sufficient, LDs were surrounded by INV, whereas no INV or LDs were found in the majority of starved cells. With a supply of oleic acid (OA), LDs re-appeared and so did INV localized to LDs. In this system, inhibition of protein kinase C (PKC) disrupts INV's re-localization to LDs. As I found INV to be phosphorylated by PKC *in vitro* (residues within the N-terminus might be phosphorylated by PKC), I conclude that PKC might regulate INV's re-localization in the starvation / re-feeding system.

3T3-L1 mouse fibroblasts can differentiate into adipocytes in vitro; this is termed adipogenesis. Since INV is a LD associated protein, the role of INV in adipogenesis is of interest. INV localized on LDs in the early stage of differentiation but disassociated from LDs in mature adipocytes. The levels of INV mRNA and protein were significantly increased upon differentiation to adipocytes. On the other hand, INV decreased when adipocyte differentiation was inhibited by PKC and PI3K inhibitors, suggesting that the increase of INV is required for adipocyte differentiation.

I was interested to examine the possible role of INV in InR/PI3K/Akt signalling, and therefore compared wild type with mutant INV (*Drosophila* INV^{4Y7}). Decreased levels of phospho-Akt and phospho-S6K, and increased mRNA levels of d4E-BP were observed in INV^{4Y7} mutant larvae, suggesting that INV may be required for InR/PI3K/Akt signalling. In addition, a decreased level of Lsd2 (LD binding protein) was found in INV^{4Y7} mutants. These correlations between INV and molecules important for signaling suggest that INV might be a mediator of nutritional metabolism. In light of these data, I speculate that INV plays a homeostatic role, possibly by affecting the InR/PI3K/Akt signaling pathway.

In conclusion, the localization of INV to LDs is dependent on the activity of PKC. An increase in invadolysin accompanies adipogenesis, in which PKC and PI3K may be mediators. Examining mutant *Drosophila*, I found INV to be involved in InR/PI3K/Akt signalling. Collectively, I conclude that INV may serve as a regulator in adipogenesis and the InR/PI3K/Akt signaling pathway.

Chapter 1: Introduction

1.1 Background of Invadolysin (IX-14)

Why study Invadolysin?

Invadolysin (IX-14) was identified in a study of *Drosophila* mutants that were defective in mitotic chromosome condensation. This *Drosophila* mutant, named *l(3)IX-14*^{1}, was generated using ICR-170, a chemical mutagen in a screen for mutations affecting development of the imaginal discs (precursors of adult structures) and *l(3)IX-14*^{1} is a late larval lethal mutation (Shearn *et al*, 1971). *Drosophila* larval tissues grow largely by endoreduplication, whereas, some tissues remain diploid and require mitosis to form structures in the adult, such as cells in the brain, imaginal discs and histoblasts. The imaginal discs are completely unnecessary for larvae growth since larvae lacking these tissues survive until the larval-pupal transition (late larval stage). Therefore, Gatti and Baker reasoned that many of these late larval lethal mutants may actually represent cell cycle phenotypes rather than developmental defects (Gatti & Baker, 1989). Indeed, analysis of the *l*(3)*IX-14*^{1} mutant larval neuroblasts showed hypercondensed chromosomes and metaphase arrest (Gatti & Baker, 1989). Furthermore, the *IX-14* allele was mapped to the 85E10-F16 region by crossing to deficiency lines with known breakpoints (McHugh *et al.*, 2004).

To further assist in identification of the *IX-14* gene, Sue Ann Krause, a former Ph.D. student in the Heck laboratory, generated a P-element insertion allele of *l*(3)*IX-14*^{1} by local hopping of a nearby P-element, *1(3)04017*. This allele was termed *l(3)IX-14*^{4Y7} and inverse PCR was used to clone and identify the *IX-14* gene. A candidate *IX-14* gene was cloned by identifying a 3.6-kb full length *Drosophila* adult

head library EST whose sequence overlapped with the flanking region of *l(3)IX-14*^{4Y7}. Furthermore, the P-element insertion was mapped to 40 bp upstream of the transcription start region of *IX-14* gene. The P-element insertion upstream of the *IX-14* gene abolished its expression as shown by Northern blot analysis. This 3.6-kb mRNA was missing in larval extracts prepared from both *IX-14* mutant alleles (Figure 1.1).

A detailed analysis of the two alleles was published (McHugh *et al.*, 2004). Both *l*(3)*IX-14*^{1} and *l(3)IX-14*^{4Y7} revealed similar defects. The third instar larvae of both alleles have small brains and missing imaginal discs. In addition, mutant larval neuroblasts showed hypercondensation of mitotic chromosomes (Figure 1.2A). In addition to the difference in chromosome structure between wild type and the mutants, the cell division defects were also observed in *IX-14* mutant alleles. Neuroblasts of *IX-14* mutants exhibited abnormal spindle and centrosomal morphology. The spindles were monopolar, asymmetric bipolar or completely disorganized in mutant mitotic neuroblasts cells. In addition, nearly 70% of mitotic cells in *IX-14* mutant neuroblasts appeared to have one centrosome (Figure 1.2B). Moreover, dsRNA-mediated interference of IX-14 in *Drosophila* Schneider 2 (S2) cells phenocopied the neuroblast defects (McHugh *et al.*, 2004). These data suggested that the *IX-14* gene has essential roles both in chromosome and spindle architecture in *Drosophila* cells.

The IX-14 gene encodes a novel metalloprotease

The *Drosophila IX-14* gene has 9 exons spread over 15 kb of genomic DNA. The 2052 nucleotide open reading frame in the *IX-14* cDNA encodes a 683 amino acid protein. The protein is predicted to be about 71 kDa in size. Sequence analysis

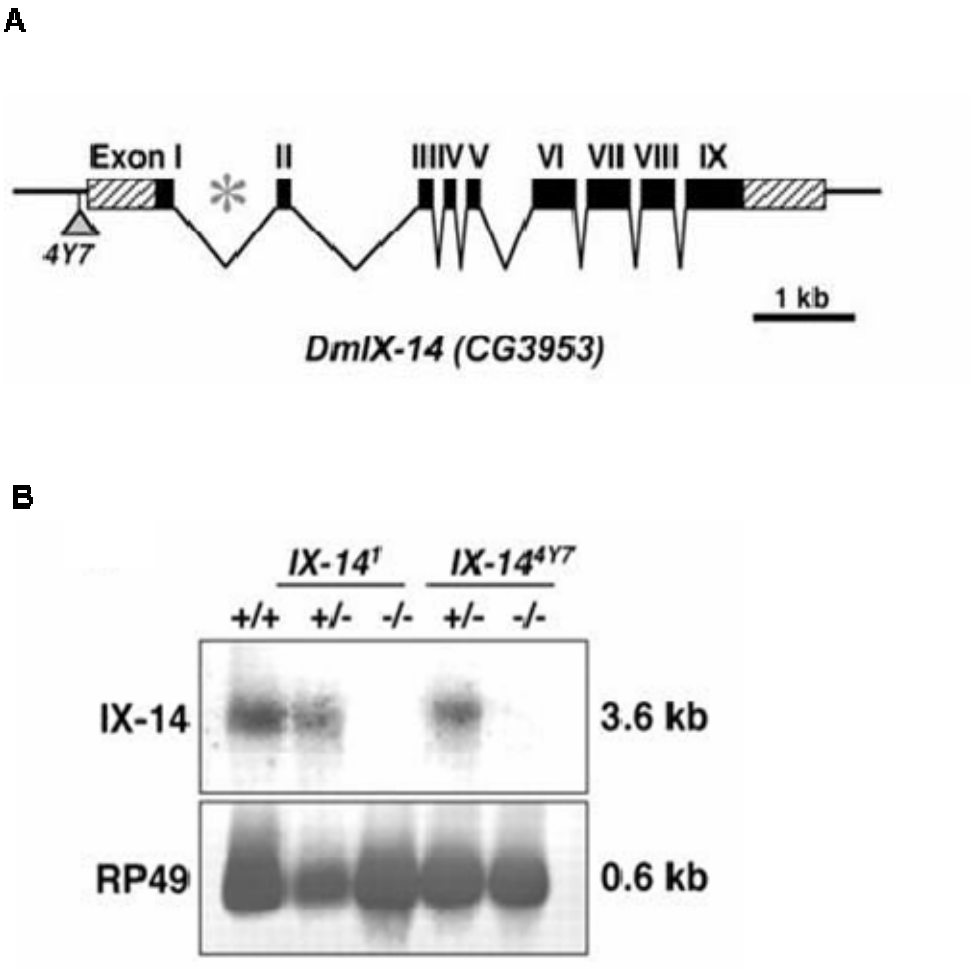

Figure 1.1 Molecular characterization of Drosophila IX-14 gene. A.) Schematic representation of the *IX-14* gene. The *IX-14* gene contains 9 exons shown as black boxes and the 5' and the 3' UTR shown as hatched boxes. The P element insertion is 40 bp upstream of the transcription start site depicting as gray triangle. B. Northern blot showed that the expression of *IX-14* RNA is undetectable in both *l(3)IX-14*^{1} and *l(3)IX-14*^{4Y7} homozygous mutants. (Figure taken from McHugh *et al.,* 2004.)

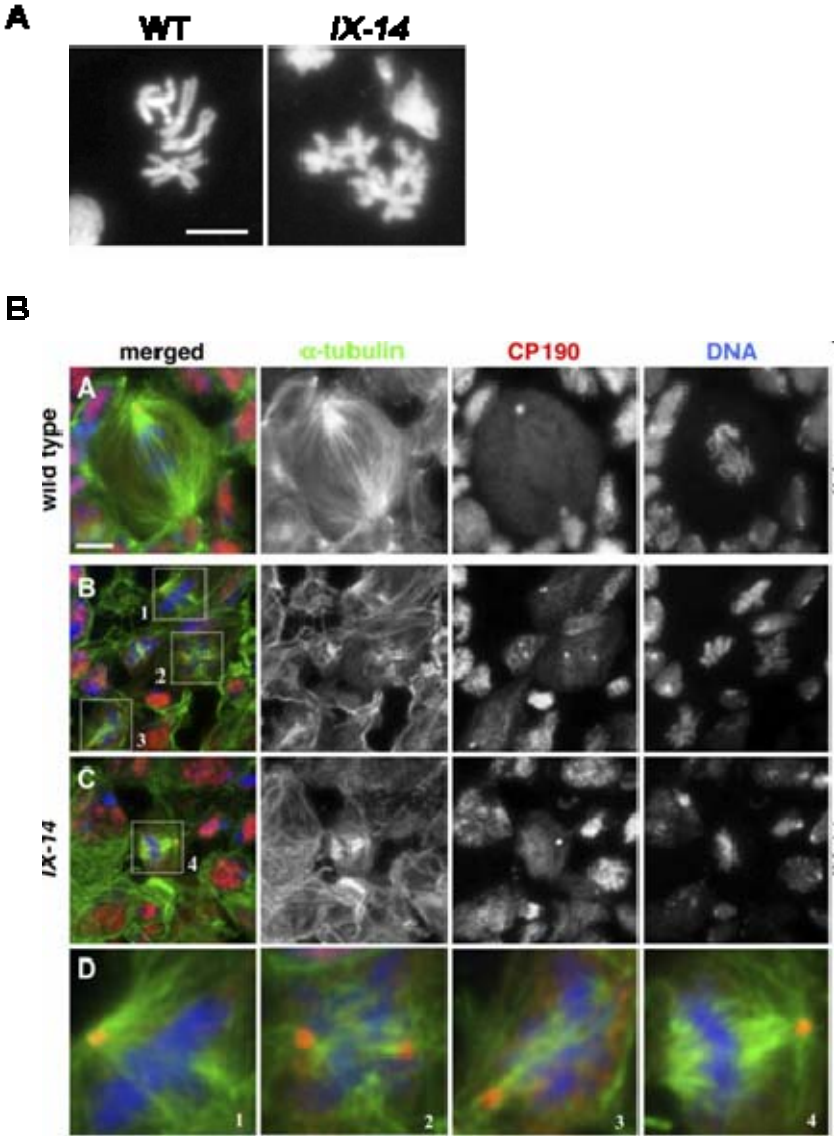

Figure 1.2 The phenotype observed in l(3)IX-14 mutants. A) The chromosome defect in *l(3)IX-14*. Mitotic chromosome spreads from wild type (WT) and the *l(3)IX-14* mutant. Chromosome hypercondensation with fuzzy periphery was observed in *IX-14* mutants. B) Centrosome and spindle phenotype of *l(3)IX-14*. Laval neuroblasts were stained for α-tubulin (green), a centrosome marker, CP190 (red) and DAPI. The aberrant spindle and centrosomes were observed in *IX-14* mutants. (Figure taken from McHugh *et al.,* 2004)

of the protein showed one conserved sequence belonging to the pathogen *Leishmania major*, named Leishmanolysin or GP63. GP63 belongs to the M8 class of metalloprotease with a conserved "HEXXHXXG[X]$_N$H" catalytic motif (Figure 1.3A) (Gomis-Rüth, 2003). The homologues of IX-14 were identified in all higher eukaryotic species for which sequence exists. Sequence alignment of the worm (*Caenorhabditis elegan*s), fly (*Drosophila melanogaster*), mouse (*Mus musculus*) and human with GP63 showed that the most obvious region of homology with GP63 is centered on the conserved metalloprotease motif (Figure 1.3A). The N and C-terminal regions are more divergent. There are nine blocks (Figure 1.3, number 1-9) that are shared among the worm, fly, mouse and human homologues, but absent from GP63. Despite this difference between GP63 and IX-14 of higher eukaryotic organisms, the positions of 14 cysteines are remarkably conserved between GP63 and the higher eukaryotic protein (Figure 1.3, green boxes) which suggests that the core of IX-14 should resemble that of GP63. The crystal structure of GP63 has been determined (Schlagenhauf *et al.*, 1998). The potential conformation of IX-14 was modelled on this structure and the indicated insertions (numbered 1-9) were found to lie at the surface of this structure (Figure 1.3B, black numbered spheres).The internal zinc ion essential for protease activity is indicated by a magenta sphere (Figure 1.3B). These sequence analyses of IX-14 suggested that it encodes a novel conserved zinc-metalloprotease in metazoan species with sequence homology to GP63.

So far there is only one known IX-14 variant in *Drosophila*, zebrafish (*Danio rerio*) and mouse, but four distinct splice variants of this gene have been identified in humans cells (Figure 1.4). Variant 1 (accession: AM920777 or AJ312399) of IX-14 has a longer first exon. An additional human splice variant, variant 2 (accession: AJ312398 or AM920778) has been identified in which the N-terminus is also

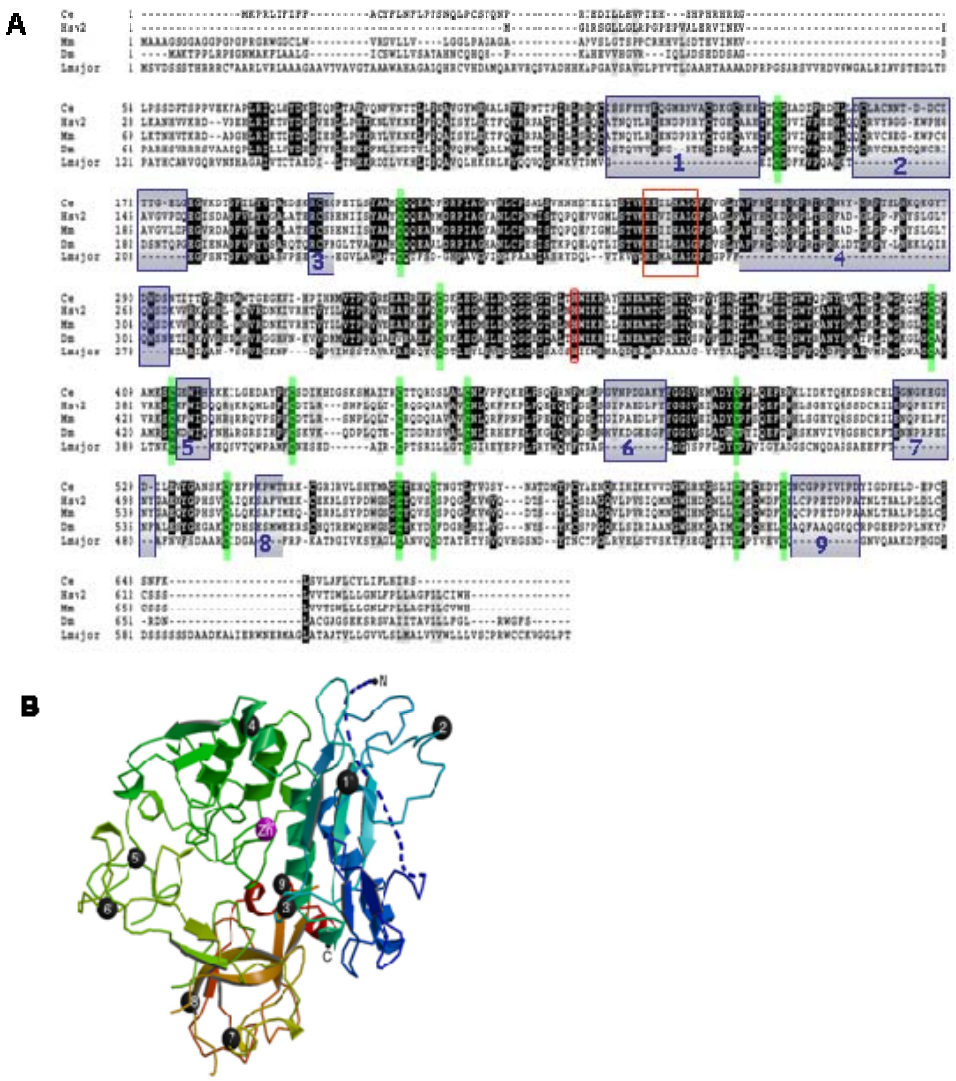

Figure 1.3 T-COFFEE alignments of IX-14 homologues and the structure analysis based on Leishmanolysin. A) T-COFFEE alignment showing homologues of IX-14 conserved between *Caenorhabditis elegans* (Ce), *Homo sapiens* variant 2 (Hs V2), *Mus musculus* (Mm), *Drosophila melanogaster* (Dm) and *Leishmania major* (Lmajor) with the conserved HEXXHXXG[X]NH zinc-metalloprotease motif (red box). There are 14 conserved cysteine residues (green) between all the homologues. Number 1-9 regions shared among the higher eukaryotic orthologues (absent in leishmanolysin) are indicated by blue boxes. B) Structure of leishmanolysin. The black numbered spheres represent the insertions (correlating to the number 1-9 regions) that map by prediction to the surface of the leishmanolysin structure. The internal magenta sphere represents the zinc ion required for catalysis. (Figure taken from McHugh *et al.,* 2004.)

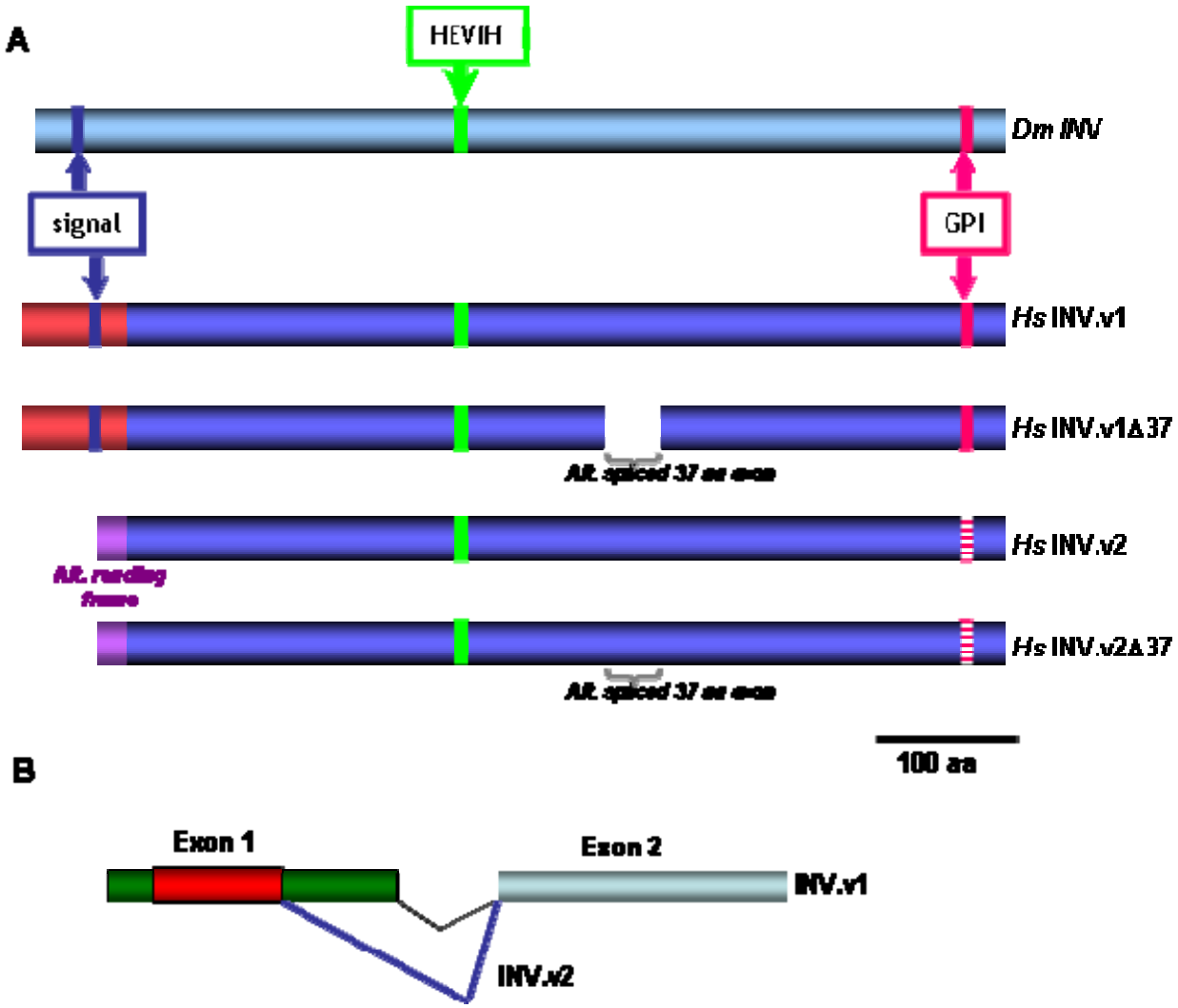

Figure 1.4 IX-14 (invadolysin) variants in Drosophila and human. A) This schematic picture represents one variant of fly INV and four variants of human INV. The conserved metalloprotease motif is depicted by a green box. In human, variant 1 is encoded by the longer first exon (red) containing a signal sequence at the N-terminus (blue arrow). Human variant 2 is translated in a different reading frame of first exon (purple box) and is spliced in a different way as shown in B). Both variants also exist in two different forms with regard to 37 amino acid exon 12. The GPI-anchor site (dark pink box) is predicted at the C-terminal of all INV variants. The variant 2 form of INV does not contain a signal sequence, therefore we predicted that the post-translational process addition of GPI moiety region would not occur in variant 2 (hatched dark pink box).

encoded by the first exon but translated in a different reading frame. The alternative first exon found in human variant 2 does not appear to have a counterpart in the available sequences of other species (except for orangutan or chimpanzee). In addition, each of the human IX-14 N-terminal splice variants may also exist in two alternative forms differing by the presence (accession: AM920777 or AM920778) or absence (accession: AJ312399 or AM920778) of a 37 amino acid region encoded by exon 12 (Cobbe et al., submitted). GP63 itself is a major GPI-linked (glycosylphosphatidylinositol-anchored proteins) surface protease present in diverse species of *Leishmania*. Analysis of human IX-14 variant 1 protein sequence revealed that IX-14 variant 1 contains a signal sequence in the N-terminus and the signal cleavage site is located at the 51st amino acid of IX-14 (human IX-14 variant 2 does not contain this signal sequence). In addition, the GPI modification sequence was also predicted at the C-terminus of IX-14 and a potential GPI anchor site (ω site) is localized at the 664th amino acid of IX-14.

The localization of invadolysin (IX-14)

The localization of the protein was originally studied in *Drosophila* S2 cells into which GFP-tagged Dm IX-14 was transfected. However, due to the limited resolution with such relatively small cells and non adherent properties, the transfected signal in S2 cells was rarely observed. Therefore, the study of IX-14 localization was examined in human cells. Intracellular staining with antibodies generated against recombinant human IX-14 showed ring-like localization patterns in HeLa cells (Figure 1.5) (McHugh *et al.*, 2004). This ring-like localization pattern was observed in many cell types, such as melanoma cell lines (A375, A375 MM and HBL), a human hepatoma cell line (HuH7) and an ovarian carcinoma cell line

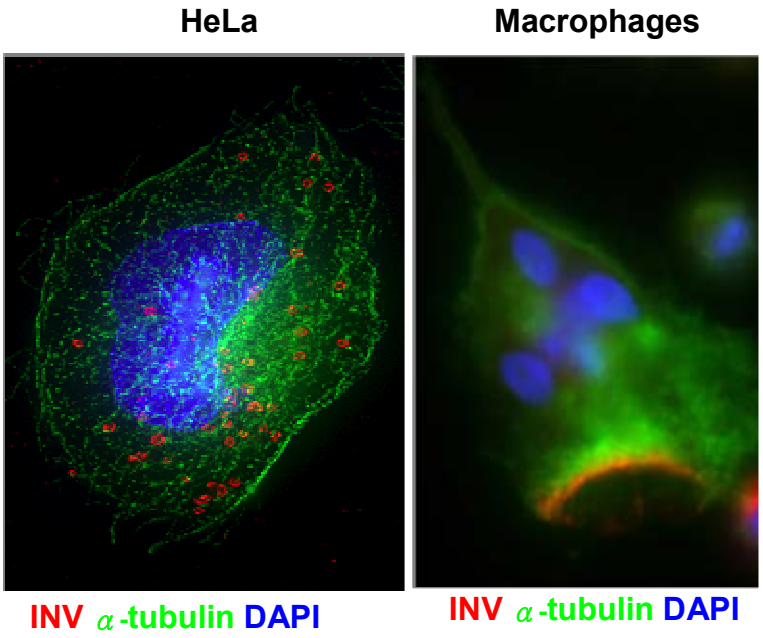

Figure 1.5 The localization of IX-14/INV in HeLa cells and macrophages. Intracellular staining with INV antibody showed the ring-like localization pattern in human HeLa cells (red). However, the localization of INV in normal human migrating macrophages revealed a leading edge localization (red). (Figure taken from McHugh *et al*. 2004.)

(PEO14) (Cobbe *et al*., submitted). The ring-like structure did not colocalize with Golgi, proteasomes, mitochondria or lysosomes. McGwire showed that GP63 plays an important role in the migration of the parasitic protozoan pathogen *Leishmania* through the extracellular matrix of the host organism (McGwire *et al.*, 1996) thus, the localization of IX-14 was also examined in migrating macrophages. Interestingly, the human IX-14 protein concentrated at the leading edge of migrating human macrophages, suggesting that IX-14 plays a role in cell migration (Figure 1.5) (McHugh *et al.*, 2004). Invadopodia are actin-based projections that are important for extracellular matrix degradation and cell migration in transformed cells, they are around 1 μm diameter structures in cultured cells (Baldassarre *et al.*, 2003; Buccione *et al.*, 2004). Therefore, it was postulated that the ring-like structures observed might be invadopodia due to their resemblance in size and distribution. Taking into account the homology to GP63 (leishmanolysin) and the proposed localization to invadopodia, the protein was named invadolysin (INV). However, additional experiments showed that INV does not appear to coincide with actin-rich projections associated with extracellular proteolytic degradation, which indicated that INV ring-like structures were not invadopodia (Cobbe *et al.*, submitted).

In the absence of colocalization between INV and an invadopodia marker, cortactin, the localization of INV and other endocytic vesicles was considered. Co-staining with INV antibody and cholera toxin B (CtxB) was used to examine for caveolar endocytosis (Orlandi & Fishman, 1998). This showed that CtxB was associated with some INV rings (Cobbe et al., submitted). Moreover, CtxB can also target to lipid vesicles, known as lipid droplets (LDs) (Lian & Ho, 1997). LDs are organelles that exist in most eukaryotic cell types to store neutral lipid (Murphy, 2001). Immunofluorescent detection of INV antibody and BODIPY (a dye specific

for LDs) in cultured cells revealed that INV was associated with the surface of LDs, suggesting that INV is a lipid droplet binding protein (Cobbe *et al.*, submitted).

Other phenotypes described in INV mutants

INV mutant cells accumulate high levels of nuclear envelope proteins

The nuclear envelope separates nucleus from cytoplasm. It is composed of outer and inner nuclear membranes, a perinuclear space, nuclear pore complexes and the nuclear lamina. The nuclear lamina is located between the inner nuclear membrane and the peripheral chromatin and interacts with lamin-associated proteins, nuclear scaffold proteins, and chromatin. Lamins are classified as type A and type B according to sequence homology, expression pattern, biochemical properties, and subcellular localization in mitosis (Stuurman *et al.*, 1998; Gruenbaum *et al.*, 2000). There are two lamin genes in *Drosophila*, one B-type lamin, termed lamin Dm0 (Gruenbaum *et al.*,1988) and one A-type lamin, termed lamin C (Bossie & Sanders,1993).

During mitosis, proper disassembly and reassembly of the nuclear lamina are required to progress through the cell cycle (Gant & Wilson, 1997). Chromosome condensation and spindle assembly are accompanied by disassembly of the nuclear envelope. Previously, members of the Heck lab examined nuclear envelope proteins in the *IX-14*^{4Y7} mutant and found that lamin Dm0, lamin C and otefin accumulated to higher levels in *INV* mutant neuroblasts than in wild type. INV was also shown to cleave lamin Dm0 *in vitro*, suggesting that lamin Dm0 could be a substrate of INV. (McHugh *et al.*, 2004).

Drosophila germ cell migration defect in INV mutants

As mentioned previously, the leading edge localization of INV in macrophages suggested a role for INV in cell migration (McHugh *et al.*, 2004). Furthermore, INV's involvement in cell migration was also shown by observation of germ cell migration in *Drosophila* embryos. In *Drosophila*, the primordial germ cells (PGCs) are the first cells to be formed and set aside from the rest of the embryos early during development (around 2.5 hours after egg laying at 25˚C) (Kunwar *et al.*, 2006). Germ cells migrate along and through various somatic tissues soon after their specification to reach the somatic component of the gonad (Santos & Lehmann 2004). Impaired germ cell migration was observed in *INV* mutant embryos (Figure 1.6). In *INV* mutants, germ cells were formed but did not migrate to make gonads and hence gonads were also absent in the mutant larvae (McHugh *et al.*, 2004). Thus phenotypic characterization of *INV* mutants and the localization of INV in human cells indicated that INV might be involved in both mitosis and cell migration.

1.2 Zinc metalloproteases

Overview of zinc metalloproteases

Zinc metalloproteases constitute a family of enzymes from the group of proteinases, which have catalytic motifs that can bind a metal ion such as zinc (Gomis-Rüth, 2003). Metalloproteases are involved in many aspects of biology, including cell proliferation, differentiation, remodelling of the extracellular matrix, vascularisation and cell migration (Chang & Werb, 2001). Comparing the sequences around the zinc binding site, zinc metalloproteases can be classified into distinct families. For the majority of metalloproteases, two of the zinc ligands are histidines. The zincins are defined by a HEXXH motif. The inverted zinc motif, HXXEH, defines the inverzincin family; the HXXE motif was defined as the carboxypeptidase

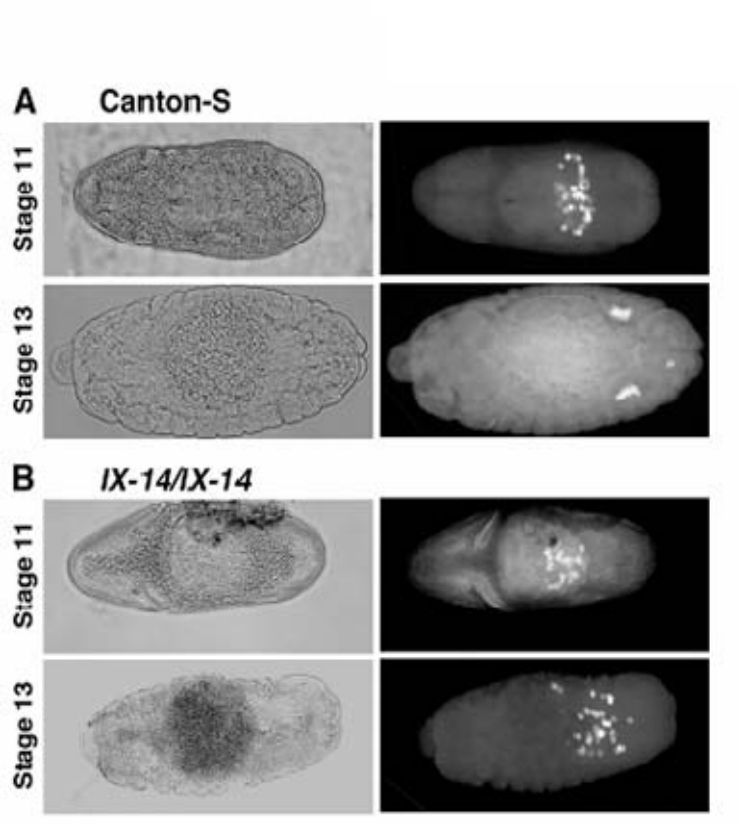

Figure 1.6 INV mutants embryos have a germ cell migration defect. Germ cells were examined both before and after the migration phase by using Vasa as a marker for germ cells. During the later stage of gonad coalescence in the embryo, the gonads were observed in wild type, however, in the *IX-14* mutants, germ cells were formed but failed to migrate to the gonads. (Figure taken from McHugh *et al*. 2004.)

family, and the HXH motif was defined as D-carboxypeptidase (Hooper 1994). Since 1996, the *MEROPS* database uses a hierarchical, structure-based classification of the peptidases (http://merops.sanger.ac.uk/). In this, each peptidase is assigned to a "family" on the basis of statistically significant similarities in amino acid sequence, and families that are thought to be related are grouped together in a "clan". Based on this, the metalloproteases can be divided into 15 clans (Figure 1.7). The metalloprotease with an HEXXH motif belongs to the MA clan, which includes 32 families (Figure 1.7). The other group such as the carboxypeptidase family (HXXE motif) belongs to the MC clan and HXXEH belongs to clan ME (Rawlings *et al.*, 2006).

Based on the nature and position of an additional third zinc ligand, the MA clan is further classified into two subclans, MA(E) and MA(M). The MA(E) subclan (also named gluzincins) provides a glutamate as third zinc ligand, and includes 19 families. The MA(M) subclan (also named metzincins) has a C-terminally elongated zinc binding motif HEXXHXXGXXH/D with an additional histidine or aspartate as third zinc ligand. Besides, metzincins additionally possess a conserved methionine within a typical Met-turn after the active site (Figure 1.8). The feature of this structure is to form a hydrophobic "pillow" for the catalytic zinc ion. Mutation of this methionine residue causes a decrease in activity of the metalloprotease (Gomis-Rüth, 2003). Therefore, a role for this Met-turn during folding of these catalytic domains has been postulated (Gomis-Rüth, 2003). The metzincin contains 13 families, including the most well-characterized MMPs (matrix metalloprotease) belonging to the M10 family, ADAMs (a disintegrin and metalloprotease) belonging to the M12 family and leishmanolysins, a homologue of invadolysin, was placed in the M8 family (Gomis-Rüth, 2003; Rawlings *et al.*, 2006).

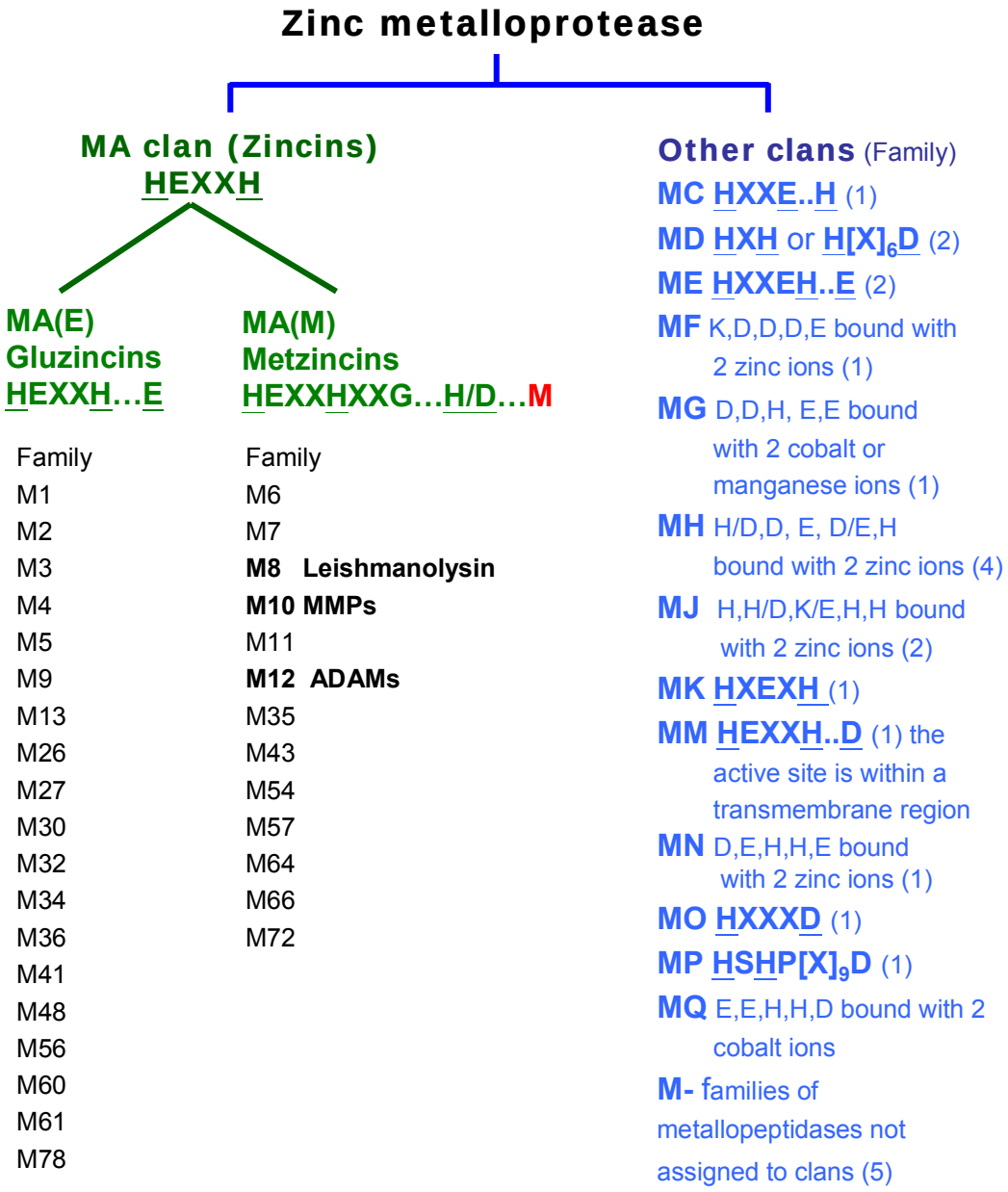

Figure 1.7 Categorization of zinc metalloproteases. The clan of metalloproteases and their inter-relationships based on sequence around the zinc-binding residues. The underlined letters represent identified zinc ligands. A conserved methionine (red letter) is present in the MA(M) subclan. (data collected from http://merops.sanger.ac.uk/)

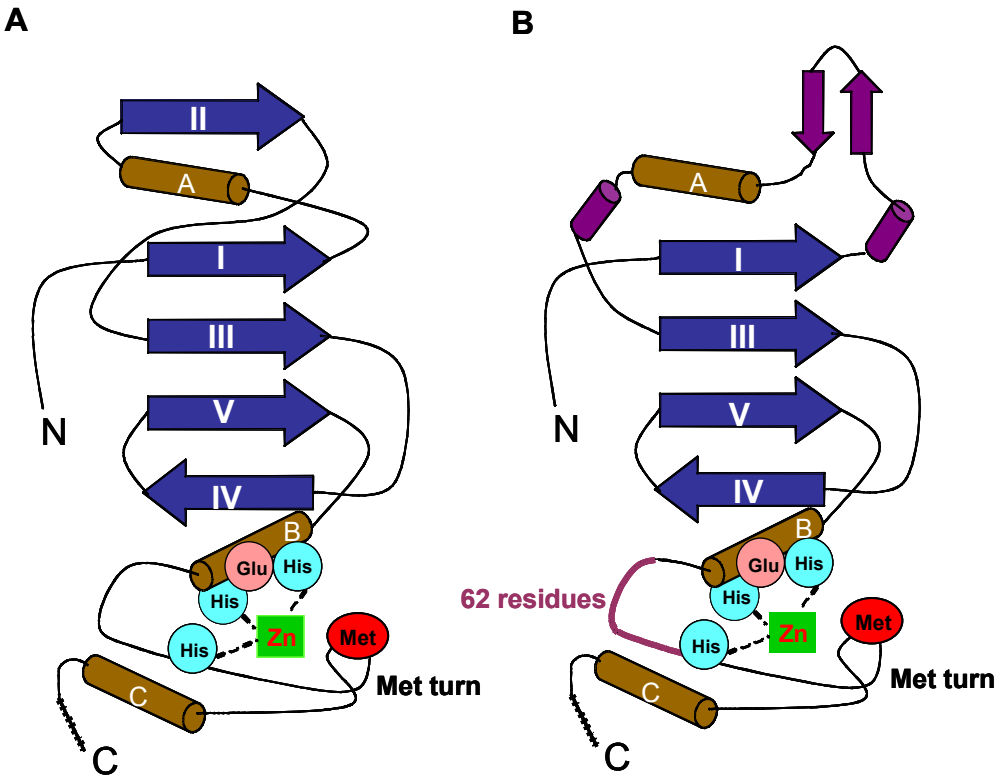

Figure 1.8 Secondary structure of a typical metzincin (A) and leishmanolysin (B). MA(M) subclan members (metzincins) share a conserved structure of 3 α- helices (represented by brown cylinders A, B, C) and 5 β-strands (represented by blue arrows I, II, III, IV, V). Three histidines are bound to a zinc ion to make the active catalytic site. A "met turn" follows the active site. Instead of β-sheet II present in other metzincins, the other 3 sequence (represented in purple) appear in Leishmanolysin. (Adapted from Gomis-Rüth, 2003.)

MMPs & ADAMs

Metzincins have been recognized as key players in a variety of biological systems. These enzymes have been found to regulate the activity of other molecules such as cytokines, growth factors and other proteases. MMPs were first described in the 1960s (Gross & Lapiere, 1962). Much attention has been focused on this family of metzincins due to their ability to degrade components of the extracellular matrix (Gomis-Rüth, 2003; Page-McCaw *et al*., 2007). However, processing of cell adhesion molecules, growth factors, cytokines, and receptors has also been documented. For example, MMP1 cleavage of laminin-5 induces cell migration; MMP3 (stromelysin-1) and MMP7 (matrilysin) cleavage of E-cadherin disrupts adhesion junctions and stimulates cellular migration and invasion (Noe *et al*., 2001). Membrane-type matrix metalloprotease (MT1-MMP) cleavage of CD44 results in the release of specific, biologically active fragments in culture to medium and in increased invasive behaviour (Kajita *et al*., 2001). MMP9 and MMP12 contribute to proteolytic shedding of the lipopolysaccharide (LPS) receptor CD14, and therefore influence innate host defense (Senft *et al*., 2005).

Advances in knowledge about ADAMs is growing quickly. As major ectodomain "sheddases", ADAMs release a variety of cell-surface proteins including growth factors, cytokines, cell adhesion molecules and receptors. Thus, ADAMs are important modulators of cell signaling (Murphy, 2008). For example, ADAM10 (Kuzbanian) is a sheddase involved in Notch signaling and it mediates cell-cell communication by cleaving ephrin, a ligand of the Eph family of receptor tyrosine kinases (Six *et al.*, 2003; Mishra-Gorur *et al.*, 2002; Mancia & Shapiro, 2005). ADAM17, also known as the TNFα converting enzyme (TACE), is involved in the activation of pro-TNFα (Black *et al*., 1997). Besides, ADAM17 is also required for

generation of the active form of epidermal growth factor receptor (EGFR) ligand, and its function is essential for development of epithelial tissue (Peschon *et al.*, 1998).

The MMPs are synthesized as inactive precursors. Activation of the MMPs proenzymes occurs via a "cysteine switch" (Van Wart & Birkedal-Hansen, 1990; Grams *et al.*, 1993; Wasserman, 2005). In this, there is an interaction between a conserved cysteine in the prodomain and the catalytic zinc ion in the active site that prevents the binding and cleavage of substrate, keeping enzyme in an inactive form. Dissociation of this cysteine from the zinc ion results in activation of the enzyme (Figure 1.9). Because of the importance of cysteine in the latency of the proenzymes, they can commonly be activated by thiol-blocking agents such as aminophenylmercuric acetate (APMA) (Van Wart & Birkedal-Hansen, 1990; Wasserman, 2005).

Leishmanolysin

Leishmanolysin is one of the cell surface proteins identified from *Leishmania major* (Russell and Wilhelm, 1986). It is a 63 kDa glycosylated GPI-linked protein, also known as GP63 and it was placed into family M8 in the MA clan according to its tertiary structure (Schlagenhauf *et al.*, 1998). The difference between GP63 and MMPs is the insertion of 62 residues between the glycine residue and the third histidine residue of the consensus motif HEXXHXXG…H (Figure 1.8B). The GP63 protein is the structural prototype for membrane-bound metalloproteases and they are found not only in protozoa but also in some bacteria (eg. *Deinococcus radiodurans*), nematode, the fruit fly and humans (Gomis-Rüth, 2003; McHugh *et al*., 2004).

Although GP63 and MMPs were placed into different families, leishmanolysin

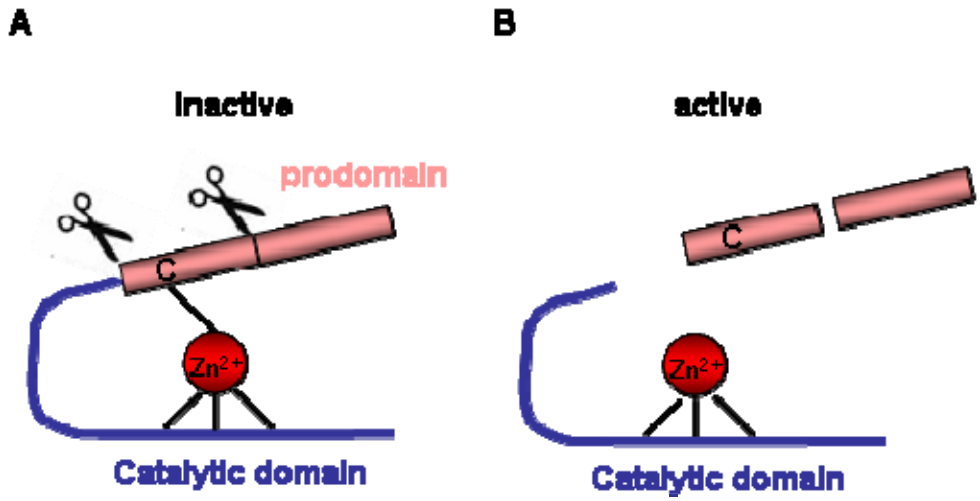

Figure 1.9 The mechanism of cysteine switch. Matrix metalloproteinases (MMPs) and Leshimanolysin are expressed as pro-proteins. A. The conserved cysteine residue (C in the pink box) in the pro-domain coordinates the zinc ion (red circle box) to result in an inactive form of the protease. B. The pro-domain is removed by combination of a cleavage in the prodomain and between the pro-domain and the catalytic domain.

has a similar cysteine switch mechanism of activation like MMPs. *L. major* GP63 has been predicted to be synthesized as a 602 amino acid precursor protein containing an NH_2-terminal signal sequence of 39 amino acids; a putative regulatory pro-region of 61 amino acids, which includes a highly conserved cysteine residue and a COOH-terminal GPI attachment signal sequence of 25 amino acids (Button & McMaster 1988). Post-translational modifications are important for forming active, mature GP63. Aside from the signal peptide, a prodomain is presumably cleaved from the NH_2-terminal end of nascent GP63 by autocatalytic processing (McGwire & Chang, 1996), thereby unblocking the active site via a "cysteine switch" mechanism and liberating the mature active protein (Button *et al.,* 1993). Leishmanolysin is a major component of the promastigote surface. It cleaves CD4 molecules on the surface of human T cells and protects promastigotes from lysis by complement proteins (Yang *et al.*, 1991). This suggests that GP63 plays a role as a virulence factor (Yang *et al.*, 1991).In addition, *Leishmania* expressing high levels of active GP63 have enhanced capacity for migration through the ECM *in vitro* by degradation of ECM components, such as gelatin, casein, hemoglobin and fibrinogen (Yao *et al.*, 2003; McGwire *et al.*, 2003).

1.3 Lipid droplets

Structure of LDs

Lipid droplets (LD) are organelles that are present in different organisms, ranging from yeast to human. They share many features and consist of a core of neutral lipid with triglycerols or cholesterol ester and they are usually surrounded by a monolayer of phospholipids and associated proteins (Martin *et al.*, 2005; Imanishi *et al.*, 2004). The size and number of LD varies between different cell types;

large-sized LDs are predominantly found in adipocytes, which are highly specialized for lipid storage. In other mammalian cell types, the size of LDs is around 1 μm (Listenberger & Brown, 2008). Interestingly, it has been observed that all cell types examined have the ability to generate LDs in response to elevated fatty acid levels (Martin & Parton 2006). Based on the rapid increase in studies on LDs, the question about how and where LDs form, how proteins are recruited to LDs, and what the function of LDs in cells are being addressed.

Lipid droplet formation

LDs form quickly in response to an increase in fatty acid levels in most cultured cells (Pol *et al.*, 2004). The mechanism of LD formation is still poorly understood. The most acceptable hypothesis for LD formation is from Murphy & Vance (Murphy & Vance, 1999). They propose that neutral lipid is synthesized between the leaflets of the endoplasmic reticulum membrane (ER membrane). Continued lipid synthesis causes the disc to swell into a sphere, then a mature LD buds from the ER membrane to form an independent organelle in the cytoplasm (Figure 1.10A) (Murphy & Vance,1999). Several observations suggest that LD formation occurrs in the ER. When GFP tagged ALD1 (associated with LD protein 1) was expressed in cells, it localized to the ER prior to entering LDs in response to lipid loading. Thus, it was suggested that ALD1 might target to newly formed LDs in ER that eventually form independent LDs (Turoo *et al.*, 2006). On the other hand, trafficking of lipid to LDs in living cells by feeding cells with a fluorescent fatty acid (all-trans-6,8,10,12,14-hexadecapentaenoic acid) revealed a diffuse fluorescent signal in the ER by 2 minutes. Upon longer incubation, the fluorescent vesicles were found in the cytoplasm (Kuerschner *et al.*, 2008). However, LD budding from the ER has

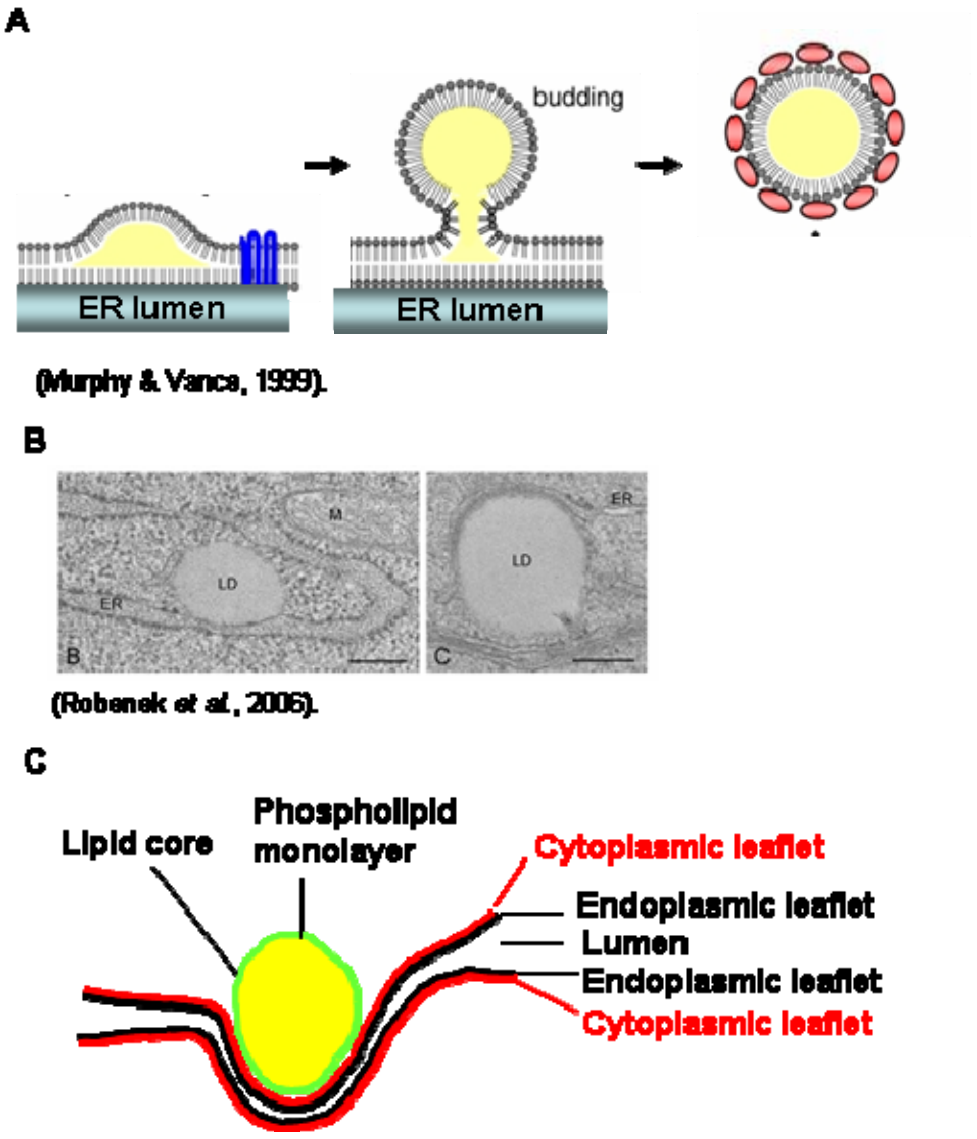

Figure 1.10 Models of lipid droplet formation. A) A model from Murphy & Vance. The neutral lipid is synthesized between the outer leaflets of the ER membrane, the mature LD buds from the ER membrane to form an independent structure (Murphy & Vance, 1999). B) Conventional thin section electron microscopy images showed a close association between lipid droplets and the ER after lipid loading in macrophages (Robenek *et al*., 2006). C) The second model assumes that the formation of a lipid droplet occurs at a specialized site of the cytoplasmic surface of ER (Robenek *et al*., 2006).

never been unequivocally observed (Robenek *et al.*, 2006; Listenberger & Brown, 2008). Another hypothesis assumed that formation of a LD occurs at a specialized site of the cytoplasmic surface of the ER (Brown, 2001; Robenek *et al.*, 2006; Listenberger & Brown, 2008). Freeze-fracture immunocytochemistry revealed that the LD develops alongside but not within the ER membrane (Figure 1.10B). Their data showed that whereas LDs and ER membranes are often seen in close association, LDs always lie adjacent to the paired membranes of the ER; lipid accumulation is never seen within the ER membrane (Figure 1.10C). The ER membrane partially encloses LDs in a manner similar to an egg cup holding an egg (Robenek *et al.*, 2006).

Recently, several molecules have been identified as regulators controlling the formation of LDs. For example, phospholipase D1 (PLD1) and extracellular signal-regulated kinase (ERK2) stimulated the formation of LDs (Andersson *et al.* 2006); siRNA depletion of Prp19p (a nuclear protein involved in DNA repair) in 3T3-L1 cells repressed LD formation with a decrease in the levels of expression of perilipin and S3-12 (Mahajan & Mitchell, 2003; Cho *et al.*, 2007). Endoplasmic reticulum resident membrane proteins fat-inducing transcript (FIT), FIT1 and FIT2 can induce LD accumulation in cell culture. shRNA-mediated silencing of FIT2 in 3T3-LI adipocytes prevented accumulation of LDs, and depletion of FIT2 in zebrafish blocked diet-induced accumulation of LDs in the intestine and liver (Kadereit *et al.*, 2008).

The protein composition of LDs

As with other membranous organelles, the LD surface monolayer also contains a characteristic set of proteins. The best understood LD components are PAT family

proteins, named after the first identified members' Perilipin, ADRP (Adipose Differentiation Related Protein or Adipophilin) and TIP47 (Tail Interacting Protein of 47 kDa) (Martin & Parton, 2006; Thiele & Spandl, 2008). The N-terminal regions of PAT family proteins are very similar, constituting the so-called PAT domain (perilipin amino-terminal domain) (Olofsson *et al.*, 2008). Perilipin is restricted to adipocyte and steroidogenic cells which are specialized for lipid storage (Brown, 2001). ADRP is expressed in a wide range of non-adipocytes (Brasaemle *et al.*, 1997), where it binds to the LD to promote the accumulation of triacylglycerols and uptake of fatty acids (Gao & Serrero, 1999; Imamura *et al.*, 2002). TIP47 coats the membrane of LDs and is known to transport the mannose-6-phosphate receptor from endosomes to the Golgi (Barbero *et al.*, 2002; Miura *et al.*, 2002). Recently, lipid storage droplet protein 5 (LSDP5 or OXPAT), myocardial lipid droplet protein (MLDP or PAT-1) and S3-12 have been categorized as members of the PAT family (Dalen *et al.*, 2007; Wolins *et al.*, 2006; Yamaguchi *et al.*, 2006; Wolins *et al.*, 2003; Dalen *et al.*, 2004) because their N-terminal regions are similar to PAT domains.

However, the PAT domain does not seem to be important for binding to the LD. Perilipin contains central hydrophobic domains (H1, H2, H3) for its targeting to LDs (Garcia *et al.*, 2003). The central domain of ADRP directs ADRP to LDs (Nakamura *et al.*, 2003). PAT domain proteins are evolutionarily conserved in *Drosophila*. For example, lipid storage droplet-2 (LSD2), a *D. melanogaster* PAT protein, has been proposed to regulate lipid catabolism and is required for LD motion (Welte *et al.*, 2005; Gronke *et al.*, 2003). In addition, the enzymes involved in lipid metabolism were also frequently found in LD proteomic studies, including acyl-CoA synthetase; ATGL (Adipose triglyceride lipase) and CGI-58 (Smirnova *et al.*, 2006; Yamaguchi *et al.*, 2007).

In principle, LDs can be relatively easily isolated with high purity due to their unique density and their ability to float on top of sucrose gradients (Brasaemle & Wolins, 2006). Recently, a number of mass spectrometric analyses of the LD proteome have been performed from different cell types and tissues (Table 1). Mass spectrometric analyses have identified several proteins that were thought to be unique to other subcellular organelles. The list contains proteins from ER, Golgi and mitochondria and also proteins related to signaling, cytoskeketal proteins and chaperones. Surprisingly, more than 10 Rab proteins were detected (Bartz *et al.*, 2007; Wan *et al.*, 2007; Cho *et al.*, 2007; Turro *et al.*, 2006; Beller *et al.*, 2006; Cermelli *et al.*, 2006; Liu *et al.*, 2004; Fujimoto *et al.*, 2004). Among these, Rab18 is probably the only Rab that was confirmed to localize to LD (Martin *et al.*, 2005; Ozeki *et al.*, 2005). Caveolin is a major component of caveolae (flask-shaped structures that function in signaling transduction and endocytosis) (Martin & Parton, 2005) and was found in the LD fraction with both Brefeldin A (BFA) treatment and in response to the intracellular accumulation of lipid (Pol *et al.*, 2001; Fujimoto *et al.*, 2001; Martin & Parton, 2005). When cells are loaded with lipid, caveolin translocates to LDs depending on the activity of Src tyrosine kinase and protein kinase C (Le Lay *et al.*, 2006).

Caveolin proteins have a 30-40 amino acid long hydrophobic region which forms a hairpin helix structure to bind to LDs (Fujimoto *et al.*, 2001; Pol *et al.*, 2001). Interestingly, nuclear proteins have also been found in LD fractions analyzed by mass spectrometric analyses (Cermelli *et al.*, 2006; Beller *et al.*, 2006; Cho *et al.*, 2007).

Table 1.1 The proteomic analysis on lipid droplets

Paper	**Source of LDs for proteomic studies**	
Fujimoto *et al*., 2004	Hepatocyte cell line HuH7	17 proteins were identified
Liu *et al.*, 2004	Chinese Hamster Overy K2 cell (CHO K2)	40 proteins were identidfied including Rabs and caveolin
Brasaemle *et al.*, 2004	3T3-L1 adipocyte	To isolate LDs from basal and lipolytic stimulated adipocyte
Umlauf *et al*., 2004	A431 cell line which stable expressed stomatin (stomatin localizes to plasma membrane and the late endosomal compartment. it is targeted to lipid bodies (LBs) on overexpression)	cytoskeletal components, chaperones, Rab 1,6,7,10,18 association of the Rab proteins 1, 6, 7, 10, and 18
Beller *et al.*, 2006	*Drosophila* fat body tissue	248 proteins were indentified
Cermelli *et al.*, 2006	*Drosophila* embryo	H2A, H2B and lamins were identified from embryo LDs
Turró *et al.*, 2006	Rat liver after hepatectomy	50 proteins were identified.
Wang *et al.*, 2006	Luminal LDs from mouse liver microsomes	Many ER proteins were identified, including, HSP70
Bartz *et al.*, 2007	CHO K2 cell	125 proteins were identified of which 70 proteins had not been identified on LDs of mammalian cells. They also carried out phosphoprotein proteomic analysis, 7 functional LD protein were determined to be phosphorylated.
Wan et al., 2007	Monocytic cell line U937	ribosomes, ER membrane-associated and ER luminal proteins
Cho *et al.*, 2007	3T3-L1 adipocyte	Previous nuclear protein Prp19p was found to associated with LD

Functions of LDs

The LD plays a major role in lipid homeostasis. Lipids stored in LDs are hydrolysed and may be used for oxidation, membrane synthesis, protein modification and generation of signaling molecules and other lipid products (Fujimoto *et al.*, 2008). Chanarin-Dorfman syndrome (CDS), also called "neutral lipid storage disease with ichthyosis", is characterized by excessive accumulation of triacyglycerol in cells of many organs (Yen & Farese, 2006). Mutations in CGI-58 such as Q130P, E7K, and E260K were identified in patients with CDS (Lefevre *et al.*, 2001). CGI-58 interacts with perilipin and localizes to LDs, mutation of CGI-58 in CDS patients (Q132P and E262K) weakens its binding to perilipin and disrupts its binding to LDs (Yamaguchi *et al.*, 2004). However, an increasing variety of proteins found in LDs revealed that the LD has functions that are not restricted to lipid metabolism.

Recent research showed that the LD can be a temporary storage site for proteins to be degraded (Fujimoto & Ohsaki 2006; Ohsaki *et al.*, 2006; Cole *et al.*, 2002). Apolipoprotein B (ApoB) is the primary protein component of VLDL (very low-density lipoprotein). Nascent lipoproteins are first assembled in the ER. After maturation, they are secreted by exocytosis (Davis, 1999). ApoB has been shown to exist in the ER and Golgi (Sakata *et al.*, 2001). A recent study found that ApoB accumulates on LDs markedly when the proteasomal or autophagic process is inhibited in hepatocytes (Fujimoto & Ohsaki 2006; Ohsaki *et al.*, 2006). This result suggested the LD as a temporary storage site for ApoB degradation. The degradation of excess ApoB has been reported to occur by both proteasomal and nonproteasomal pathways (Cavallo *et al.*, 1999; Fisher *et al.*, 1999). LDs may offer another advantage for the processing of ApoB. A major protein of Lewy bodies (abnormal aggregates of protein that develop inside nerve cells), α-synuclein, found in

Parkinson's disease, also has an affinity to LDs (Cole *et al.*, 2002) and it can be degraded by the proteasome and via autophagy (Webb *et al.*, 2003). Hydrophobic segments are found in both ApoB and α-synuclein and they are likely to form aggregates when left free in an aqueous environment (Giasson *et al.*, 2001; Segrest *et al.*, 2001). The LD may provide a surface that these proteins can bind through hydrophobic interactions, and this aids in the disposal of potentially toxic protein aggregates (Fujimoto & Ohsaki *et al.*, 2006).

LDs can also be a temporary storage site for abundant proteins. A massive amount of histones are stored in LDs of the *Drosophila* embryo and they are later utilized to package chromatin in the nucleus (Cermelli *et al.*, 2006). Newly laid *Drosophila* eggs contain histones in thousand-fold excess relative to DNA (Cermelli *et al.*, 2006). It has been reported that free histones can interfere with growth and development (Gunjan *et al.*, 2003; Gunjan *et al.*, 2005). Therefore, it was suggested that LDs may offer sequestration sites to store histones, such as H2A and H2B or even inactivate them. However, H3 and H4 are not found there (Cermelli *et al.*, 2006; Welte, 2007).

LDs can also be a target of pathogens. Hepatitis C virus (HCV) is a causative agent of chronic liver disease and it appears to need LDs for its proliferation (Miyanari *et al.*, 2007). HCV targets to the LDs through its structural "Core" protein, which recruits nonstructural (NS) proteins and the replication complex to LDs. This recruitment is critical for producing infectious viruses, as deletion or mutation of Core (disrupting its LD targeting) suppressed HCV production (Miyanari *et al.*, 2007). *Chlamydia trachomatis*, a causative agent of trachoma and sexually transmitted disease, causes accumulation of LDs around a bacteria-containing vacuole (Kumar *et al.*, 2006). It has been suggested that the bacterium utilizes the

stored lipid for its growth (Kumar *et al.*, 2006).

As more proteins were identified from LDs, so more hints were obtained to allow speculation about additional functions of LDs. LDs may co-ordinate several cellular processes either directly or indirectly. LDs cross talk with lysosomes, endosomes and caveolae by transiently sharing proteins and influencing cellular processes from lipolysis to membrane trafficking. Spartin, also known as SPG20, is mutated in a rare neuronal disease, called Troyer syndrome (Patel *et al.*, 2002). The localization of SPG20 has been reported on endosomes and mitochondria (Bakowska *et al.*, 2005; Lu *et al*., 2006). Recently, new findings show that SPG20 associates with the surface of LDs and can regulate the size and number of LDs. The mutant SPG20 present in Troyer syndrome is not able to bind LDs. This suggests that SPG20 can regulate LD turnover and potential pathological mechanisms in Troyer syndrome (Eastman *et al*., 2009). An increase in LD numbers was found in osteoarthritis, liver degeneration, cartilage over-proliferation and breast cancers, but the detailed mechanism for LD accumulation is still unclear (Welte, 2007).

1.4 Adipocyte differentiation

Models of adipocyte differentiation

Adipocyte differentiation, also termed adipogenesis, is the development of fat cells from preadipocytes. It is one of the most intensely and faithfully modelled processes of cellular differentiation (Rosen *et al*., 2000; Fleming *et al*., 1998). Many LD binding proteins are regulated during this differentiation process. The expression of LD binding proteins CGI-58 and ADRP increases during adipocyte differentiation (Yamaguchi *et al.*, 2004). Adipose triglyceride lipase (ATGL) catalyzes the initial step in triglyceride hydrolysis and displayed a difference in its expression level

during adipogenesis (Zimmermann *et al.*, 2004)**.**

The differentiation of adipose cells has been an experimentally accessible system of study since the development of a preadipocyte cell line by Green and colleagues in the 1970s (Green & Kehinde 1974, 1975, 1976, 1979). The most well-characterized models for studying the conversion of preadipocytes into adipocytes are 3T3-L1 and 3T3-F442A. These cells were isolated from non-clonal Swiss 3T3 cells and they are morphologically indistinguishable from fibroblasts. When the 3T3-L1 cell line was injected into nude mice, the cells developed into adipocyte cells that were indistinguishable from normal adipose tissue (Green & Kehinde, 1979). In culture, differentiated 3T3-L1 cells possess most of the ultrastructural characteristics of adipocytes from animal tissue (Novikoff *et al.*, 1980).

Confluent 3T3-L1 preadipocytes can be differentiated by a defined biochemical adipogenic cocktail. Maximal differentiation is achieved upon treatment with the combination of insulin, glucocorticoids, and an agent that elevates cAMP levels (Student *et al.*, 1980). Insulin is known to act through the insulin-like growth factor1 (IGF-1) receptor. IGF-1 can be substituted for insulin in the adipogenic cocktail (Smith *et al.*, 1988). Dexamethasone (Dex), a synthetic glucocorticoid agonist, is used to stimulate the glucocorticoid receptor pathway. Methylisobutylxanthine (MIX), a cAMP phosphodiesterase inhibitor, is traditionally used to stimulate the cAMP dependent protein kinase pathway. The first stage in the differentiation of fat cells is growth arrest. Initial growth arrest is achieved in the cultured cell line after contact inhibition. Following induction with an adipogenic cocktail, cells are committed to the differentiation process. After induction by the adipogenic cocktail, cells change their shape due to a reorganization of extracellular matrix and

cytoskeleton proteins. In the early stage of differentiation, clonal expansion (a limited number of mitosies) allows an increase in the final proportion of differentiated fat cells. Finally, cells enter the maturation phase. During this process, cells became able to transport a large amount of glucose into the cells in response to insulin, synthesize fatty acids and to store triacylglycerols (Féve, 2005; Rosen & Spiegelman 2000).

Transcriptional control of adipocyte differentiation

Adipose differentiation is the result of transcriptional remodelling that leads to activation of a large number of adipose-related genes. Several transcription factor families that exhibit different modes of activation and function appear to be key regulators of the adipogenesis process. CCAAT-enhancer binding proteins (C/EBP) β and δ are the first transcription factors induced after exposure of preadipocytes to the differentiation cocktail (Schwarz *et al.*, 1997; Elberg *et al.*, 2000). The importance of C/EBP β and δ during adipogenesis is demonstrated by loss-of-function and gain-of-function studies in mice. Overexpression of C/EBP β and δ enhances adipogenesis (Yeh *et al.*, 1995; Darlington *et al.*, 1998). On the other hand, embryonic fibroblast cells derived from mice lacking either C/EBP β or δ have reduced levels of adipogenesis compared with wild type (Tanaka *et al.*, 1997). In addition, embryonic fibroblast cells derived from C/EBP β and δ double knock-out mice do not differentiate into adipocytes (Tanaka *et al.*, 1997). The activities of C/EBP β and δ are thought to mediate the expression of the central transcriptional regulators of adipogenesis, peroxisome proliferator activated receptor γ (PPARγ) and C/EBP α (Clarke *et al.*, 1997, Wu *et al.*, 1995). PPARγ is a member of a nuclear-receptor superfamily and is necessary and sufficient for adipogenesis (Rosen

& Spiegelman, 2000). This has been demonstrated by the observation that overexpression of PPARγ is able to induce adipocyte differentiation in non-adipogenic fibroblastic NIH3T3 cells (Tontonoz *et al.*, 1994), and no factor has been discovered that promotes adipogenesis in the absence of PPARγ (Rosen & MacDaugald, 2006). PPARγ is not only crucial for adipogenesis but is also required for maintenance of the differentiation state. Expression of a dominant-negative PPARγ in mature adipocytes causes de-differentiation with loss of lipid accumulation and decreased expression of adipocyte markers (Tamori *et al.*, 2002). Ligand activation of PPARγ, induces many target genes involved in lipogenesis and adipogenesis (such as adipocyte lipid-binding protein aP2, CD36, GLUT4, perilipin) and it also turns on the expression of C/EBP α. Other transcription factors that promote adipogenesis include KLFs (krüppel-like family, a large family of C2H2 zinc-finger proteins) (Mori *et al.*, 2005; Gray *et al.*, 2002), SREBP1c (sterol regulating element binding protein) (Kim *et al.*, 1998) and CREB (cyclic AMP response element-binding protein) (Zhang *et al.*, 2003).

Signaling pathways in adipogenesis

The process of adipogenesis is modelled by sequential activation of transcription factors (Figure 1.11). These transcription factors function downstream of signaling pathways that transduce information about the suitability of intracellular and extracellular conditions for differentiation. There are many pathways that influence adipocyte differentiation, such as Wnt, TGFβ (the transforming growth factor β), Notch and insulin signaling (Rosen & MacDougald, 2006). Those signaling pathways can subsequently affect the expression of C/EBPα and PPARγ, and finally regulate the expression of adipocyte genes (Rosen & MacDougald, 2006). The

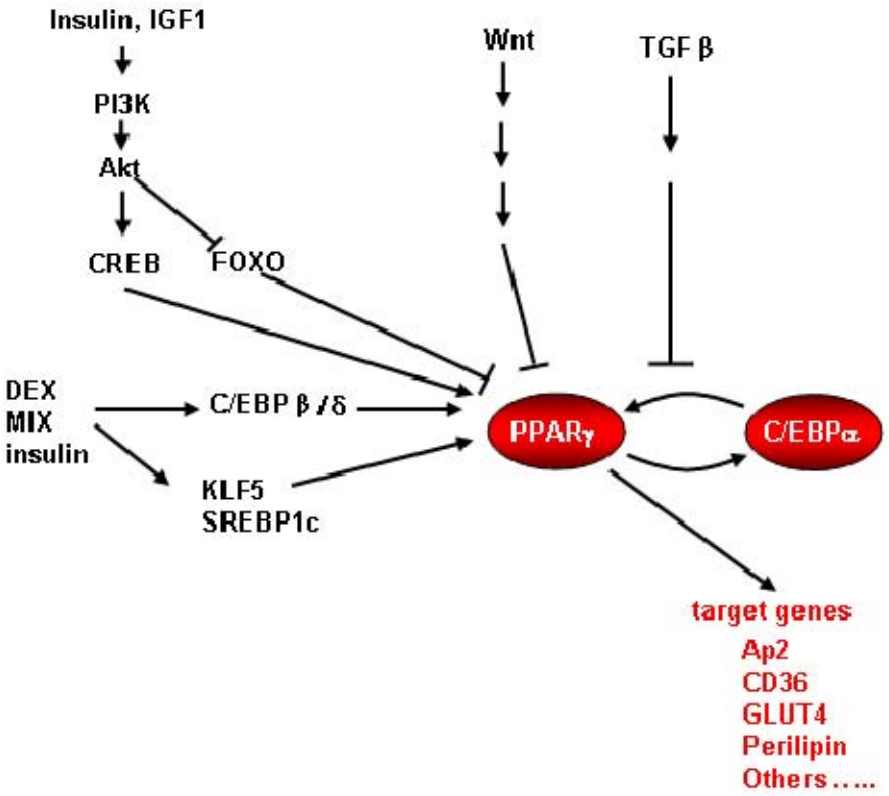

Figure 1.11 Extracellular signaling in adipogenesis. PPARγ is the master regulator of adipogenesis which can turn on the expression of C/EBPα. A feedback loop exists between PPAR γ and C/EBPα. Activation of PPARγ promotes differentiation through induction of a variety of target genes important for triacylglycerol uptake, including ap2, GLUT4, perilipin and other. A variety of signaling pathways have been identified that act upstream of PPARγ. Insulin signaling promotes adipocyte differentiation; Wnt and TGF β pathways inhibits adipogenesis (details of the pathway have been omitted). In addition, many transcription factors such as C/EBP β / δ , CREB (cyclic AMP response element-binding protein), KLF (krüppel-like family) and SREBP1c (Sterol regulatory element binding protein) can regulate adipocyte differentiation (diagram modified from Rosen & MacDougald, 2006).

earliest observations revealed that efficient differentiation *in vitro* requires insulin. Insulin and insulin-like growth factor-1 increases the percentage of cells that differentiate and also increases the amount of lipid accumulation in each fat cell (Girard *et al.*, 1994). 3T3-L1 cells with partial inactivation of the *insulin receptor* gene (*InR*) display impaired adipocyte differentiation, and InR knock-out mice have marked adipose tissue hypotrophy (Accili & Taylor, 1991; Cinti *et al.*, 1998).

Downstream components of the insulin signaling cascade are also important for adipogenesis. The loss of an individual insulin-receptor substrate (IRS) protein inhibits adipogenesis (Tseng *et al.*, 2004). Adipocyte differentiation is associated with a transient increase of phosphatidylinositol-3 kinase (PI3K) activity (Sakaue *et al.*, 1998). Inhibition of PI3K and Akt/protein kinase B (PKB) repress adipogenesis (Rosen & MacDougald, 2006). Mouse embryonic fibroblasts (MEFs) from mice that lack both *Akt1* and *Akt2* can not undergo differentiation (Garofalo *et al.*, 2003). In addition, several Akt targets which have a role in adipogenesis have been discovered. These include the Foxo transcription factor, Foxo1, which is negatively regulated by Akt phosphorylation (Kops & Burgering, 1999). It is an anti-adipogeneic transcription factor in that constitutively active Foxo1 prevents the differentiation of adipocytes, while a dominant negative Foxo1 construct can rescue adipogenesis of insulin-receptor-deficient MEFs (Nakae *et al.*, 2003). Furthermore, the serine/ threonine kinase mammalian target of rapamycin (mTOR), an indirect target of Akt, has been shown to be involved in adipogenesis (Lawrence *et al.*, 2004; Kim & Chen 2004). The glycogen synthase kinase 3 (GSK-3), an important Akt substrate, is also implicated in adipogenesis (Cross *et al.*, 1995; Ross *et al.*, 1999).

Almost every important cellular signaling pathway has a positive or negative effect on adipocyte development. These signaling pathways converge on a tightly

regulated cascade of transcription events (Rosen & MacDougald, 2006). Some proteins which have been reported to affect adipogenesis were also found to have an effect on the expression of PPARγ. The overexpression of nuclear lamin A was associated with inhibition of PPARγ and GLUT4, and subsequently inhibited lipid accumulation, triglyceride synthesis and adipocyte differentiation (Boguslavsky *et al.*, 2006). In contrast, embryonic fibroblasts lacking A-type lamins accumulated more lipid and those cells had increased phosphorylation of Akt, a mediator of insulin signaling (Boguslavsky *et al.*, 2006).

Recent studies have indicated that matrix degradation might also be essential for adipogenesis. MMP-2 and MMP-9 were secreted by adipocytes and their proteolytic activities were important for adipogenesis (Brown *et al.*, 1997; Bouloumie *et al.*, 2001). Inhibition of the activity of MMP by several metalloprotease inhibitors, such as BB-94 or GM6001, blocked adipocyte differentiation (Bouloumie *et al.*, 2001; Alexander *et al.*, 2001). Further study showed that in BB-94 treated cells, expression of PPARγ was undetectable at day 3 and 80% less compared with control cells at the end of the protocol (Chavey *et al.*, 2003).

Adipocytes provide a safe place to store lipid. When these cells are absent, as in lipodystrophy, lipid accumulates in muscle, liver and other locations. This is believed to cause significant metabolic abnormal, including insulin resistance and hepatosteatosis that leads to cirrhosis (Agarwal & Garg, 2006). Several genetic causes of human lipodystrophy have been discovered. Mutations in the nuclear proteins (lamin A and lamin C), zinc metalloprotease (ZMPSTE24), Akt 1/2 and PPARγ affect adipocyte development and cause human lipodystrophy (Boguslavsky *et al*., 2006; Rosen & MacDougald, 2006).

1.5 Insulin signaling pathway

Overview of insulin signaling pathway

The insulin signaling pathway is a conserved signaling cascade in animals. The mechanisms of insulin receptor signaling are similar in mammals and *Drosophila* (Lizcano & Alessi, 2002). This pathway functions as a nutrient-sensing pathway and plays a role in the regulation of cell growth and metabolism in the organism (Grewal, 2008). Insulin signaling is mediated by a complex, highly integrated network that controls several processes. In the presence of insulin, the insulin receptor (IR) and insulin-like growth factor receptor (IGFR) are activated by autophosphorylation (Van Obberghen *et al.*, 2001). Receptor activation leads to phosphorylation of key tyrosine residues on insulin receptor substrate proteins that are linked to the activation of two main signaling pathways: the phosphatidylinositol 3-kinase (PI3K)–Akt pathway and Ras mitogen-activated protein kinase (MAPK) pathway (Figure 1.12) (Taniguchi *et al.*, 2006).

The phosphorylated-IRS is capable of interacting with the PI3K regulatory subunit, which associates with the PI3K catalytic subunit. Actived PI3K leads to the generation of a lipid second messenger called PIP3 (phosphatidylinositol-3,4,5-triphosphate), the contribution of which is to recruit Akt via its PH (pleckstrin homology) domain to the plasma membrane. After translocation to the plasma membrane, Akt is phosphorylated at the activation loop threonine 208 and hydrophobic motif serine 473 by PDK1 (3-phosphoinositide-dependent protein kinase-1) and PDK2, respectively. Akt mediates most of the PI3K-mediated metabolic actions of insulin through the phosphorylation of several substrates, including other kinases, signaling proteins and transcription factors. Insulin regulated Akt acts on two effector pathways. In one

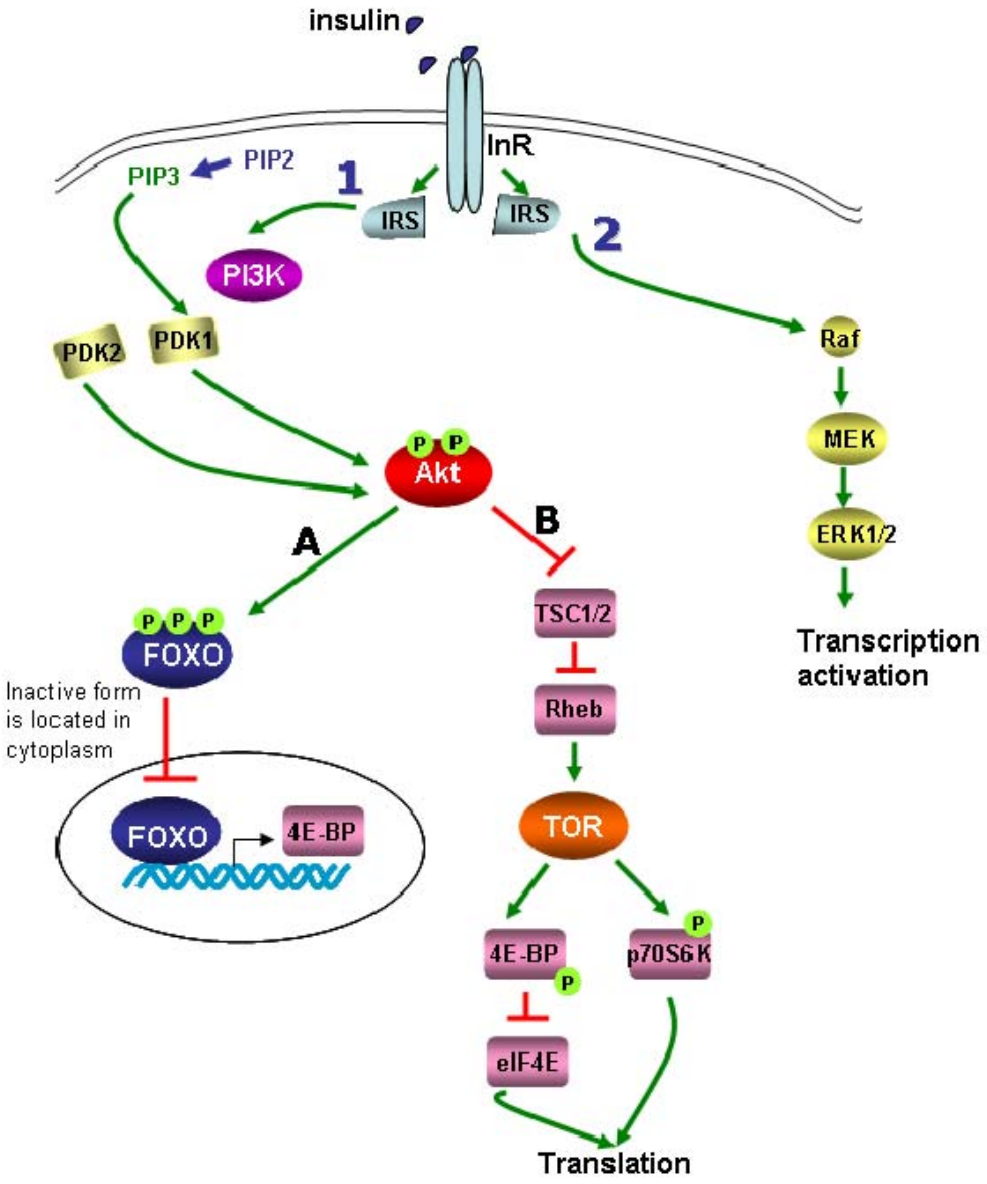

Figure 1.12 An overview of the insulin signaling pathway. The response to insulin is linked to two main signaling pathways, the PI3K/kt (1) and MAPK (2) pathway. Downstream of PI3K/Akt, there are two effector pathways that are regulated by Akt. One branch of the pathway (A) regulates the transcription factor, FOXO. Akt phosphorylates FOXO, which leads to retention of FOXO in the cytoplasm. The second branch (B) activates TOR through the inhibition of TSC2. Activated TOR increases protein synthesis by phosphorylating p70S6K and phosphorylating and inactivating the translation inhibitor 4E-BP.

pathway it regulates the activity by phosphorylation of the transcription factor FOXO (forkhead box, subgroup O) and the second pathway is to activate TOR (Figure 1.12) (Grewal, 2008). FOXO protein is phosphorylated by Akt at three conserved serine/threonine residues, which leads to retention of the FOXO transcription factors in the cytoplasm (Burgering & Kops, 2002), thereby down-regulating transcription of specific target genes that affect cell cycle progression (Demontis & Perrimon, 2009; Burgering, 2008) and modulation of metabolic genes (Baker & Thummel, 2007).

Akt can also regulate the activity of TOR. Akt directly phosphorylates and inhibits TSC2 (Tuberous sclerosis complex 2) on multiple sites, which is complexed with TSC1. These phosphorylations inactivate the function of TSC1/TSC2, allowing GTP-bound Rheb (Ras-homolog enriched in brain) to activate TOR. Activated TOR phosphorylates the p70 ribosomal protein S6 kinase (p70S6K) and eukaryotic translation initiation factor 4E binding protein (4E-BP). These phosphorylations regulate ribosomal biogenesis, protein synthesis, cell cycle progression and inhibition of autophagy (Soulard & Hall, 2007).

4E-BP can bind eIF4E (eukaryotic initiation factors) and block its normal function of recruiting the initiation complex (containing the 40S ribosomal subunit) to the m^7GpppX cap structure present at the 5′-end of all eukaryotic cellular mRNAs (Gingras *et al.*, 1999). Most cellular mRNAs are poorly translated in the absence of this cap-dependent recruitment. When TOR activity is low, 4E-BP is hypophosphorylated, allowing it to bind efficiently to eIF4E and block translation. When TOR activity increases, it phosphorylates 4E-BP, causing its affinity for eIF4E to drop and allowing cap-dependent translation to occur. S6K is a well-characterized downstream target of TOR. S6K is fully activated by phosphorylation at multiple Ser/Thr residues (Tee & Blenis, 2005). Phospho-S6K mediates phosphorylation of

ribosomal protein S6 (rpS6) which stimulates translation (Tee & Blenis, 2005).

Insulin/TOR signaling components in lipid metabolic control

Mutations in the core components of the insulin/TOR pathway such as InR, PI3K, PDK1, Akt, FOXO, TSC1/TSC2, TOR and S6K all cause tissue growth abnormalities and lethality (Hafen, 2004). Flies and mice with reduced InR and PI3K activity are small and have increased fat levels (Brogiolo *et al.*, 2001; Wither *et al.*, 1998). Mice mutant for Akt2 become insulin resistant and develop lipoatrophy (loss of fat tissue) (Cho *et al*, 2001). Cytoplasmic activated dAkt regulates LD accumulation in *Drosophila* nurse cells (Vereshchagina & Wilson, 2006). FOXO transcription factors have been shown to function in the control of fat metabolism and lifespan in *C. elegans*, flies and mice (Accili & Arden, 2004). Constitutively expressed active Foxo1 prevents the differentiation of preadipocytes, while dominant-negative Foxo1 restores adipocyte differentiation of fibroblasts from InR-deficient mice (Nakae *et al.*, 2003). Activated dFOXO (Akt phosphorylation site is mutated) results in increased lipid levels as assessed by Nile Red staining and measurement of triglyceride levels (Luong *et al.*, 2006). The TOR pathway has been implicated in lipid metabolism as well. S6K mutant mice are resistant to diet-induced obesity (Um *et al.*, 2004). A knock-out mouse for one of the three mammalian 4E-BP proteins, 4E-BP1 is viable and has elevated metabolism and reduced adipose tissue (Tsukiyama-Kohara *et al.*, 2001). Likewise, 4E-BP mutant flies showed increased sensitivity to nutrient deprivation, leading to abnormal fat loss (Teleman *et al.*, 2005).

Recently, more and more groups utilize *Drosophila* as a model for characterization of carbohydrate, sterol and lipid metabolism (Baker & Thummel,

2007). *Drosophila* shares most of the same basic metabolic functions as vertebrates. The fly maintains appropriate circulating sugar levels, sensing for the change of environmental conditions and storing excess energy in the forms of glycogen and lipid (Rusten *et al.*, 2004; Scott *et al.*, 2004). In *Drosophila*, the organ that metabolizes nutrients and stores lipid and glycogen is called the fat body, which acts like the mammalian liver and adipose tissue (Canavoso *et al.*, 2001). In addition, there is a specialized cluster of *Drosophila* cells, called oenocytes, which accumulates lipid upon starvation. Under starvation conditions, lipid was mobilized from the fat body and incorporated into LDs that accumulate in oenocytes. This feature of oenocytes is similar to the atypical lipid uptake that occurs in mammalian hepatocytes during starvation (Gutierrez *et al.*, 2007).

Observation of the fat body and oenocytes could provide a hint as to how a particular protein acts in lipid metabolism. For example, Lsd2 (a homologue of perilipin) plays a role in storage lipid in LDs. The *Lsd2* mutant exhibits impaired lipid storage, thus the fat body of *Lsd2* mutant seems more transparent than wild type due to less lipid being stored in the fat body (Teixeira *et al*., 2003). Conversely, overexpression of Lsd2 in the fat body results in reduced lipolysis in fat cells and suppression of lipid uptake by oenocytes in starved animals. The difference in size of LDs was observed between feeding and starvation. Many small LDs are evident in fat body cells of starved control larvae relative to fed controls, consistent with the mobilization of stored lipid for energy production (Palanker *et al*., 2009). *Drosphila* HNF4 (hepatocyte nuclear factor 4) contributes to mobilizing stored fat for energy. Under conditions of starvation, *dHNF4* null mutant larvae retain lipid in the fat body, thus the LDs in the mutant were larger than wild type, suggesting that the mutants are unable to efficiently mobilize stored fat (Palanker *et al*., 2009).

Genetic studies in *Drosophila* have established the basis for our understanding of the regulatory mechanisms that control development. Well-known signaling pathways such as Notch, wingless and hedgehog were discovered by *Drosophila* genetic studies (Baker & Thummel, 2007). Based on genetic screens in *Drosophila*, more genes that modulate the insulin/TOR signaling pathway have been identified, such as *melted* and *slimfast*. Melted is a novel modulator of the insulin/TOR pathway which can interact with both TSC1 and FOXO. In the *melted* mutant, TOR activity is reduced. The flies with the *melted* mutation are lean and have less triglyceride in the fat body (Teleman *et al.*, 2005). Reduction of dTOR function also decreased lipid levels in the fat body (Luong *et al.*, 2006). By measuring the level of ketone bodies (β-hydroxybutyrate level, whose levels serve as an indicator of lipid utilization), they proved that the lipid consuming rate is quicker in a dTOR mutant (Luong *et al.*, 2006). In a genetic screen for growth modifiers, *slimfast* was identified as a gene that encodes an amino acid transporter and functions as a nutrient sensor in the larval fat body, controlling a systemic response that links amino acid levels with organismal growth (Colombani *et al.*, 2003). The observation that fat body-specific inactivation of either *slimfast* or *dTOR* leads to similar phenotype. This suggests that slimfast can signal through dTOR in the fat body to regulate growth and metabolism in response to amino acid level.

Insulin/TOR signaling components in glucose homeostic control

Insulin is a hormone released by pancreatic β cells in response to elevated levels of nutrients in the blood. Insulin triggers the uptake of glucose, fatty acids and amino acids. Downstream molecules of the insulin signaling pathway are important to regulate glucose storage and uptake. Glycogen synthase kinase-3 (GSK3) was the

first physiological target of Akt to be identified (Cross *et al*., 1995). Phosphorylation of GSK3 by Akt leads to a decrease in its own activity but increases glycogen synthesis (Frame *et al*., 2001). Akt can also regulate glucose uptake by phosphorylating and inhibiting the Rab-GTPase-activating protein, AS160 (for Akt substrate of 160 kDa) (Sano *et al*., 2003). This triggers the activation of Rab small GTPases that are involved in the cytoskeletal re-organization that is required for the translocation of the glucose transporter GLUT4 (glucose transporter type 4) to the plasma membrane. In addition, constitutive FOXO activation in the liver and pancreatic β cells causes hyperglycemia in mammals (Nakae *et al.*, 2002).

In *Drosophila*, there are 7 insulin-like peptides (DILPs) which are structurally and functionally related to insulin and IGF (Brogiolo *et al.*, 2001). DILPs are produced from insulin producing cells (IPCs) in the *Drosophila* brain. Increased blood glucose levels were observed in the absence of IPCs, this elevation of glucose level can be rescued by overexpression DILPs (Rulifson *et al.*, 2002). Thus, loss of insulin/IGF production and signaling is related to altered glucose homeostasis in *Drosophila* (Rulifson *et al.*, 2002). A hypomorphic mutation in dTOR (reduction of dTOR function) causes an increase in DILP2 mRNA and protein level and lowers glucose levels (Luong *et al.*, 2006).

Insulin/TOR signaling pathway in growth control

The insulin signaling pathway acts as a key regulator of growth, cell and tissue size in *Drosophila* and mammals (Saucedo & Edgar, 2002; Hafen & Stocker, 2003). The function of the insulin/TOR signaling pathway has been analyzed in detail in the imaginal discs that develop into wings and eyes of the fly. Overexpression of InR, PI3K or Akt in the discs enhances cellular growth, resulting in enlarged cells and

organ, whereas disc cells mutant for these genes are small and grow more slowly (Zhang *et al*., 2000; Leevers *et al*., 1996; Verdu *et al*., 1999; Weinkove *et al*., 1999). Similar studies to show that insulin/TOR control cell growth have also been performed in other organs in *Drosophila*. Inhibition of PI3K activity by overexpression of PTEN (phosphatase and tensin homologue, the negative regulator of PI3K) in the larval fat body reduces cell size (Britton *et al*., 2002). An additional negative regulator of insulin signaling, *Susi* (Suppressor of signaling by insulin), is a coiled-coil domain protein that plays a role in negatively regulating dPI3K activity. Loss of *Susi* function increases body size whereas overexpression of *Susi* in the eyes and wing reduces cell and tissue size (Wittwer *et al.*, 2005).

1.6 Aims of the PhD. project

Invadolysin encodes a novel, conserved metalloprotease. As previously stated, the INV mutant in *Drosophila* showed a wide range of phenotypes affecting aspects of mitosis and cell migration. Thus it was concluded that the protein has pleotropic functions. The lab has recently shown that invadolysin localized to lipid droplets. Thus, this opens additional ways to approach the function of INV. My Ph.D. project aimed to address the following questions: First, what is required for the localization of invadolysin to lipid droplets, and which part of INV is required for the localization to LD? LD binding protein such as perilipin and caveolin encircle LD depending on the phosphorylation of PKA and Src. Protein phosphorylation is often crucial for regulating activity, localization or molecular interaction. Thus, whether the localization of INV is regulated by protein kinase is of interest. Second, in order to gain a better understanding of the localization of invadolysin on LDs, I chose to examine a cellular differentiation model in which the dynamic of LDs may be

modulated. Therefore, 3T3-L1 cell differentiation into adipocyte model was carried out to address the role of INV in adipogenesis. The final aim was to utilize *Drosophila* as a model. *Drosophila* is a multi-cellular model ideally suited for the genetic analysis. A mutation that results in the loss-off-function of invadolysin has been generated, providing an opportunity to study the pathways invadolysin is involved in a multi-cellular organism.

Chapter 2: Materials and Methods

2.1 Preparation of competent cells for heat shock transformation

One ml of overnight culture of either *E. coli* BL21 or *E. coli* DH5α was transferred to 100 ml fresh LB (Luria-Bertrani broth, 1% Bacto-tryptone, 0.5% Bacto-yeast extract, 1% NaCl, pH7.4) medium. The bacterial culture was incubated at 37˚C with shaking (250 rpm) until the optical density (OD_{600}) reached 0.4-0.6. After chilling cells on ice for 10 minutes, all of the subsequent steps were performed on ice. The bacterial culture was transferred to sterile, pre-chilled 50 ml falcon tubes and the cells were harvested by centrifugation at 4300 rpm at 4˚C for 10 minutes. The supernatant was removed and the cell pellet was resuspended in 30 ml ice-cold sterile magnesium /calcium solution (80 mM $MgCl_2$ & 20 mM $CaCl_2$) and the cells were placed on ice for 10 minutes. The resuspended cells were centrifuged again at 4300 rpm at 4˚C for 15 minutes and the cell pellet was resuspended in 2 ml of calcium solution (0.1M $CaCl_2$ & 10% glycerol). Next, 200 µl aliquots were snap-frozen in liquid nitrogen and stored at -80˚C.

Table 2.1 Bacterial strain information

Bacteria	Genotype
E. coli BL21	F- *omp*T *hsd*SB (*r*B-*m*B-) *gal dcm* (DE3)
E. coli DH5α	F-, φ80dlacZΔM15, Δ(lacZYA-argF)U169, deoR, recA1, endA1, hsdR17(rk-, mk+), phoA, supE44, λ-, thi-1, gyrA96, relA1

2.2 Ligation and transformation

An insert to vector molar ratio of 3:1 was routinely used in reactions for ligation.

The insert and vector mixture was performed by a supplement of T4 DNA ligase (3 U/μl) with appropriate reaction buffer (30 mM Tris-HCl, pH7.8 , 10 mM $MgCl_2$, 10 mM DTT and 1mM ATP [Promega]) and the reaction was incubated at 4˚C overnight. Next day, 10 μl of the ligation sample (or 1 μl plasmid DNA, for direct plasmid transformation) was incubated with 200 μl of competent cells and then incubated on ice for 30 minutes. Next, the DNA and bacteria mixture was incubated at 42˚C for 1 minute for heat shock reaction and the mixture was subsequently cooled on ice for 2 minutes. Following, 1 ml of SOC medium (2% Bacto-tryptone, 0.5% Bacto-yeast extract, 0.05% (8.5 mM) NaCl, 2.5 mM KCl pH7.0, 20 mM glucose) was added to the mixture and the mixture was incubated at 37˚C for 1 hour. Dilutions of the mixture were spread on agar plates (with the appropriate antibiotic: ampicillin 50 μg/ml, kanamycin 50 μg/ml).

2.3 Plasmid DNA extraction and agarose gel electrophoresis

For small scale plasmid DNA isolation, one colony from a selective plate was inoculated in 3 ml of LB with appropriate antibiotic (ampicillin 50 μg/ml or kanamycin 50 μg/ml) and bacterial cells were cultured overnight at 37˚C with shaking. One ml of this culture was collected for plasmid DNA extraction. Small scale plasmid DNA extraction was performed using the QIAprep Spin® MiniPrep Kit (QIAGEN, 27106), according to manufacturer's instructions. The large scale extraction (up to 50 ml) was performed by using the Qiafilter® Plasmid Maxi Kit (QIAGEN, 12243), according to the manufacturer's instructions.

To check for positive constructs, restriction enzyme digestion of DNA plasmids was performed in 1.5 ml eppendorf tubes as follows: mixture includes 5-8 μl of plasmid DNA (mini preps), 1 μl of 10X NEB buffer, 1μl of restriction enzyme

(NEB), the mixture was made up to 10 µl with sterile deionized water. Restriction digestion was normally performed at 37˚C for 2-4 hours. The sizes of the fragments were checked by electrophoresing an aliquot of the plasmid digest on a Seakem LE agarose gel (0.8% to 1.2%) along with 100 bp DNA ladder (Promega, G210A) or 1Kb DNA ladder (Promega, G571A). Agarose gel was normally prepared containing 200 ng/ml of ethidium bromide in 1X TAE buffer (50X TAE includes 2M Tris base, 1M acetic acid and 50 mM EDTA). Agarose gels were set in electrophoresis tanks (Owl Scientific Plastics) with 1X TAE buffer for electrophoresis at 100V.

2.4 BigDye Terminator sequencing

Sequencing reactions were performed with 250-500 ng of plasmid DNA (normally ~ 5 µl of plasmid DNA was used), 0.5 µM of the appropriate primer, 2 µl of BigDye (Perkin Elmer, Applied Biosystems) and sterile deionized water (dH_2O) was added up to 20µl. Reactions were performed in a Biometra Personal Cycler with the following thermal cycle: a) 95˚C for 5 minutes, b) 95˚C for 30 seconds, c) 55˚C for 15 seconds, d) 60˚C for 4 minutes (b-d were repeated for 25 cycles), and eventually held at 4˚C. Reactions were then transferred to 0.2 ml tubes for sequencing (sequencing facility of ICMB / Ashworth building, University of Edinburgh). The table below shows the primers used for sequencing.

Table 2.2 Primers used for sequencing reactions to check constructs in Chapter 6 and 7

GFPC1F	5’-CCAACGAGAAGCGCGATCAC-3'
GFPC1R	5’-GCAAGTAAAACCTCTACAAATGTGG-3'
GFPN1 PN1	5’-ATGGGCGGTAGGCGTGTA -3'
GFPN1 PN13	5’- TACGTCGCCGTCCAGCTC -3'

GST F	5’-GGGCTGGCAAGCCACGTTTGGTG-3'
GST R	5’-CCGGGAGCTGCATGTGTCAGAGG-3'
T3 F	5’-AATTAACCCTCACTAAAGGG-3'
T7 R	5’-GTAATACGACTCACTATAGGGC-3'
INVBin2	5’-CCAGACCAAGAAGGCATCTC-3' (601-620)
INVBin3	5’-TGGAGAGATTATGGGATGTTCGA-3' (972-992)
INVBin4	5’-CAGCGCAGCTCAGATTGTAG-3' (1599-1616)

2.5 Polymerase Chain Reaction

PCR reactions were performed in a 50 µl volume containing 500 nM of each forward and reverse primer, 1.5 mM $MgCl_2$, 200 µM of each dNTP, 100 ng of plasmid DNA and 1 µl of Expand High Fidelity enzyme (3.5 U/µl, Roche, 11732650 001). PCR reactions were performed in a Biometra Personal Cycler according to the following protocol: a) 95˚C for 5 minutes, b) 95˚C for 30 seconds, c) 55˚C-58˚C for 30 seconds, d) 72˚C for 2-4 minutes which is dependent on the size of the product (step b-d were repeated for 30 cycles), 72˚C for 7 minutes and eventually held at 4˚C.

2.6 DNA Purification

2.6.1 DNA purification from agarose gels

Electrophoresis was performed in 0.8% to 1.2% agarose gels containing 200 ng/ml ethidium bromide in 1X TAE buffer. The selected band was excised under UV irradiation using a razor blade and placed into 1.5 ml eppendorf tubes. DNA was purified from the agarose gel by using QIAquick® Gel Extraction kit according to manufacturer’s instructions (Qiagen, 28704).

2.6.2 Purification of DNA from PCR reactions

PCR reaction products were purified by using the QIAquick® PCR Purification Kit (Qiagen, 28104). The entire PCR reaction was used and 5 volumes of the SpinBind reagent were added. The DNA was finally purified using the Spin Filter columns by following the manufacturer's instructions and the DNA was eluted in 20-30 µl of sterile dH_2O.

2.7 Oligonucleotide annealing for cloning

Oligonucleotides were dissolved in dH_2O to a final concentration 3 µg/µl. 1 µl of each oligo was mixed in 48 µl of annealing buffer (10 mM Tris pH8.0, 1 mM EDTA pH8.0, 100 mM NaCl or 50 mM HEPES pH7.4, 100 mM NaCl). The mixture was incubated in a series of thermal reactions: 90˚C for 4 minutes, 70˚C for 10 minutes, 60˚C for 4 minutes, 50˚C for 4 minutes, 40˚C for 4 minutes, 30˚C for 4 minutes, 20˚C for 4 minutes, 10˚C for 4 minutes. Finally, 2 µl of the annealed oligo was used for cloning.

2.8 Total RNA extraction

Total RNA from cultured cells or *Drosophila* larvae was extracted using RNeasy ® Mini Kit (Qiagen, 74104) according to manufacturer's instructions. For cell lines: The cell culture medium was removed and rinsed by PBS. 350 µl of RLT buffer containing 3.5 µl ß-mercaptoethanol (ß-ME) was added to a culture dish and the cells were harvested by cell scraper (Corning) and transferred into a QIAshredder (Qiagen, 79654) spin column, followed by centrifugation at 13,000 rpm for 2 minutes. An equal volume of 70% ethanol was added to the homogenized lysate. After mixing well by pipetting, the mixture was transferred to an RNeasy spin column and

centrifuged for 15 seconds at 10,000 rpm. 700 µl of buffer RW1 was added to the column and the column was centrifuged for 15 seconds. Next the column was washed twice with 500 µl of RPE buffer, followed by centrifuging for 1 minute. Finally, 50 µl of the RNase-free water was added to elute the RNA.

For larval samples, 5 wild type and 10-15 mutant larvae were collected in RNA*later* (Qiagen, 76104) to stabilize the larval tissue. The larvae were transferred to 350 µl of RLT buffer containing 3.5 µl of ß-ME and homogenised using a hand pestle and then the mixture was transferred into a QIAshredder spin column, following by centrifugation at 13,000 rpm for 2 minutes. 350 µl of 70% ethanol was added to the homogenized lysate. After mixing well by pipetting, 700 µl of the mixture was transferred to an RNeasy spin colum and centrifuged for 15 seconds at 10,000 rpm. 700 µl of buffer RW1 was added to the column and the column was centrifuged for 15 seconds. Next the column was washed twice with 500 µl of RPE buffer, followed by centrifuging for 1 minute. Finally, 50 µl of the RNase-free water was added to elute the RNA.

2.9 RT-PCR reactions

2.9.1 One-step RT-PCR

Reactions were performed using the Access RT-PCR system (Promega, A1250) in a 25 µl reaction. Each reaction contained 5 µl of 5X AMV/*Tfl* reaction buffer, 200 µM of each dNTP, 1 µM of forward and reverse primer, 1 mM $MgSO_4$, 200 ng of the total RNA, 0.1 U/µl of AMV reverse transcriptase and 0.1 U/µl *Tfl* DNA polymerase. The reactions were performed in the Biometra Personal Cycler at 45˚C for 45 minutes for the reaction of the reverse transcription and at 94˚C for 2 minutes to inactivate the AMV reverse transcriptase. After finishing the cDNA synthesis,

targeted fragments of DNA were amplified by the gene specific primers by the following reactions: a) 94˚C for 2 minutes, b) 95˚C for 30 seconds, c) 55˚C for 30 seconds, d) 68˚C for 1 minute (b-d were repeated for 30 cycles), 68˚C for 7 minutes and then held at 4˚C.

2.9.2 Two-step RT-PCR

Two-step RT-PCR reaction was performed by using Superscript^{TM}III reverse transcriptase (Invitrogen, 18080044) in 20 μl reactions. The reactions contained 1 μg of RNA,1 μl of 150 ng/μl of random primer (or 50 μM oligo dT), 1 μl of 10 mM each dNTP and 1 μl of DEPC H_2O. This mixture was incubated at 65˚C for 5 minutes and placed on ice for over 1 minute. Then 4 μl of 5X first strand buffer, 1 μl of 0.1M DTT, 1 μl of RNase out (40 U/μl) and 1 μl of Superscript^{TM}III reverse transcriptase (200 U/μl) was added to the mixture. The mixture was mixed by pipetting gently. If using random primers, the reaction tube was incubated at 25˚C for 5 minutes and the reactions were performed in the Biometra Personal Cycler according to the following protocol: 50˚C for 60 minutes and then 70˚C for 15 minutes. The cDNA was then ready to serve as template for PCR or quantitative PCR (qPCR) reaction.

PCR reactions to amplify fragments of cDNA were performed by the Taq DNA polymerase (Roche, 11146173001). Each 25 μl reaction contained 800 nM of forward and reverse primer, 1.5 mM $MgCl_2$, 400 μM of each dNTP, 2 μl of cDNA and 0.2 μl of Taq DNA polymerase (5 U/μl). PCR reactions were performed in the Biometra Personal Cycler according to the following protocol: a) 95˚C for 5 minutes, b) 95˚C for 30 seconds, c) 55˚C for 30 seconds, d) 72˚C for 45 seconds (b-d were repeated for 28 or 30 cycles), 72˚C for 7 minutes and subsequently held on 4˚C. The

table below is a list of primers used in this thesis.

Table 2.3 Primers used for the RT-PCR reactions

Primers used in Chapter 4			
Target Gene	**primer**	**Sequence**	**PCR product**
ADRP	mADRPF	5'-CTGATTGAATTCGCCAGGAAG-3'	**505 bp**
	mADRPR	5'-CTGAGCTTTGACCTCAGACTG-3'	
β-actin	mactinF	TCTGGCACCACACCTTCTAC	**214 bp**
	mactinR	GAGGCATACAGGGACAGCAC	
Invadolysin	mINV2/3F	5'-ATCACGTCCTTTCGGACACT-3'	**173 bp**
	mINV2/3R	5'-AGCTTGAGGGAAAAGTTTGTT-3'	
	mINV10/12F	5'-TTGAAGAAGCTCGGAAGCAT-3'	**182 bp**
	mINV10/12R	5'-GGCTTTGTACCAGCCAGTGT-3'	
	mINV15/16F	5'-AACTACGGGGCAGAGCAGTA-3'	**184 bp**
	mINV15/16R	5'-CCCGGCTACACAGATAGGAA-3'	
	mINV12bF	5'-GCGTTAATGGAGGACACTGG-3'	**183 bp**
	mINV12bR	5'-CTGCAGCGGGTTACTTCTG-3'	
Perilipin	mplinF	5'-ATGTGGATCCCGGGTGTGGCACCC-3'	**366 bp**
	mplin R	5'-TGCAGGACCTTCCCACCGTGCC-3'	
TIP47	mTIP47F	5'-GCTCAGCTGGAACCAGAAGAC-3'	**410 bp**
	mTIP47R	5'-TTCTCTGTGATTCCAGGAGCG-3'	
Primers used in Chapter 5			
	Dm 4EBP F	5'-GATCACCAGGAAGGTTGTC-3'	**457 bp**
	Dm 4EBP R	5'-GGTCAATATGACCGAGAGAA-3'	

Dm rp49 F	5'-AGGGTATCGACAACAGAGTG-3'	**122 bp**
Dm rp49 R	5'-CACCAGGAACTTCTTGAATC-3'	

2.10 Quantification of mRNA using real-time PCR

qPCR was performed using the LightCycler® 480 System and the LighterCycler® 480 probes Master kit (Roche, 04707494001). Primers and probes used in qPCR reactions were designed by Universal Probe Library Assay Design Center (https://www.roche-applied-science.com/sis/rtpcr/upl/index.jsp?id=UP030000) by entering the sequence ID from Ensembl (http://www.ensembl.org/index.html). The PCR mix was added to 2.2 µl of water, 0.2 µl of 100 µM forward and reverse primer mix, 0.1 µl of appropriate Hydrolysis Probe and 5 µl of the probe master (vial 1). Reaction was transferred into the LightCycler®480 Multiwell plate (Roche, 04729749001). Next, 2.5 µl of the cDNA (1/10 dilution) was added to each well. qPCR reactions were performed by the following steps: Pre-incubation at 95˚C for 5 minutes, amplification at 95˚C for 10 seconds, 55˚C for 15 seconds, 72˚C for 1 second, the last three steps were repeated for 50 cycles and subsequently the reactions were cooled at 4˚C for 10 seconds. The table below is a list of the primers and probes used in the thesis.

Table 2.4 Primers and probes for qPCR used in Chapter 4

β-Actin (ID: ENSMUST00000031564),104 nt. Use probe **#**64

Qm actin F	5'-CTAAGGCCAACCGTGAAAAG-3'
Qm actin R	5'-ACCAGAGGCATACAGGGACA-3'

Adipose differentiation-related protein (ID: ENSMUSG00000028494),72 nt. Use probe **#**17

	Qm ADRP F	5'-GACCAGTACTTCCCTCTCACTCA-3'
	Qm ADRP R	5'-AACCATATCAAATCCTTCCACCT-3'
Invadolysin (ID: ENSMUST00000023497), 63 nt. Use the probe **#**6		
	Qm INV F	5'-AGCTGCCAACCTGACTCG-3'
	Qm INV R	5'-ACCACCAGGCTAGAAGAGCA-3'
Perilipin (ID: ENSMUST00000032762), 77 nt. Use the probe **#**64		
	Qm Plin F	5'-AACGTGGTAGACACTGTGGTACA-3'
	Qm Plin R	5'-TCTCGGAATTCGCTCTCG-3'
TIP47 (ID: ENSMUST00000019726), 76 nt. Use probe #106		
	Qm TIP47 F	5'-CCACAGGATGCTGAAAAGG-3'
	QmTIP47R	5'-TGATGTCCCTGAACATGCTG-3'
Universal probes		
	Universal Probe 6	TTCCTCTG (Roche, cat. no. 04685032001)
	Universal Probe 17	AGGAGCTG (Roche, cat. no. 04686900001)
	Universal Probe 64	CCAGGCTG (Roche, cat. no. 04688635001)
	Universal Probe 106	AGCCAGAG (Roche, cat. no. 04692250001)

2.11 Preparation of protein extract

2.11.1 Preparation of protein extracts from cell lines

Medium was removed and the cells were rinsed with PBS. 200 µl of RIPA lysis buffer with protease inhibitors (Roche Protease Inhibitor Cocktail Tablets) was added into a well of 6 well plate (35 mm culture dish) and cells were scraped and the cell lysate was transferred to a 1.5 ml eppendorf. The lysate was mixed with 100 µl of 3X SDS-PAGE sample buffer and the mixture was sonicated 5 times (2 seconds sonication with 5 second rest intervals), and subsequently boiled for 10 minutes. To

remove the debris, the tube was centrifuged at 13,000 rpm for 2 minutes at 4˚C, and the supernatant was collected and stored at -20˚C until required.

2.11.2 Preparation of protein extracts from larvae

Three-day old adult flies with the appropriate genotype were transferred into a cage containing an apple juice agar in 10 cm plate with fresh yeast paste and allowed to lay eggs for one day. The next day, adult flies were removed and the plate with eggs was placed in a 25˚C incubator. 72 hours after hatching from eggs, approximately 8-10 larvae were transferred to a vial containing fresh fly food supplemented with yeast paste. 24 hours later, larvae with the appropriate genotype were collected (5 wild type larvae and 15 mutant larvae) and rinsed with PBS and transferred to 1.5 ml eppendorf tubes with 100 µl EBR lysis buffer (10X Ephrussi-Beadle Ringer's solution: 1.3 M NaCl, 47 mM KCl, 19 mM $CaCl_2$, 100 mM HEPES, pH6.9) with protease and phosphatase inhibitors. The larvae were then homogenized on ice with a hand pestle. Another 200 µl of cold EBR lysis buffer was added to the tubes and mixed gently by pipetting. The homogenate was mixed with 150 µl of 3X SDS-PAGE sample buffer (6% SDS, 150 mM Tris pH6.8, 30% glycerol, 0.03% Bromophenol blue, 6 mM EDTA) and 10 µl of 1 M DTT. The mixture was then sonicated for 2 seconds with 5 second rest intervals for 5 times and subsequently boiled for 10 minutes. To remove the debris, the tube was centrifuged at 13,000 rpm for 2 minutes at 4˚C, and the supernatant was collected and stored at -20˚C.

2.11.3 Preparation of protein extracts from the fat body of Drosophila

96 hours old larvae with the appropriate genotype were collected and rinsed

with PBS. In a glass dish pre-filled with cold-PBS and protease inhibitors. The larvae were dissected by the pull and drag method with two pairs of forceps. This leaves all the inner organs exposed to the PBS. The fat bodies were picked up and transferred to an eppendorf containing 100 µl EBR lysis buffer (10 fat bodies from wild type and 40 fat bodies from *INV* mutant were collected). The fat bodies were then homogenized on ice with a hand pestle. Another 200 µl of cold EBR lysis buffer was added to the tubes and mixed gently by pipetting. The homogenate was mixed with 150 µl of 3X SDS-PAGE sample buffer and 10 µl of 1 M DTT. The mixture was then sonicated for 2 seconds with 5 second rest intervals for 5 times and subsequently boiled for 10 minutes. To remove the debris, the tube was centrifuged at 13,000 rpm for 2 minutes at 4˚C, and the supernatant was collected and stored at -20˚C.

Table 2.5 *Drosophila* Stocks

Strain	Source
Canton S	Bloomington *Drosophila* Stock Center (USA)
l(3)IX-14^{4Y7}/TM6B	Heck laboratory

2.12 Electrophoresis of protein samples

Protein samples were resolved by SDS-PAGE on 4-12% Bis-Tris pre-cast gels (Novex) in 1X MOPS buffer (20X MOPS: 1 M 3-(N-morpholino) propane sulphonic acid, 1 M Tris base, 2% SDS and 20 mM EDTA) at 150-180V for 1 hour. In some experiments, 10% Tris-Glycine pre-cast gels were used with 1X Tris-Glycine buffer (5X Tris-Glycine: 125 mM Tris base, 1.25 M Glycine, 0.5% SDS)

2.13 Transfer of SDS-PAGE gels to nitrocellulose membrane and immunobloting

The SDS-PAGE gel was assembled in the transfer cassette with the order of (negative anode pole) - sponge / Whatman blotting paper / PAGE / nitrocellulose membrane (sigma, Z613657) / Whatman blotting paper / sponge - (positive cathode pole). The transfer cassette was placed in a transfer tank with transfer buffer (25 mM Tris, 192 mM glycine, 0.1% SDS and 20% methanol) and the transfer was performed at 450 mA for 3.5 hours at 4˚C.

After transfer, the nitrocellulose membrane was rinsed with H_2O and stained by Ponceau-S (0.2% Ponceau-S in 3% trichloroacetic acid) to check the efficiency of transfer and then washed by TBST (150 mM NaCl, 20 mM Tris pH7.4, 0.1% Tween-20) buffer. The membrane was blocked in 5% skimmed milk powder (Sainsbury) solution (prepared in TBST) for 1 hour at room temperature. The membrane was incubated with antibodies at appropriate dilutions (in 5% milk in TBST) for 1 hour at room temperature or overnight at 4˚C. To remove excess antibody, the membrane was washed by TBST for 3 times, 5 minutes each. The membrane was incubated with horseradish peroxidase-linked (HRP) secondary antibody (1 :10,000 dilution in 5% skimmed milk / TBST) for 1 hr at RT. The immune-signal was detected by ECL reagent (GE Healthcare, RPN2106) with Lumi-Film Chemiluminescent detection film (Roche, REF 11666657001). The antibodies used in this study were listed in below table.

Table 2.6 The list of the primary and secondary antibodies

Primary Antibody	Host animal	Source (Catalogue number)	Dilution

Anti-actin	Rabbit	Sigma (A2066)	1:1000
Anti-ADRP (clone C-20)	Goat	Santa Cruz (sc-32450)	1:500
Anti-AKT	Rabbit	Cell Signaling (9272)	1:500
Anti-Phospho-AKT (505)	Rabbit	Cell Signaling (4054)	1:500
Anti-Caveolin-1	Mouse	Invitrogen (036000)	1:500
Anti-Flag	Rabbit	Sigma (F7425)	1:500
Anti-GFP	Rabbit	Sigma (G1544)	1:500
Anti-HA (3F10)	Rat	Roche (1867423)	1:500
Anti-HA (12CA5)	Mouse	Roche (11583816001)	1:500
Anti-Invadolysin 3645	Rabbit	Heck laboratory Antigen region is from a.a 188-201: (YRGGKWPHGAVGVP) which was designed by Neville Cobbe and Margarete Heck. Antibody was then validated by Sharron Vass, Ching-Wen, Chang and Kate Marshall	1:500
Anti-Invadolysin 996	Rabbit	Abcam (ab58996)	1:500
Anti-Lsd2	Rabbit	Ronald Kühnlein (Max planck Gesellschaft)	1:2000
Anti-Lsd2	Rat	Luis Teixeira (University of Cambridge)	1:1000
Anti-perilipin	Rabbit	Sigma (P1998)	1:2000
Anti-Phospho- p70 S6 kinase (Thr 398)	Rabbit	Cell Signaling (9209)	1:500
Anti-S6 ribisomal protein	Mouse	Cell Signaling (2317)	1:500
Anti-SBP	Mouse	William Earnshaw (University of Edinburgh	1:250
Anti-TIP47	Guinea pig	Progen (03-GP30)	1:500
Anti-Tubulin(B-5-1-2)	Mouse	Sigma (T5168)	1:5000

Secondary antibodies	Host animal	Source (Catalogue number)	Dilution
Anti-mouse HRP	Sheep	Amersham (NA931V)	1:10,000
Anti-rabbit HRP	Donkey	Amersham (NA9340V)	1:10,000
Anti-goat/sheep HRP	Donkey	Santa Cruz (sc-2020)	1:10,000
Anti-guinea pig HRP	Goat	BETHYL (A60-117P)	1:5000
Anti-Rat HRP	Mouse	Amersham (NA932)	1:1000

2.14 Stripping nitrocellulose membranes

A nitrocellulose membrane can be re-used for another immunological detection. Previous immune-complexes were removed by incubating the membrane in stripping solution (100 mM β-mercaptoethanol, 2% SDS and 50 mM Tris-HCl pH6.8) for 30 minutes at 50˚C. The membrane was washed 4 times with TBST, before being used for another probing.

2.15 Coomassie Brilliant Blue staining of polyacrylamide gels

In some experiments, proteins were assessed by Coomassie Blue staining (0.5%Coomassie Brilliant Blue in 45% methanol, 10% acetic acid in dH_2O) after electrophoresis. The gel was stained in 0.5% Coomassie Blue for 1-2 hour, destained with destain solution (45% methanol, 10% acetic acid in dH_2O) and subsequently dried with the gel dry system (Novex, N12387). The gel was placed between two layers of DryEase mini Cellophane (Invitrogen, NC2380) with a supplement of the Gel-Dry™ drying solution (Invitrogen, LC 4025), and dried overnight at room temperature.

2.16 Fusion of INV fragments with GST tag

DNA fragments encoding different portions of invadolysin were generated by PCR of cDNA clones, fused in-frame with glutathione-*S*-transferase (GST) and constructed in the pGEX-4T plasmid (Amersham, Piscataway, NJ). The constructs of invadolysin fragments for bacterial expression were generated by using primers listed in the following table. And then all the constructs were verified by DNA sequencing by the primers GST F, GST R, INVBin2, 3 and 4 (section 2.4).

Table 2.7 Different portions of invadolysin constructs and the corresponding primers

Construct name	**Primers for the cloning (forward/reverse)**	**Protein size (kDa)**
GST-VINK (74-661)	BF88 BglII / BG BamHI	90 kDa
GST-SBG (53-661△37)	BSBgl II / BG BamHI	88 kDa
GST-V1N (1-300)	V1F2Bgl II / FC2R	59 kDa
Primers	**Sequence (the underlined bold capital letters represent the restriction enzyme sites)**	
BSBgl II	5'-CG**AGATCT**ACATCTACTCCCGTCTCCTTG-3'	
BF88Bgl II	5'-CG**AGATCT**GATGTTGATGAGCATTTAAGAATC-3'	
BG Bam HI	5'-GT**GGATCC**CTAAAGATCAAGTGGCAGAGCTCGG-3'	
V1F2Bgl II	5'-CG**AGATCT**ATGGTAACGACGCTCGGCCCG-3'	
FC2R	5'- CC**AGATCT**ATGAACATGGACAGGCCAATAG	

2.17 Expression and purification of recombinant proteins

2.17.1 Overexpression and purification of GST-tagged fusion proteins

Overexpression and affinity purification of GST recombinant proteins was based on previously described work (Frangioni & Neel, 1993). In brief, an overnight culture (1 ml) was added to 100 ml fresh LB medium containing 100 μg/ml ampicillin. Bacteria were cultured at 37˚C until the OD_{600} reached 0.6. Protein expression was

induced by adding 0.4 mM Isopropyl β-D-1-thiogalactopyranoside (IPTG). After an induction for 3-4 hours at 30˚C, the bacterial cells were pelleted and washed with ice-cold STE buffer (10 mM Tris pH8.0, 150 mM NaCl, 1 mM EDTA). The pellet was then suspended in 6 ml STE buffer containing 100 µg/ml lysozyme and protease inhibitor (1mM PMSF) and placed on ice for 15 minutes. Bacteria were lysed by adding sarkosyl to STE buffer (0.5% final concentration) and the lysate was sonicated for 3 minutes on ice (10 seconds of sonication and 20 seconds of rest in turn). Extracts were clarified by centrifugation for 20 minutes at 13,000 rpm at 4˚C. The supernatant was collected and adjusted to contain 2% Triton X-100 and incubated with glutathione beads for 2 hours. The beads were washed with ice-cold wash buffer (10 mM Tris pH8.0, 200 mM NaCl and 1 mM EDTA) for 6 times and resuspended in storage buffer (50 mM HEPES pH7.5, 150 mM NaCl, 1 mM DTT, 10% glycerol).

To elute the protein from GST beads, the beads were incubated with 20 mM of reduced glutathione (Sigma G4251, prepared in 50 mM Tris, pH9.0 buffer) at 4˚C for 30 minutes. For electrophoresis analysis, GST-fusion protein was eluted directly from glutathione beads by boiling for 10 minutes in SDS-PAGE sample buffer (2% SDS, 50 mM Tris pH6.8, 10% glycerol, 0.01% Bromophenol blue, 2 mM EDTA, 20 mM DTT).

2.17.2 Overexpression and purification of His-tagged fusion proteins

Bacteria containing His-tag fusion protein construct (clone of V1C-His was constructed by Brian McHugh) was cultured and induced to express protein as 2.17.1. After induction with IPTG, bacterial cells were pelleted and resuspended with 5 ml BugBuster (Novagen, 70751-3REF) reagent with 5 µl of Benzonase Nuclease (25 U/µl) and 1 mM PMSF. The cell suspension was then incubated for 20 minutes at

room temperature on a shaking platform. To remove insoluble cell debris, the cell suspension was centrifuged at 15,000 rpm for 20 minutes at 4˚C. The supernatant was transferred to a fresh tube and the proteins were purified by binding directly to BugBuster Ni-NTA His•Bind buffer kit (Novagen). For preparation of the resin beads, 1 ml of the 50% Ni-NTA His-beads was mixed with 4 ml 1X Ni-NTA binding buffer (300 mM NaCl, 50 mM sodium phosphate buffer, 10 mM imidazole pH8.0) and settled by gravity. Next, 4 ml of buffer was removed and then the beads were ready to use.

Ni-NTA beads were added into the cleared lysate, and the mixture was set on a rotator and incubated for 1 hour at 4˚C. The beads were pelleted at 2000 rpm for 5 minutes at 4˚C and washed 3 times with 4 ml 1X Ni-NTA wash buffer (300 mM NaCl, 50 mM sodium phosphate buffer, 20 mM imidazole pH8.0). Bound proteins were eluted from the beads by adding 0.5 ml Elution buffer (300 mM NaCl, 50 mM sodium phosphate buffer, 250 mM imidazole pH8.0). After spinning for 5 minutes at 2000 rpm, the eluted supernatant was transferred to a new eppendorf. The elution step was repeated 4 times and the beads were kept at -80˚C afterwards. All fractions were stored at -80˚C.

2.18 *In vitro* kinase assay

The *in vitro* phosphorylation assay of invadolysin was performed at 30 ˚C in a 20 µl reaction. The reaction contained 1X kinase buffer (25 mM Tris-HCl pH7.5, 5 mM ß-glycerophosphate, 2 mM DTT, 0.1 mM Na_3VO_4, 10 mM $MgCl_2$), 200 µM cold ATP (Cell signaling, 9804), 1 µg of purified protein kinase C (Calbiochem, 539494), 0.1-1 µg of substrate, and 0.2 µl of γ-^{32}P-ATP (Perkin Ekmer, 250UC, NEG 502Z). After a 30 minute incubation, 10 µl of the 3X SDS sample buffer (6% SDS,

150 mM upper buffer Tris (pH6.8), 30% Glycerol, 0.03% Bromophenol blue, 6 mM EDTA) was added to the reaction mixture and the mixture were boiled for 10 minutes. Following, the samples were resolved by 4-12% SDS-PAGE. After electrophoresis, the gel was transferred to Whatman blotting paper and was dried by gel dryer for 2 hours. The dried-gel was transferred to a cassette with Lumi-Film Chemiuminescent detection film, followed by autoradiography.

2.19 Detection of protease activity by zymography

Gelatin- or casein-containing Zymogram gels (Novex) were used for zymography. Purified GST-fusion protein was mixed with 2X Zymogram sample buffer (Bio-Rad, 1610764) and incubated at room temperature for 10 minutes. Samples were loaded into 10% or 12% Tris-Glycine Zymogram gel and electrophoresed at 125 V. After electrophoresis, the gel was rinsed with renaturing buffer (Novex, LC2670) for 30 minutes and equilibrated in developing buffer (Novex, LC2671) for 30 minutes, then subsequently incubated overnight at 37˚C in developing buffer. Gels were stained with 0.5% Colloidal Coomassie blue (0.5% Colloidal Coomassie blue in 45% methanol, 10% acetic acid in H_2O) to visualize the signal.

2.20 Cell culture

Cells were cultured in a humidified incubator at 37˚C with 5% CO_2. For HeLa (epithelial cervical carcinoma) and A375 (human melanoma) cells, Dulbecco's modified essential medium (DMEM) (GIBCO, 41966) with 10% FBS was used. For 3T3-L1 cells (mouse embryonic fibroblast), DMEM with 10% newborn calf serum (NCS) was used.

For starvation and re-feeding experiments in Chapter 3, cells were starved in DMEM without serum for 24 hours, and cells were re-fed by DMEM with 10% FBS and 10 μM oleic acid (Sigma, O3008). In some experiments, inhibitors were added 1 hour ahead of supplement of 10% FBS and 10 μM oleic acid (OA/FBS). The inhibitors applied in this study were listed in the following table.

Table 2.8 The inhibitors used in Chapters 3 & 4

Product	Target protein	Source (catalogue number)	Concentration used
Cycloheximide	80S ribosomal protein	Sigma (C4859)	10 μM
Gö 6979	PKC α, βand γ	Calbiochem (36520)	10 μM
GF 109203	PKC α, βand γ	Biosource (PHZ1083)	1 μM
Genisten	Tyrosin kinase	Sigma (G6649)	50 μM
MG132	26 S Proteasome	Sigma (C2211)	10 μM
LY294002	PI-3 kinase (PI3K)	Cell Signaling (9901)	50 μM
U1026	ERK	Sigma (U120)	10 μM
PD9805	ERK	Biosource (PHZ1164)	20 μM
Ro-31-8220	All PKC isozymes	Sigma (R136)	5 μM
Ste-MEK1$_{13}$	ERK2	Calbiochem (328000)	25 μM

2.21 Adipocyte differentiation

Mouse embryonic fibroblast 3T3-L1 cells were cultured in 10% NCS/DMEM until confluent. Two days after confluence, cells were stimulated with 10% FBS/DMEM medium containing 100 μM of 3-isobutyl-l-methylxantin (IBMX) (Sigma, I7018), 0.25 μM of dexamethasone (DEX) (Sigma, D4902) and 1 μg/ml of insulin (Sigma, I5500). A change of cellular morphology would be observed in the

next 2 days. After stimulation, culture medium was replaced with fresh medium containing 1 μg/ml of insulin every other day for 2 times. Afterwards, culture medium was replaced with 10% FBS/DMEM medium. At day 8, cells would become fully differentiated (Student *et al*., 1980). The differentiation procedure was summarized below.

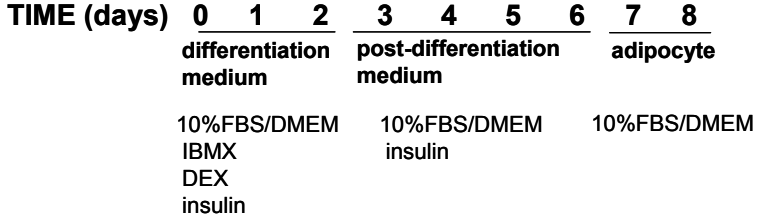

2.22 Construction of invadolysin vectors for transfection into mammalian cells

DNA fragments encoding either full length or different portions of the invadolysin coding sequence were generated by PCR from cDNA clones and inserted in-frame into either vector of pEGFP –N1 (Clontech) and pEdG (modified by removing GFP from the pEGFP-N1 vector). The following primers were used to generate the various constructs of invadolysin coding sequence for expression in mammalian cells. And then all the constructs were verified by DNA sequencing by the primers GFPN1PN1. GFPN1 PN13, INVBin2, 3 and 4 (section 2.4).

Table 2.9 The constructs and primers used for cloning of INV fragments in Chapter 6

Construct name	Primer for the clone (forward/reverse)
INV.v1△37:GFP	V1F*Bgl*II / VR*Bam*HI
INV.v2:GFP	V2F*Bgl*II / VR*Bam*HI
$V1N_{1\text{-}300}$:GFP	V1F*Bgl*II / RV2*Eco*RI
INV_{CT}:GFP	Fc*Bgl*II / VR*Bam*HI

GFP-:INV$_{CT}$	Fc*Bgl*II / VR*Bam*HI
pEdG-v1△37:GFP	V1F*Bgl*II / M2RI, gfpRIF/ gfp*Nco*IR, M2*Nco*IF/ INVRBStop
pEdG-v1:SSBP	V1F*Bgl*II/ M2RI, ssbpRIF / ssbp*Nco*IR, M2*Nco*IF2/ INVRBStop
pEdG-v1:HA	V1F*Bgl*II/ M2RI, HARIF HA*Nco*IR, M2*Nco*IF/ INVRBStop
pEdG-v1:HA[HIII]	*Hind*3HAF/ *Hind*3HAR

Primers	**Sequence (the underlined bold capital letters represent the restriction enzyme sites)**
V1F*Bgl*II	5’-CG**AGATCT**CATGGTAACGACGCTCGGC-3'
V1F2*Bgl*II	5’-CG**AGATCT**ATGGTAACGACGCTCGGCCCG-3'
V2F*Bgl*II	5’-CG**AGATCT**CATGGGGCGGAGGAGTGGG-3’
RV2*Eco*RI	5’-CA**GAATTC**GAAATCTTGAAGTTGAGAGG-3'
VR*Bam*HI	5’-GT**GGATCC**CGGTGCCATATACACAGAAG-3'
FC2*Bgl* II	5’-CC**AGATCT**ATGAACATGGACAGGCCAATAG
M2RI	5’-GT**GAATTC**AGGCCACTTACCCCCACGGTAG-3'
gfpRIF	5’-AC**GAATTC**ATGGTGAGCAAGGGCGAGGAG-3'
gfpNcoIR	5’-CATG**CCATGG**CTTGTACAGCTCGTCCATGC-3'
M2NcoIF	5’-CATG**CCATGG**CATGGGAGCAGTGGGTGTGCC-3'
INVRBStop	5’-GT**GGATCC**CTAGTGCCATATACACAGAAG-3'
ssbpRIF	5’-AC**GAATTC**AAAGAAACCGCTGCTGCTAAATTC-3'
ssbpNcoIR	5’-TGCT**CCATGG**GGCTCCCGCTGGCCCTGAGG-3'
M2NcoIF2	5’-AGCC**CCATGG**AGCAGTGGGTGTGCCAG-3'
HARIF	5’-**GAATTC**TACCCATACGATGTTCCAGATTACGCT-3'

HANcoIR	5’-**CCATGG**AGCGTAATCTGGAACATCGTATGGGTA-3'
HAF	5’-AGCTTTACCCATACGATGTTCCAGATTACGCTA-3'
HAR	5’-AGCTTAGCGTAATCTGGAACATCGTATGGGTAA-3'

2.23 Transfection of mammalian cells

2.23.1 Transfection by electroporation

HeLa cells were cultured to 80-90 % confluence in 75 cm^2 flasks and trypsinized with 3 ml 0.25% trypsin-EDTA to detach the cells from flask. Cells were harvested by adding 7 ml of fresh medium and centrifuging at 1500 rpm for 5 minutes to pellet cells. After centrifugation, 10 ml of OPTI-MEM®I (GIBICO, 31985) were added to resuspend the cells and the cell number was determined. After another centrifugation as above, cells were resuspended at a concentration of 5 x 10^6 / ml in OPTI-MEM®. 0.4 ml of the cells and 10 μg of the DNA were mixed and transferred to a 0.4 cm electrode gap cuvette (Bio-Rad, 165-2088) for electroporation. The electroporation was carried out with the following condition: voltage at 300V, capacity at 0.95 μFD and time constant at 18-21 seconds. After pulsing, 1 ml of pre-warm medium was added to the cuvette and the mixture was subsequently transferred to a cell culture dish.

2.23.2 Transfection by lipofectamine 2000

Transfection with lipofectamine™ 2000 (Invitrogen, 11668-019) was performed according to the manufacturer’s protocol. The day before transfection, 3-4 x10^5 cells were seeded in a well of 6 well plate (or 35 mm culture dish) and cultured to 90% confluence. Samples for transfection were prepared as followed: 4 μg of plasmid DNA and 10 μl of lipofectamine 2000 was added in 250 μl of OPTI-MEM® in

separate 1.5 ml eppendorf tubes and the mixtures were incubated at room temperature for 5 minutes. After incubation, DNA and lipofectamine 2000 solution were mixed together and incubated for 15 minutes at room temperature. The 500 µl mixture was added to a well containing pre-seeded cells and 1.5 ml of OPTI-MEM®. The cells were incubated at 37˚C in a CO_2 incubator for 4 hours and then the OPTI-MEM® was exchanged by fresh 10% FBS/DMEM.

2.24 Immunofluorescence of human cultured cells

Cultured cells were seeded overnight onto round cover slips in normal culture conditions (as 2.20). Cover slips were removed from the culture dish and fixed for 3 minutes with 4% formaldehyde in D-PBS (10X Dulbecco's Phosphate Buffered Saline: 1.37 M NaCl, 26.8 mM KCl, 14.7 mM KH_2PO_4, 64.6 mM Na_2HPO_4, pH7.4). After two times two minute washes by PBST (D-PBS with 0.05% TritonX-100), cells were permeabilized with D-PBS containing 0.1% TX-100 for 3 minutes. After twice washing by PBST, cells were blocked with 3% BSA in PBS at room temperature for 30 minutes. After washing for twice by PBST, cells were incubated with the primary antibody (all antibodies were diluted in 0.3% BSA/D-PBS) for 1 hour at room temperature. After washing for 3 times by PBST, cells were incubated with the secondary antibody (all secondary antibodies and DAPI were diluted in 0.3% BSA/D-PBS) at room temperature for 45 minutes. After washing 3 times by PBST, the cover slips were mounted on glass slides with Mowiol solution (10% Mowiol 4-88 (Calbiochem), 20% glycerol in PBS). Cells were visualized with an Olympus AX-70 Provis epifluorescence microscope and equipped with a Hamamatsu Orca II CCD camera using SmartCapture3 software. The antibodies used for the study were listed below.

Table 2.10 The fluorescent dyes, primary and secondary antibodies used for this study

Fluorescent dyes		**Source (Catalogue number)**	**Dilution**
Alexa Fluor 488 phalloidin		Invitrogen (A12379)	1:500
Alex Fluor 594 phalloidin		Invitrogen (A12381)	1:500
BODIPY (493/503), 1 mg/ml in EtOH		Invitrogen (B2103)	1:100 (10 μg/ml)
BODIPY (630/650), 1 mg/ml in EtOH		Invitrogen (B22802)	1:100 (10 μg/ml)
DAPI 1 mg/ml in dH_2O		Sigma (D9564)	1:10,000
Primary antibodies	**Host animal**	**Source (Catalogue number)**	**Dilution**
Anti-Golgin-97 (CDF4)	Mouse	Molecular Probes (A-21270)	1:250
Anti-HA (3F10)	Rat	Roche (1867423)	1:250
Anti-HA (12CA5)	Mouse	Roche (11583816001)	1:250
Anti-Invadolysin 1318	Rabbit	Heck laboratory Antigen region is from a.a 327-692 of INV which was designed and validated by Brian McHugh (McHugh *et al*. 2004.).	1:250
anti-Perilipin	Rabbit	Sigma (P1998)	1:500
Anti-caveolin	mouse	Zymed Laboratories (03-6000)	1:500
Anti-SBP	Mouse	William Earnshaw (University of Edinburgh)	1:250
Secondary antibodies	**Host animal**	**Source**	**Dilution**
Anti-mouse Alexa 488	Donkey	Molecular Probes (A21202)	1:500
Anti-mouse Alexa 594	Donkey	Molecular Probes (A21203)	1:500
Anti-rabbit Alexa 488	Donkey	Molecular Probes (A21206)	1:500
Anti-rabbit Alexa 594	Donkey	Molecular Probes (A21207)	1:500
Anti-rat Alexa 594	Goat	Molecular Probes (T6392)	1:500

Anti-rat Alexa 488	Goat	Molecular Probes (O6382)	1:500
Anti-goat Alexa 594	Donkey	Jackson Immunoresearch (705-075-147)	1:50
Anti-guinea pig Alexa 594	Donkey	Jackson Immunoresearch (706-075-148)	1:50

2.25 Immunoprecipitation

HeLa cells or transfected HeLa cells were washed with cold PBS and lysed with 1 ml RIPA lysis buffer (20 mM Tris-HCl pH7.5, 150 mM NaCl, 1 mM Na_2EDTA, 1 mM EGTA, 1% NP40, 1% sodium deoxycholate, 1 mM beta-glycerophosphate, 1 mM Na_3VO_4, 1 μg/ml leupeptin, aprotinin, chymostatin, pepstatin and 1mM PMSF). Cells were scraped and placed on ice for 10 minutes, then, the cells were sonicated for 2 seconds with 5 second rest intervals for 5 times. The cell lysate was clarified by centrifuging for 15 minutes at 4˚C at 13000 rpm. The supernatant was transferred to a new tube and incubated with 20 μl of protein A or protein G sepharose beads (GE Healthcare, 17-6002035) on a rotating wheel at 4˚C for 1 hour. The mixture was centrifuged for 1 minute at 4˚C at 2000 rpm. The supernatant was transferred to a new tube and mixed with 2 μg of desired antibody. After incubation on rotating wheel at 4˚C for 2 hours, 40 μl of protein A or G agarose beads were added and the incubation was continued for another hour. The beads were washed for 5 times with 1 ml lysis buffer and resuspended in 20 μl of lysis buffer. 10 μl of 3X SDS-PAGE sample buffer was added to elute the protein complexes.

Chapter 3: Identification of molecules which regulate the localization of invadolysin to lipid droplets

3.1 Introduction

Invadolysin (INV) is a member of the M8 family of metzincin metalloproteases. Intracellular immuno staining with rabbit antibodies generated against recombinant human INV exhibit intriguing localization patterns in cultured human cells. The protein localized to the leading edge of normal migrating macrophages and to 'ring-like' structures in cultured cells (McHugh *et al.*, 2004). This suggested that INV may participate in cell migration. Furthermore, INV "rings" were postulated to be invadopodia in cultured cells. However, recent experiments showed that INV does not appear to coincide with the cortactin-enriched foci associated with proteolytic degradation (Cobbe *et al.*, submitted; Buccione *et al*., 2004). In a different experiment, co-staining with INV antibody and cholera toxin B (CtxB) was applied to examine caveolar endocytosis (Orlandi & Fishman, 1998). This work showed that some CtxB was associated with INV rings (Cobbe *et al.*, submitted). CtxB has additionally been shown to target to lipid vesicles (Lian & Ho, 1997). Immunofluorescent detection of INV and BODIPY (a specific dye for LDs) in cultured cells reveals that INV-like immunoreactivity was localized to the surface of LDs (Cobbe *et al.*, submitted). INV ring-like structures of similar size and shape were also found in different cell types, though some cell lines contained different numbers of these ring. As the number of INV ring-like structure were more and consistently observed in A375 human melanoma cells, this cell line was selected for further study.

The LD is an intracellular organelle specialized for lipid storage (Welte *et al.*, 2007). Identification of the protein composition is one step towards the molecular dissection of an organelle's function (Bartz *et al.*, 2007). Recently, several proteomic studies have been reported using LDs purified from different cell types and tissues (Bartz *et al.*, 2007; Liu *et al.*, 2004; Wu *et al.*, 2000; Umlauf *et al.*, 2004; Fujimoto *et al.*, 2004; Brasaemle *et al.*, 2004; Sato *et al*., 2006; Turro *et al.*, 2006; Beller *et al.*, 2006; Cermelli *et al.*, 2006; Wan *et al.*, 2007). The Liu group classified LD proteins into the following groups: lipid metabolism, membrane trafficking, signaling, cytoskeleton, endoplasmic reticulum, Golgi, lysosomes, mitochondria, chaperones and protein of unknown (Bartz *et al.*, 2007). Interestingly, most of these proteins are not uniquely present on lipid droplets, but also found in other cell compartments (Bartz *et al.*, 2007). For example: caveolin (which belongs to the membrane trafficking group) is primarily involved in membrane-related functions and has been found to associate with LDs upon Src kinase regulation (Blouin *et al.*, 2008). In our lab, INV has recently been shown to be associated with LDs, however, how INV is localized on LDs is not clear. The focus of this chapter is to approach the mechanism of "INV on LDs".

3.2 Results

3.2.1 INV localizes to LDs

Rabbit antibody to human INV was raised against the 327 to 692 amino acid region (Δ37 variant) of human INV (Figure 3.1 A). The primmune serum was first examined to observe the background level of activity from serum. As shown in Figure 3.1B, strong nuclear staining was observed in A375 melanoma cells by using preimmune serum. However, cytoplasmic ring-like structures were observed in A375

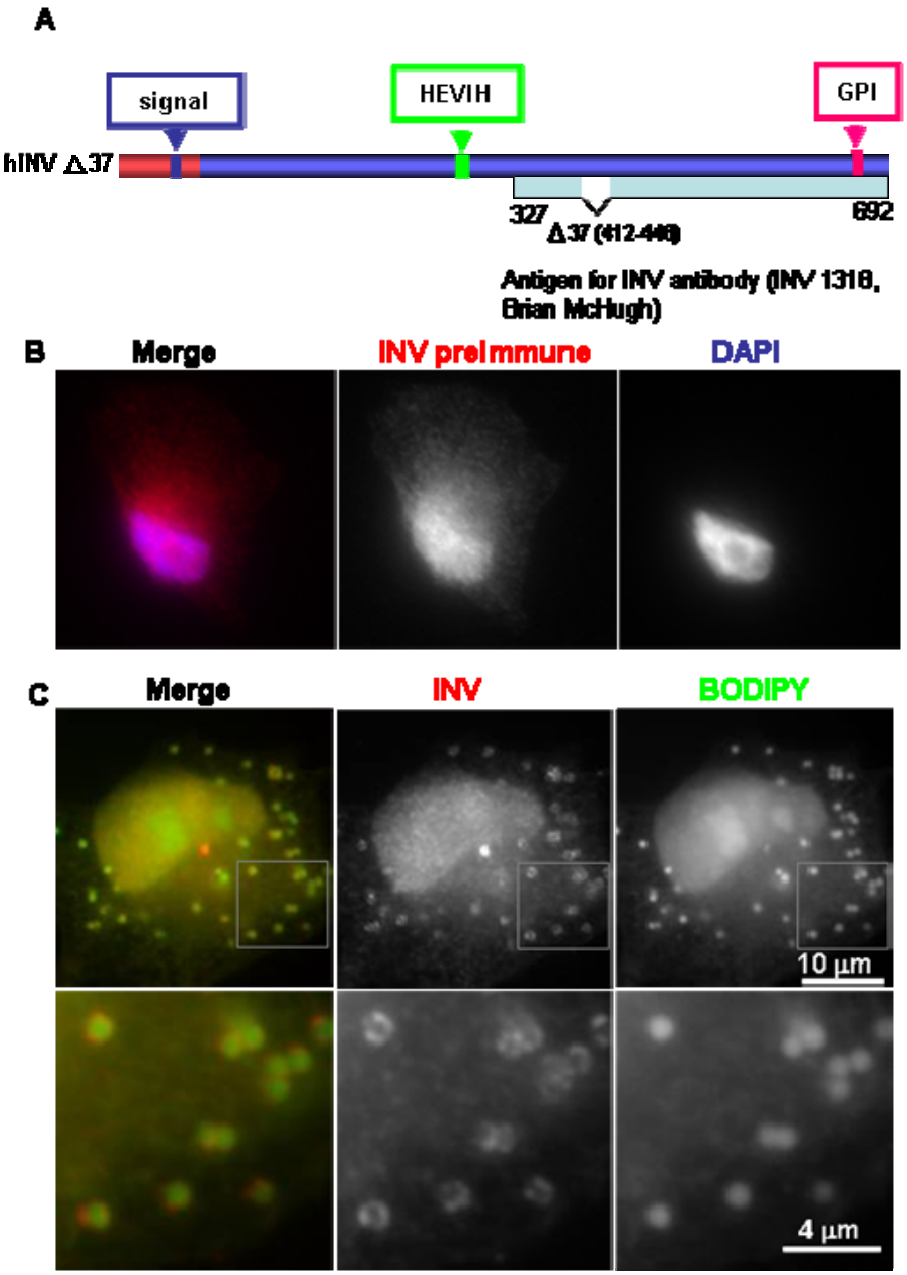

Figure 3.1 Invadolysin is localized on the surface of lipid droplets. A) A diagram of the antigen used for invadolysin (R1318) antibody. B) Human A375 melanoma cells were stained with INV 1318 pre immune antibody and DAPI for DNA. C) Human A375 melanoma cells were stained with INV antibody (red), neutral lipid dye BODIPY 493/503 for lipid droplets (green). Bottom panel was the higher magnification (~2.5X) of the area surrounded by the gray line square. INV stains the surface of lipid droplets

cells, when the cells were stained with INV antibody. The average diameter of these structures was around 1 μm. BODIPY is a neutral lipid binding dye which has been widely used to label LDs and used in the study of LD associated proteins such as TIP 47 (tail-interacting protein of 47 kDa), ADRP (adipocyte differentiation-related protein), perilipin and ATGL (adipose triglyceride lipase) (Wolins *et al.*, 2001; Londos *et al.*, 1996; Londos *et al.*, 1999; Smirnova *et al.*, 2006). A375 cells were fixed and stained with INV antibody and BODIPY. BODIPY binds LDs which are observed as stained spheres and are surrounded by a ring surface structure which was formed by INV, suggesting that INV is a LD binding protein (Figure 3.1C).

Oleic acid (OA) accumulates in LDs, which grow in size in response to the fatty acids (Brasaemle *et al.*, 1997). To examine whether INV still encircles LDs when a cell has taken up more fatty acid, I treated cells with various concentrations (0 μM, 50 μM, 100 μM and 300 μM) of oleic acid for 24 hours. After treatment, cells were fixed and co-stained with INV antibody and BODIPY. The size and the number of LDs increased markedly with an increasing concentration of OA. BODIPY-labeled LDs were much brighter in cells treated with high concentration of the OA, suggesting that more lipids accumulated in LDs (Figure 3.2A, B). The size of LDs in human cultured cells is generally around 1 μm. With an increased concentration of OA up to 300 μM in cell culture medium, the diameter of LD increase up to 2-4 μm. Likewise, the diameter of INV rings was also observed to increase after OA treatment. The enhanced size of LDs after OA treatment does not change INV's localization around LDs, confirming an intimate association between INV and LDs (Figure 3.2A, B)

3.2.2 Caveolin co-localized with INV in the presence of Brefeldin A

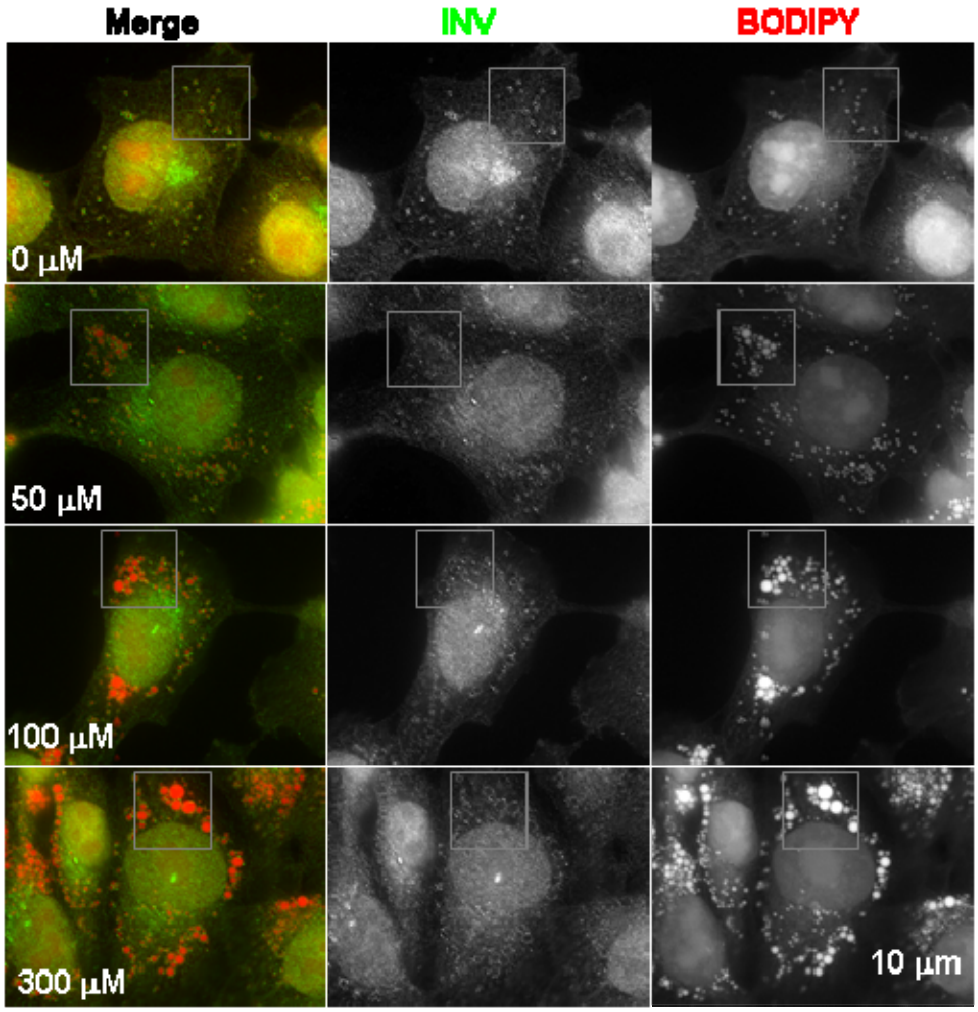

Figure 3.2A Oleic acid treatment increases the size of invadolysin rings. Human A375 cells were treated with different concentrations of oleic acid (50, 100 or 300 μM) for 24 hours and stained for INV (green), neutral lipid dye BODIPY 630/650 (red). The higher magnification of the areas enclosed by the gray lines are shown in Figure 3.2B.

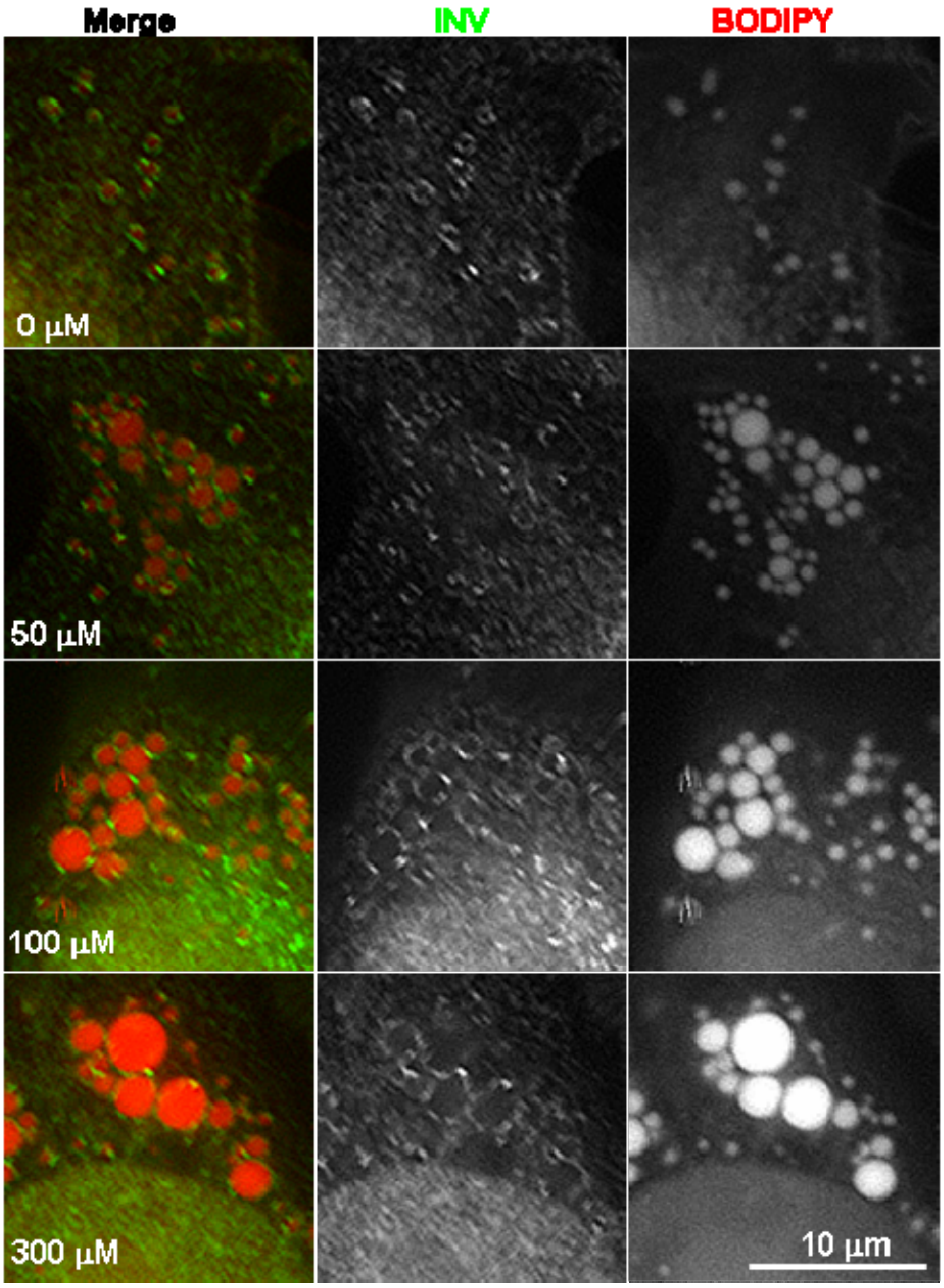

Figure 3.2B Oleic acid treatment increases the size of invadolysin rings. The higher magnification (4X) of Figure 3.2A. The diameter of the invadolysin rings surrounding lipid droplets increased with respect to the increasing concentration of oleic acid.

INV surrounds lipid vesicles which are CtxB positive (Cobbe *et al.*, submitted). Fluorescently-labeled CtxB is a marker for tracing caveolar endocytosis (Orlandi *et al.*, 1998). Caveolae are specialized membrane microdomains present in the plasma membrane. Its predominant coat protein is caveolin (including caveolins-1, -2 and -3) (Cohen *et al.*, 2003). The caveolin scaffolding domain (CSD) can interact with numerous signaling molecules including the insulin receptor (Cohen *et al.*, 2003). Based on biochemical analysis, there are two similar caveolin-binding motifs present within all known caveolin-associated proteins. They are "ΦXXXΦXXΦ" and "ΦXΦXXXXΦ" (Φ can be amino acid W, F and Y) (Cohen *et al.*, 2003). Interestingly, three potential caveolin binding sites were found within the protein sequence of INV variant 1. The potential caveolin binding sites are located at amino acid 29-36, 280-288 and 307-314, the 2nd and 3rd also in variant 2 (Figure 3.3A).

Therefore, I assessed the co-localization between INV and caveolin. A375 cells grown in normal culture condition (DMEM + 10% FBS) were stained with INV and caveolin antibodies. INV again exhibited ring-like staining, however, not many caveolins localized to INV-positive vesicles but accumulated in the cytosol (Figure 3.3 B). Most of the caveolin-positive spots were present in the nucleus and possibly the endoplasmic reticulum (ER). A few foci of caveolin may co-localize with INV (Figure 3.3B, lower panel), suggesting that only a partial co-localization between caveolin and INV occurs in normal cell culture conditions.

Endogenous caveolin moves to LDs after Brefeldin A (BFA) treatment and in response to the intracellular accumulation of lipid (Pol *et al.*, 2003). BFA blocks the export pathway at the transition between the ER and the Golgi complex (Klausner *et al.*, 1992). The reason for caveolin redistribution to LDs is unclear. To confirm the previous report, BFA treatment was performed prior to immunostaining for INV and

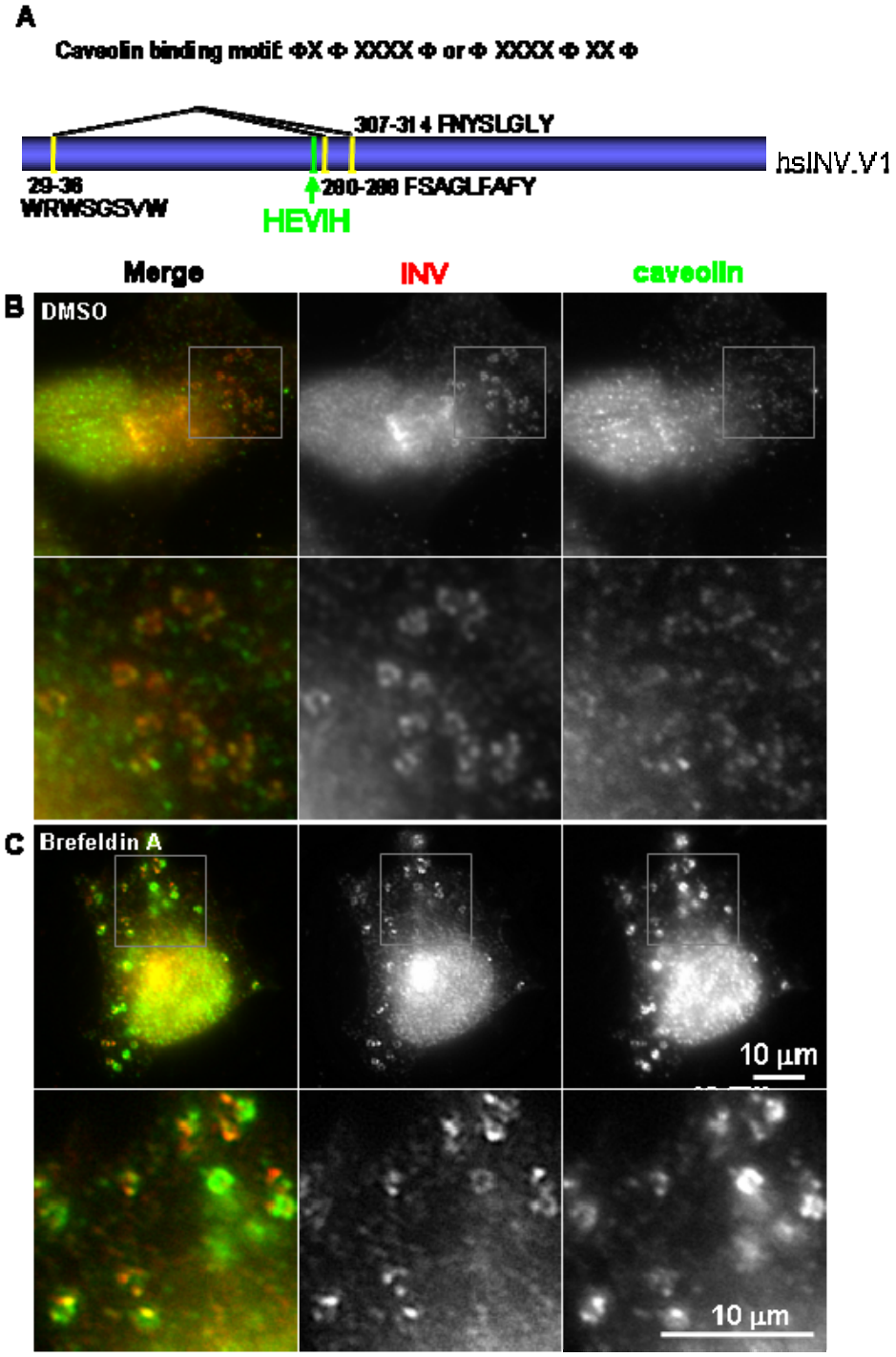

Figure 3.3 Caveolin co-localized with INV in the presence of Brefeldin A. A) Schematic representation of human INV putative caveolin binding sites. Either DMSO (B) or 5 µg/ml Brefeldin A (C) was added to the cells and cells were incubated for 3 hours. Afterwards, cells were stained for INV (red), caveolin (green). Bottom panel was the higher magnification (~2.5X) of the area surrounded by the gray line square.

caveolin. A375 cells were treated with 5μg/ml BFA for 3 hours. After treatment, cells were fixed and stained with INV and caveolin antibodies. As figure 3.3C shows, a large amount of caveolins was released to the cytosol, confirming published observations (Pol *et al.*, 2003). INV was co-localized with caveolin and surrounded vesicles to generate ring-like structures. According to the previous results shown in section 3.2.1, those vesicles are LDs. To further confirm that INV and caveolin remain localized on LDs under the treatment of BFA, cells were fixed and stained with INV and BODIPY, or caveolin and BODIPY after BFA treatment. As expected, in the presence of BFA, Golgi structure was disrupted (Figure 3.4A). The data revealed that both INV and caveolin still encircle LDs in the presence of BFA (Figure 3.4). These data indicated that INV and caveolin are differentially associated with LDs depending on the various circumstances of intracellular membrane dynamic.

3.2.3 Time course for the recruitment of INV to LDs

The formation of LDs is dependent on the nutritional status of cells and starvation can disrupt the formation of LDs in cells. Serum contains phospholipids, proteins, salts, sugars, vitamins, minerals, hormones, receptors and growth factors. Growing cells in 2% lipoprotein-deficient serum reduced LD formation (Ozeli *et al.*, 2005). The serum-starvation condition can disrupt LDs formation and it has been used to study the relationship between newly formed LDs and LD binding proteins (Andersson *et al.*, 2006, Ozeli *et al.*, 2005). To assess the localization of INV under serum-starvation condition, A375 cell were cultured in serum free medium for 24 hours and then re-fed with fresh medium (DMEM + 10% FBS + 10μM oleic acid: OA/FBS). Cells were fixed and stained with INV antibody at

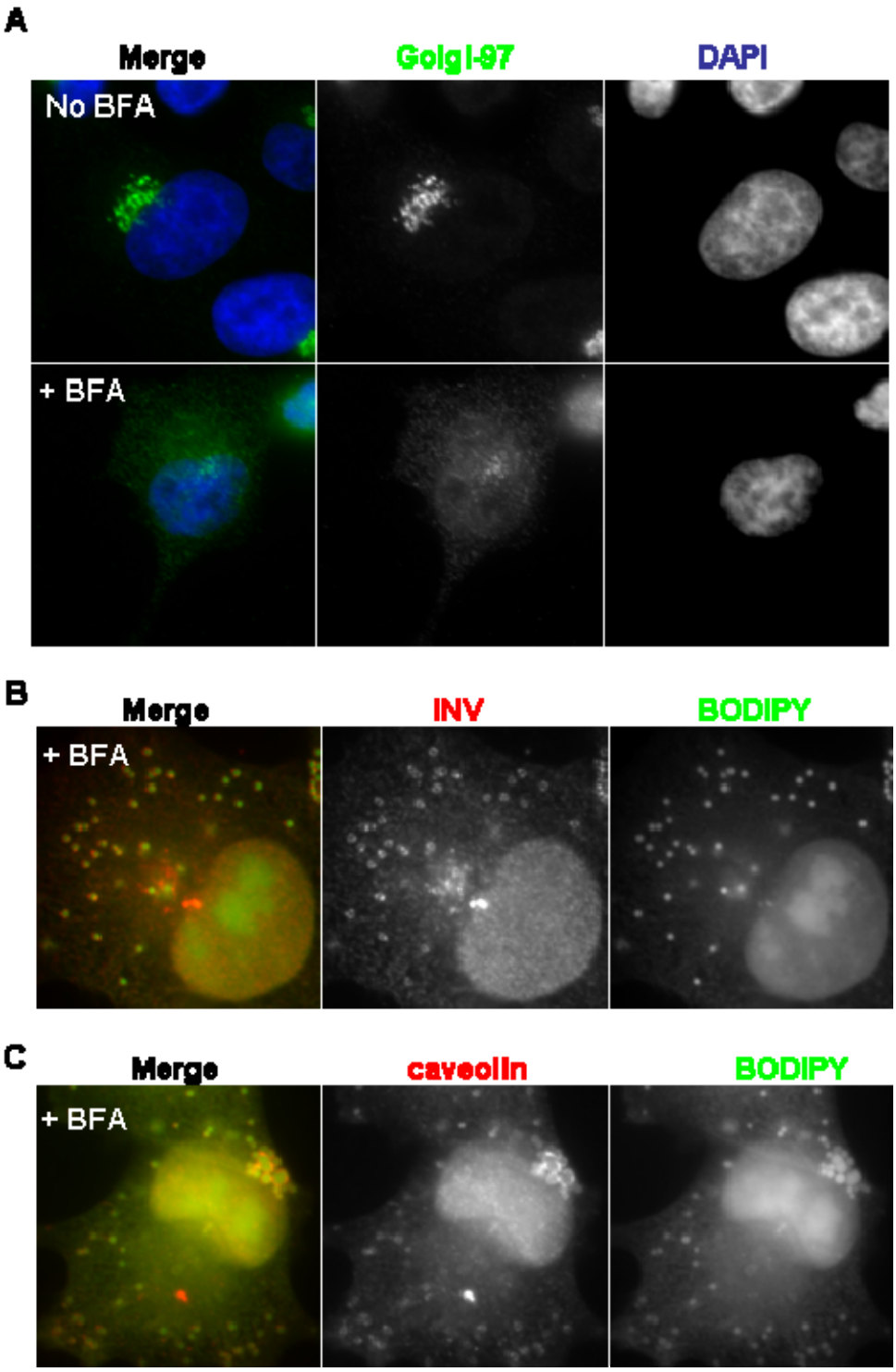

Figure 3.4 Both INV and caveolin bind with LDs in the presence of Brefeldin A. 5 µg/ml Brefeldin A was added to the cells and incubated for 3 hours. Then the cells were stained with either A) Golgi specific marker, Golgi-97 and DAPI for DNA, B) INV and BODIPY and C) caveolin and BODIPY. Golgi structure was disrupted in the presence of 5 µg/ml BFA. Whereas, INV and caveolin still encircle LDs.

indicated time points. Under normal cell culture conditions (DMEM + 10% FBS), the INV ring-like staining pattern was observed in every single cell, whereas, the INV staining was not observed after 24 hours of serum-starvation (Figure 3.5A, B). After only 30 minutes feeding with OA/FBS after 24 hours of serum starvation, INV rings/dots could be seen in cells. In response to OA/FBS, INV staining positive cells were increased with respect to the incubation time (Figure 3.5).

To examine whether the re-appearance of INV was related to the formation of newly generated LDs, cells were co-stained for INV and BODIPY after serum-starvation. In normal cell culture condition, LDs labeled with BODIPY were clearly surrounded by INV, whereas no INV "rings" or LDs were detectable in the majority of serum-starved cells (Figure 3.6A, B). After an addition of OA, LDs re-appeared within 30 minutes. As soon as LDs were apparent, INV was localized to them. With prolonged OA/FBS incubation, more INV and LDs were visible, and the number of double-positive cells (INV and BODIPY) was dependent on the incubation time. LDs were surrounded by INV when the cells were incubated in the medium with sufficient serum, suggesting that INV is recruited to newly formed LDs as soon as they form.

In order to determine the frequency of BODIPY positive cells after OA treatment, 400-500 cells were assessed at the time points indicated. A cell containing five or more LDs was identified as a BODIPY positive cell. BODIPY positive cells increased with the time of OA incubation. The frequency of the appearance of INV on LDs was time dependent. The increased incubation time gave more BODIPY positive cells and INV was found on every LD. Around 50 percent of cells were BODIPY-positive after 1hr incubation in OA/FBS and the majority of cells showed BODIPY-positively after 3 hours incubation in OA/FBS (Figure 3.6C).

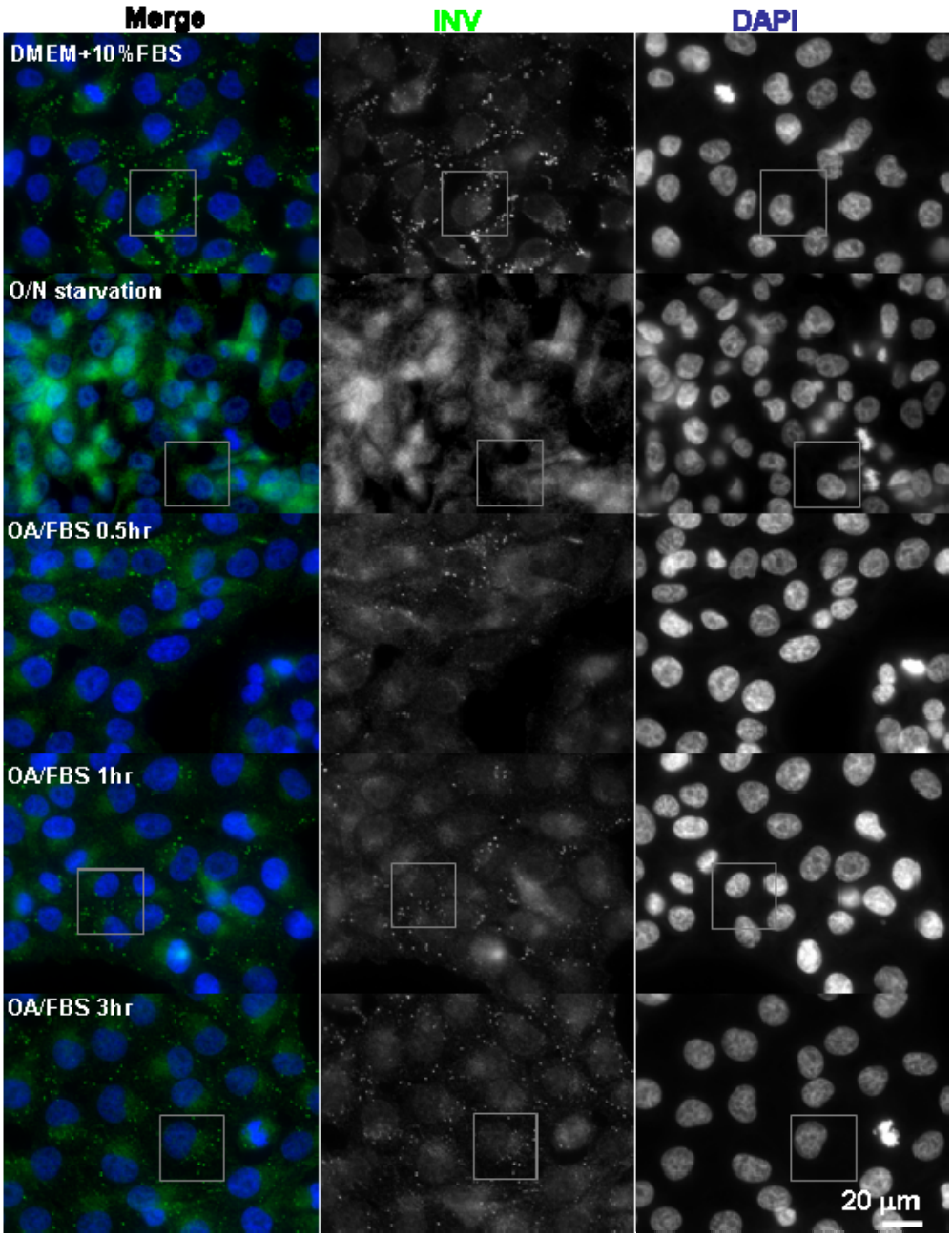

Figure 3.5A Time course of invadolysin localization in human A375 cells loaded with oleic acid. Human A375 cells were cultured in serum free medium for 24 hours, and then re-fed with OA/FBS. Afterwards, the cells were fixed and stained for INV (green), and DAPI (blue) at the time indicated. INV rings/dots can not be detected in serum free medium. INV rings/dots were observed clearly in cytosol after incubating the cell in OA/FBS medium. The higher magnifications of the areas enclosed by the gray lines are shown in figure 3.4B.

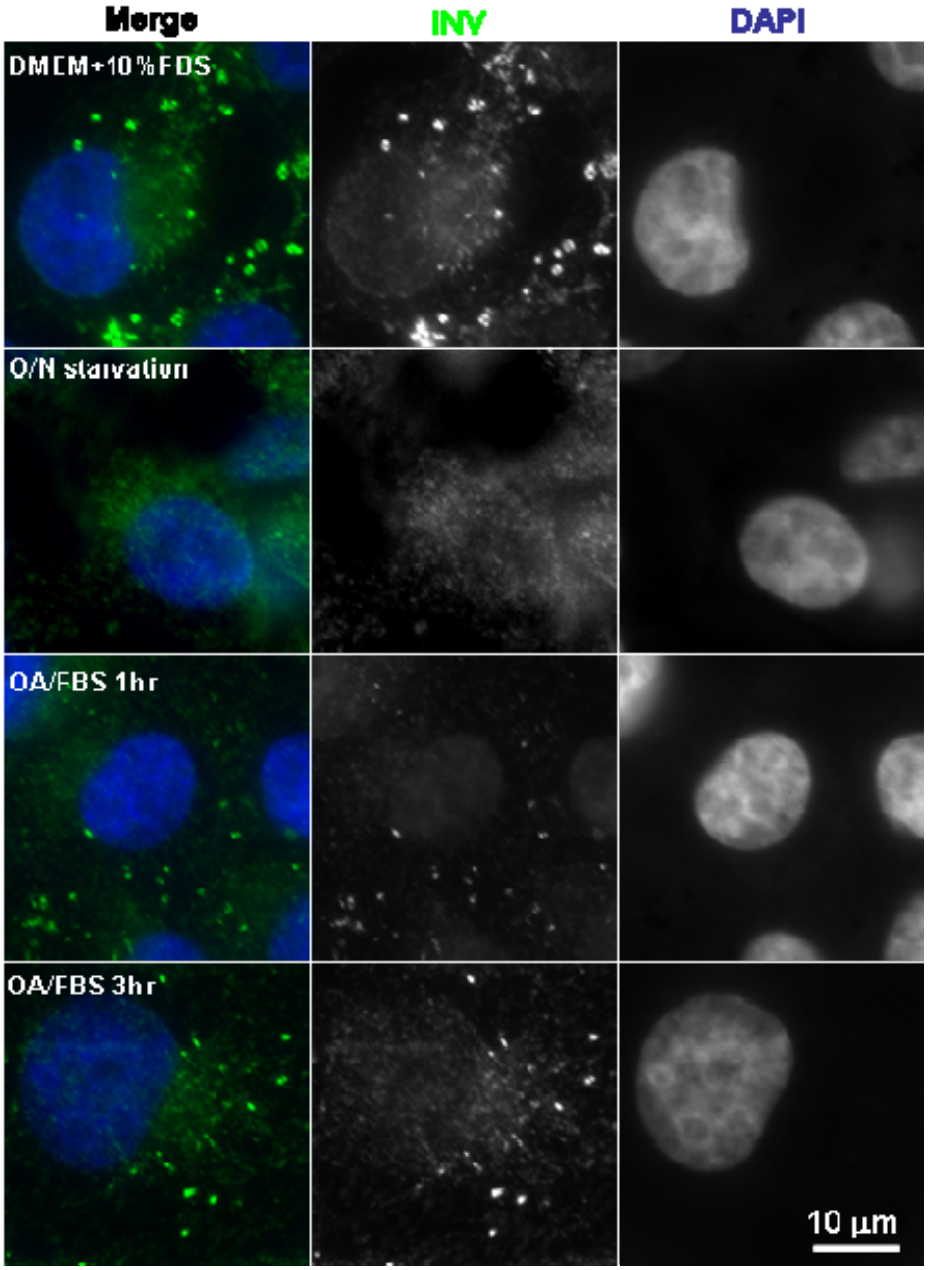

Figure 3.5B Time course of invadolysin localization in human A375 cells loaded with oleic acid. The higher magnification (3X) of the areas enclosed by the gray lines showed in figure 3.5A.

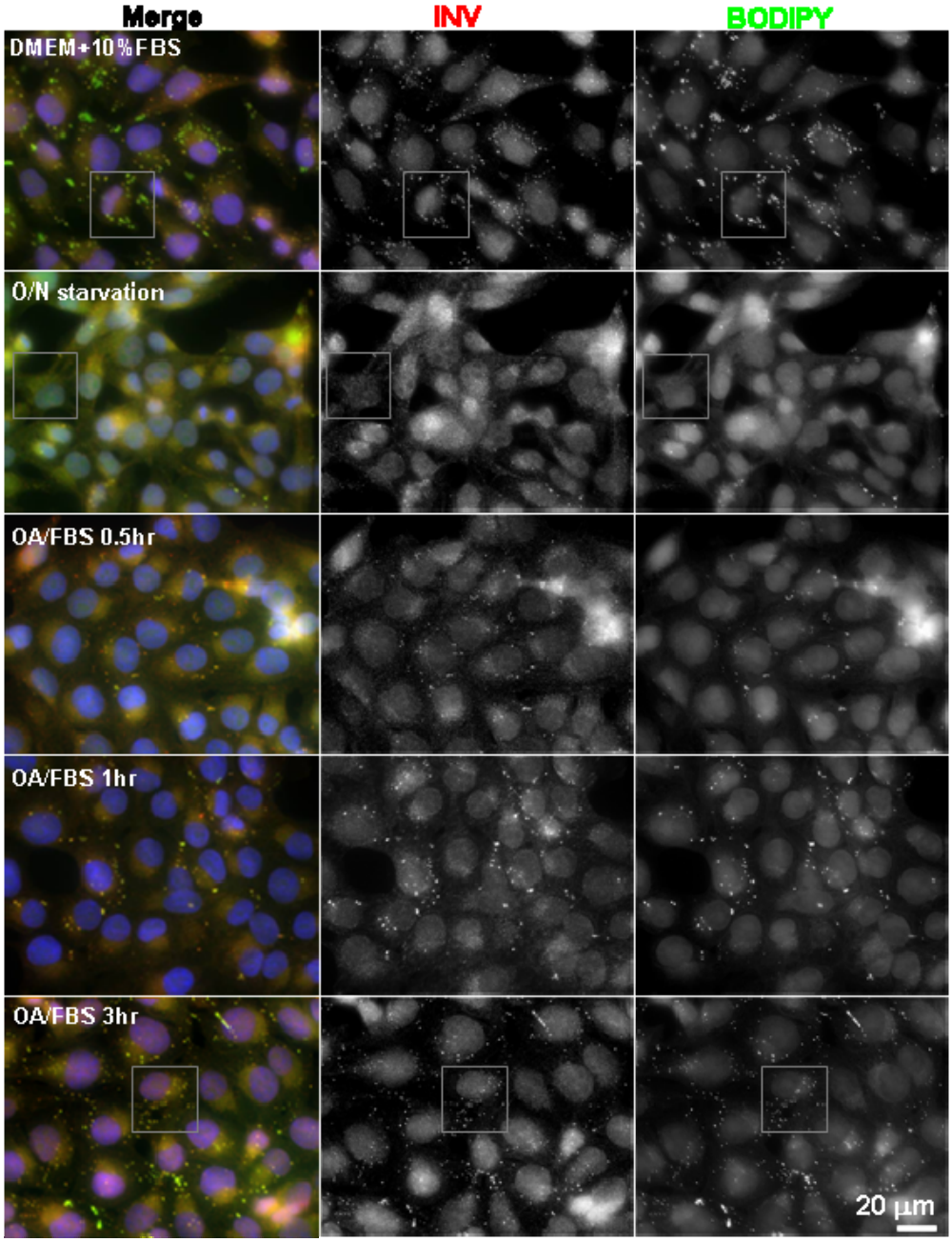

Figure 3.6A Invadolysin is recruited to newly formed lipid droplets. Human A375 cell were cultured in serum free medium for 24 hours, and then re-fed in OA/FBS. Afterwards, the cells were fixed and stained for purified-INV 1318 antibody (red, the antibody was purified by Francesca Di Cara), BODIPY (green) and DAPI (blue). INV rings/dots and LDs can not be detected in serum free medium. However, INV ring/dot and LDs were observed clearly in cytosol after incubating the cells in OA/FBS medium. The higher magnification of the areas enclosed by the gray lines are shown in Figure 3.6B.

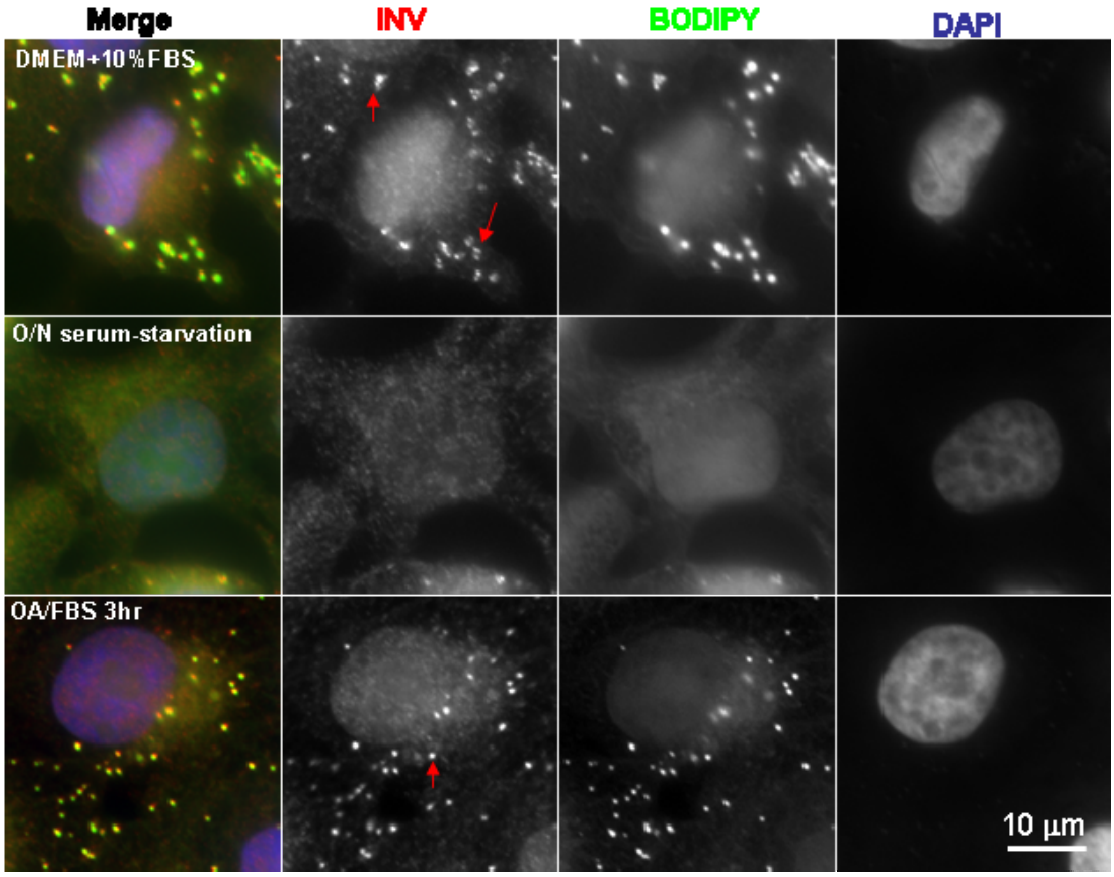

Figure 3.6B Time course of invadolysin localization in human A375 cells loaded with oleic acid. The higher magnification (3X) of the areas enclosed by the gray lines showed in figure 3.6A. INV rings/dots and LDs can not be detected in serum free medium. However, INV ring/dot (red arrow) and LDs were observed clearly in cytosol after incubating the cells in OA/FBS medium.

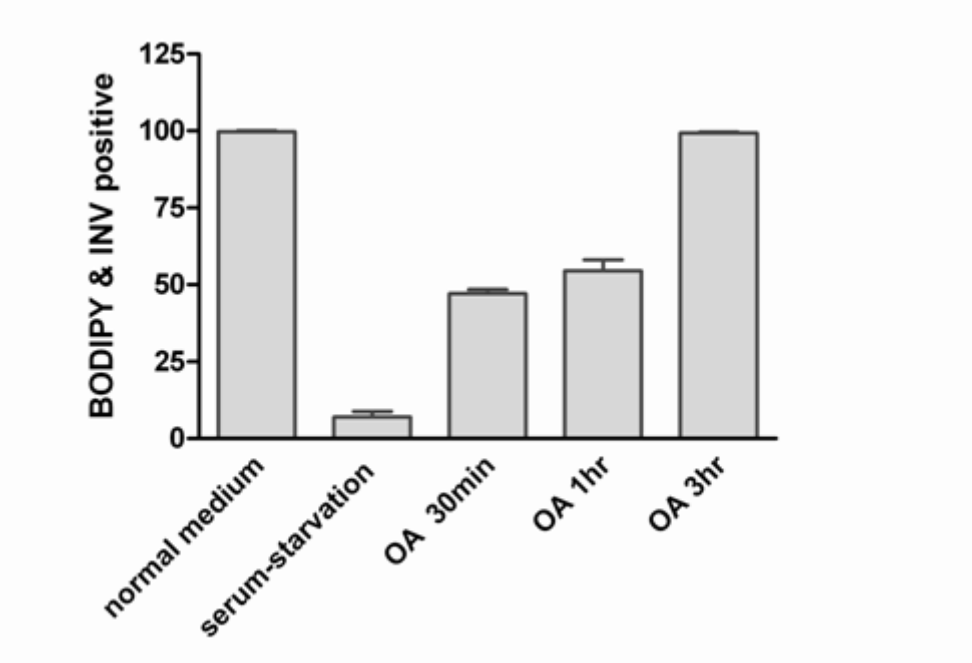

Figure 3.6C The BODIPY positive cells were increased by re-feeding the cells with OA/FBS medium after overnight starvation. A375 cells were starved in serum-free for 24 hours, then cells were re-fed with OA/FBS medium. At different time points, cells were fixed and stained with INV/DAPI or INV/BODIPY. Cell containing five or more LDs was identified as BODIPY positive. Data represent 3 independent experiments where 400 to 500 cells were counted for each time point for every experiment. The graph shows the mean value and standard deviation (SD) from 3 independent experiments. The data shows that the LDs and INV stained positive cells gradually increased over time.

3.2.4 The targeting of INV to LDs is independent of newly synthesized INV

INV rings were not observed after overnight starvation. Previous reports have shown that ADRP is localized to LDs in most mammalian cells. Cells cultured with fatty acid have elevated levels of ADRP mRNA and protein (Gao *et al.*, 1999; Gao *et al.*, 2000). Conversely, depletion of serum from culture medium can affect the accumulation of LDs and appear to down-regulate the level of ADRP (Xu *et al.* 2005). Following the same logic, the level of INV might also be modified after starvation. However, the mRNA level of INV did not alter after starvation (data not shown). To confirm whether INV is resynthesized and recruited to LDs, cycloheximide, an inhibitor of protein biosynthesis in eukaryotes, was added to cell cultures before OA/FBS treatment (Figure 3.7). A375 cells were starved in serum free medium overnight to deplete LDs. Next, cells were pretreated with 10 μM cycloheximide for 1, 2 or 3 hours to inhibit protein translation, followed by 3h incubation with OA/FBS and cycloheximide. Subsequently, cells were fixed and stained with INV and BODIPY. LDs can regenerate during OA/FBS treatment in A375 cells, this procedure was not affected by cycloheximide treatment. Likewise, INV can locate to LDs during OA/FBS and cycloheximide treatment, these data suggested that the localization of INV to LDs was not dependent on synthesis of new INV. Based on these data, I hypothesis that starvation results in the delocalization of INV from LDs. INV may disperse in the cytosol and be recruited to LDs upon OA/FBS treatment.

3.2.5 Tyrosine kinase may not affect the localization of INV to LDs

Src kinases have been described as key players in caveolar endocytosis (Sharma *et al.*, 2004). Activation of Src family kinases is known to increase the fusion of

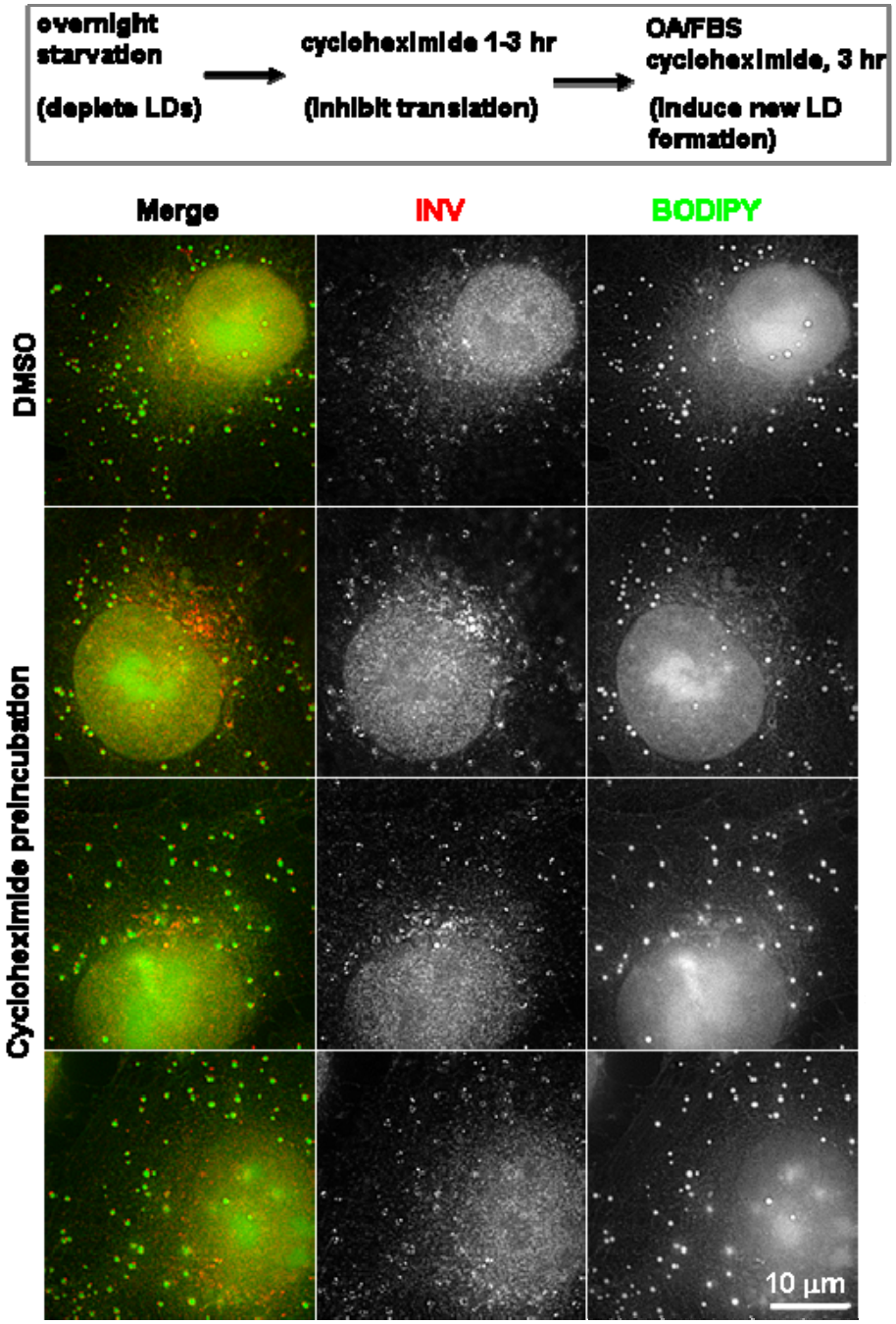

Figure 3.7 Targeting of INV to LDs is independent of newly synthesized INV. A375 cells were starved in serum free medium for 24 hours. Either 10 µM cycloheximide or DMSO was added to cells to inhibit protein translation. After 1-3 hours incubation, cells were re-fed with OA/FBS containing cycloheximide for another 3 hours. Finally, cells were stained with INV (red) and BODIPY (green). Cycloheximide treatment did not affect the localization of INV to LDs.

caveolar vesicles, whereas Src knockout stabilizes plasma membrane caveolae (Sharma *et al.*, 2004; Pelkmans & Zerial, 2005; Lay *et al.*, 2006). As mentioned before, INV showed a partial localization with caveolin (Figure 3.3B) and co-localized with caveolin after BFA treatment (Figure 3.3C). Importantly, cholesterol-induced translocation of caveolin to LDs is regulated by Src kinases (Lay *et al.*, 2006). INV contains three potential caveolin binding sites (Figure 3.3 A) and endogenous INV shows a partial localization with caveolin. Therefore, to address whether Src kinase might be involved in the regulation of the re-localization of INV to LDs during starvation/re-feeding, genistein, a general tyrosine kinase inhibitor was used. A375 cells were starved in serum free medium for 24 hours, and then 50 μM genistein was added to cells and incubated for 1 hour to inhibit kinase activity. Afterwards, cells were incubated in fresh medium with OA/FBS plus genistein. Cell were fixed and subsequently and stained for INV and BODIPY. As shown in Figure 3.8, the BODIPY-positive stained LDs were INV positive in either the genistein treated or the control group (Figure 3.8), indicating that the general inhibition of tyrosine kinases probably has no effect on the localization of INV to newly synthesized LDs. However, to further confirm this idea, the inhibition effiency of the inhibitor needed to be exaimined by blotting with phosphotyrosine antibody.

3.2.6 Protein kinase C is required for the localization of INV to newly synthesized LDs

Several proteins related to cell signaling such as protein kinase C (PKC) δ, diacylglycerol kinase (DGK) δ, PKA, Ras, Raf and P-MAPK have been found also localized with LDs by mass spectrometry proteomics analyses (Turro *et al.*, 2006). PKC α and PKC δ can be translocated to LDs in RAW 264.7 Macrophages after

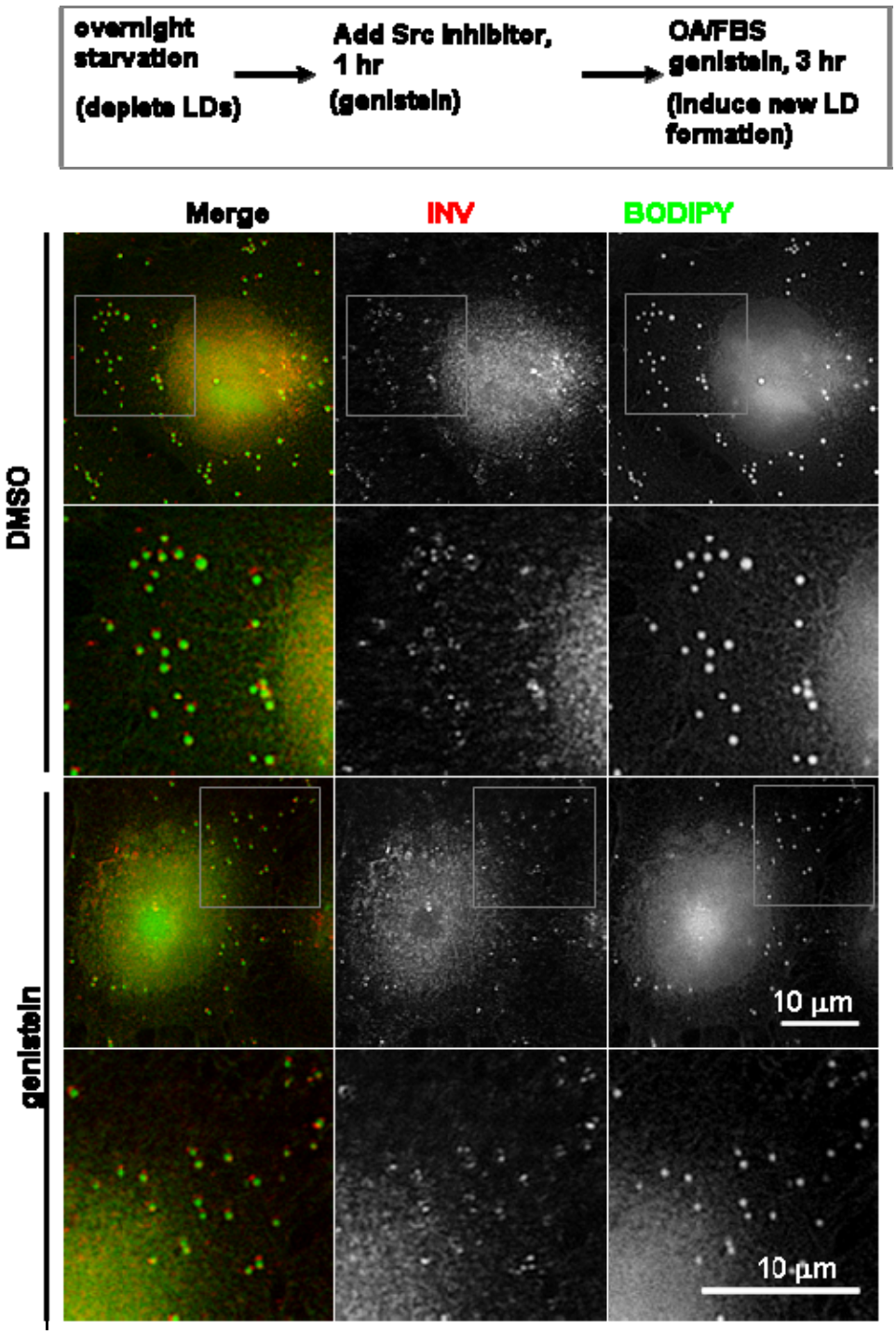

Figure 3.8 Src kinase inhibitor may not affect the re-localization of INV. A375 cells were starved in serum free medium for 24 hours. Either 50 μM genistein or DMSO was added to the cells. After 1 hour incubation, cells were re-fed with fresh medium containing OA/FBS and genistein and incubated for another 3 hours. Finally, cells were stained with INV (red) and BODIPY (green). The area surrounded by the gray line was magnified to 2-fold and showed in the bottom panel.

stimulating with OA (Chen *et al.*, 2002). In addition, PKC activation has been reported to be involved in fatty acid-stimulated insulin secretion (Littman *et al.*, 2000) and in the regulation of LD formation in neutrophils (Weller *et al.*, 1991). To address any potential role of PKC in regulating the localization of INV while new LDs are generated, the general PKC inhibitor (Ro31-8220, which inhibits all PKC isozymes) was applied in thestarvation/re-feeding protocol. A375 melanoma cells were starved in serum free medium for 24 hours to disrupt the formation of LDs, and were then treated with 5 μM of Ro31-8220 for 1 hour to inhibit the activity of PKC. After PKC inhibition, cells were re-fed for another 3 hours with OA/FBS (containing 5 μM Ro31-8220), subsequently fixed and stained for INV and BODIPY.

INV underwent de-localization and re-localization after starvation/re-feedingprocedure, as expected, however, PKC inhibition disrupted the re-formation of LDs, as well as INV localization. As figure 3.9 shows, fewer LDs were regenerated during Ro31-8220 treatment, compared to DMSO treated control cells. Meanwhile, most of INV was located in the cytosol and appeared as aggregates (Figure 3.9A (B), 3.9B (B)). Although some LDs still existed in the presence of PKC inhibitor, Ro31-8220, INV positive LDs were hardly observed (Figure 3.9A, arrow). These data suggested that the localization of INV to nascent LDs was dependent on PKC activity.

To observe whether INV can re-locate to LD after Ro31-8220 was removed, A375 cells were starved and re-fed with OA/FBS containing Ro31-8220 for 3h. Afterwards, medium was replaced with fresh OA/FBS and the cells were incubated for another 1 hour or 16 hours. One hour after the PKC inhibitor was removed, aggregated complexes of INV were still observed in cells, whereas INV re-located to LDs after 16 hours of Ro31-8220 removal (Figure 3.10). Again, this experiment

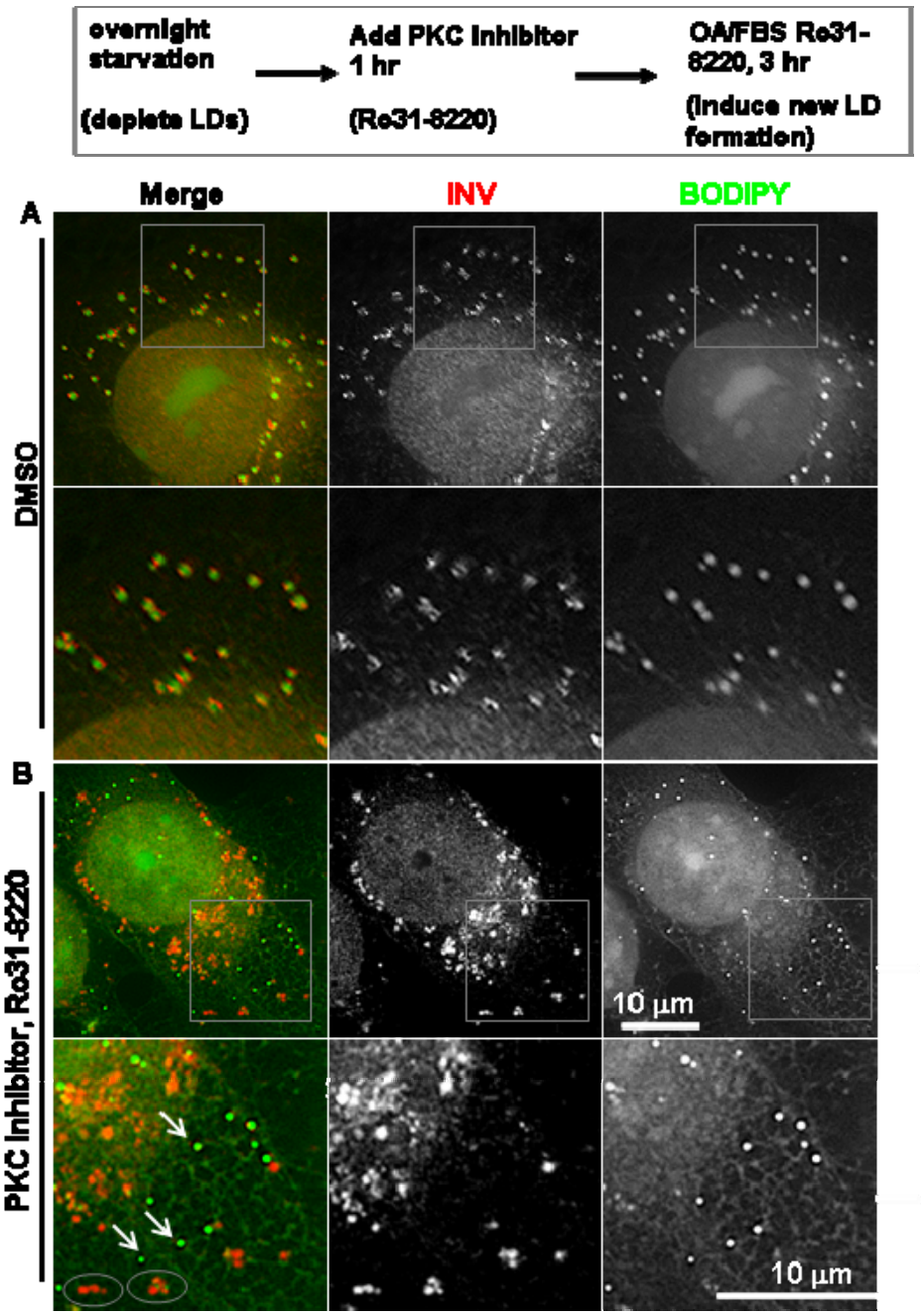

Figure 3.9A Recruitment of INV to some newly formed LDs was inhibited by Ro31-8220 treatment. A375 cells were starved in serum free medium for 24 hours. Either 5 μM Ro31-8220 or DMSO was added to the cells to inhibit the activity of PKC. After 1 hour incubation, cells were re-fed with fresh medium containing OA/FBS/Ro31-8220 and incubated for another 3 hours. Finally, cells were stained with INV (red) and BODIPY (green). The gray square in (A) shows INV binding to LDs; the gray square in (B) shows INV aggregates (gray circle) and did not bind to LDs (arrow) upon Ro31-8220 treatment.

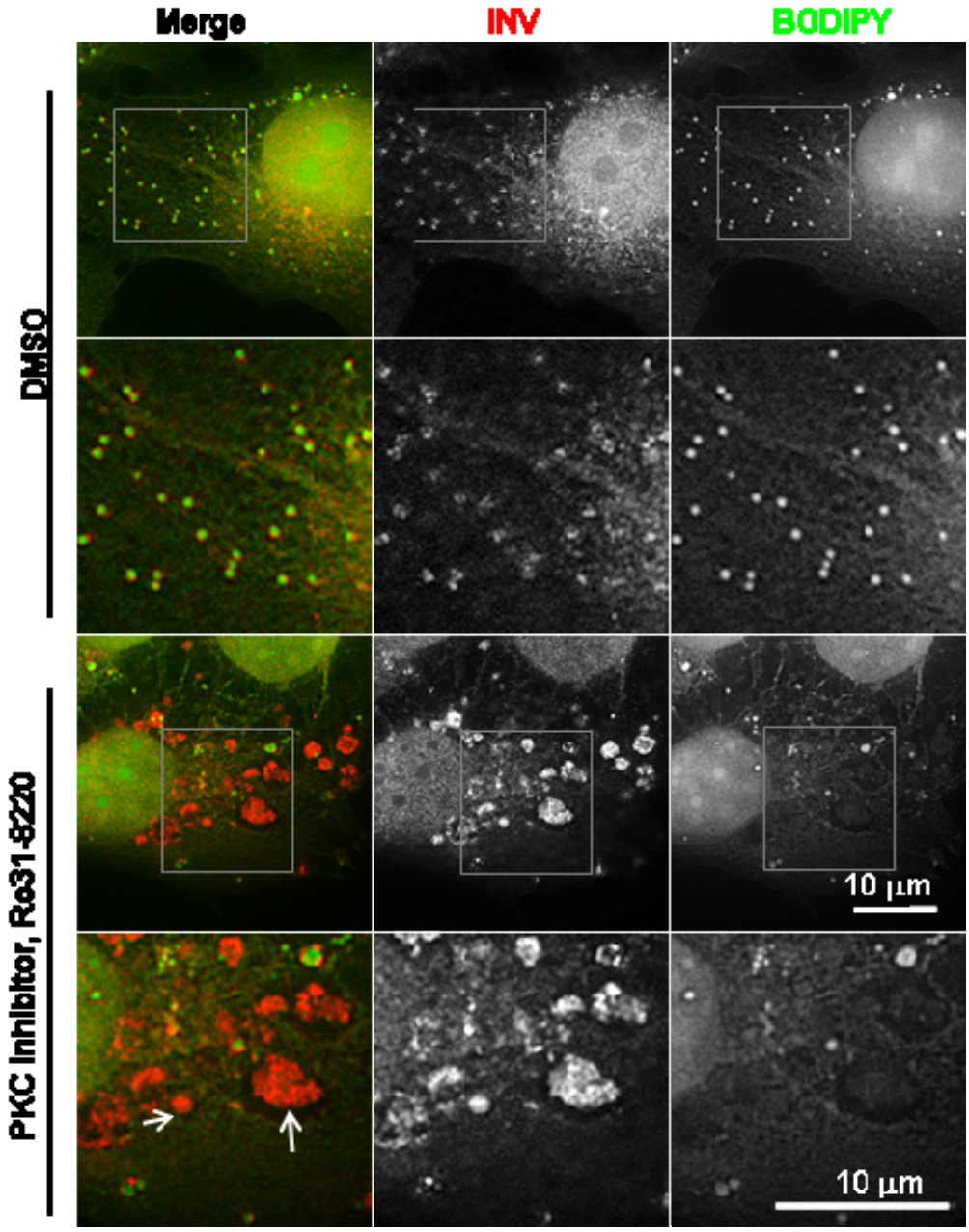

Figure 3.9B INV formed as aggregates in the cytoplasm after Ro31-8220 treatment.

A375 cells were starved in serum free medium for 24 hours. Either 5 µM Ro31-8220 or DMSO was added to cells. After 1 hour incubation, cells were incubated with fresh medium containing OA/FBS/Ro31-8220 and incubated for another 3 hours. Afterwards, cells were stained with INV (red) and BODIPY (green). In the presence of Ro31-8220, INV forms aggregates (arrow).

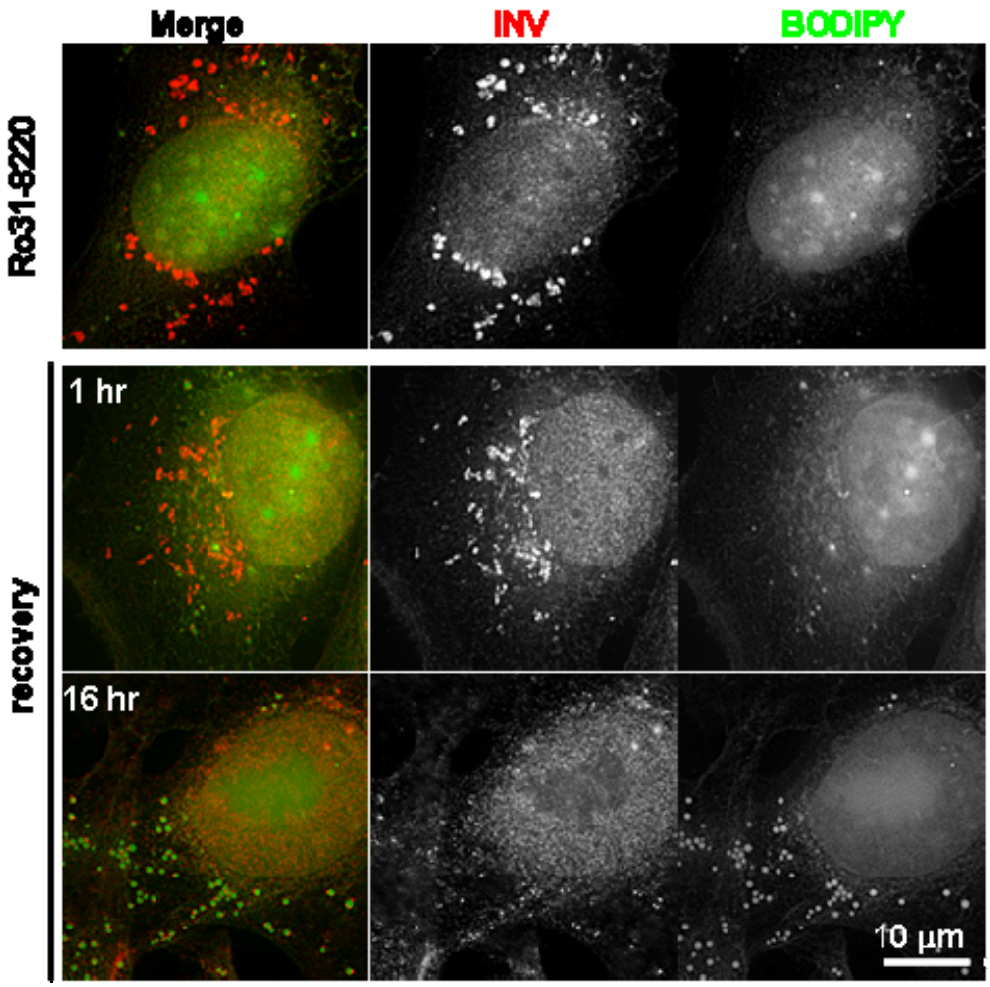

Figure 3.10 Re-localization of INV to lipid droplets after removal of PKC inhibitor. A375 cells were starved in serum free medium for 24 hours. Either 5 µM Ro31-8220 or DMSO was added to the cells. After 1 hour incubation, cells were re-fed with fresh medium containing OA/FBS/Ro31-8220 and incubated for another 3 hours. Next, medium containing PKC inhibitor was replaced by fresh medium containing OA/FBS (no inhibitor). Afterwards, cells were stained with INV (red) and BODIPY (green).

suggested that the activity of PKC was important for the localization of INV.

At least 11 isozymes of PKC have been reported with different biochemical properties, tissue distribution, subcellular localization, and substrate specificities. They are classified as conventional (α, β1, β2, γ), novel (δ, ε, η, θ, μ), and atypical (ζ, λ) isozymes (Newton, 2008; Steinberg, 2008). To further address which PKC isozyme might regulate the localization of INV to LDs, more specific inhibitors, Gö6976 and GF109203, were used for suppressing Ca^{2+}-dependent PKC α, β and γ.A375 cells were starved in serum free medium for 24 hours, and then 10 μM of Gö6976 or GF109203 were added to the cells. After 1 hour incubation, cells were supplied with fresh OA/FBS plus inhibitor. Finally, cells were fixed and stained for INV and BODIPY. After serum starvation and re-feeding, INV was re-localized on LDs as showed in Figure 3.11 after either Gö6976 or GF109203 treatment. This data may suggest that novel and atypical PKC isozymes and not PKC α, β, γ may regulate the localization of INV to LD during serum re-feeding. However, further verification of the effiency of inhibitors is required.

3.2.7 Extracellular signal-related kinase 2 (ERK2) does not affect re-localization of INV to LDs after starvation/re-feeding

Using a cell free system, phospholipase D1 (PLD1) and ERK2 were identified as key factors in the formation of insulin-stimulated lipid droplets (Adersson *et al.*, 2006). In Adersson's report, inhibition of the expression of PLD1 or ERK2 prevented the insulin-promoted formation of LDs. My previous results showed that the OA-induced formation of LDs and the re-localization of INV can be disrupted by general inactivation of PKC enzymes (Figure 3.9A, B). As ERK is a downstream molecule in PKC signaling (Caunt *et al.*, 2008), I wanted to address whether

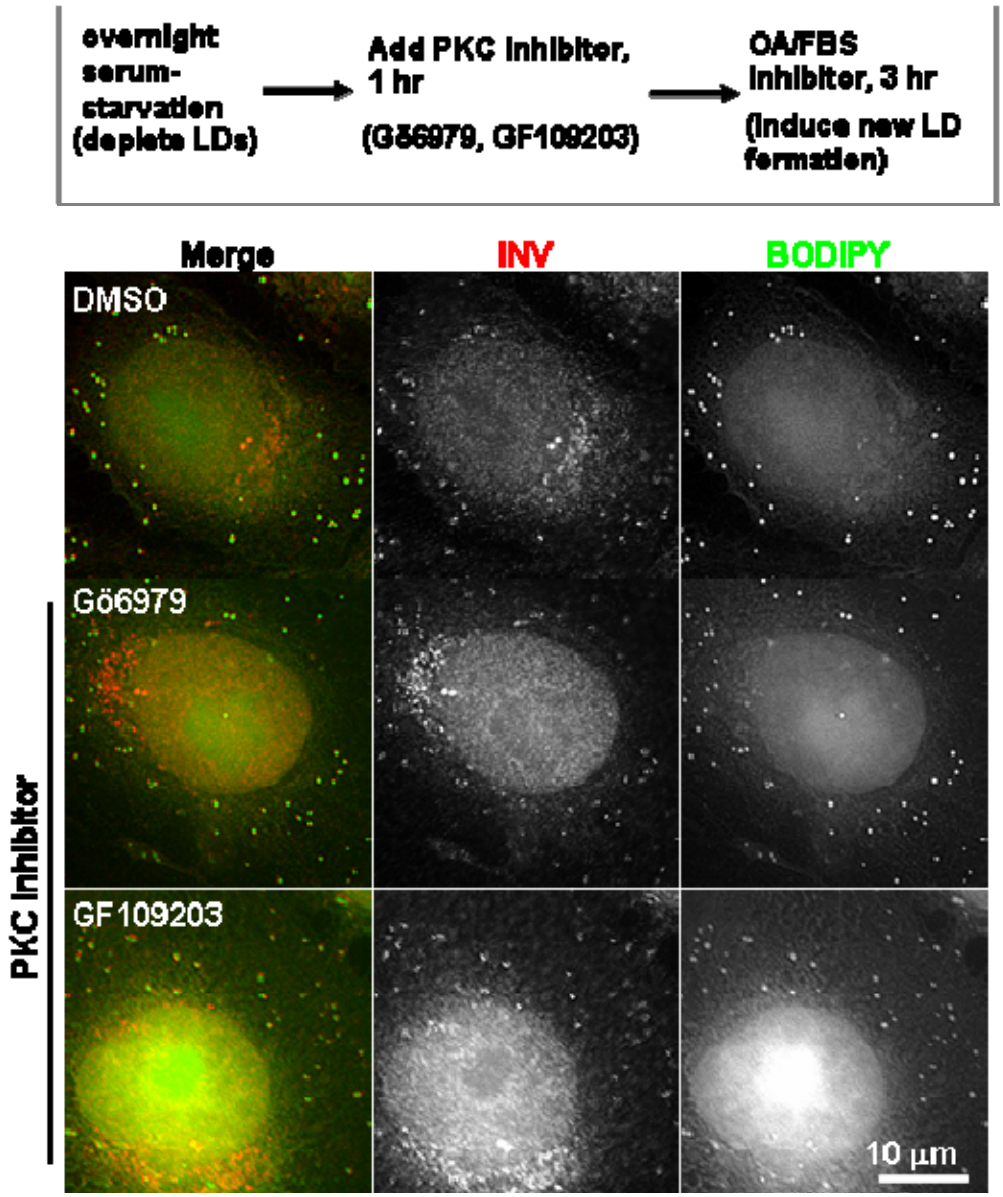

Figure 3.11 PKC inhibitors, Gö6979 and GF109203 treatment may not change the localization of INV to lipid droplets in A375 cells. A375 cells were starved in serum free medium for 24 hours. 10 μM Gö676, 1 μM GF109203 or DMSO was added to the cells. After 1 hour incubation, cells were re-fed with fresh medium containing OA/FBS and selected PKC inhibitor and incubated for another 3 hours. Finally, cells were stained for INV (red) and BODIPY (green). Ca2+-dependent PKC inhibitor may not affect the re-localization of INV/LDs.

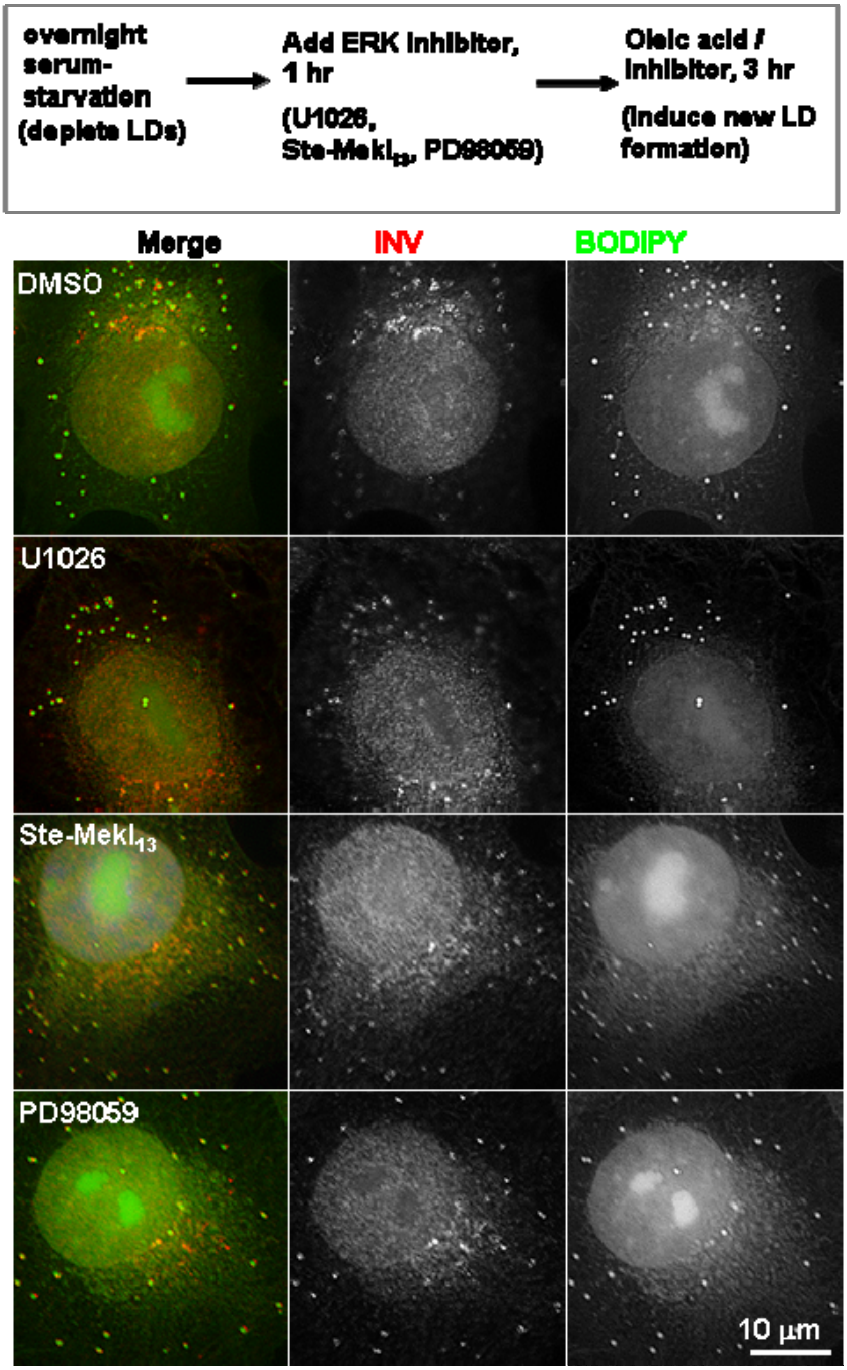

Figure 3.12 ERK inhibitors treatment may not affect the localization of INV. A375 cells were starved in serum free medium for 24 hours. 10 µM U1026, 10 µM Ste-Mekl$_{13}$, 50 µM PD9805 or DMSO was added to the cells. One hour later, fresh medium containing OA/FBS and selected inhibitor was added and cells were cultured for another 3 hours. Finally, cells were stained for INV (red), BODIPY (green) and DAPI (blue).

inhibition of ERK2 had a similar effect to the inhibition of PKC. A375 cells were starved in serum free medium for 24 hours. Either 10 µM U1026 (an inhibitor of ERK1/2), 25 µM Ste-Mek1$_{13}$ (a specific inhibitor of ERK2) or 50 µM PD98059 (an inhibitor of ERK1/2) was added to the medium and cells were incubated for 1 hour to inhibit the activity of ERK. Afterwards, cells were incubated with OA/FBS plus inhibitor for another 3 hours. Cells were fixed and stained for INV and BODIPY. In the presence of inhibitor, the BODIPY positive particles were INV positive (Figure 3.12), indicating that inhibition of ERK2 probably has no effect on the formation of new LDs after starvation or the re-localization of INV to these LDs. However, further verification of the inhibition effiency is required to support this data.

3.2.8 Invadolysin is a substrate of protein kinase C

Protein phosphorylation is a common post-translational modification frequently used to regulate activity, localization or molecular interactions of the modified protein (Bartz *et al.*, 2007). To investigate the potential phosphorylation of INV by PKC, the sequence of human INV.v1 was analyzed with NetPhosK 1.0 server (http://www.cbs.dtu.dk/services/NetPhosK/). The server produces neural network predictions of kinase specific eukaryotic protein phosphorylation sites. Five positions in INV sequence showed high scores over, 0.80. Four of them were potential PKC phosphorylation sites. They are S-34 (serine-34), T-220 (threonine-220), T-269 and T-458. A potential PKA phosphorylation site was predicted at position T-339 (Figure 3.13A).

Recruitment of INV to newly formed lipid droplets is PKC dependent (Figure 3.8A& 3.8B). PKC might regulate the localization of INV by directly

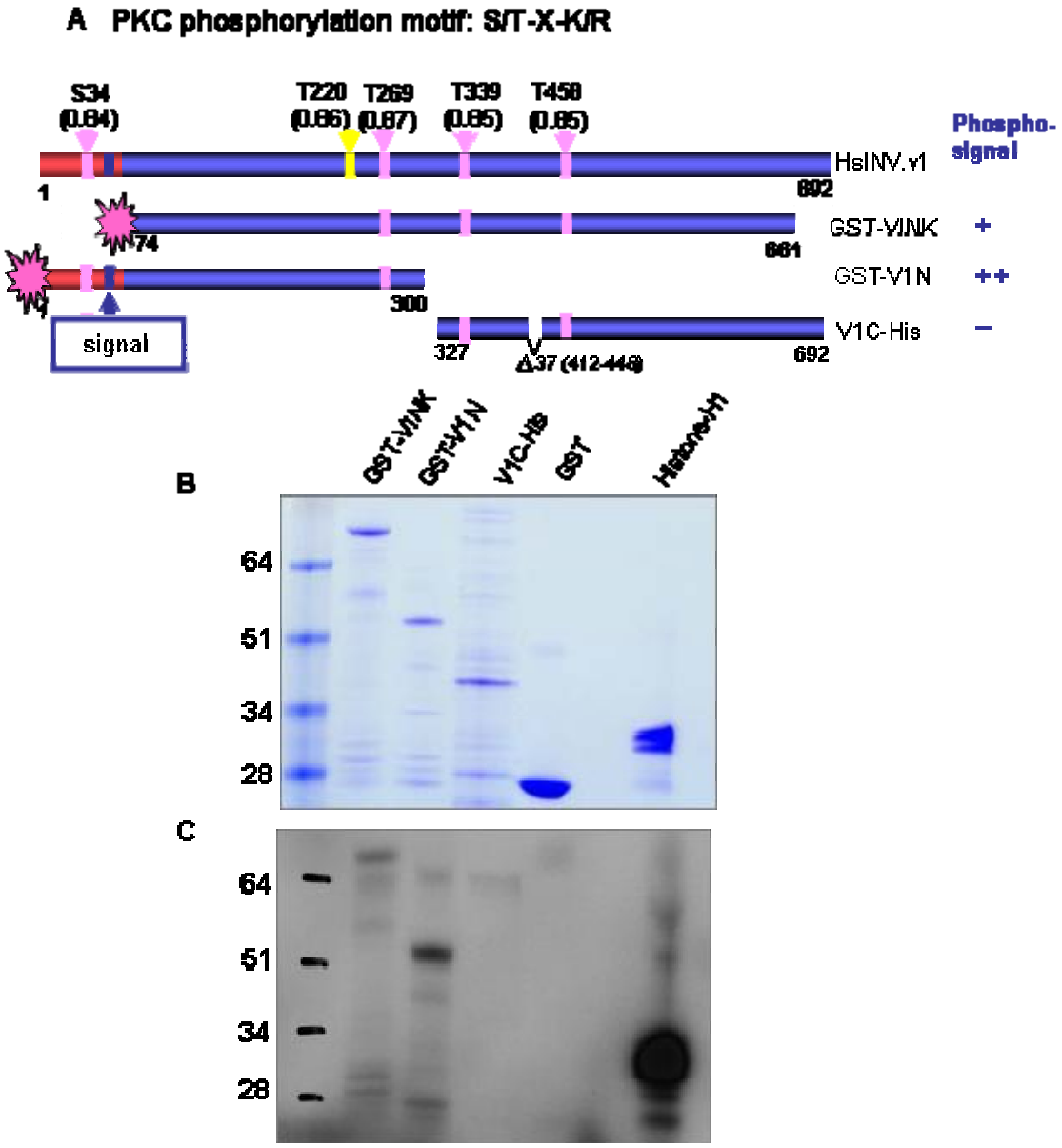

Figure 3.13 INV is a substrate of protein kinase C. A) Schematic representation of human INV putative phosphorylation sites of protein kinase C (pink arrows) and protein kinase A (yellow arrow) and the truncated forms of INV constructs which were tagged with GST or His-tag. B) Coomassie blue shows the amount of protein used for the *in vitro* kinase assay. C) Recombinant invadolysin proteins, GST (negative control) and Histone H1 (positive control) were incubated with protein kinase C and γ-^{32}P-ATP and then analyzed by 4-12% NuPAGE and autoradiography. GST-VINK and GST-V1N becomes the phosphorylated while V1C-His does not. This result suggests that a site within the N-terminal half of INV is a substrate of PKC.

phosphorylating INV or indirectly by other mechanisms. To determine whether INV can be phosphorylated by PKC *in vitro*, bacterially expressed recombinant INV (different truncated forms of INV) was affinity purified using glutathione beads or His-Bind resin (Figure 3.13A and B). The details of solubilization and purification of INV recombinant proteins from bacteria were discussed in Chapter 2. Three constructs were used to perform *in vitro kinase* assay. To perform *in vitro* kinase assays, recombinant protein was incubated with protein kinase C and γ-^{32}P-ATP at 30˚C for 30 minutes. There was a strong phosphorylation band in Histone-H1 positive control, which is a substrate of PKC. Radioactivity was incorporated in the GST-VINK constructs, suggesting that INV can be phosphorylated by protein kinase C. N-terminal fragment construct was also phosphorylated while the C-terminal INV fragment construct showed no phosphorylation, indicating that one or more potential phosphorylation sites may be located on the N-terminal fragment of INV. This might include the sites of S34 and/or T269.

3.3 Discussion

INV appears to be ubiquitously expressed and the ring-like localization of INV appears in several cell lines with similar size and shape (Cobbe *et al.*, submitted). The formation of LDs is dependent on nutritional status of the cells. In serum starved cells, LDs and INV could not be detected. When re-fed with serum and 10 μM oleic acid containing medium, newly-synthesized LDs were re-formed and the INV staining found on those newly-synthesized LDs. The newly-supplied serum (which contains a high amount of lipids) may play a major source to induce new LD formation. The concentraction of the olecic acid used in this experiment is too low to have an effect on the regulation of LD formation. According to the results showed in

Figure 3-6, the re-generation of LDs is time dependent. As re-feeding time increases, more and larger newly-synthesized LDs were found in the cells (Figure 3.5 and Figure 3.6). Based on the time course observation between INV and LDs, every detectable LD was surrounded with INV. Presumably, INV can be recruited to LDs immediately once the new LDs were synthesized or INV is initiated in the LD assembly procedure. LDs are composed of a hydrophobic neutral lipid core and a phospholipid monolayer surface coated with proteins (Zweytick *et al.*, 2000). Mainly LD associated proteins are PAT family proteins defined by their similarity of sequence, including perilipin (in adipocyte and steroidogenic cells), ADRP and TIP47 (Brasaemle *et al.*, 2004; Liu *et al.*, 2004). Although INV does not contain a PAT domain, it has been shown that GPI-anchored proteins can be transiently associated with LDs (Muller *et al.*, 2008). Thus, the association of INV to LD might be achieved by INV's GPI anchor site.

The procedure of serum starvation and re-feeding provides a model for studying the relationship between INV and newly-synthesized LDs. Based on this protocol, de novo synthesis of INV is not required for the recruitment of INV to newly-synthesized LDs (Figure 3.7). These data suggest that INV distributed in the cytosol when the nutrient supply is insufficient. Some of the PAT proteins, such as perilipin and ADRP, are always associated with LDs. In the absence of LD, these proteins are targeted to proteasomes and degraded (Wolins *et al*., 2006; Brasaemle *et al.*, 1997; Xu *et al.*, 2005). However, other PAT proteins have alternative fates. TIP 47 and S3-12 are distributed in the cytosol when LDs are absent (Wolins *et al.*, Yamaguchi *et al.*, 2006). Data in this chapter suggest that INV may be recruited onto LDs under a lipid rich environment (re-feeding with 10% FBS and 10 μM OA), whereas INV may distribute in the cytosol when cells lack LDs.

INV contains potential caveolin binding sites and the co-localization of INV and caveolin in the presence of BFA suggested a possibility of their interaction (Figure 3.3). Src kinase regulates the localization of caveolin to LDs and also regulates caveolar endocytosis (Blouin *et al.*, 2008; Sharma *et al.*, 2004). However, INV re-localization does not alter in the presence of genistein, this may suggests that INV and caveolin are independent of their association to LDs in this model (Figure 3.8). However, a control experiment, such as detection of the efficiency of the inhibitor is required to draw a firm conclusion.

A similar model was used to dissect the potential regulators of the localization of INV to newly-synthesized LDs. My results suggest that the activity of PKC is essential for INV's re-localization to LDs. In the presence of Ro31-8220, a general PKC inhibitor, INV aggregates were observed in the cytosol, distinct from LDs (Figure 3.8 & 3.9). Notably, PKC inhibitor treatment also affects new LD formation; fewer LDs were formed in the presence of Ro31-8220 (Figure 3.9 & 3.10). PKC is believed to serve as a lipid regulated kinase, providing a signal for lipid-controlled kinase activation (eg. Akt kinase) (Newton, 2009). In addition, I found that INV could be phosphorylated by PKC *in vitro* and that one or more potential phosphorylation sites are located in N-terminal half of INV (potentially at S34 or T269) (Figure 3.13).

Protein phosphorylation is often crucial for regulating activity, localization or molecular interaction (Bartz *et al.*, 2007). Therefore, PKC may control the formation of LDs by regulating the activity of Akt and it is also possible that INV's localization is regulated by phosphorylation catalyzed by PKC. In the future, experiments using point mutations at the potential catalytic sites should be tested to identify the PKC's exact target site. It is also possible that the activity of PKC can regulate other

proteins and subsequently affect the localization of INV indirectly. Phosphorylation status is essential for many LD-associated proteins. Previous studies have shown that phosphorylated perilipin did not bind to LDs and phosphorylated hormone-sensitive lipase (HSL) was bound to LDs, and subsequently induced cell lipolysis (Londos *et al.*, 1996; Su *et al.*, 2003). In addition, Src phosphorylated-caveolin bound to LDs (Blouin *et al.*, 2008). Overall, phosphorylation of the protein (perilipin, HSL and caveolin) would suggest mechanisms for regulating LD localization and the function (Bartz *et al.*, 2007). However, some LD proteins may undergo alternative regulation process, such as by acylation. Acylation is necessary for SNAP23 (synaptosomal-associated protein) to localize to LDs (Boström *et al*., 2007). My results showed that INV dispersed in the cytosol when cells were starved, whereas INV may home to LD after re-feeding. This process appears to be strongly regulated by PKC.

Inhibition of the expression of PLD1 or ERK2 or using the specific inhibitor of ERK2, Ste-Mek1$_{13}$, prevented the insulin-promoted formation of LDs (Andersson *et al*., 2006). However, when ERK2 inhibitors were applied to the serum starvation/re-feeding model in this chapter, LDs still re-formed and the re-localization of INV to newly-formed LDs was not affected (Figure 3.12). Although this experiment was followed as per the published conditions by Andersson, it is still can not rule out the possibility that Ste-Mek1$_{13}$ may not work efficiently in this serum starvation/ re-feeding model. Thus, the further comfirmation of the inhibition efficiency of Ste-Mek1$_{13}$ is required. Besides, as a component of multiple pathways, ERK may be activated by insulin as well as by PKC. Although insulin-stimulated formation of LDs is regulated by ERK2, a different regulation may be occurring in the starvation/re-feeding model. ERK inhibition did not decrease

the re-formation of LDs in our model, suggesting that formation of new LDs is independent of ERK. Likewise, ERK inhibition also indicates that INV's localization to LD was independent of ERK. My results do not exclude the possibility that PKC can mediate ERK and its downstream signaling, however, data presented here suggest that ERK may not participate in PKC-mediated co-localization of INV with LD.

In conclusion, the aim for this chapter was to identify some of the molecules that regulate the INV's localization to LDs. My data suggest that INV is associated with LD when nutrition is plentiful. Under conditions of serum starvation, cells lost their LDs and INV disperses in the cytoplasm. When cells are re-fed (with OA/FBS), LDs were re-synthesized and INV was again observed on LDs. In the serum starvation/re-feeding model, the activity of PKC was required for the re-formation of LD and the re-localization of INV. This conclusion is strengthened by the *in vitro* kinase assay in which I showed that PKC can phosphorylate INV, possibly at one or more phosphorylation sites within the N-terminal half of INV.

Chapter 4: Studying invadolysin expression during adipocyte differentiation

4.1 Introduction

The subcellular localization of human INV on LDs was shown in the previous chapter. LDs have been implicated in playing some obvious roles, such as regulating lipid homeostasis (Smirnova *et al* 2006; Naslavsky *et al.*, 2006) and in some less obvious processes, such as cancer (Accioly *et al*., 2008) Parkinson's disease (Scherzer *et al*., 2004) hepatitis C infection (Miyanari *et al*., 2007), protein degradation (Ohsaki *et al*., 2006), and act as a transient protein storage place (Cermelli *et al.*, 2006).

Adipocyte differentiation, also termed adipogenesis, is the development of fat cells from preadipocytes. It is one of the most intensely and faithfully modeled *in vitro* processes of cellular differentiation (Rosen *et al*., 2000; Fleming *et al*., 1998). Since human INV is located on LDs (Chapter 3), the role of INV in adipocyte differentiation warrants investigation. 3T3-L1 cells are the most commonly used preadipocyte cells. When 3T3-L1 cells grow to confluence, they can be treated with a combination of hormones (including glucocorticoids and insulin-like growth factor 1/ insulin) committing the cells to undergo adipocyte differentiation (Green & Kehinde, 1974; Green & Kehinde, 1976). During adipogenesis, cells undergo gene expression changes that lead to a morphological and biochemical metamorphosis towards the adipocyte phenotype. Differentiating cells become round in shape and generate cytoplasmic droplets which accumulate lipids and are easily detected by phase-contrast microscopy (Rosen & Spiegelman *et al*., 2000). During differentiation, the size and number of LDs increases and the level of endogenous LD binding

proteins, including ADRP and perilipin is also elevated (Yamaguchi *et al*., 2004). To approach the role of INV in adipogenesis, the 3T3-L1 adipocyte differentiation model was utilized to analyze the association between INV and adipocyte differentiation.

4.2 Results

4.2.1 Invadolysin localized to lipid droplets in mouse 3T3-L1 fibroblast cells

Human INV localizes to LDs; to determine whether mouse INV is also localized on LDs, mouse fibroblast cells were used for indirect immunostaining of INV. 3T3-L1 cells were fixed and stained with an INV antibody and BODIPY, a LD specific dye. A fuzzy BODIPY staining pattern was observed in 3T3-L1 cells (Figure 4.1A), perhaps due to lower levels of neutral lipids in the LDs of this cell type. More brighter and sphere-like BODIPY staining was observed when the cells were cultured with 50 μM oleic acid (Figure 4.1B). Antibody to human INV stained 3T3-L1 cells, showing punctate staining pattern in both conditions. These punctate dots were localized to LDs (Figure 4.1A, B), suggesting that antibody to human INV can cross react with mouse INV and that mouse INV is also a LD associated protein.

4.2.2 The localization of invadolysin during adipocyte differentiation

To determine the subcellular localization of INV during adipocyte differentiation, 3T3-L1 cells were induced to differentiate to adipocytes, followed by examination of the cells for INV (Figure 4.2) or perilipin (Figure 4.3) at day 2, day 4, day 6 and day 8 of differentiation. After inducing differentiation by 3-isobutyl-1-methylxantin (IBMX), dexamethasone (DEX) and insulin, cell morphology changed and the cell medium became viscous at day 2. On the same day,

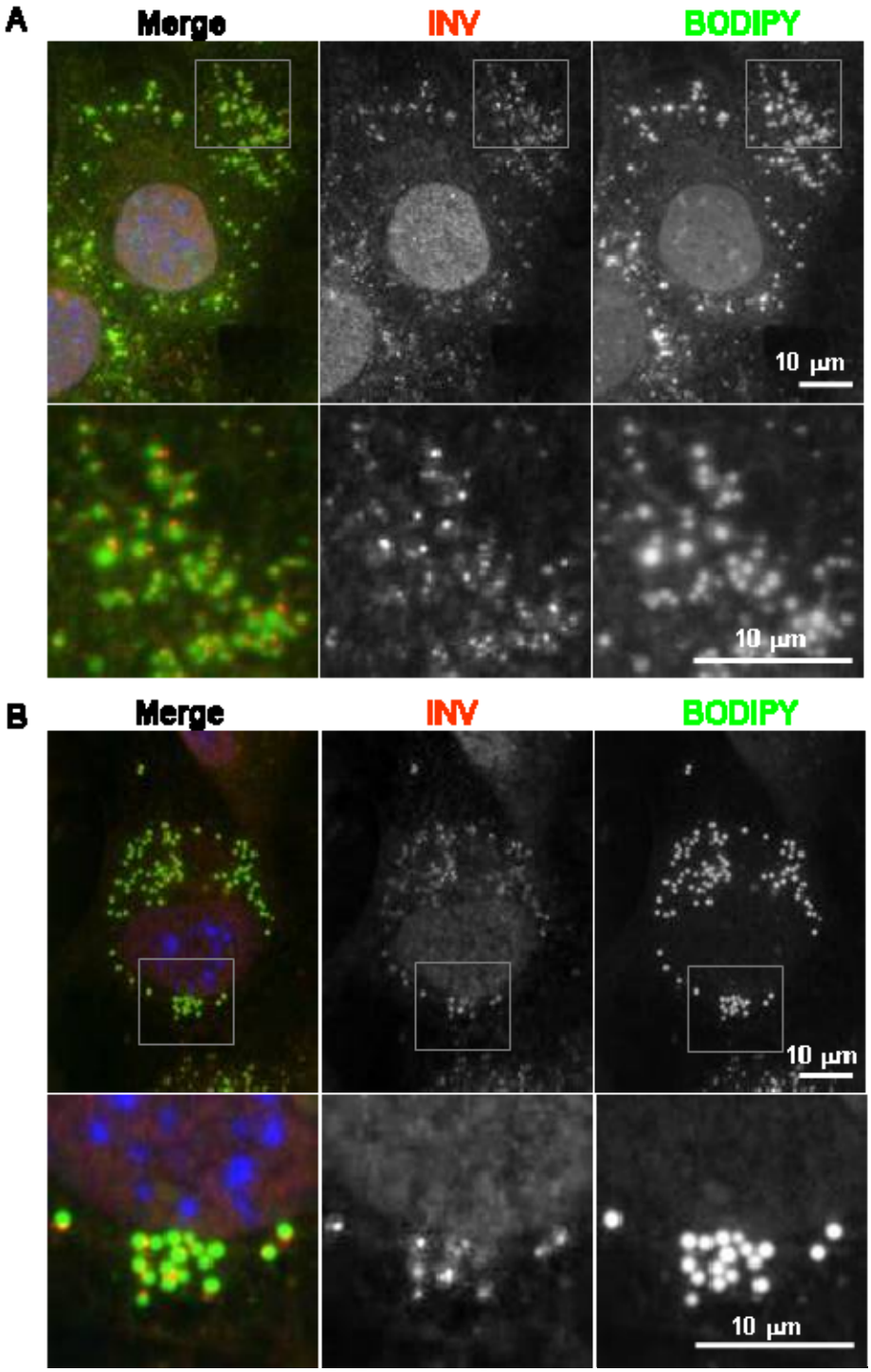

Figure 4.1 The localization of invadolysin in mouse 3T3-L1 fibroblast cells. Cells were treated without (A) or with (B) 50 μM oleic acid for 24 hours and were fixed and stained for INV antibody (red), the BODIPY (green) and DAPI (blue). Invadolysin was localized on lipid droplets in mouse 3T3-L1fibroblast cells.

endogenous INV showed a punctate staining pattern in the cytosol (Figure 4.2). At day 4, the size of LDs increased and the morphology of the cells was round. Endogenous INV displayed a cytoplasmic ring-like distribution at day 4 (Figure 4.2). At day 6, INV rings were not as obvious as day 4, however INV disperse cytoplasmic staining was observed in fully differentiated adipocytes (day 8). These data suggested that INV localized on LDs in the early stages of differentiation, whereas it disassociated from LDs in the later stages of differentiation.

Perilipin is a protein localized on LD surfaces in adipocytes and steroidogenic cells (Akther *et al*., 2008). To compare the localization with INV, 3T3-L1 cells were fixed and stained for perilipin during adipocyte differentiation. Both INV and perilipin antibody were all generated from rabbit, thus the co-staining of INV and perilipin can not be perform. When compared with INV, the endogenous perilipin showed a different localization pattern. Perilipin localized in the nucleus on day 2 of differentiation. However, it mainly displayed a ring-like distribution pattern from day 4 of differentiation (Figure 4.3).

The adipocytes were cultured in 10% FBS/DMEM until day 14 and then fixed and stained for INV and BODIPY, or perilipin and BODIPY (Figure 4.4). Under these culture conditions, small and large LDs were observed within the same adipocyte. Interestingly, INV encircled smaller LDs (Figure 4.4, arrow) rather than larger LDs, whereas perilipin still encircled every LD (Figure 4.4).

4.2.3 Invadolysin mRNA level increased significantly during adipocyte differentiation

In order to determination the changes in the mRNA level of INV occurred during differentiation of 3T3-L1 adipocytes, RT-PCR and qPCR were performed

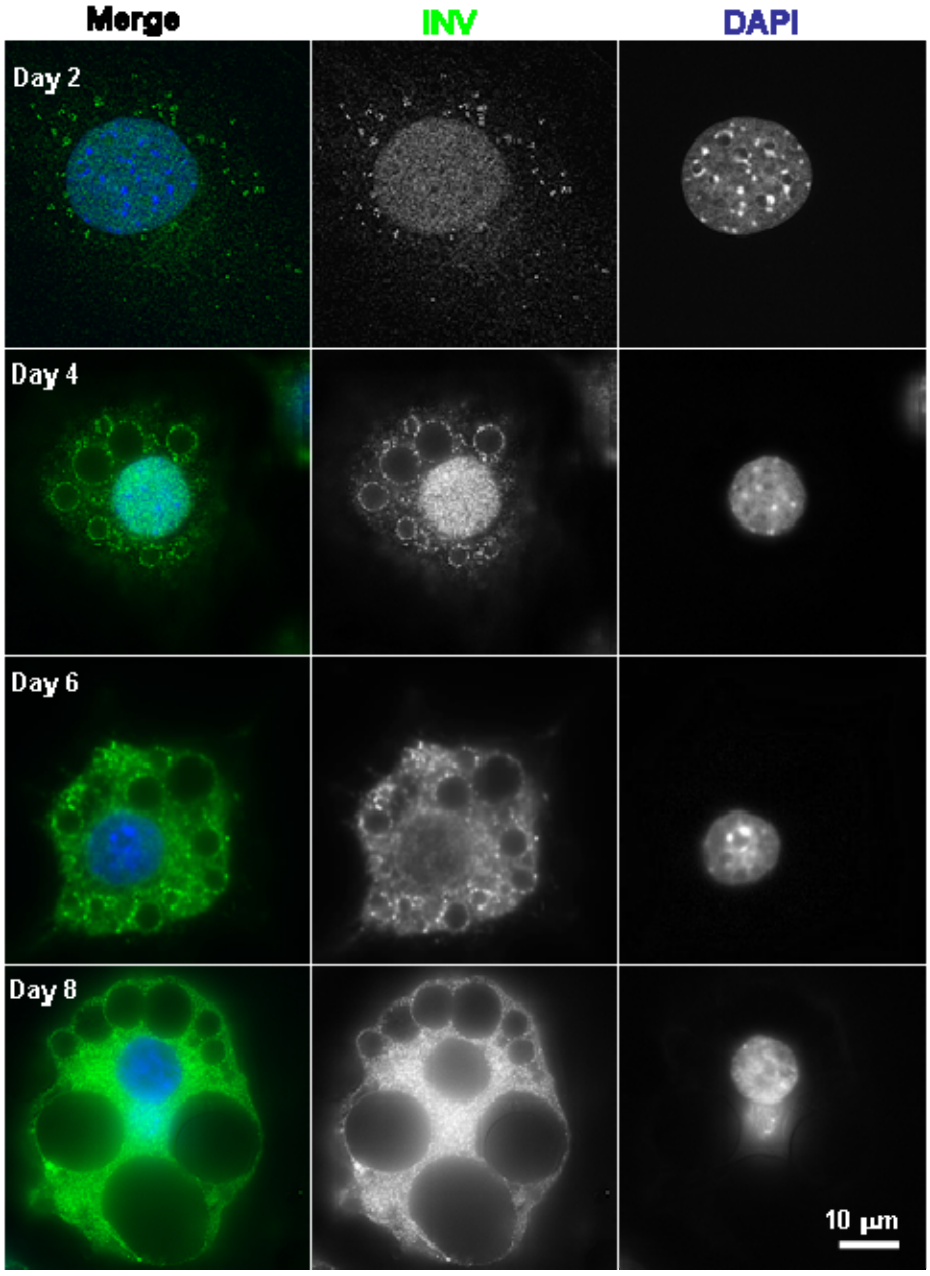

Figure 4.2 Determination of invadolysin localization during adipocyte differentiation. During differentiation, 3T3-L1 cells were fixed and stained for INV (green) and DAPI for DNA (blue). In early stages of differentiation (Day 2 and 4), invadolysin was observed around lipid droplets. At day 8, invadolysin dispersed in cytosol in fully differentiated 3T3-L1 cells.

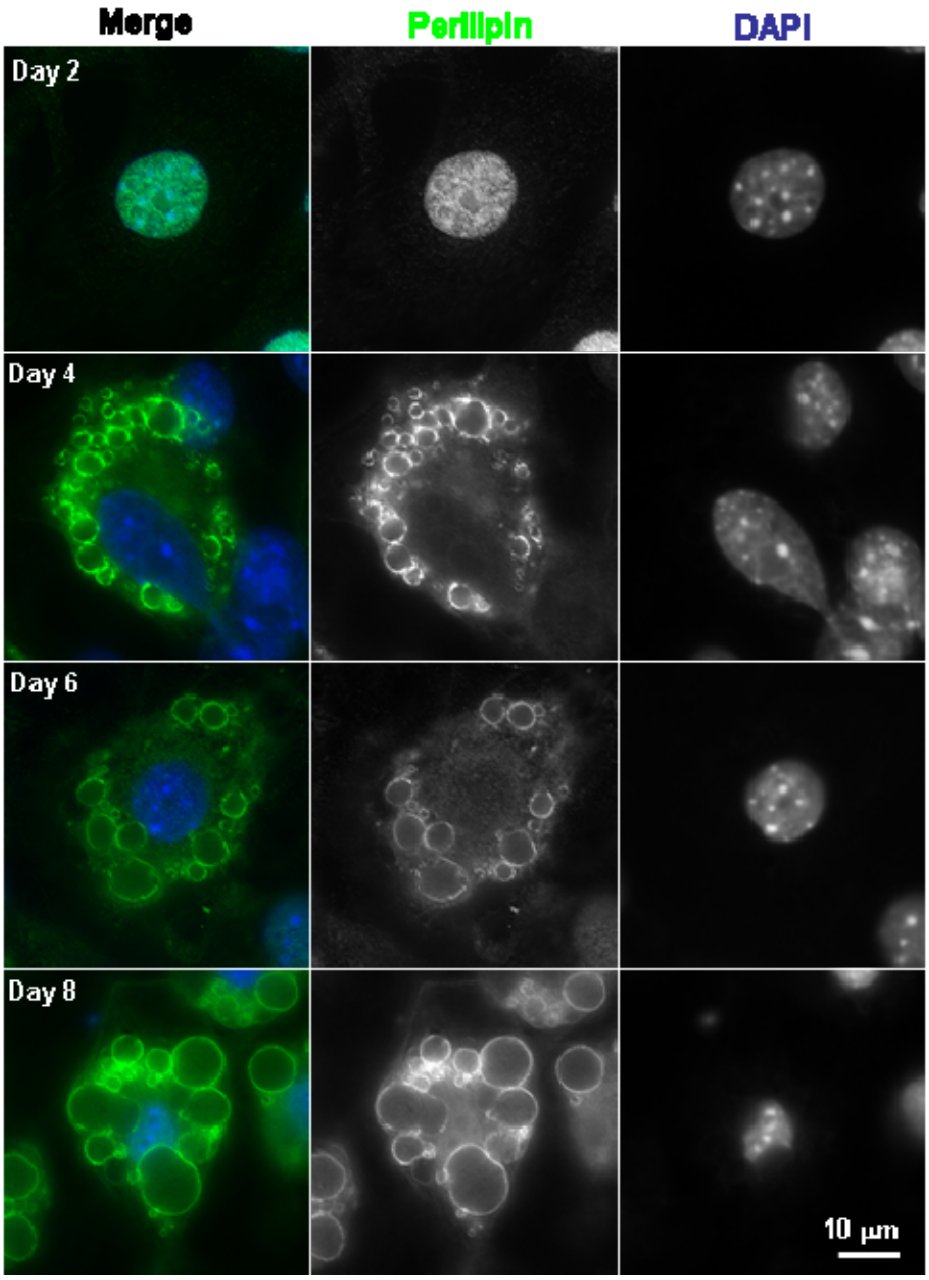

Figure 4.3 The localization of perilipin during adipocyte differentiation. During differentiation, 3T3-L1 cells were fixed and stained for perilipin (green) and DAPI for DNA (blue). Perilipin was to localize in the nucleus at day 2. After day 4, perilipin encircled lipid droplets.

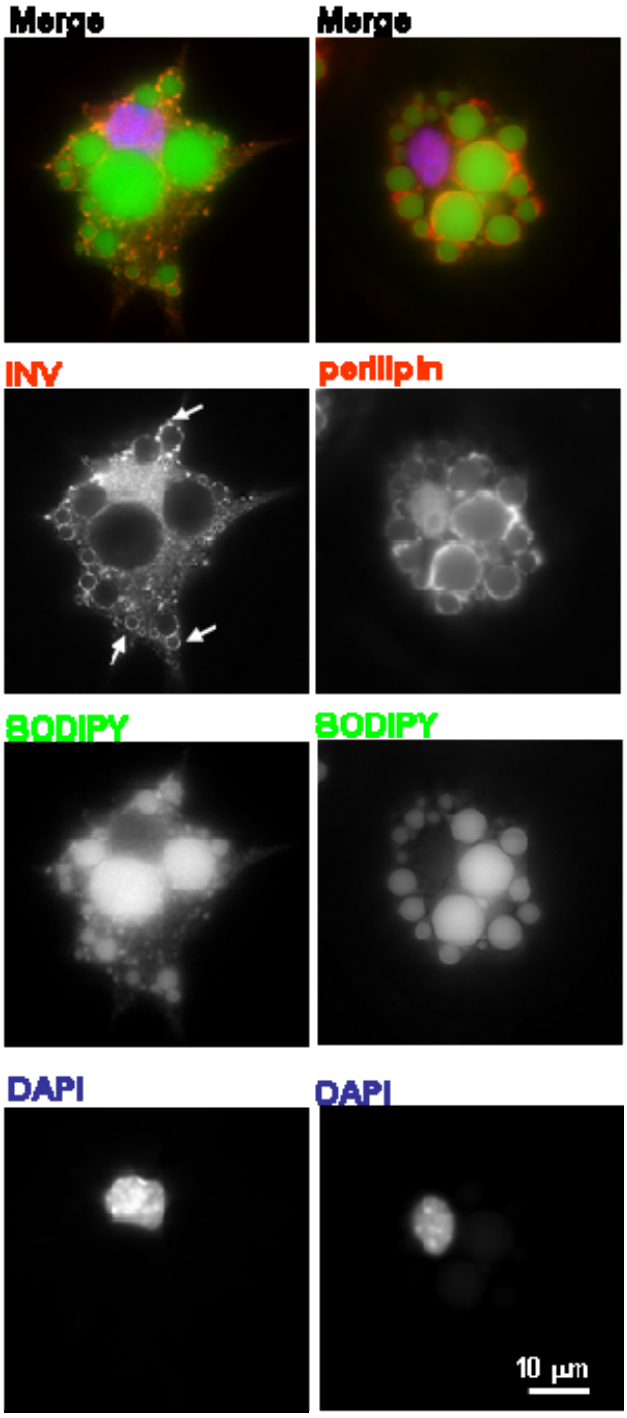

Figure 4.4 Comparison of the localization of invadolysin and perilipin in adipocyte.

Day 14 adipocytes were fixed and stained for INV (red) and BODIPY (green) or perilipin (red) and BODIPY (green). Invadolysin encircled with small LDs. Perilipin was accumulated around all LDs. White arrows were indicated that INV encircle with small lipid droplets.

using total RNA prepared from cells at day 0, day 2, day 4, day 6 and day 8. INV mRNA levels were compared with levels for perilipin and TIP 47 (PAT proteins). β-actin was used as an internal control. To control for the integrity of cDNA, four pairs of primers were designed to amplify the N-terminal (INV-A), middle (INV-B, -C) and C-terminal (INV-D) fragments of INV cDNA (Figure 4.5). At day 0 and day 2 of differentiation, INV mRNA was expressed at a low level, whereas after day 4 of differentiation, the mRNA level increased and remained constant until day 8 (Figure 4.5), the same increasing pattern was observed for the four different pairs of INV primers, indicating that the quality and integrity of cDNA prepared for RT-PCR was high. Perilipin expression is limited to adipocytes and steroidogenic cells (Brasaemle *et al*., 1997; Miura *et al*., 2002). Thus, perilipin mRNA can not be detected at day 0. However after induction to differentiate, perilipin mRNA level increased from day 2 and continued to rise (Figure 4.5). TIP 47 also shows a low mRNA level at day 0, however after induction, TIP47 mRNA levels remain constant until day 8 (Figure 4.5).

To further confirm the RT-PCR result shown in Figure 4.5, the mRNA levels of INV, perilipin and ADRP were assessed by qPCR. The expression of actin was used to normalize the expression of the above genes. The relative expression of the transcripts at various time points was further normalized to day 0 control values, in order to represent a relative-fold change of expression. Data from the qPCR experiments confirmed that the levels of INV (Figure 4.6A), ADRP (Figure 4.6B) and perilipin ((Figure 4.6C) mRNA were elevated during adipocyte differentiation. INV mRNA level increased gradually during differentiation and the mRNA level showed a 10-fold increase in adipocytes (day 8) when compared with preadipocytes (day 0). ADRP expression was strongly induced in cells increased lipid load (Chang

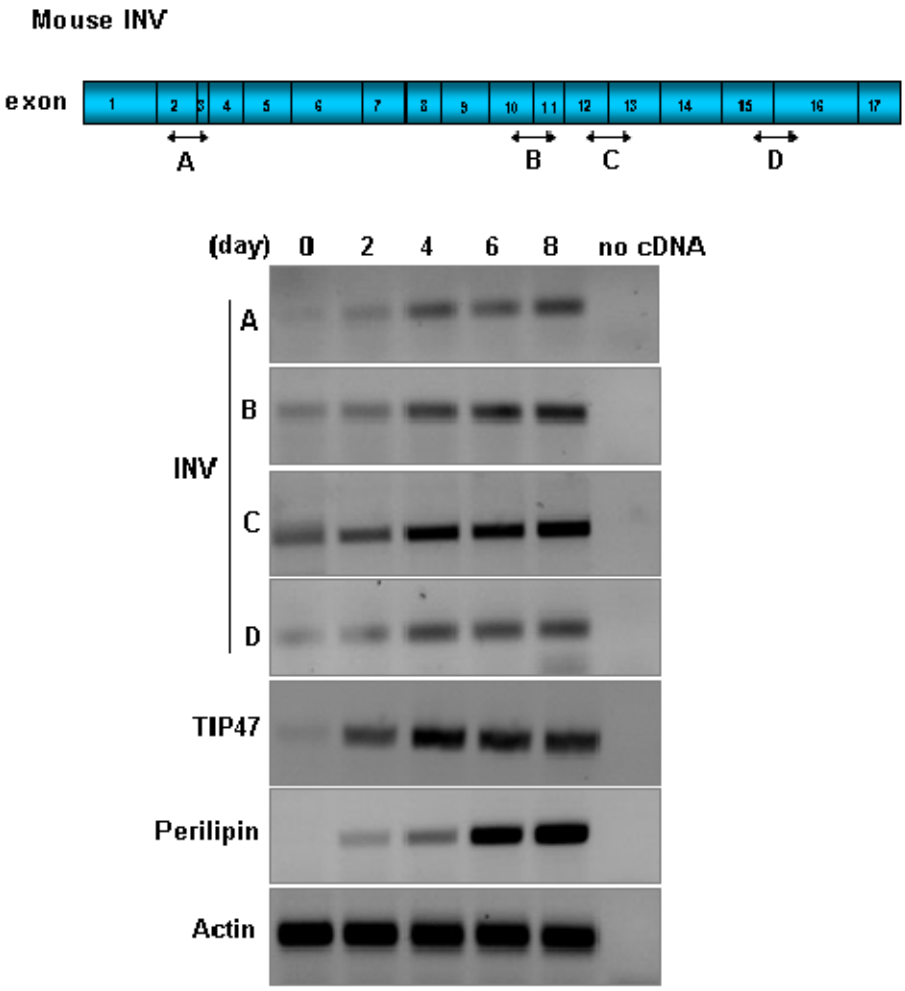

Figure 4.5 Levels of Invadolysin mRNA increase during adipocyte differentiation.

3T3-L1 cells were induced to differentiate. Total RNA was prepared on the days indicated. The expression of mRNA was examined by RT-PCR using appropriate primers. 25 cycles of PCR were performed for actin, 28 cycles for INV and perilipin, and 30 cycles for TIP47. Levels of INV mRNA appeared to increase after day 4 of differentiation.

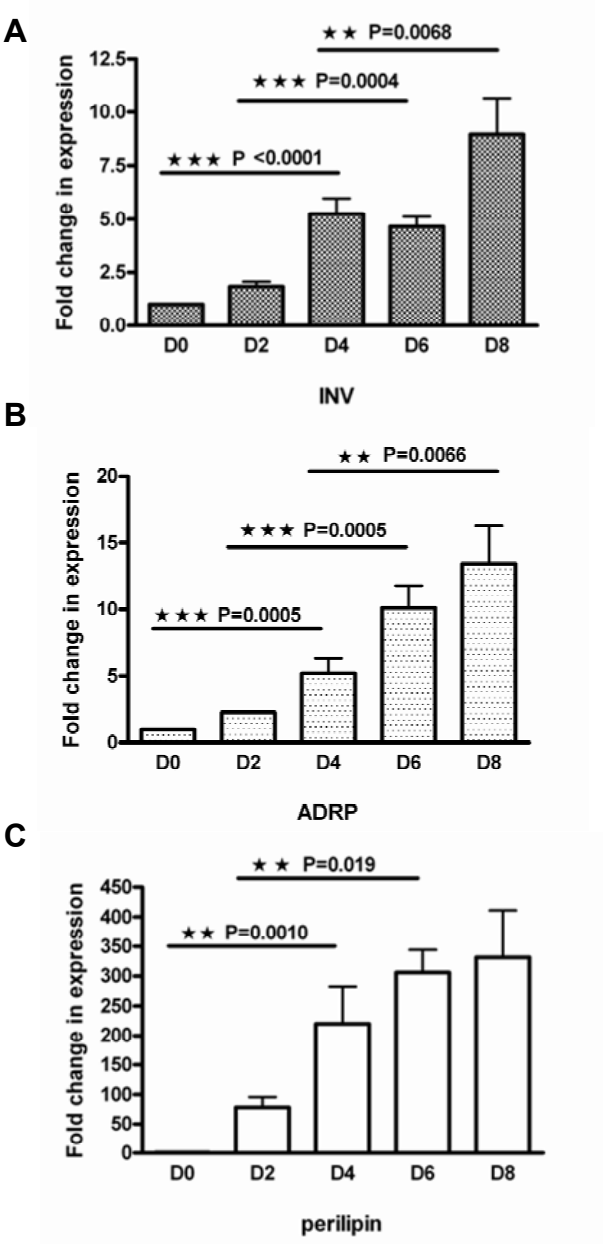

Figure 4.6 INV mRNA increases significantly during adipocyte differentiation. 3T3-L1 cells were induced to differentiate. Total RNA was prepared on the days indicated. The expression of; A) INV, B) ADRP, and C) perilipin mRNA was quantified by qPCR using appropriate primers and probes. The expression of each gene was normalized to actin and the fold-changes of expression were normalized to day 0. The data is representative of 3 individual experiments and each experiment was done in triplicate. The graph shows the mean value and standard deviation (SD) for 3 independent experiments. For comparison the difference between each day, was further analyzed by one way ANOVA (nonparametric) in 95 % confidence intervals ($P < 0.05$).

illustrated in Figure 4.6, ADRP mRNA showed a significant increase during adipogenesis, with mRNA levels rising around 15-fold as compared to preadipocyte levels. Moreover, expression of the perilipin gene exhibited a dramatic increase (100-fold) at day 2 of differentiation and continued to increase to more than 250-fold at day 4 (Figure 4.6).

4.2.4 Invadolysin protein levels are increased during adipocyte differentiation

Since INV mRNA increased during adipocyte differentiation, it was important to address whether the level of INV protein also increased. The precursor of mouse INV (mINV) is predicted to be 75 kDa (681 amino acids), with mINV processed to remove its 42 amino acid signal peptide and 28 amino acids downstream of the GPI predicted site its apparent mol. wt. should be 68 kDa. While the biosynthetic processing of INV is still unclear, it is also likely that a prodomain will be cleaved to generate active protease. The INV protein level was compared with perilipin and β-actin was used as a protein loading control. An INV antibody reportedly recognizing INV's prodomain (abcam 996, http://www.abcam.com/Invadolysin-antibody-ab58996.html) was used to probe protein extracts of differentiating 3T3-L1 cells. If a prodomain is removed, this antibody will not detect the active form of INV. In order to detect the putative processed form of INV, the 3645 antibody (raised against amino acids 188-201 of human INV (amino acids 177-190 of mouse INV) was used to probe the same protein extracts.

The results of immunoblotting show that perilipin levels began to rise at day 2 after differentiation was induced, with maximal levels reached after 8 days (shown in Figure 4.7). Using the 996 antibody to detect INV in differentiating cells, the expression of a form of INV containing the prodomain also increased dramatically

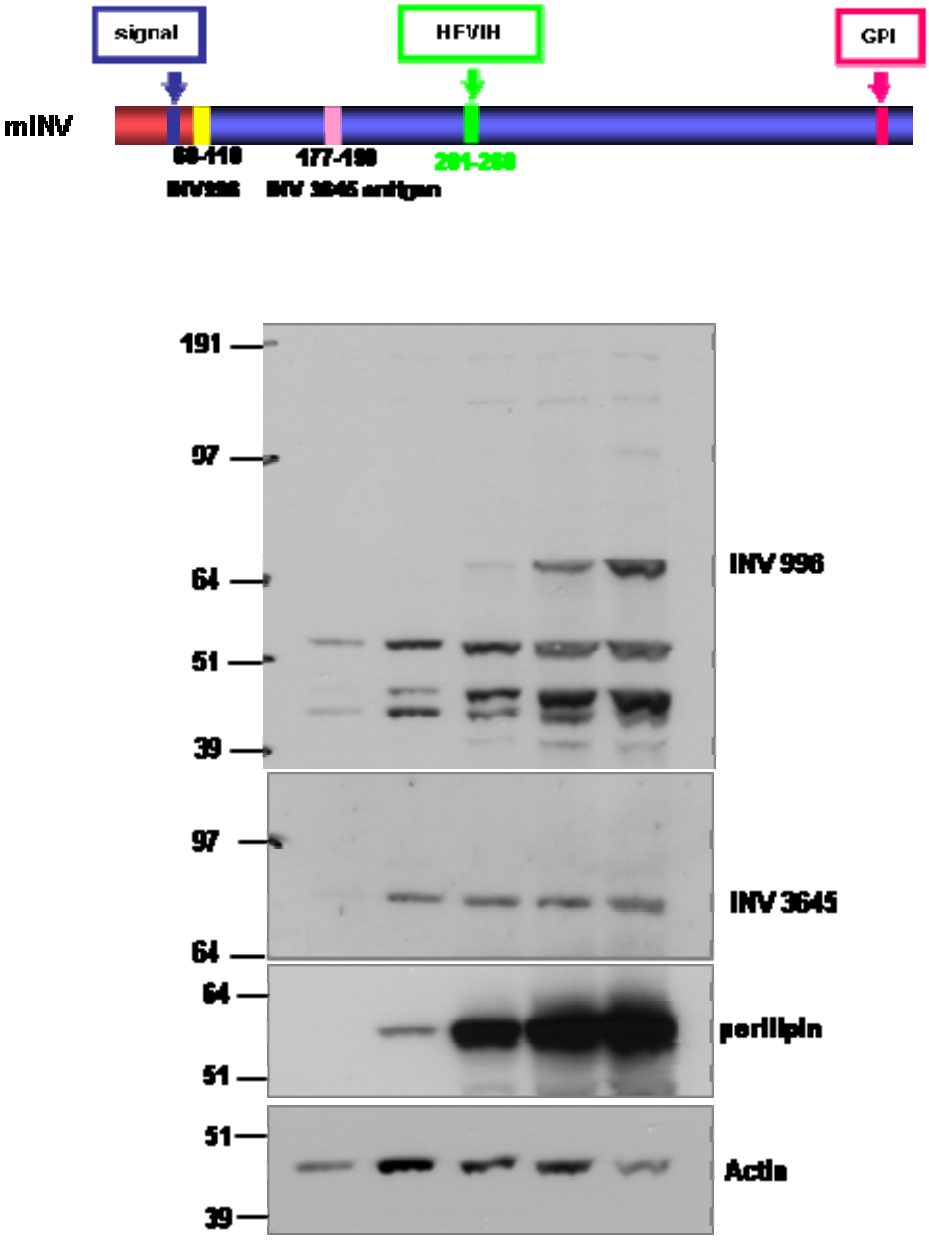

Figure 4.7 Expression of INV and perilipin is increased during adipogenesis. 3T3-L1 cells were induced to differentiate. Cell lysates were prepared on the days indicated. Protein expression was detected by immunoblotting using appropriate antibodies.

during the differentiation process. However, the putative processed INV protein recognized by the 3645 antibody appeared to remain relatively constant during adipogenesis (Figure 4.7). Thus, it is possible that the immunoblot with 996 shows an accumulation of *de novo* synthesized INV. However, it is possible that the level of processed INV (recognized by 3645) must be very tightly controlled within the cell. Whether the level of INV on isolated lipid droplets changes has not been analyzed.

4.2.5 Inhibition of adipocyte differentiation by PKC and PI3K inhibitors diminished the expression of invadolysin

To examine whether the increase of INV upon adipocyte differentiation is under the control of gene expression in adipogenesis procedure, INV levels were examined when adipocyte differentiation was inhibited pharmacologically.

As described in the previous chapter, the PKC family plays important roles in cellular signaling and various biological events such as cell proliferation, differentiation, survival and cell death (Breitkreutz *et al.*, 2007). A number of reports showed that PKC may regulate adipocyte differentiation (Fleming *et al*., 1998; McGown *et al*., 1996, Zhou *et al.* 2006). The depletion of specific PKC isoforms, via anti-sense oligodeoxynucleotides, demonstrated that PKC α, δ, and μ might exert an inhibitory influence on adipocyte differentiation (Fleming *et al*., 1998).

Previous results illustrated that INV mRNA and protein levels did not show a dramatic difference between day 0 and day 2, however a significant increase was observed between days 2 and 4. Therefore, after induction of differentiation by IBMX, DEX and insulin on day 0, the broad-spectrum PKC inhibitor Ro31-8220 was added to the cells on day 2 and incubated till day 8. The mRNA and protein extracts were prepared before inhibitor treatment on day 2, and with and without inhibitor

treatment on day 8. Afterwards, mRNA levels for INV, perilipin, TIP47 and actin were determined by RT-PCR and qPCR. Most 3T3-L1 cells in control cultures differentiated into mature adipocytes at day 8. However, in the presence Ro31-8220, cells failed to differentiate (Figure 4.8A). Consistently, the mRNA expression levels of INV and perilipin were decreased in PKC inhibitor-treated cells, whereas the TIP 47 mRNA level did not change (Figure 4.8 B, C). Furthermore, I examined INV and perilipin protein levels, with actin as a loading control. INV and perilipin were also decreased in Ro31-8220 treated cells (Figure 4.9). Taken together, these data indicate that inhibition of PKC blocked adipogenesis and diminished the expression of both INV and perilipin.

Insulin has marked effects on adipogenesis (Rosen & MacDougald, 2006). Differentiation of 3T3-L1 preadipocytes into adipocytes requires insulin or insulin-like growth factors (Smith *et al*., 1988). Furthermore, downstream components of the insulin signaling cascade are crucially important for adipocyte differentiation (Tseng *et al*., 2004; Rosen & MacDougald, 2006). Adipogenesis is repressed by the inhibition of phosphatidylinositide 3-kinase (PI3K), as well as Akt1 or Akt2 (Garofalo *et al*., 2003). Also, the presence of PI3K inhibitors completely blocks the differentiation process (Tomiyama *et al.*, 1995; Christoffersen *et al.*, 1998; Xia & Serrero, 1999). To determine whether the level of INV can be altered upon the inhibition of the adipocyte differentiation, PI3K inhibitor LY294002 was added at day 2 till day 8, to block adipocyte differentiation. mRNA and protein was prepared from cells on day 2 and day 8. As expected, adipocyte differentiation was inhibited by PI3K inhibitor treatment (Figure 4.10A). In the presence of PI3K inhibitor, the level of INV and perilipin mRNA was decreased (Figure 4.10 B, C). Whereas, TIP 47 mRNA level was increased around 2.5-fold in the present of PI3K inhibitor (Figure

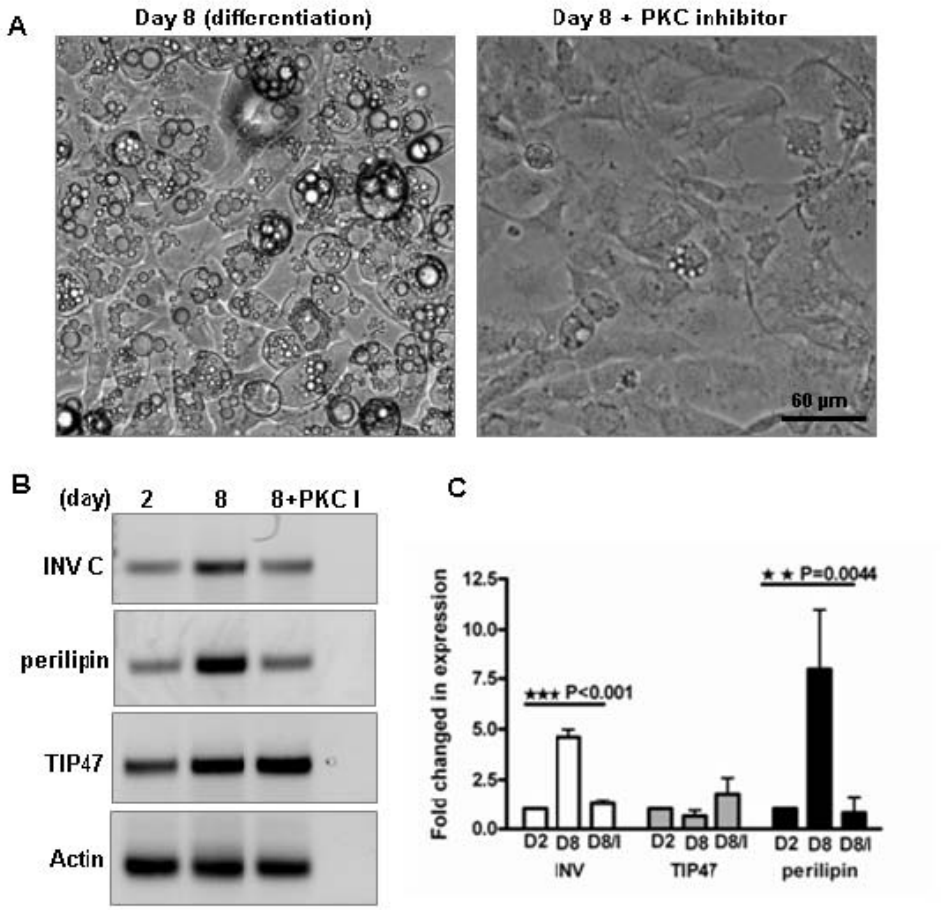

Figure 4.8 The mRNA levels of INV and perilipin were decreased with inhibition of PKC. 3T3-L1 cells were induced to differentiate to adipocytes. On day 2, cells were treated with or without 5 μM Ro31-8220 and the culture medium was replaced with fresh medium every two days until day 8. A) Inhibition of adipocyte differentiation was observed after treatment with PKC inhibitor (the image was taken by Nikon ECLipse T*i*). B) Total RNA was prepared from day 2 and day 8. The expression of mRNA was examined by RT-PCR using appropriate primers. Number of PCR cycles was 28 for INV and perilipin; 30 for TIP 47 and 25 for actin. C) mRNA expression was quantified by qPCR using appropriate primers and probes. The expression of each gene was normalized to actin and the fold changes of expression were normalized to day 2. Data are representative of 3 individual experiments and each experiment has triplicate samples. The graph shows the mean value and standard deviation (SD) for 3 independent experiments. For differential comparison the data was further analyzed by one way ANOVA (nonparametric) in 95 % confidence intervals ($P < 0.05$).

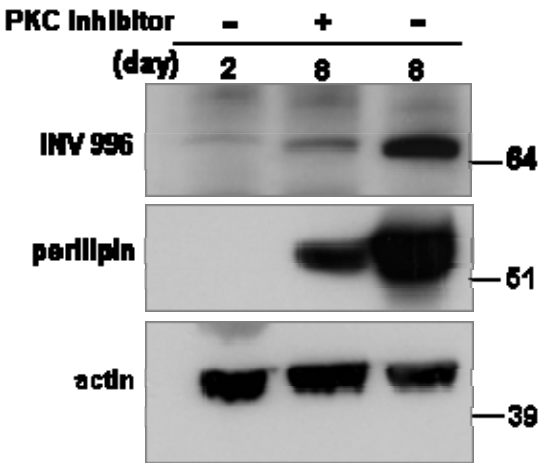

Figure 4.9 Protein levels of invadolysin and perilipin were decreased in the presence of PKC inhibitor. 3T3-L1 cells were induced to differentiate to adipocytes. On day 2, cells were treated with or without 5 μM Ro31-8220 and the culture medium was replaced with fresh medium every two days until day 8. The cell lysates were collected on the day indicated. The expression of protein was detected by immunoblotting using appropriate antibodies.

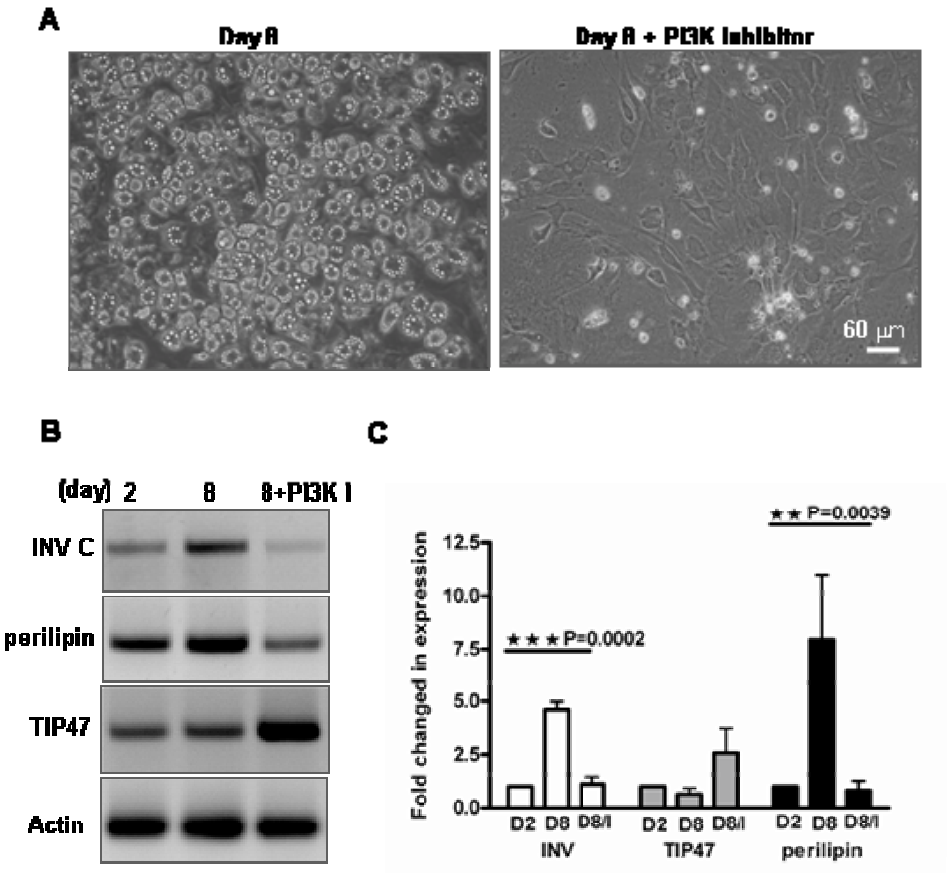

Figure 4.10 The mRNA levels of INV and perilipin were decreased with the treatment of PI3K inhibitor, LY294002. 3T3-L1 cells were induced to differentiate to adipocytes. On day 2, cells were treated with or without 50 μM LY294002 and the culture medium was replaced with fresh medium every two days until day 8. A) Inhibition of adipocyte differentiation was observed after the treatment of LY294002 (Olympus microspore was used to take the image). B) Total RNA was prepared on day 2 and day 8. The expression of mRNA was examined by RT-PCR using appropriate primers. Number of PCR cycles was 28 for INV and perilipin; 30 for TIP 47 and 25 for actin. C) mRNA expression was quantified by qPCR using appropriate primers and probes. The expression of each gene was normalized to actin and the fold changes of expression were normalized to day 2. Data are representative of 3 individual experiments and each experiment has triplicate samples. The graph shows the mean value and standard deviation (SD) for 3 independent experiments. For differential comparison, the data was further analyzed by one way ANOVA (nonparametric) in 95 % confidence intervals ($P < 0.05$).

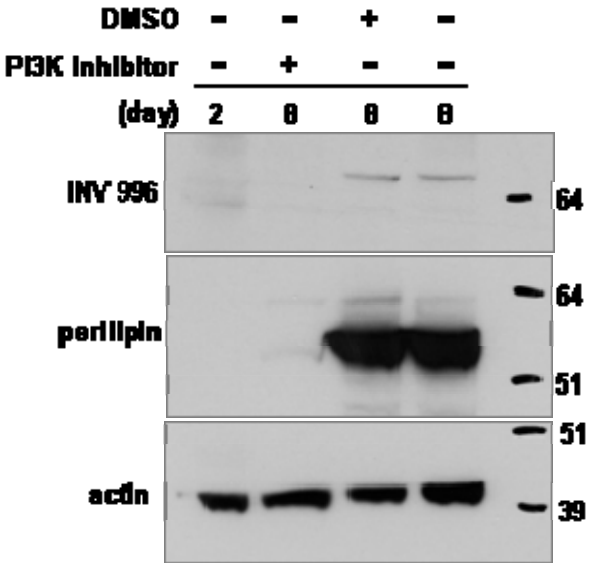

Figure 4.11 Protein levels of invadolysin and perilipin were decreased in the presence of PI3K inhibitor, LY294002. 3T3-L1 cells were induced to differentiate to adipocytes. On day 2, cells were treated with or without 50 μM LY29400 and the culture medium was replaced with fresh medium every two days until day 8. The cell lysates were collected on the days indicated. The expression of protein was detected by immunoblotting using appropriate antibodies.

4.10 B, C). To confirm that the decrease in INV and perilipin mRNA resulted in a decrease in protein level, cell lysates were blotted with INV and perilipin antibodies, with actin as a loading control. The data in Figure 4.11 show that INV and perilipin protein levels were also decreased in the presence of LY294002. These data suggest that INV and perilipin are down-regulated when adipogenesis is inhibited by treatment with PI3K inhibitors.

4.2.6 Phospho-Akt levels are decreased when PKC activity is inhibited

Treatment with both PKC and PI3K inhibitors can block adipocyte differentiation and decrease the level of INV at the mRNA and protein levels. The lipid (PIP3) produced by PI3K has been implicated as a secondary messenger which leads to the activation of Akt (Toker & Cantley, 1997). The role of Akt in adipogenesis has been demonstrated by various knock-out mouse studies (Peng *et al*., 2003; Baudry *et al*., 2006). PKCs are involved in a number of signaling pathways, including MAPK (the mitogen-activated protein kinase) (Cobb & Goldsmith 1995), Akt (Newton, 2009) and PI3K (Maines, 2007) pathways. To approach whether the treatment with PKC inhibitor in 3T3-L1 preadipocytes can modulate the activity of Akt, phospho-Akt was assessed by immunoblotting with an antibody against phospho Ser 473-Akt. Without PKC inhibitor treatment, Akt phosphorylation was observed in adipocytes. However, upon addition of Ro31-8220, which inhibits the activity of PKC, phosphorylation of Akt decreased (Figure 4.12A). Inhibition of PI3K activity by LY294002 also inhibited the activity of Akt without altering the basal level of Akt (Gagnon *et al*., 1999). As anticipated the phosphorylation level of Akt was decreased after treatment with LY294002 (Figure 4.12 B).

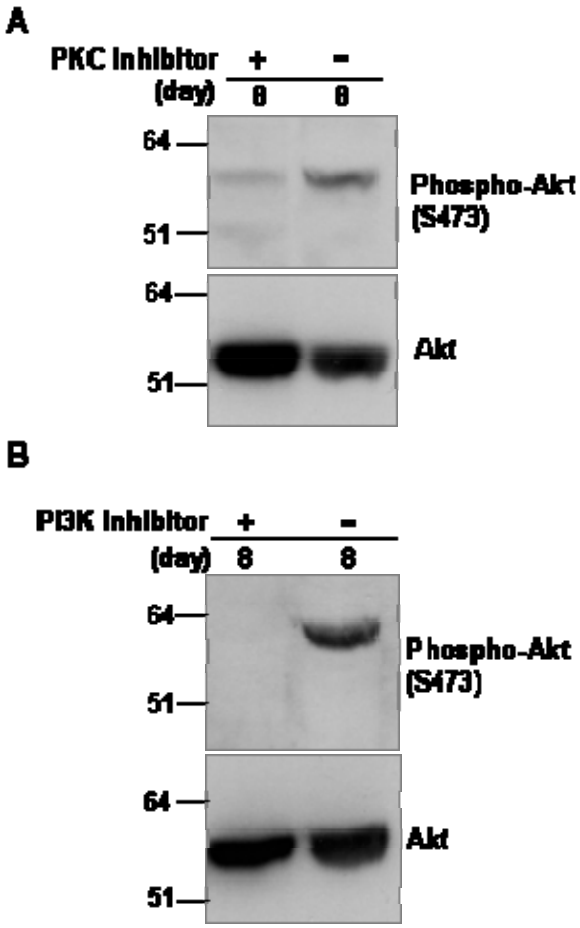

Figure 4.12 Levels of Phospho-Akt are decreased in the presence of PKC and PI3K inhibitors. 3T3-L1 cells were induced to differentiate to adipocytes. The PKC inhibitor (Ro31-8220) or PI3K inhibitor (LY294002) was added at day 2 and incubated until day 8 to block adipocyte differentiation. Cell lysates were harvested at day 8. Active Akt was detected by immunoblotting for phospho-Akt (S473).

4.3 Discussion

As INV was shown to be a LD binding protein, it is probable that INV might alter or have a role in the model system of *in vitro* adipocyte differentiation. Adipocyte differentiation is a multi-step process that requires growth inhibition by cell-to-cell contact and hormonal induction for mitotic clonal expansion, followed by accumulation of triacylglycerol storage in LDs, and subsequently differentiation (Rosen & Spiegelman, 2000). This system can therefore be used to characterize INV throughout the adipocyte differentiation process. During adipogenesis, INV exhibited a different localization pattern as compared to perilipin (Figure 4.1 and 4.3). INV appeared on LDs at day 2 and day 4 after differentiation. After the terminal differentiation stage of adipogenesis, INV's localization changed from LD to dispersal within the cytosol (Figure 4.2). However, INV still encircled small LDs on day 14 after differentiation. It is possible that the absence of INV from large LDs reflects INV release from the droplet surface during maturation or growth of LDs. Meanwhile, adipocyte differentiation was accompanied by the increase in level of PAT proteins including perilipin and ADRP. Although the function of INV in response to adipogenesis is still unclear, significant increases in INV and PAT proteins during adipogenesis suggest physiological and possible functional linkages between INV and adipocyte differentiation.

The results presented in Chapter 3 suggested that INV re-localization to newly formed LDs required the activity of PKC. It is possible that PKC activity also plays a role in regulating the localization of INV during adipogenesis. Further experiments would be required to prove this point. Levels of INV mRNA and protein significantly increased during adipocyte differentiation, whilst inhibition of adipocyte differentiation by PKC and PI3K inhibitors resulted in a decrease the levels of INV

mRNA and protein. These suggested that the increase of INV during adipogenesis might depend on the activity of PKC and/or PI3K.

Peroxisome proliferator-activated receptor γ (PPARγ) and CCAAT-enhancer-binding proteins (C/EBPs) are the crucial transcription factors that promote adipogenesis (Rosen *et al*., 2000). PPARγ sense cellular free fatty acid levels, and when high levels are detected, PPARγ drove transcription of genes involved in fatty acid metabolism, such as CD36, lipoprotein lipase (LPL) and phosphoenol pyruvate carboxykinase (Tontonoz & Spiegelman, 2008). Many adipocyte-specific proteins, including perilipin (Shimizu *et al.*, 2004; Arimura *et al*., 2004; Nagai *et al.*, 2004) and adipose fatty acid-binding protein (aP2) are also regulated by PPARγ (Nanbu-Wakao *et al*.,2000). The decrease of the expression of PPARγ in the presence of PKC and PI3K inhibitor treated cells (Zhou *et al*., 2006; Yu *et al*., 2008; Goetze *et al*., 2002) might be related to the reduction of INV and perilipin expression. To further elucidate if PPARγ regulates INV expression in adipocyte differentiation, inhibition of PPARγ by specific inhibitors, siRNA or even studies on PPARγ null mice, might help to address this question (Rosen *et al*., 1999; Barak *et al*., 1999)

An important issue remaining to be resolved is the physiological function of INV on the surface of LDs. Previous studies showed that *Drosophila INV* mutant larvae exhibit increased levels of nuclear envelope proteins, lamin Dm0, lamin C and otefin; moreover, INV cleaved lamin *in vitro* (Mchugh *et al*., 2004). The lamin A knock-out mouse exhibits both muscular dystrophy and lipodystrophy (Sullivan *et al.*, 1999). Recently, Worman's group found that lamin A acts as an inhibitor of adipocyte differentiation, possibly by affecting PPARγ and insulin signaling (Boguslavsky *et al*., 2006). Overexpression of lamin A inhibited lipid accumulation, triglyceride synthesis

and expression of adipogenic markers, subsequently affecting adipocyte differentiation. There is only one variant of INV present in mouse cells and mINV's metzincin protease motif is conserved. Thus, it is possible that mINV may also play a role in regulating lamin A level and subsequent adipocyte differentiation. Moreover, the inhibition of PKC can decrease phospho-Akt levels (Figure 4.12), which may result in the disruption of insulin signaling. Since the overexpression of lamin A has been found to decrease phospho-Akt levels and *lamin* knock-out embryonic fibroblasts have increased levels of phospho-Akt, lamin may be an inhibitor of adipocyte differentiation through affecting the phosphorylation level of Akt (Boguslavsky *et al*., 2006). Therefore, INV is a strong candidate by affecting lamin A and Akt in the adipocyte differentiation pathway.

Chapter 5: Characterization of the InR/PI3K/Akt signaling pathway in Invadolysin mutant larvae

5.1 Introduction

Previous results presented in Chapter 4 have shown that the LD associated protein, invadolysin, is increased at mRNA and protein levels during adipocyte differentiation. However, whether INV plays an active role during the process of adipocyte differentiation still remains unclear. Previous studies showed that loss of function alleles of INV led to the accumulation of nuclear proteins lamin Dm0 (B-type lamin) and lamin C (A-type lamin) in *Drosophila* (McHugh *et al.*, 2004). This data suggests that INV might regulate the protein levels of lamins. In addition, the overexpression of lamin A can inhibit lipid accumulation in mouse 3T3-L1 cells (Boguslavsky *et al.*, 2006). Notably, the overexpression of lamin A leads to a decrease in phospho-Akt level which is the active form of Akt. On the other hand, increased levels of phospho-Akt was observed in lamin$^{-/-}$ embryonic fibroblast cells, indicating that lamin A might act as an inhibitor of adipocyte differentiation (Boguslavsky *et al.*, 2006).

Akt, one of the survival kinases, is involved in the regulation of a wide array of cellular process, including cell metabolism, growth, proliferation and apoptosis (Luo *et al.*, 2003; Brazil *et al.*, 2004; Hay & Sonenberg, 2004). We observed that *INV* mutant larvae are dramatically reduced in size, suggesting that INV might be involved in the metabolic systems required for cell growth regulation. Previous studies have elucidated signaling through the insulin receptor/PI3K/Akt (InR/PI3K/Akt) pathway and suggested that InR/PI3K/Akt is the major regulator of

cell growth (Leevers & Hafen, 2004).

The InR/PI3K/Akt signaling cascade exhibits a broad range of evolutionarily conserved functions, including the regulation of cell growth, differentiation, control of lifespan and metabolic homeostasis (Buch *et al.*, 2008; Gershman *et al.*, 2007; Guertin *et al.*, 2006; Teleman *et al.*, 2008; Zinke *et al.*, 2002; Grewal, 2009). Insulin exerts its effect by binding to InR which results in phosphorylation of Akt at the activation loop site Threonine308 (Thr 342 in *Drosophila* Akt, dAkt) and hydrophobic motif site Serine 473 (Ser 505 in dAkt) by PDK1 (3-phosphoinositide-dependent protein kinase 1) and PDK2 (Cho *et al.*, 2001; Toker & Newton, 2000; Belham *et al.*, 1999). Phospho-Akt in turn influences gene expression through the transcription factor FOXO by phosphorylating FOXO at conserved Ser/Thr residues (Burgering and Kops, 2002). This leads to the retention of FOXO in the cytoplasm, thereby down-regulating the transcription of target genes (Burgering & Kops, 2002; Puig *et al.*, 2006). In addition, TOR (target of rapamycin) kinase can be activated through InR/PI3K/Akt activity (Grewal *et al.*, 2009). Phospho-Akt leads to the inhibition of TSC1 (Tuberous sclerosis complex)-TSC2 heterodimer, which then leads to the activation of TOR by GTP-bound Rheb (Ras-homolog enriched in brain). Activated TOR increases protein synthesis by phosphorylating and activating S6 kinase and by phosphorylating and inactivating the translation inhibitor 4E-BP (eukaryotic initiation factor 4E-binding protein) (Soulard & Hall, 2007) (Figure 1.12).

Invadolysin mutant neuroblasts showed increased levels of nuclear envelope proteins, lamin Dm0, lamin C and otifen in *Drosophila*. The overexpression of lamin A in mouse preadipocytes was found to result in decreased phospho-Akt levels. Thus, we hypothesized that INV might be playing a role in the regulation of Akt activity,

thus regulating downstream effects of insulin signaling. *Drosophila* has been commonly used as a genetic model to elucidate various components of the InR/PI3K/Akt pathway. *Drosophila* loss of function allele, INV^{4Y7}, was utilized to investigate the possible involvement of INV in the regulation of Akt activity in insulin signaling.

5.2 Results

5.2.1 Levels of Phospho-dAkt are decreased in INV^{4Y7} mutant larvae

Previous studies in *Drosophila* have shown an essential role of InR/PI3K/Akt signaling in linking cellular metabolism to nutritional conditions (Britton *et al.*, 2002). InR signaling is initiated upon binding of insulin to InR and subsequent recruitment of its downstream effector, Akt kinase, to the cell membrane. To examine whether INV plays a role in InR/PI3K signaling, 72-hour wild type and INV^{4Y7} mutant larvae were collected and transferred to a new vial with fresh food containing fresh yeast paste. The next day, total larval extracts were prepared and analyzed by immunoblotting. As Figure 5.1 show, a reduced level of phospho-Akt was found in INV^{4Y7} mutant larvae compared with wild type larvae, however, the basal level of dAkt did not alter, suggesting that INV may affect phospho-Akt level in *Drosophila* larvae (Figure 5.1A, B, C and D).

5.2.2 INV affects the activity of Akt downstream effectors, d4E-BP and S6K1

Insulin signaling leads to the activation of Akt, which can phosphorylate FOXO and led to the inhibition of 4E-BP (Teleman *et al.*, 2005). INV^{4Y7} larvae have reduced levels of phospho-Akt, thus we hypothesize that INV^{4Y7} mutants might have an

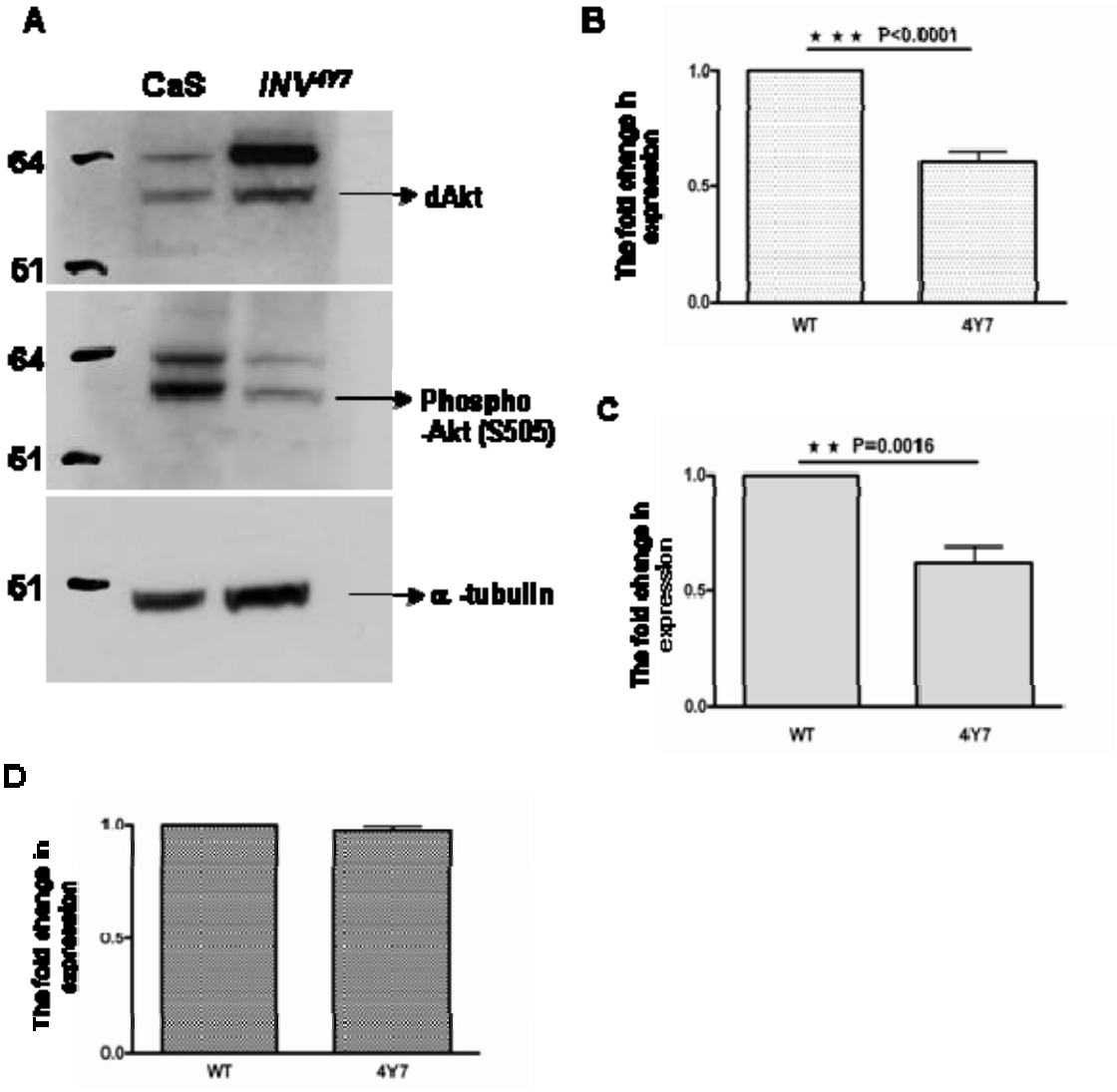

Figure 5.1 The phosphorylation level of dAkt is decreased in the *INV^{4Y7}* mutant. Protein extracts was prepared from third instar (96 hours) wild type (CaS) or *INV^{4Y7}* mutant larvae. A) Samples were resolved by electrophoresis and probes with antibodies recognizing dAkt, phospho-dAkt and α-tubulin. Immunoblotting on protein extracts revealed a decreased level of phospho-Akt in *INV^{4Y7}* mutant. Quantification of pAkt levels shown in left. B) The fold change of phospho-Akt level which was normalized to the expression of α-tubulin. C) The fold change of phospho-Akt level which was normalized to the expression of dAkt. D) The fold change of Akt level which was normalized to the expression of α-tubulin. Data represent means ± SD from four independent expression. The unpaired, two-tailed t test was used to compare the data from wild type and mutant larvae.

increased expression of d4E-BP. This was assessed by examining the at d4E-BP mRNA level in wild type and mutant *Drosophila* larvae. mRNA extracted from wild type and INV^{4Y7} mutant larvae was analyzed, with rp49 (ribosomal protein 49) used as the internal control. As we hypothesize, the expression of d4E-BP was elevated in the INV^{4Y7} mutant, suggesting that INV may be affecting the transcription of d4E-BP (Figure 5.2). Collectively, these data suggest that *INV* loss of function mutants show decreased phospho-Akt, which affects the subsequent signals including FOXO and results in the increase of d4E-BP in the INV^{4Y7} mutant.

Akt can directly phosphorylate TSC2 and block formation of the TSC1/TSC2 complex, leading to subsequent activation of TOR (Potter *et al.*, 2002; Inoki *et al.*, 2002; Manning *et al.*, 2002). S6 kinase (S6K) is a critical effector and downstream substrate of TOR (Fingar & Blenis, 2004). Knockdown of dTOR (*Drosophila* TOR) can eliminate the phosphorylation of dS6K (Yang *et al.*, 2006). Since phospho-dAkt levels were decreased in INV^{4Y7} mutant larvae, the expression of activated p70 S6 kinase was assessed in wild type and mutant larvae. As Figure 5.3 shows, a significantly reduced level of phospho-dS6K was observed in INV^{4Y7} mutant larval extract in comparison to wild type extract. As phospho-Akt regulates dTOR activity which in its turn regulates dS6K, it is reasonable that INV may affect the activity of S6K via Akt, furthermore suggesting a regulatory role for INV in insulin signaling.

5.2.3 Perilipin homolog Lsd2 is decreased in INV^{4Y7} mutant larvae

In vertebrates, triglyceride storage is regulated by conserved lipases and LD associated proteins, such as perilipin (a member of the PAT family). Perilipin can promote LD formation and its expression and activity are regulated by insulin (Vereshchagina & Wilson, 2006; Holm 2003; Prusty *et al.*, 2002; Akimoto *et al.*,

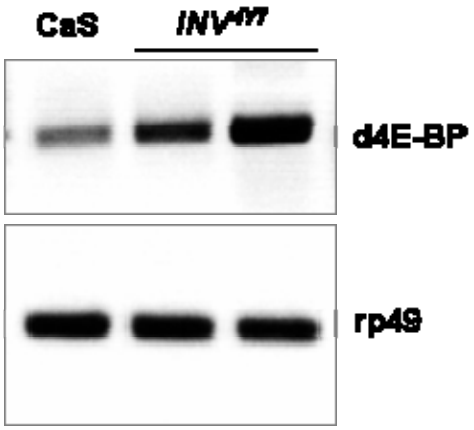

Figure 5.2 The expression of d4E-BP was elevated in *INV* ^{4Y7} mutant. Total RNA were prepared from third instar (96 hours) wild type (CaS) or *INV*^{4Y7} mutant larvae. The expression of mRNA was assessed by RT-PCR with appropriate primers. PCR were performed with 28 cycles for d4E-BP and 25 cycles for rp49. mRNA levels of d4E-BP were increased in *INV* ^{4Y7} mutant compared to wild type.

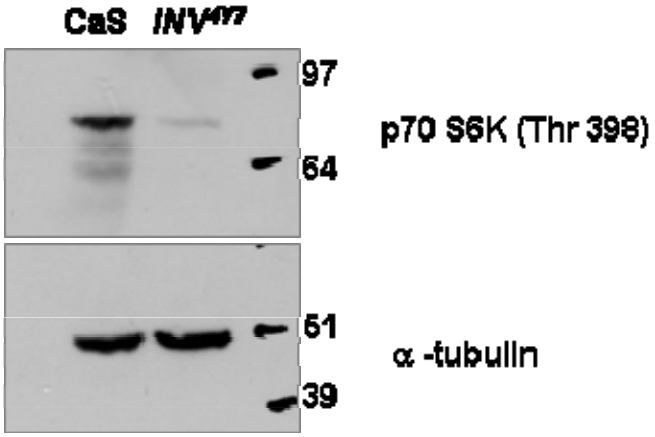

Figure 5.3 The phosphorylation level of p70S6 kinase is decreased in *INV*^{4Y7} mutant.

The 96 hour-larval protein extract from wild type (CaS) and *INV*^{4Y7} mutant were resolved by electrophoresis. Phospho-dS6K and α-tubulin were detected by immunoblotting. A decreased level of phospho-dS6K in the *INV*^{4Y7} mutant extract was observed.

2005). Two members of the PAT family in *Drosophila*, Lsd1 and Lsd2, have been identified (Lu *et al.*, 2001). Ectopically expressed GFP-tagged Lsd1 and Lsd2 can localize to LDs in *Drosophila* the fat body and in mammalian cells (Miura *et al.*, 2002), suggesting that targeting to LDs is a feature conserved between *Drosophila* and mammalian PAT members.

Akt can promote the transcription of genes involved in lipid biosynthesis and storage pathways (Eberle *et al.*, 2004). For example, Akt controls the expression of lipid storage protein, Lsd2. Ovarian nurse cells lacking *Pten,* a negative regulator of Akt, exhibit an elevated level of phospho-Akt and Lsd2 (Vereshchagina & Wilson, 2006), suggesting a potential correlation between Akt and Lsd2. The phosphorylation levels of Akt were reduced in INV^{4Y7} mutants. Thus, we hypothesized that Lsd2 expression levels might be altered in INV^{4Y7} mutants. To test this hypothesis, protein extracts from 96-hour wild type and INV^{4Y7} mutant larvae were analyzed. The level of Lsd2 protein was decreased in INV^{4Y7} larval extracts compared to wild type larval extracts (Figure 5.4).

Expression of Lsd2 was also analyzed in isolated fat body from wild type and INV^{4Y7} mutants. In *Drosophila*, the fat body is the main lipid-storage tissue similar to mammalian adipocytes, providing the major energy reserve for *Drosophila*. Fat body protein extracts prepared from the 96-hour wild type and INV^{4Y7} mutants were examined for Lsd2 level. Lsd2 protein was decreased in INV^{4Y7} mutant fat body, compared to fat body from wild type larvae (Figure 5.4). This suggests that *INV* mutants may affect Lsd2 levels, possibly through Akt.

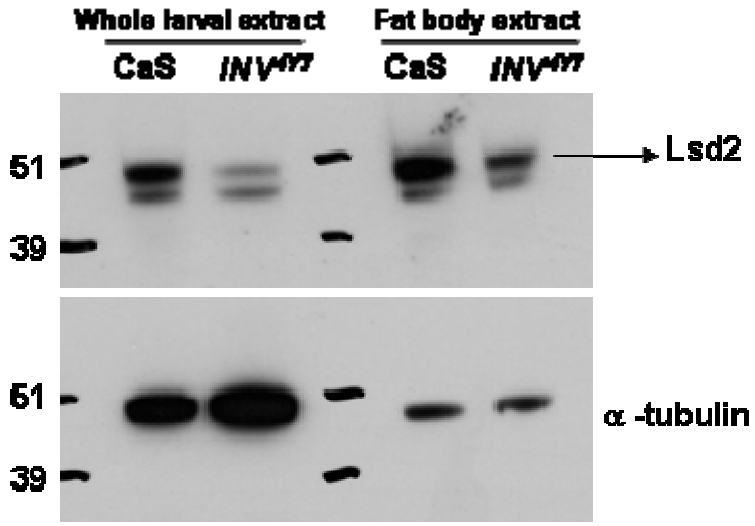

Figure 5.4 The level of Lsd2 protein is decreased in *INV*^{4Y7} mutant. 96 hour-wild type or *INV*^{4Y7} mutant larval or isolated fat body protein extracts were resolved by electrophoresis and probed with antibodies to Lsd2 and α-tubulin. Immunoblotting of protein extracts revealed a decreased level of Lsd2 in *INV*^{4Y7} mutant larvae and isolated fat body.

5.3 Discussion

According to the data presented in this chapter, I found *INV* mutant appeared to affect the phospho-Akt level and subsequently affect its downstream molecules and lipid storage protein, Lsd2 (Figure 5.5).

InR/PI3K/Akt signaling links cell metabolism to nutritional status (Britton *et al.*, 2002). Upon its activation, PI3K catalyses the formation of ptdIns(3,4,5)P3, a lipid second messenger, which subsequently activates Akt (Lizcano & Alessi, 2002). Once activated, Akt in its turn phosphorylates multiple targets, leading to numerous downstream effects (Downward, 1998). TOR is stimulated by InR/PI3K/Akt signaling (Hennig *et al.*, 2006; Martin & Hall, 2005). Furthermore, S6 kinase (S6K) and 4E-BP act as downstream effectors of TOR signaling (Martin & Hall, 2005). In INV^{4Y7} mutant larvae, the phosphorylated forms of both dAkt and dS6 kinase were found to be decreased, whereas the transcript of d4E-BP was increased (Figure 5.1-5.3). This suggests that INV may mediate InR/PI3K/Akt signaling.

The insulin signaling pathway affects sugar metabolism (Rulifson *et al.*, 2002), as well as lipid storage during *Drosophila* development (Vereshcagina & Wilson., 2006; Teleman *et al.*, 2005; Holm, 2003). Data presented in this chapter suggest that a decrease of Lsd2, a homologue of perilipin which is located on LDs, is observed in whole larval and fat body protein extracts in INV^{4Y7}. The *Drosophila* fat body is thought to act similarly to the mammalian liver and white adipocyte tissue, metabolizing nutrients and storing glycogen and lipid (Arquier & Leopold, 2007).

A recent report has demonstrated that activated cytoplasmic Akt regulates lipid accumulation in *Drosophila* ovarian nurse cells (Vereschagina & Wilson, 2006). Thus, Akt is not only involved in insulin signaling, but also in lipid storage. Decreased levels of phospho-Akt in INV^{4Y7} mutant larvae suggest a regulatory role

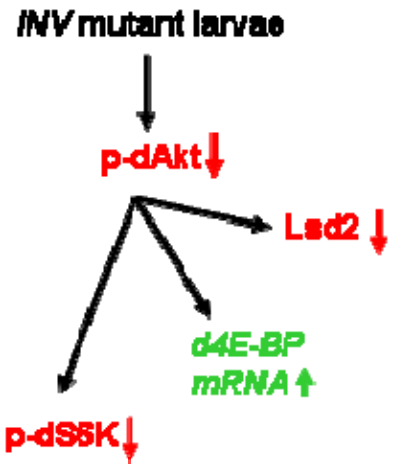

Figure 5.5 INV mutant exhibits impaired insulin signaling. A decreased level of phospho-Akt was found in *INV* mutant larvae. In addition, the activity of its downstream effector molecule S6K was decreased and d4E-BP was increased in the transcription levels. Furthermore, a decreased level of Lsd2 in *INV* mutant larvae was proved. Thus, INV might play a role in regulating cellular metabolism by affecting the insulin signaling.

for INV in insulin signaling and lipid storage in *Drosophila*. Moreover, Lsd2 is regulated by phospho-Akt (Vereschagina & Wilson, 2006). The decrease in Lsd2 in INV^{4Y7} mutants may result from the decrease of phospho-Akt (Fighre 5.4).Thus, we can conclude that the *Drosophila* nurse cell may not be the only place where Akt regulates lipid accumulation. Via Akt, INV seems to contribute to lipid metabolism.

Another recent report has demonstrated that Bride of sevenless (BOSS), a G protein couple receptor, has impaired insulin signaling that affects sugar and lipid metabolism (Kohyamma-Koganeya *et al.*, 2008). During insulin signaling, Akt mediated phosphorylation of FOXO leads to its retention in the cytoplasm and phospho-FOXO is unable to trigger transcription of its target genes (Teleman *et al.*, 2005). The active (non-phosphorylated-) FOXO can translocate into the nucleus and trigger the transcription of 4E-BP which subsequently controls lipid metabolism (Teleman *et al.*, 2005; Baker & Thummel, 2007). *Drosophila* d4E-BP mutants are sensitive to nutritional starvation. They have an impaired frequency of survival under starvation conditions due to aberrant lipid metabolism (Teleman *et al.*, 2005). I observed an increase in d4E-BP transcript in INV^{4Y7} mutants (Figure 5.2). And interestingly, INV^{4Y7} mutant larvae can survive longer than wild type larvae under conditions of starvation (E. Duca, personal communication).

Taken together, correlations between INV and metabolic-mediated components suggest that INV might play a role in cellular metabolism. In the light of these data, we might speculate that INV is involved in the cellular homeostasis of metabolism, possibly by affecting the InR/PI3K/Akt signaling pathway.

Chapter 6: Tagging invadolysin for studies of localization

6.1 Introduction

Overexpression of wild type and mutant forms of a protein of interest in cells can help to decipher the localization and function of the protein. For example, overexpression of wild type adipose triglyceride lipase (ATGL) has been found to localize to LDs and resulted in a decreased size of LDs, whereas overexpression of the catalytically-dead form of ATGL did not affect the size of LDs (Smirnova *et al.*, 2006). To date, four invadolysin variants have been found in human cells (Figure 1.4). Human invadolysin variant 1 froms (HsINV.v1 +/-37aa) are predicted to encode a signal sequence at the N-terminus and a GPI modification site at the C-terminus. The signal sequence should direct the protein's synthesis to the ER through docking of the Signal Recognition Particle and the C-terminal GPI anchor modification site should modify the protein for insertion into a membrane (Pollard & Earnshaw, 2002). The N-terminus of human invadolysin variant 2 forms (HsINV.v2) is translated in a different reading frame from the first exon of variant 1. HsINV.v2 lacks the predicted signal sequence and therefore would be predicted to display a different intracellular localization. Each of these variants is present in two alternative forms differing by the presence or absence of 37 amino acids encoded by exon 12. A previous study has shown that GFP-tagged full length INV (INV.v1-GFP) could accumulate on some vesicles in the cytosol (McHugh *et al.*, 2004), therefore INV variants were examined for their localization in human cells by the overexpression of tagged fusion proteins.

6.2 Results

6.2.1 Ectopic expression of GFP-tagged invadolysin in HeLa cells

There are four variants of INV in human cells (Figure 1.4). We postulate that these variants could play different roles in human cells based on possible different localizations. To address this question, GFP fusions of different INV constructs were made (Figure 6.1). Different cDNAs encoding full-length INV variants were subcloned in-frame into a CMV (cytomegalovirus) promoter-driven GFP-tagged expression vector (Figure 6.1). HeLa cells were transiently transfected with C-terminally GFP-tagged full length INV plasmids and then cells were fixed and stained for actin and DNA. Three variants of INV with C-terminal GFP (INV.v1:GFP, INV.v1△37:GFP and INV.v2:GFP) showed similar localization patterns. They all located in the cytoplasm with signal around the nucleus (Figure 6.2). These constructs of INV variants fused to GFP at the C-terminus did not appear to show cytosolic accumulation on vesicles.

To further confirm the protein expression of those INV variants with GFP tags, cell lysates were prepared at 24 hours after transfection and blotted with an antibody to GFP. A 26 kDa GFP band was observed in lysates prepared from empty GFP vector transfected cell (Figure 6.3). The size of INV variants (without processing) with GFP should be around 100 kDa. However, the proteins can not be detected by GFP antibody. If normalized to the background proteins in the GFP control lane, it is hard to detect full length INV variants with a GFP antibody, suggesting that the protein is unstable and does not accumulate to appreciable levels.

6.2.2 INV.v1-GFP is degraded through the proteasomal pathway

As described above, it was puzzling that GFP could be observed in transfected cells by immunofluorescence, but that the protein expression could not be detected

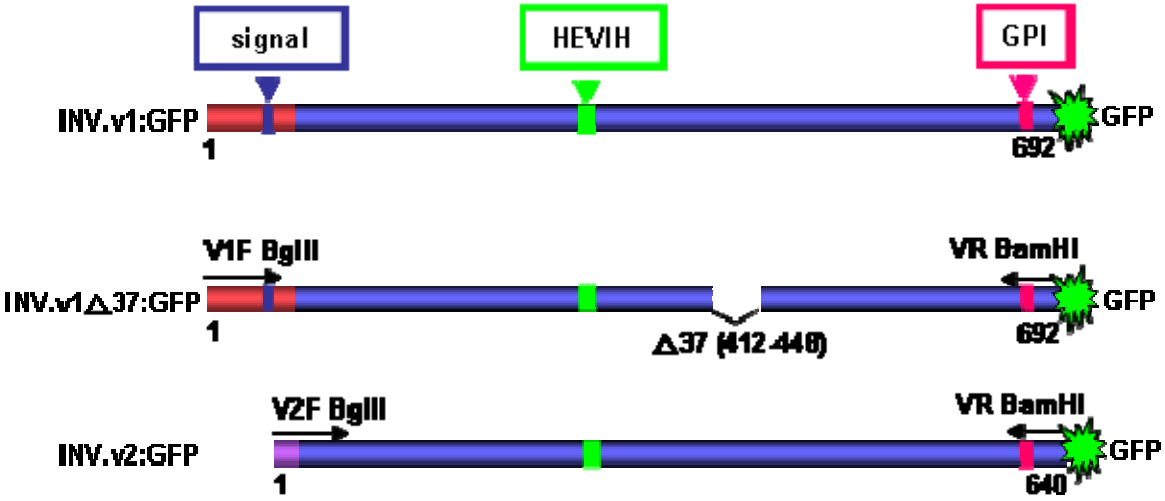

Figure 6.1 Cloning full length invadolysin variants into pEGFP-N1 mammalian transfection vector. The cDNAs of different variants were amplified from EST cDNA clones by appropriate primers with restriction enzyme sites and then cloned in-frame into pEGFP-N1 vector (INV.v1:GFP plasmid was constructed by Brian McHugh). There is a predicted signal sequence and GPI anchor site localized at the N- and C- termini of INV. HEVIH is the metalloprotease catalytic site of INV.

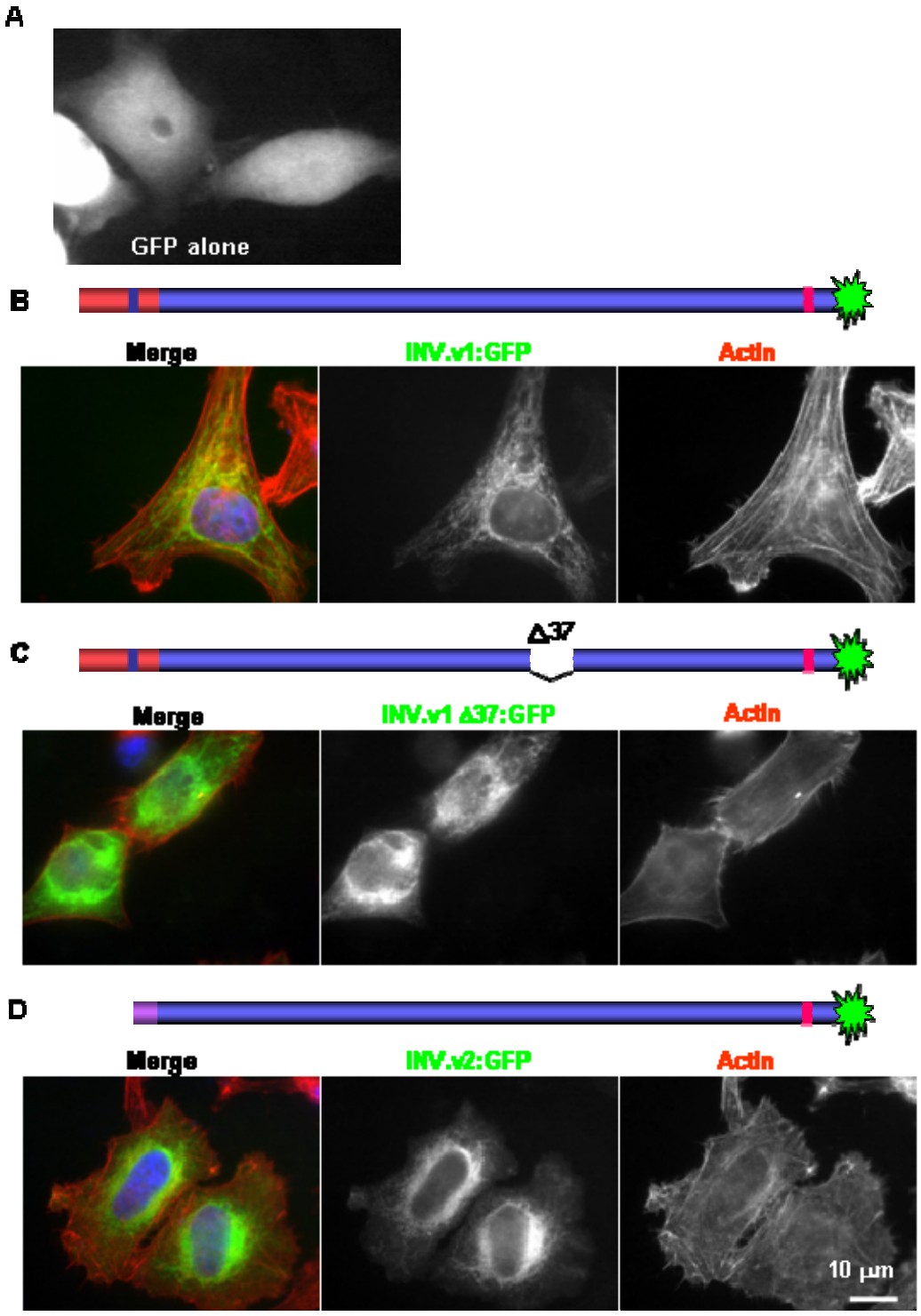

Figure 6.2 The localization of A) GFP, B) INV.v1:GFP, C) INV.v1Δ37:GFP and D) INV.v2:GFP in HeLa cells. HeLa cells were transiently transfected by electroporation with different variants of INV:GFP fusion protein constructs. The cells were fixed at 24 hours after transfection and doubly stained with Rhodamine-conjugated phalloidin (red) and DAPI (blue).

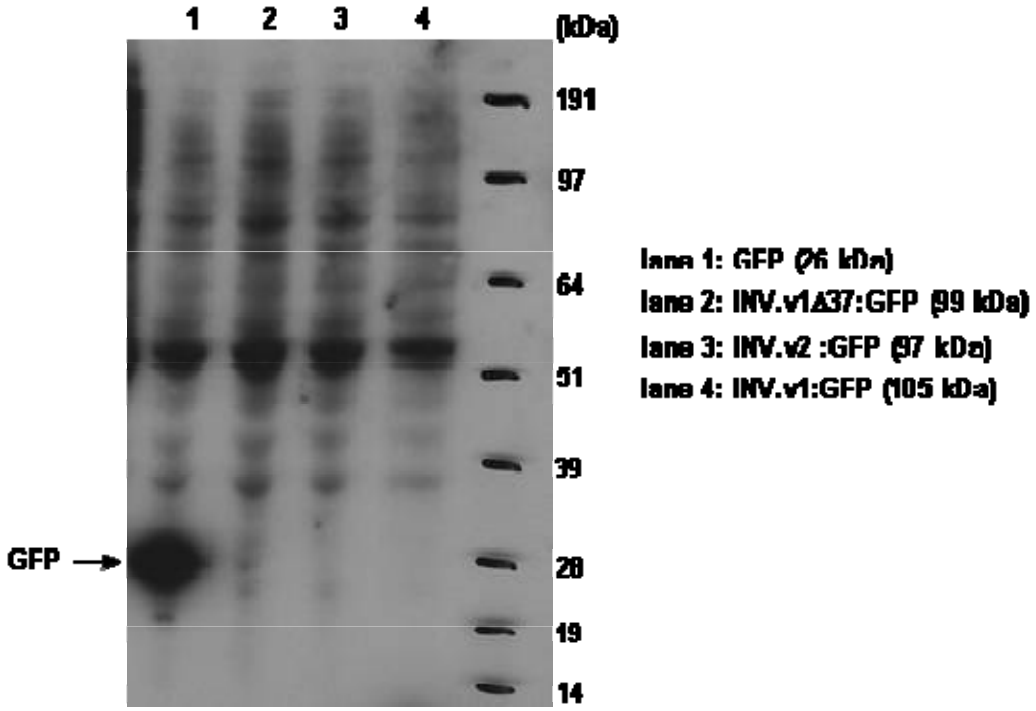

Figure 6.3 Detection of the expression of INV GFP-fusion proteins by immunoblotting. HeLa cells were transiently transfected with GFP vector only, INV.v1Δ37:GFP, INV.v2:GFP and INV.v1:GFP. At 24 hours after transfection, cells extracts were prepared and resolved by SDS-PAGE, followed by immunoblotting with a GFP antibody. The size of the GFP tag is around 26 kDa and GFP tagged INV fusion proteins should be around 100 kDa. INV fused to GFP could not be detected by immunoblotting.

by immunoblotting. The N-terminal signal sequence is present in INV variant 1, which should be cleaved off by a signal peptidase and the C-terminus of INV might be cleaved off after GPI addition. INV variants were fused to GFP at the C-terminus (Figure 6.1). Thus, it is possible that the C-terminal protein of INV including GFP was cleaved off and GFP may have remained in the ER membrane. Another possibility is that INV-GFP fusion proteins may be accumulating in the ER and Golgi due to the protein being highly expressed or improperly folded, followed by degradation.

The ER-associated degradation (ERAD) pathway is involved in the degradation of incorrectly folded proteins. Ubiquitin is an 8-kDa peptide that is ubiquitously found in all eukaryotes. Typically, ubiquitin or the polyubiquitin chain is covalently conjugated to a target protein to form a poly-ubiquitinated protein complex, which is delivered to and degraded by the 26S proteasome (Ciechanover & Schwartz, 1998; Wilkinson, 1999; Wilkinson, 2000). To examine whether proteasomal activity was involved in the processing of INV.v1:GFP, MG132, a specific proteasome inhibitor, was used to treat cell after transfection. MG132 does not prevent ubiquitination but it blocks ubiquitinated proteins from attaching to the proteasome and being degraded. HeLa cells that express INV.v1:GFP or GFP were treated for 16 hours with MG132 (2.5 μM). GFP expression (INV.v1:GFP & GFP) was analyzed by immunoblotting with the GFP antibody. The expression of GFP was not affected by MG132 treatment. While, INV.v1:GFP protein was absent without MG132 treatment, INV.v1:GFP protein accumulation was apparent in cells treated with MG132, suggesting that INV.v1;GFP protein may be degraded by proteasomes right after or during translation (Figure 6.4). To further confirm that INV.v1:GFP was degraded in proteasomes, GFP or INV.v1:GFP transfected cells were treated with different

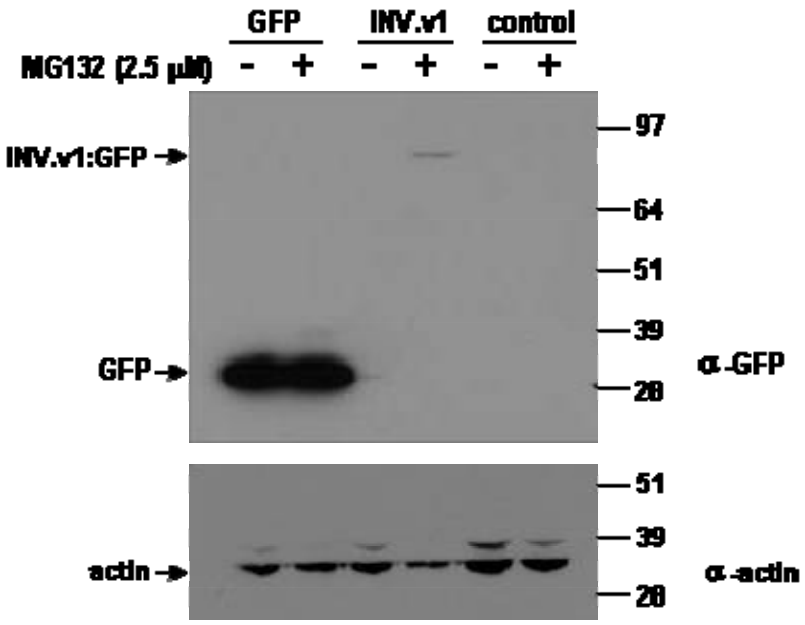

Figure 6.4 INV.v1:GFP fusion protein was degraded in proteasomes after transfection. HeLa cells were transiently transfected with GFP vector only and INV.v1-GFP. After 4 hours of transfection, cells were incubated with or without 2.5 μM proteasome inhibitor (MG132) for 16 hours. Cell lysates were harvested and resolved by SDS-PAGE, followed by immunoblotting with GFP and actin antibodies. INV.v1:GFP protein accumulated in the presence of the proteasome inhibitor.

concentrations of MG132. The expression of GFP alone did not alter with different concentrations of MG132. On the other hand, INV.v1:GFP protein accumulated in a MG132 dose-dependent manner (Figure 6.5). The MG132-stablizing effect was evident at 1 μM of MG132, and higher at 10 μM. These results provide good evidence that INV.v1:GFP may be degraded through the proteasomal pathway. Hence, an alternative position or different vector (not an overexpression system) for tagging proteins should be considered.

6.2.3 Positioning tags in region 2 of invadolysin

The transcription level of human INV.v1 suggests it is the most prevalent variant of the four so far (Cobbe *et al.*, submitted). Besides, INV.v2 does not appear to be encoded in species other than orang-utan (Cobbe *et al.*, submitted). Thus, the following experiment was focused on human INV.v1. Human INV.v1 contains a predicted N-terminal signal sequence and a GPI anchor site in the C-terminus. Therefore, it is possible that the N- and C-termini of INV might be cleaved off through post-translational modification. Thus, inserting a tag in the middle of INV might offer another way to study the localization of the different variants.

INV belongs to the M8 class of zinc-metalloproteases with sequence homology to leishmanolysin (GP63) from the pathogen *Leishmania major*. Comparison of INV sequences from the *Caenorhabditis elegans*, human, mouse and *Drosophila* with leishmanolysin reveals that there are 9 relatively conserved regions shared amongst the worm, human, mouse and fly orthologues but absent from the leishmanolysin sequence (Mchugh *et al.*, 2004). The structure of GP63 further implies that these regions should lie on the surface of the folded protein (the black numbered spheres) (Figure 6.6 A, McHugh *et al.*, 2004). The region 2 (QCRVYRGGKWPHAGVPDQ)

was

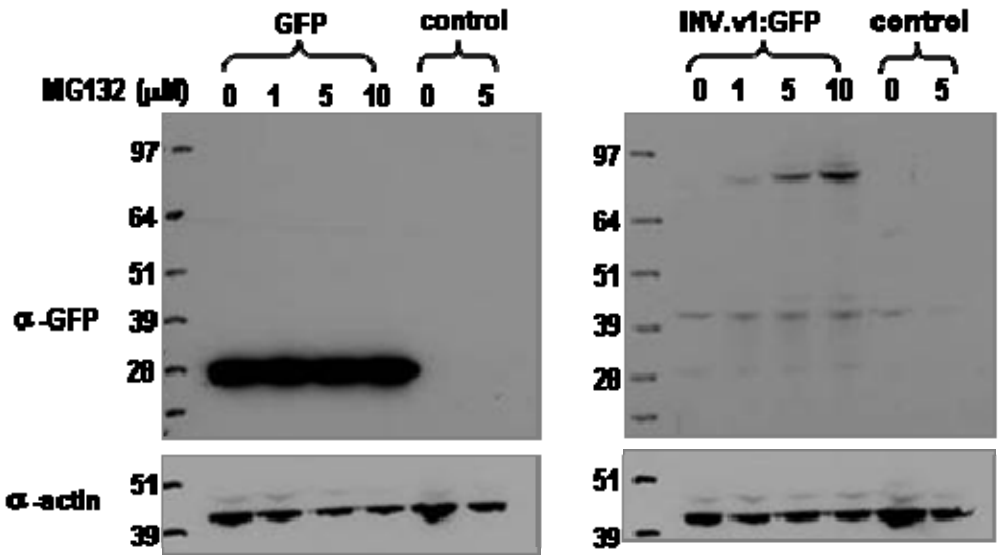

Figure 6.5 The degradation of INV.v1:GFP fusion protein is MG132 dose dependent. HeLa cells were transiently transfected with GFP vector and INV.v1:GFP. At 6 hours after transfection, cells were either untreated or treated with different concentrations of MG132 for 16 hours. Cells lysates were then prepared and resolved by SDS-PAGE, followed by immunoblotting with GFP and actin antibodies. Increasing concentration of MG132 caused an increase in the total amount of INV.v1:GFP protein.

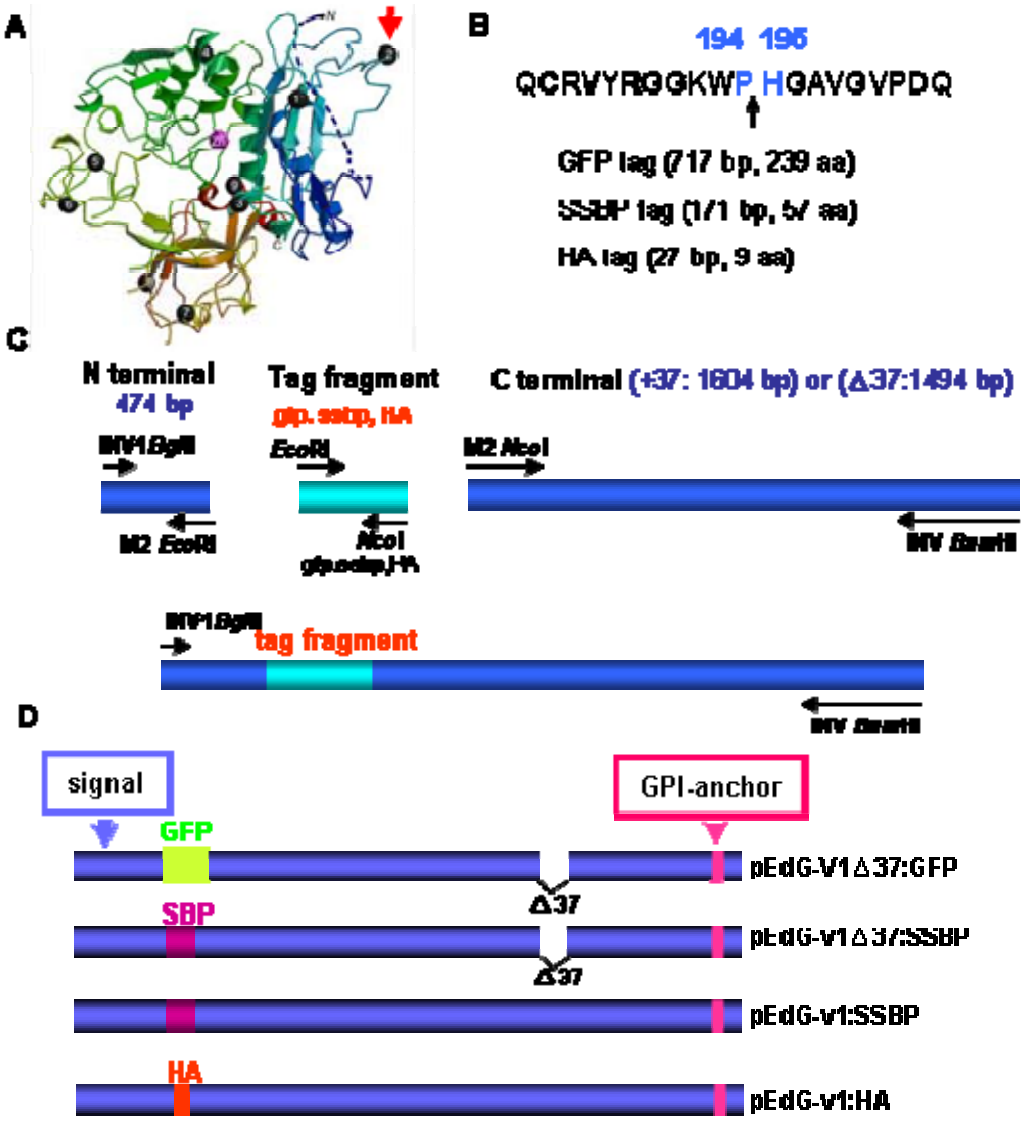

Figure 6.6 Insertion of GFP, SSBP and HA tags into region 2 of invadolysin. A) The three-dimensional structure of leishmanolysin. The black numbered spheres represent the higher eukaryotic sequences, the red arrow represent the position of the region 2. B) The protein sequence of the region 2 of human INV. The tag was inserted between a proline and a histidine. C) The strategy for cloning. Three individual fragments were made by PCR, except the HA tag fragment (HA tag oligonucleotides were annealed following the protocol described in Materials and Methods). The three fragments were combined by ligation. The full length cDNA constructs of invadolysin with GFP, SSBP and HA tag were amplified by PCR again and subcloned in-frame into pEdG vector. D) The INV constructs used for further analysis.

exposed on the surface of INV, based on the predicted INV structure. Therefore, we decided to place a tag in the middle of region 2 for further assessment (Figure 6.6 B).

Tags were inserted by PCR technology, as there is no appropriate restriction enzyme site at the required position. Thus, the N-terminal (amino acid sequence from 1-194) of INV was amplified by INV1 *Bgl*II / M2 *Eco*RI primers. The C-terminus of INV sequence (amino acids 195-692) was amplified by M2 *Nco*I / INV *Bam*HI primers (Figure 6.6 C). GFP (717 bp) and SSBP (S-tag + Streptavidin Binding Peptide tag, 171 bp) were amplified using primers containing the *Eco*RI and *Nco*I sites. HA tag only contains 27 bp, thus the primer was annealed by temperature gradient (described in Chapter 2, 2.7). Once the three fragments were ready, the fragments were mixed and ligated by T4 DNA ligase. The ligation products were amplified by INV1 *Bgl*II /INV *Bam*HI to obtain full length INV containing the tag in the region 2 and then subcloned in-frame into pEdG vector (after removal of GFP from the pEGFP-N1 vector) (Figure 6.6 C). Finally, four different constructs were obtained: v1△37:GFP, v1△37:SSBP, v1:SSBP and v1:HA (Figure 6.6 D).

6.2.4 The localization of INV with GFP, SSBP and HA tag in region 2 of INV

In order to determine the localization of v1△37:GFP, this construct was transfected into HeLa cells with the lipofectamine transfection reagent. At 24 hours after transfection, cells were fixed and stained for actin and DNA (Figure 6.7A) or with INV antibody and DAPI (Figure 6.7B). The GFP signal was observed directly by fluorescence microscopy. INV.v1△37:GFP localized in the cytosol with a mitochondrial-like pattern (Figure 6.7A, B). The GFP signal was sometimes strongly visible around the nucleus (Figure 6.7B). Staining the transfected cells with an INV antibody showed that endogenous INV has a different pattern of localization.

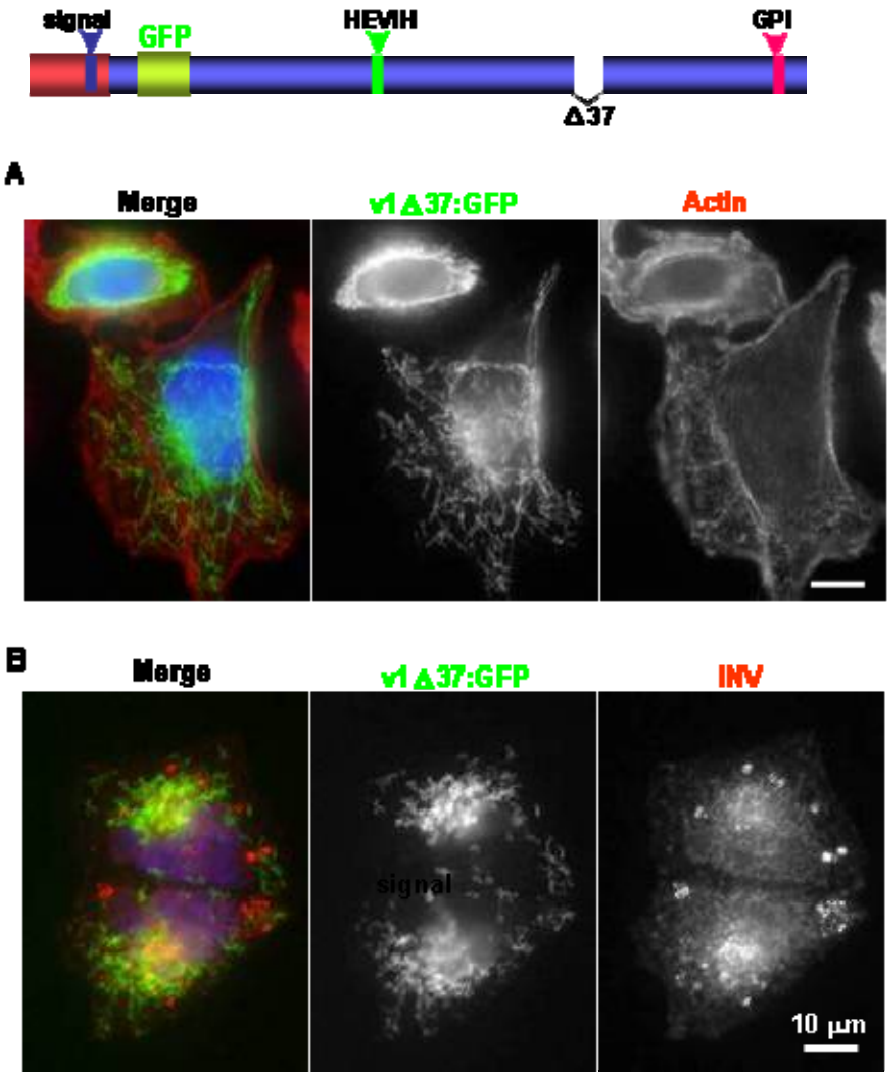

Figure 6.7 The localization of pEdG-v1Δ37:GFP in HeLa cells. HeLa cells were transiently transfected with pEdG-v1△37:GFP. After transfection, cells were fixed and doubly-stained with A) Rhodamine-conjugated phalloidin (red) and DAPI (blue) or B) stained with INV 1318 antibody (red) and DAPI (blue). GFP signal was directly observed by fluorescence microscopy.

Endogenous INV can form a ring-like structure in the cells but seemed not to localize to mitochondrial-like structures (Figure 6.7B).

The GFP tag is a 26 kDa protein, so it is possible that insertion of this big tag caused the protein conformation to be changed, therefore, the localization of INV was examined with an inserted SSBP tag. The plasmid encoding v1:SSBP was similarly transfected and the localization confirmed by immunofluorescence. The v1:SSBP transfected cells were fixed and stained with an anti-SBP antibody and DAPI. The v1:SSBP transfected cells revealed two different localization patterns (Figure 6.8). Most of the transfected cells (80-100％) had the mitochondrial-like localization pattern (Figure 6.8, upper panel) and a lower percentage of cells (0% to 20%) showed a localization as small aggregated dots in the cytosol (Figure 6.8 lower panel). However, this aggregated dot pattern did not appear in every transfection experiment. In contrast, the mitochondrial-like localization was observed consistently in every transfection experiment.

INV.v1△37 contains a signal sequence and GPI anchor but without the 37aa exon 12. To test whether this exon 12 insertion caused a difference in the localization, v1△37:SSBP constructs were transfected into HeLa cells. At 24 hours after transfection, cells were fixed and stained with anti-SBP antibody, actin and DAPI. INV.v1△37:SSBP transfected cells also showed two different kinds of localization. Most of v1△37SSBP transfected cells had a mitochondrial like localization pattern and a lower percentage of transfected cells revealed aggregated foci in the cytosol (Figure 6.9). The cells transfected with v1:SSBP and v1△37:SSBP had a similar localization pattern, suggesting that the 37 aa of exon 12 did not affect the localization. To further examine if ectopically expressed INV can co-localize with endogenous INV, v1:SSBP transfected cells were stained by anti-SBP antibody and

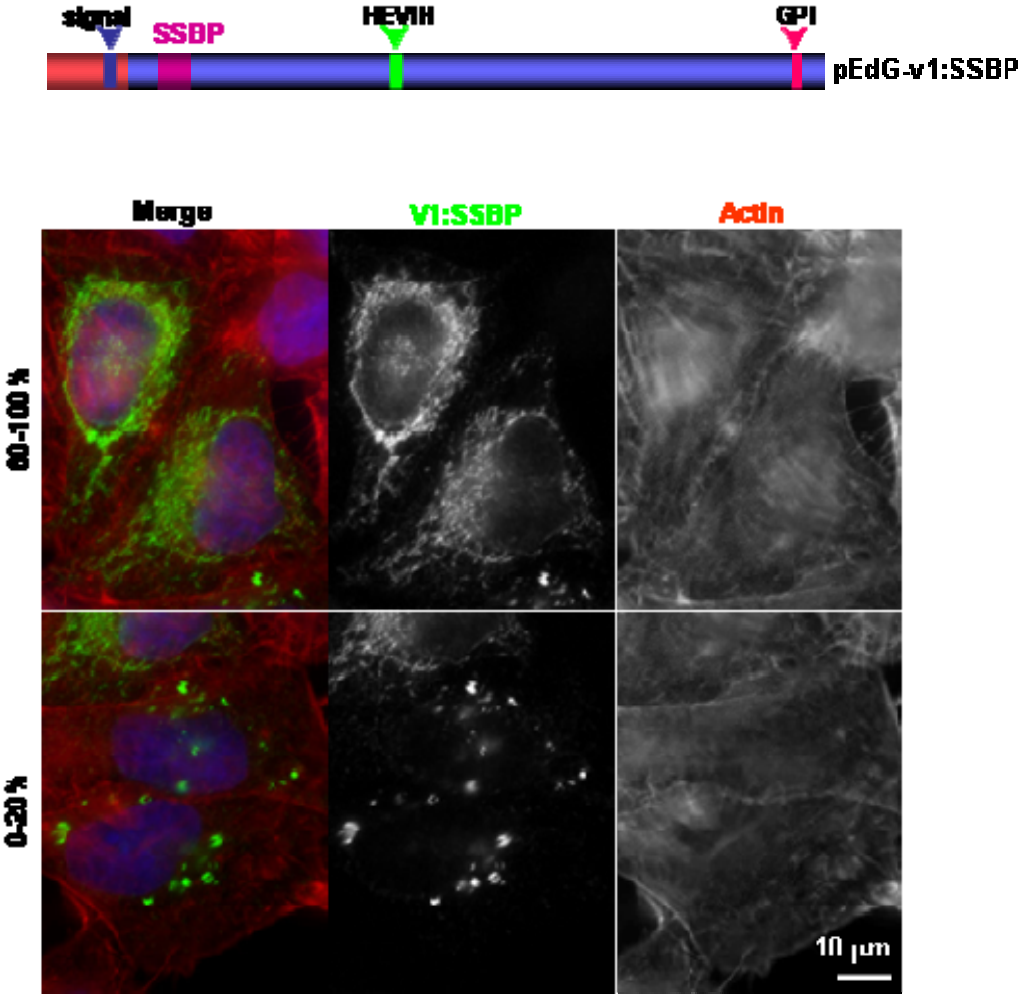

Figure 6.8 The localization of pEdG-v1:SSBP in HeLa cells. HeLa cells were transiently transfected with pEdG-v1:SSBP. At 24 hours after transfection, cells were fixed and stained with anti-SBP antibody (green), Rhodamine-conjugated phalloidin (red) and DAPI (blue). Two different kinds of localization were observed, the upper panel showed mitochondrial like localization (80-100%), the lower panel revealed punctate localization (0-20%).

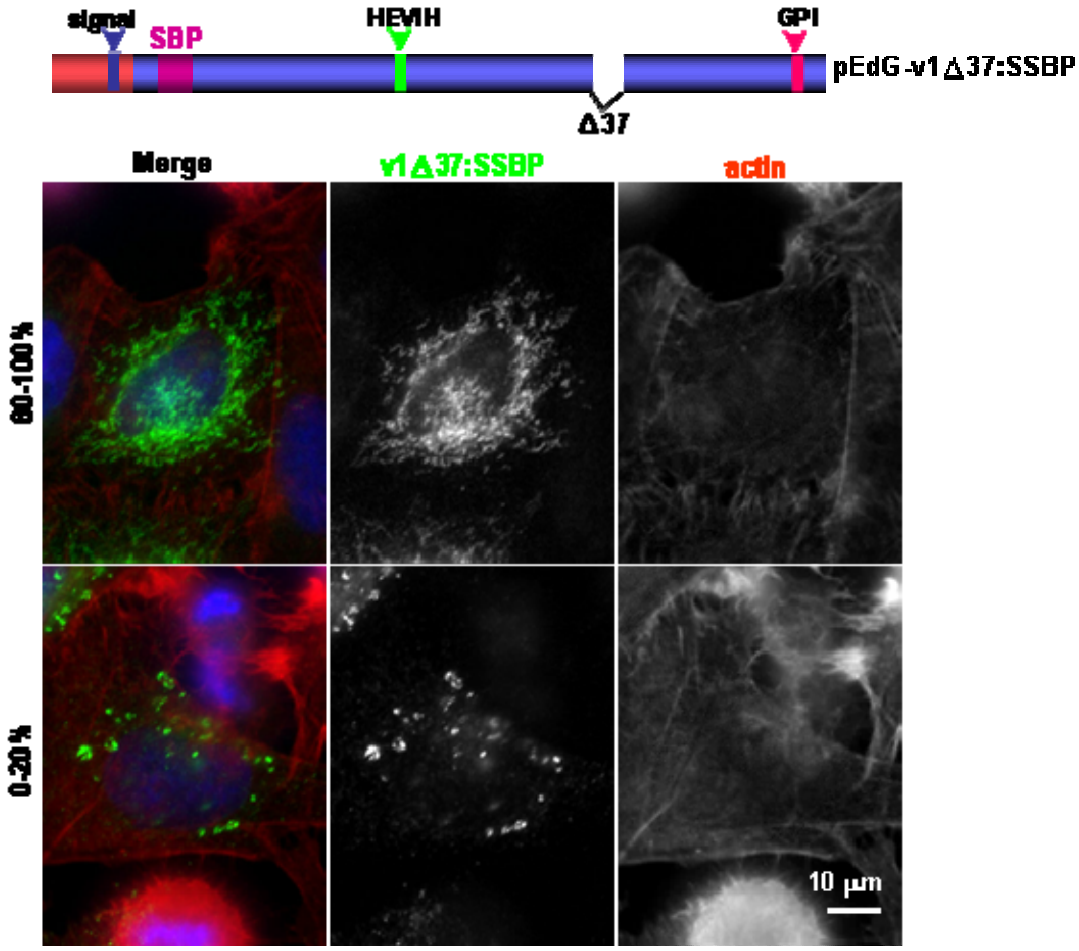

Figure 6.9 The localization of pEdG-v1Δ37:SSBP in HeLa cells. HeLa cells were transiently transfected with pEdG-v1Δ37:SSBP. At 24 hours after transfection, cells were fixed and stained with anti-SBP antibody (green), Rhodamine-conjugated phalloidin (red) and DAPI (blue). Two different kinds of localization were observed, the upper panel showed mitochondrial like localization (80-100%), the lower panel revealed small foci localization (0-20%).

INV. As shown in Figure 6.10, ectopic expression of INV with the SSBP tag revealed a mitochondrial-like localization pattern which did not co-localize with endogenous INV (Figure 6.10).

HA tag (9 amino acids) was also inserted into the region 2 of INV to examine the localization of tagged-INV. v1:HA was transfected into HeLa cell. At 24 hours after transfection, cells were fixed and stained with anti-HA antibody and DAPI. v1:HA also showed a mitochondrial-like localization in HeLa cells (Figure 6.11). LDs can be easily observed by phase contrast. As expected, the mitochondrial-like localization pattern did not coincide with LDs. These observations suggest that overexpressed tagged INV is not localized to LD.

6.2.5 Inserting the tag in invadolysin in other positions

The mitochondrial-like localization was observed consistently in all tagged INV variant 1 overexpressing cells (v1△37:GFP, v1△37:SSBP, v1:SSBP and v1:HA). The tags were inserted into region 2 of INV. To avoid the possibility that this mitochondrial-like localization was due to disrupting INV protein folding; insertion of the tag in other positions would help us to confirm the localization. A *Hind*III restriction enzyme site from 351 to 358 (amino acids 118-119) was used to insert the HA tag in this region (v1:HA [HIII]). To observe the localization of v1:HA [HIII], cells were transfected with this construct. At 24 hours after transfection, cells were fixed and stained with anti-HA antibody and DAPI. v1:HA [HIII] transfected cells also revealed a mitochondrial-like localization which did not coincide with LDs (Figure 6.12). These data confirmed the previous idea that the mitochondrial-like localization is caused by overexpression of human INV variant 1.

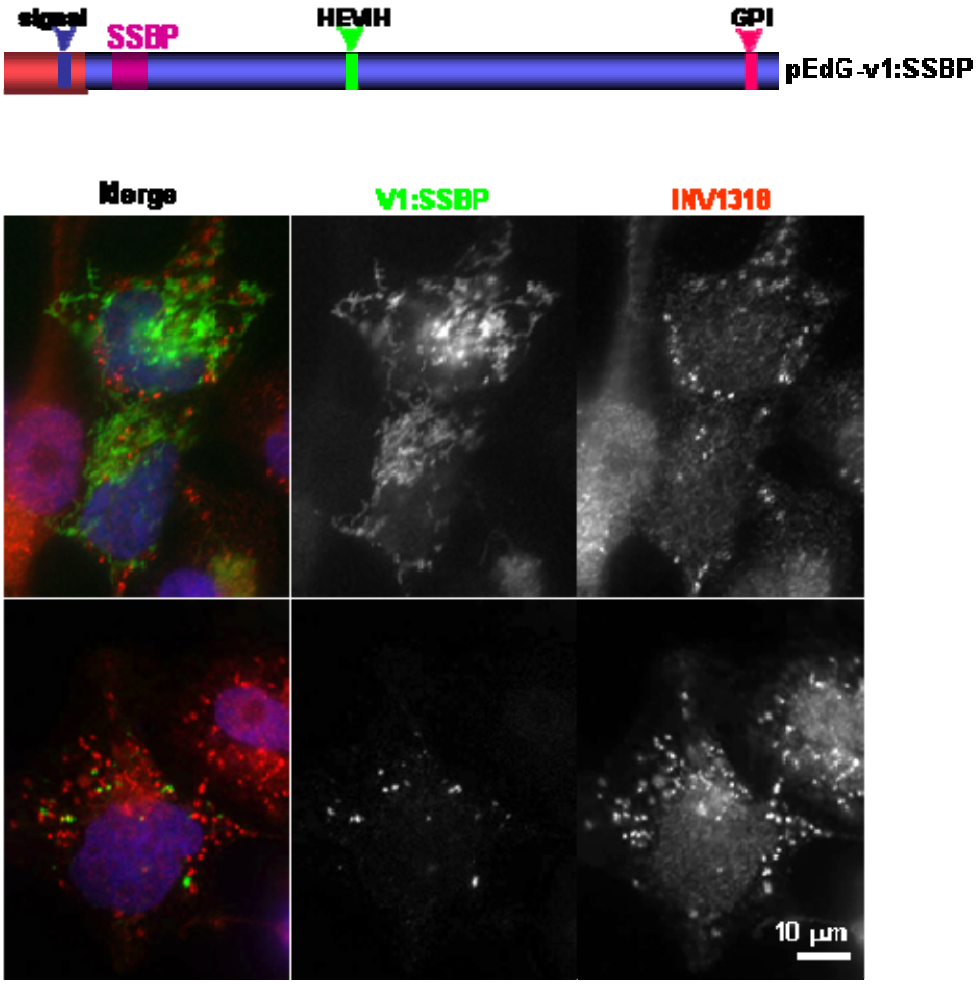

Figure 6.10 The localization of pEdG-v1:SSBP and endogenous INV in HeLa cells. HeLa cells were transiently transfected with pEdG-v1:SSBP. At 24 hours after transfection, cells were fixed and stained with anti-SBP antibody (green), INV 1318 (red) and DAPI (blue). Ectopic expression of v1:SSBP did not co-localize with endogenous INV.

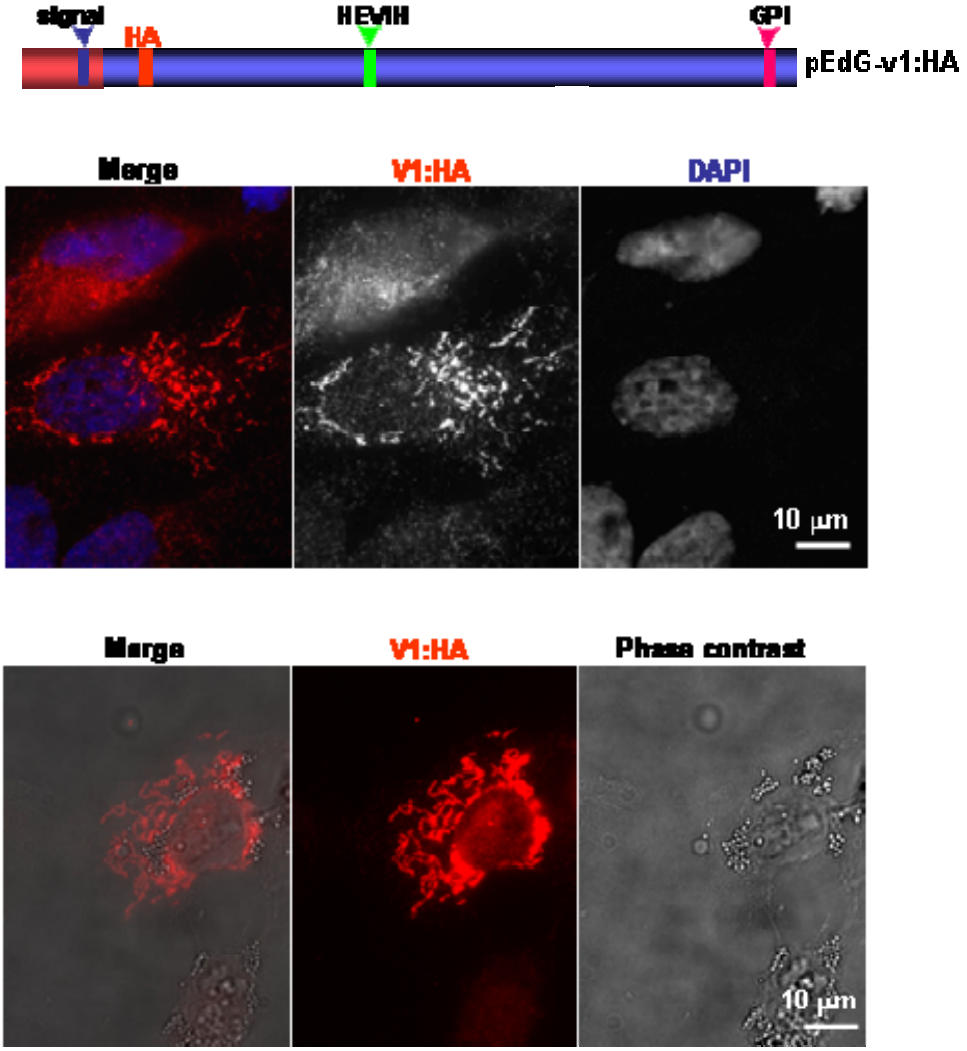

Figure 6.11 The localization of pEdG-v1:HA in HeLa cells. HeLa cells were transiently transfected with pEdG-v1:HA. At 24 hours after transfection, cells were fixed and stained with anti-HA antibody (red) and DAPI (blue). The phase contrast image reveals the lipid droplets. v1:HA transfected cells showed mitochondrial-like localization.

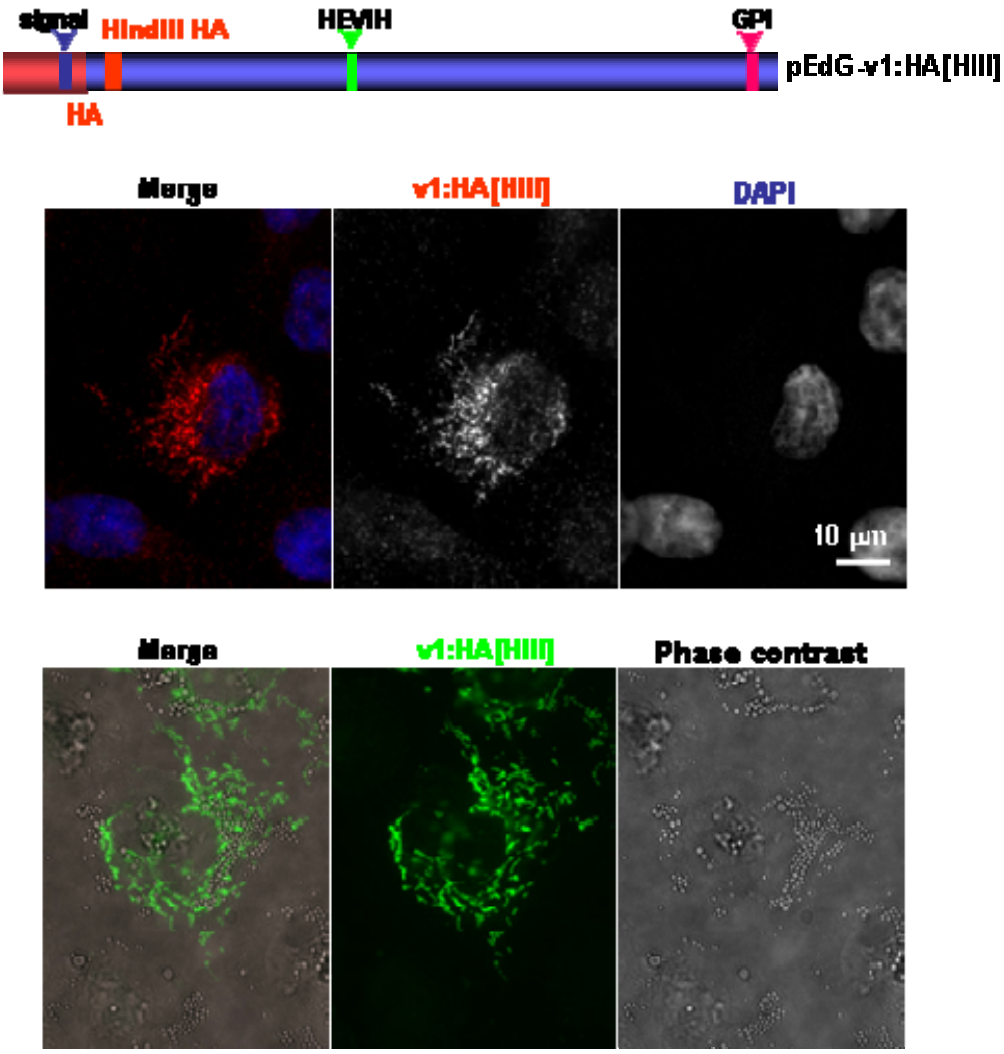

Figure 6.12 The localization of pEdG-v1:HA[HIII] in HeLa cells. HeLa cells were transiently transfected with pEdG-v1:HA[HIII]. At 24 hours after transfection, cells were fixed and stained with anti-HA antibody (red, upper panel or green, lower panel) and DAPI (blue). The phase contrast image was captured to observe the lipid droplets. v1:HA[HIII] transfected cells showed a mitochondrial-like localization that did not co-localize with LDs.

6.2.6 Region 2 tags in INV.v1 localized to mitochondria

The above observations suggested that overexpression of INV variant 1(v1△37:GFP, v1△37:SSBP, v1:SSBP, v1;HA and v1:HA [HIII]) all showed a mitochondrial-like localization in HeLa cells. To confirm this localization, the mitochondrial specific dye, MitoTracker Red CMXRos, was used after transfection. MitoTracker Red CMXRos can be used for live cell staining and as well as for visualization after permeabilization and fixation. INV constructs, v1:SSBP and v1HA:Hind3 were transfected into Hela cells. At 24 hours after transfection, cells were incubated with 125 nM MitoTracker Red dye, and then cells were fixed and stained with anti-SBP or anti-HA antibody. Normally, mitochondria display a typical worm-like staining pattern with MitoTracker Red (Figure 6.13A). HeLa cells transfected with v1:SSBP and v1:HA [HIII] showed mitochondrial-like pattern which co-localized with MitoTracker Red (Figure 6.13B). The data suggests ectopic expression of INV.v1 fused with either GFP, SSBP or HA tag localized to mitochondria.

6.2.7 Detection of expression of INV with region 2 tags by immunoblotting

At first, GFP tag was fused to the C-terminus of INV. Although GFP fluorescence was observed in transfected cells, the protein expression was difficult to detect by immunoblotting (Figure 6.1-6.3). Furthermore, I could show the degradation of INV.v1:GFP through the proteasomal pathway. This data suggested that fusion of GFP at the C-terminus of INV.v1 produced a misfolded protein, such that, INV.v1:GFP was degraded after transfection.

All the INV variant 1 constructs (v1△37:GFP, v1△37:SSBP, v1:SSBP, v1:HA and v1:HA [HIII]) showed mitochondrial-like localization, different from C-terminus

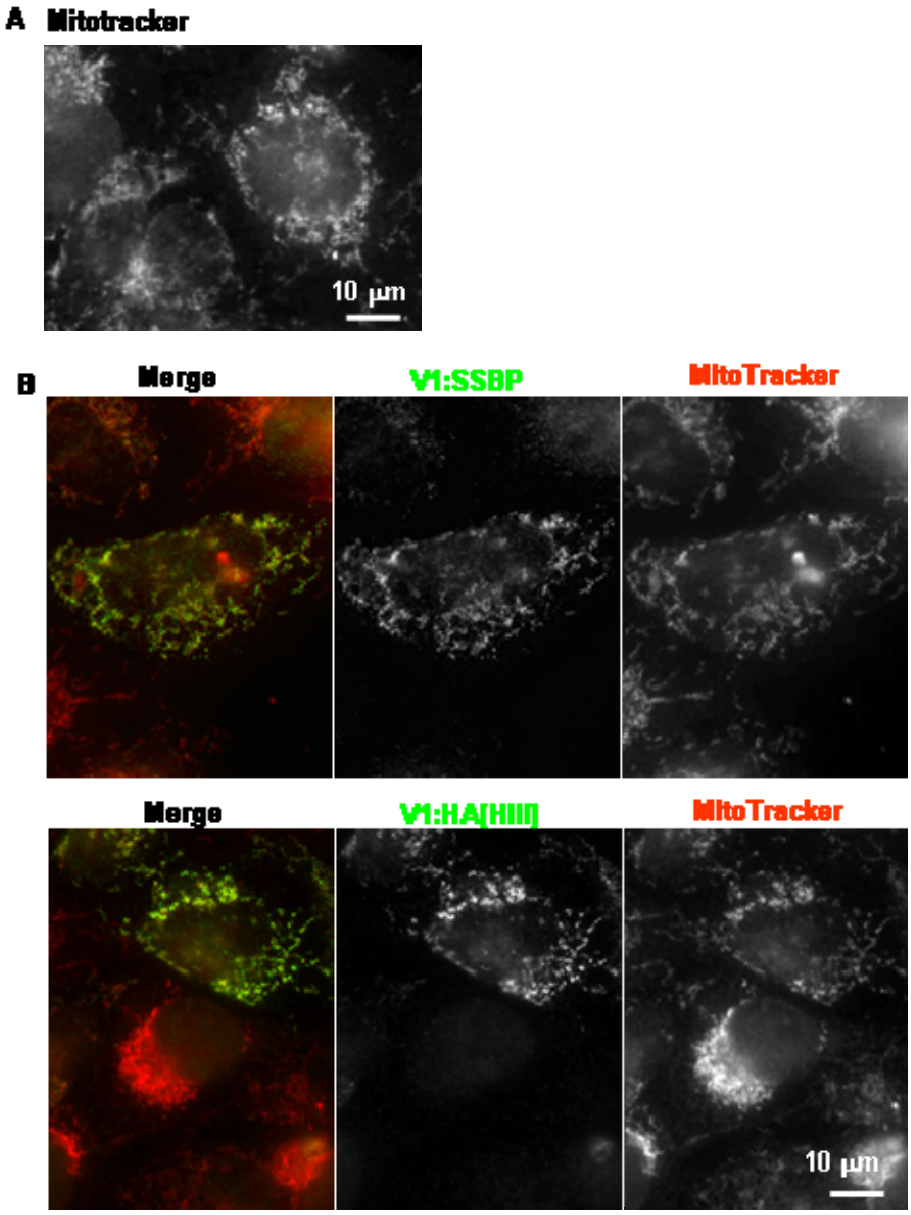

Figure 6.13 Ectopically expressed of SSBP and HA tagged Invadolysin localized with mitochondria. A) HeLa cells were incubated with 125 nM MitoTracker Red CMXRos for 45 minutes and then cells were fixed and observed directly by fluorescence microscopy. B) HeLa cells were transiently transfected with pEdG-v1:SSBP or pEdG-v1:HA[HIII]. At 24 hours after transfection, cells were incubated with Mitotrackes (red) for 45 minutes. Cells were then fixed and stained with anti-SBP or anti-HA antibody (green).

tagged INV.v1:GFP and INV.v1△37:GFP. To examine whether these constructs can be detected by immunoblotting after transfection, the proteasome inhibitor MG132 was used to inhibit the proteasomal degradation pathway. Three INV variant 1 constructs: v1 (without any tag), v1:HA and v1:SSBP were transfected into HeLa cells. At 4 hours after transfection, the transfected cells were treated with or without MG132 inhibitor for 16 hours. The next day, cell lysates were processed and probed by using INV 996 antibody (reported to be to the prodomain of INV). If these constructs (v1, v1HA, v1SSBP) produce a misfolded protein, we might expect that inhibition of the proteasomal pathway by MG132 might induce protein accumulation in the cell lysates. The overexpressed constructs (v1, v1:HA, v1:SSBP) ccould be detected by INV antibody in the absence of MG132. The treatment with MG132 did not enhance the levels of tagged proteins (v1, v1:HA, v1:SSBP), suggesting that the expressed target proteins might not be inducing ERAD (Figure 6.14A).

To confirm this result, control vector, pTrAP (contain triple tag:His-tag, S-tag and SBP tag) and v1:SSBP were transfected into HeLa cells. At 24 hours after transfection, immunoblotting was carried out on transfected cell lysates using an anti-SBP antibody (Figure 6.14 B). As expected, v1:SSBP protein could be detected after transfection. Likewise, INV with HA tags (v1:HA and v1:HA [Hind3]) were also transfected into HeLa cells and the expression of transfected protein was confirmed by probing anti-HA antibody (Figure 6.14C). v1:HA and v1:HA [HIII] protein could be detected after transfection, and the protein is around 64 kDa. These data suggest that INV can be expressed when the tag is inserted in region 2 of INV protein.

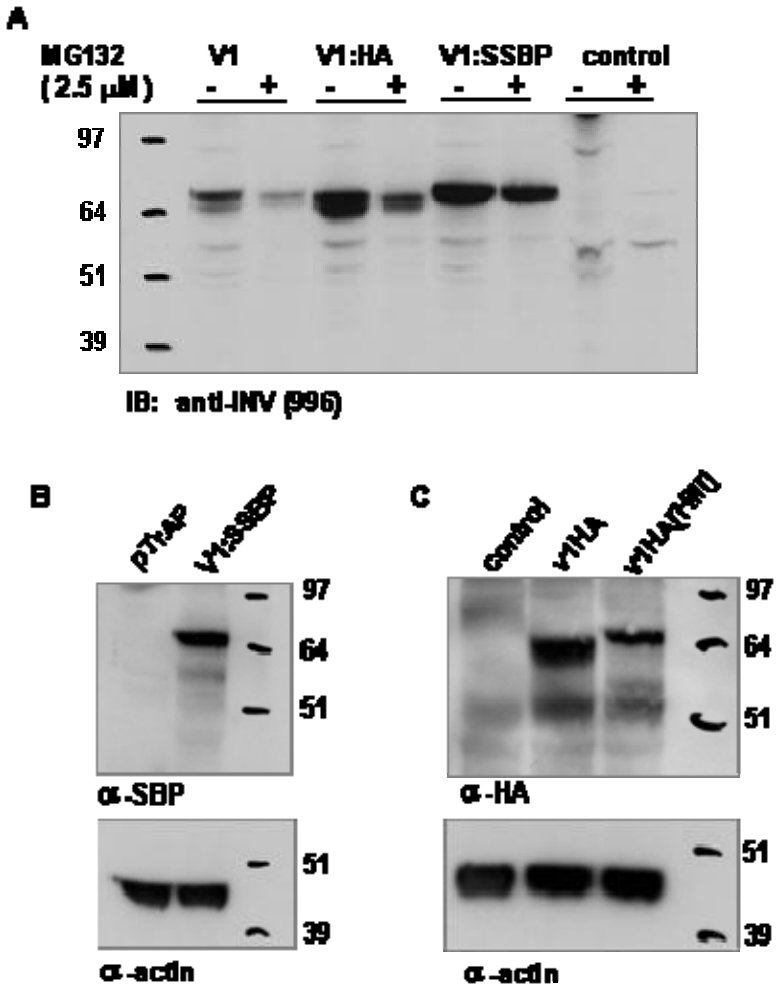

Figure 6.14 Detection of INV fused with GFP, SSBP and HA tags by immunoblotting. A) HeLa cells were transiently transfected with full length INV constructs (v1, HA and SSBP tag). At 6 hours after transfection, cells were incubated with or without MG132, proteasome inhibitor, for 16 hours. The next day, cells were harvested and lysated resolved by SDS-PAGE, followed by immunoblotting with INV 996 antibody. B) HeLa cells were transiently transfected with pTrAP control plasmid (containing His-tag, S-tag and SBP tag) and v1:SSBP. C) HeLa cells were transiently transfected with v1:HA and v1:HA[HIII]. At 24 hours after transfection, cell lysates were harvested and resolved by SDS-PAGE, followed by immunoblotting with SBP, HA and actin antibodies.

6.3 Discussion

Fluorescent proteins have become extremely popular tools for *in vivo* imaging and especially for the study of localization, motility and protein interaction in living cells (Merzlyak *et al.*, 2007). Therefore, INV variants were fused with C-terminals GFP initially. However, INV variants fused with GFP at the C-terminus showed localization around nuclei, suggestion of the ER, and the overexpressed proteins were hard to detect by immunoblotting (Figure 6.1-6.3). The results suggest the INV:GFP might fold improperly and be retained in ER and subsequently degraded. This possibility was shown by inhibiting the 26S proteasome by MG132. With increasing amounts of inhibitor, more INV.v1:GFP protein accumulated (Figure 6.4-6.5). The ER-associated degradation (ERAD)-proteasome pathway is involved in the degradation of incorrectly folded proteins, which are prevented from exiting the ER through vesicular traffic (Nakatsukasa & Brodsky, 2008). During ERAD, misfolded proteins are then targeted for ubiquitination and delivery to the 26S proteasome for degradation (Nakatsukasa & Brodsky, 2008).

As the recombinant proteins (INV.v1:GFP, v1△37:GFP and INV.v2:GFP) may fail to acquire their native conformations or lose tags during modification, the cloning strategy was changed to insert the tag inside INV. As mentioned before, human INV.v1 is more prevalent than variant 2, and INV.v2 does not appear in most other species. For these reasons, we focused on the INV variant 1 (INV.v1 and INV.v1△37). I observed a mitochondrial localization after ectopic expression of INV with GFP, SSBP and HA tag in region 2 in HeLa cells (Figure 6.8-6.13). The transfected cells showed the mitochondria localization was not due to the position of the region 2, as the tag inserted in a *Hind*III site also revealed the same localization (v1:HA [HIII]). Expression of these proteins can be detected by immunoblotting with

tag antibodies (anti-HA or anti-SBP) and with an antibody reported to recognize the prodomain of INV. The data indicate the overexpression of INV with tags in region 2 might translocate it into mitochondria.

Obviously, the localization of overexpressed tagged INV and endogenous INV showed different localization patterns (Figure 6.7 and 6.10). Ectopic expression of INV showed mitochondrial localization, whereas endogenous INV revealed LD localization. What causes the difference? The first possibility is that tagged INV was too highly expressed. Viral promoters are commonly used in transiently expressed constructs due to their strong activity in various cell lines *in vitro*. The CMV promoter is most widely used in overexpression systems. It can induce high-level constitutive expression in a variety of mammalian cell lines (Fitzsimons *et al.*, 2002). It is possible that under the control of CMV promoter, INV was too highly expressed and this caused the different localization to endogenous INV.

A similar mis-localization result was also found for cdc25. Even if only slightly overexpressed, the full protein was not located in the cell plasma membrane, but accumulated inside the cell and also in the nucleus (Tisi *et al.*, 2008). Another example is the endogenous ubiquitin ligase Chfr (Checkpoint protein with FHA and RING finger domain), which is cytoplasmic and localizes to the spindle during mitosis. Higher expression of ectopic Chfr correlated with a shift in the localization of this protein to the nucleus / PML (promyelocytic leukemia) bodies (Burgess *et al.*, 2008).

The second possibility is the unknown effects on cell physiology during transfection. For example, caveolin is a membrane bound protein involved in caveolar endocytosis, but caveolin is recruited to LDs upon oleic acid treatment of culture cells (Pol *et al.*, 2004). Matrix metalloproteinase (MMP)-1 is a collagenase,

that is important for tissue remodeling, inflammation and angiogenic processes. MMP-1 is a secreted protein, but in the mitotic phase of the cell cycle, MMP-1 showed intracellular accumulation. On induction of apoptosis, MMP-1 co-localized with aggregated mitochondria and accumulated around fragmented nuclei (Limb *et al.*, 2005). It is possible that, while cells are transfected, they may undergo physiological differences that subsequently affect the localization of overexpressed INV.

However, it is also possible that INV presents dual localization pattern. Endogenous INV is present on LDs, whereas perhaps overexpressed INV goes to mitochondria. In chapter 3, I described that endogenous INV re-localization to LDs was dependent on the activity of PKC. It is also possible that the exogenous extra INV is not phosphorylated by PKC due to limiting amounts of PKC in the cells. The phosphorylated and unphosphorylated proteins might show different affinities to different subcellular compartments. The same phenomenon has been found for the cytochrome P450 (CYP) family. Several members of the cytochrome P450 (CYP) family are targeted to both ER and mitochondrial compartments, however, phosphorylation of CYP2B1 by PKA showed reduced affinity for ER and higher affinity to mitochondria. This suggests that the localization of CYP2B1 maybe regulated through cellular cAMP / PKA levels and phosphorylation of an internal site in the protein (Robin *et al.*, 2001; Karniely & Pines, 2005).

The LDs are sometimes in the vicinity of other intracellular structures such as ER, mitochondria, Golgi and peroxisomes (Turro *et al.*, 2006; Bartz *et al.*, 2007). Mitochondria are sometimes found associated with LDs (Chanderbhan *et al.*, 1982; Nakamura & Fujimoto, 2003). Cidea, the Cide domain-containing protein localized to mitochondria and LDs, is also known to be highly expressed in adipose tissue and

regulate lipolysis (Puri *et al.*, 2008; Chen *et al.*, 2000; Zhou *et al.*, 2003). Interestingly, dissecting ADRP protein sequence has been shown to contain two LD localization sequences (1-181, 246-277) and one mitochondrial localization sequence (302-426) (Nakamura & Fujimoto, 2003). Using immunoelectron microscopy, it was found that an ADRP antibody labels not only LDs but also some adjacent membrane structures (Nakamura & Fujimoto, 2003). The reason for localization of tagged-INV to mitochondria has not been examined, but may be important in understanding the function of INV.

Chapter 7: Protease activity of invadolysin

7.1 Introduction

The zinc-metalloprotease domain encoded in INV matches the conserved metalloprotease motif, HEXXHXXG[X]$_N$H, which is the hallmark of the M8 metalloprotease family (Gomis-Rüth, 2003). The M8 family includes a protein named GP63, which has metalloprotease activity (Button *et al.,* 1993). Our lab previously showed that *INV*^{4Y7} mutant larvae have much less proteolytic activity in brain than wild type, suggesting that INV is a strong candidate for the observed activity (McHugh *et al.*, 2004). However, whether INV itself has protease activity still needs to be elucidated. The pGEX glutathione S-transferase (GST) fusion protein system is used for high level expression and rapid purification of fusion proteins from bacteria. Bacterially expressed MMP21, MMP28, matrilysin and MT1-MMP have been successfully expressed in bacteria with protease activity (Marchenko *et al.*, 2003; Lohi *et al.*, 2001; Soler *et al.*, 1995; Ho *et al.*, 1994). In this chapter, the expression of INV recombinant protein in bacteria was performed in order to begin characterization of protease activity. In addition, construction of either INV or a tagged INV was used to express protein in mammalian cells. Finally, immunoprecipitation of expressed INV protein was used to test for protease activity of INV.

7.2 Results

7.2.1 Production and purification of recombinant INV from bacteria

In order to obtain high amounts of INV, INV constructs containing the

metalloprotease motif were PCR- amplified from the cDNA of INV variant 1 or variant 1△37 with appropriate primers and subcloned in-frame to the pGEX4T vector. The prodomain may be necessary for the correct folding processing of the recombinant protein (Marchenko *et al.*, 2003), therefore, GST-SBG was designed after the N-terminal signal sequence and before the GPI anchor attachment site, from amino acid 53 to 661 (△37). Most metalloproteases are synthesized as inactive precursors (Khan & James, 1998). The prodomain of all MMPs contains a highly conserved cysteine residue; this cysteine residue can regulate metalloprotease activity (Gomis-Rüth, 2003). When binding between this cysteine and a zinc atom occurs, it turns off the activity of the enzyme. On the other hand, the dissociation from the zinc atom of cysteine activates the enzyme (Van-Wart & Birkedal-Hansen, 1990). This conserved cysteine (Cys 48) is also found in the prodomain of GP63 (Macdonald *et al.*, 1995; Button *et al.*, 1993). There is a cysteine residue at position 64 in INV. To avoid the cysteine/zinc binding, the construct GST-VINK was cloned from amino acids 74 to 661. The N-terminal construct, GST-V1N was cloned from amino acids 1 to 300 (Figure 7.1).

To express these constructs, GST-VINK, GST-SBG and GST-V1N were transformed into *E.coli* BL21 cells. Bacteria were induced to express the recombinant proteins with 0.4 mM IPTG. After induction with IPTG, the cells were pelleted and resuspended in PBS containing 0.5% TX100 (PBST), followed by sonication for disrupting bacterial cells. The predicted sizes of GST-VINK, GST-SBG and GST-V1N are 90 kDa, 88 kDa and 59 kDa, respectively. As shown in figure 7.2A, a large amount of protein was observed between 97 and 64 kDa after IPTG induction in both GST-VINK and GST-SBG transformed cells. A major band of 51 kDa was observed in GST-V1N transformed cells after induction by IPTG

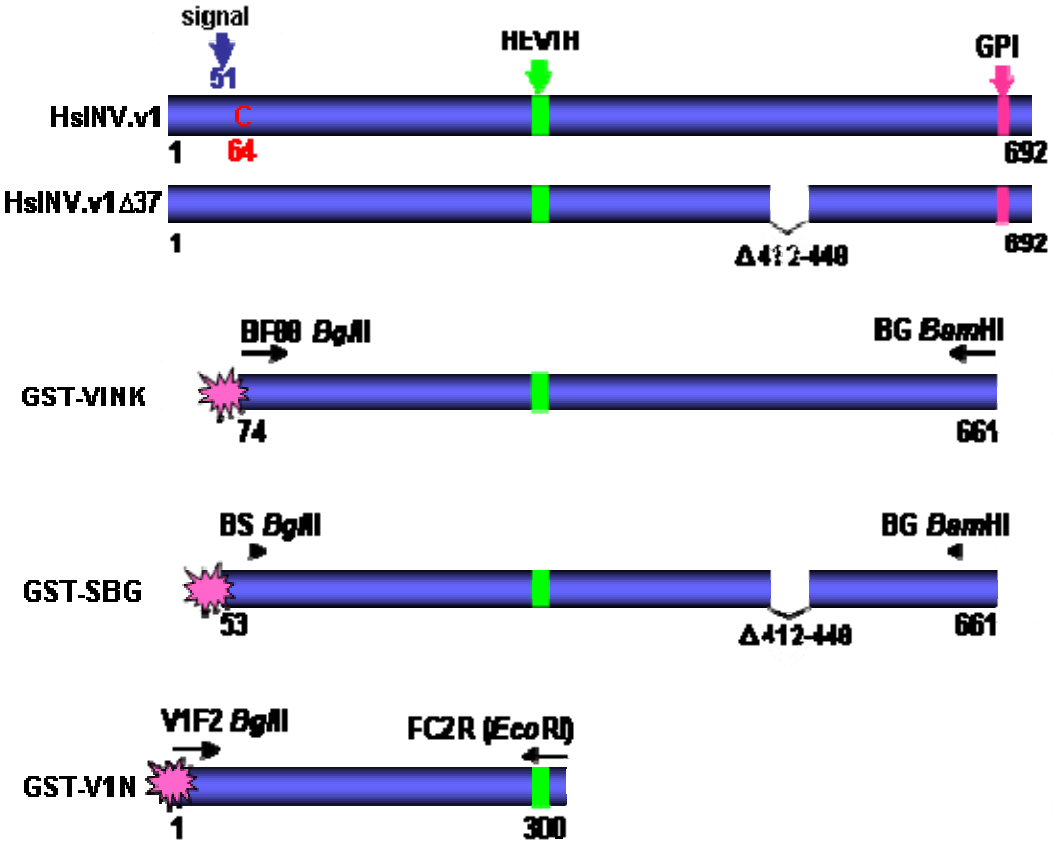

Figure 7.1 Schematic of human invadolysin fragments fused to the GST tag protein. The cDNA of truncated INV fragments was amplified from INV.v1 cDNA with appropriated primers containing restriction enzyme sites and subsequently cloned in-frame into the pGEX-4Tvector. The predicted signal sequence cleavage site is located at the 51st amino acid. 64C represent the cysteine residue in the position of the 64th amino acid, this residue might regulate the activity of the protease. HEVIH is the metalloprotease motif of INV. GPI is the GPI anchor modification site. The GST-VINK construct contains amino acids 74 to 661(from amino acids V74, I75, N76, K77 and before GPI anchor), GST-SBG begins after the signal sequence (S) and end before GPI (BG) anchor predicted site. GST-V1N is an N-terminal construct deleted of the C-terminal half of INV.

(Figure 7.2A).

To test for the solubility of the expressed proteins, induced samples were pelleted and resuspended in PBST, followed by sonication. After centrifugation, the supernatant was transferred to a new microfuge tube and the pellet was resuspended in PBST. Equal volumes of supernatant and pellet were loaded into lanes for SDS-PAGE. As shown in Figure 7.2B, the majority of the GST control was found in the supernatant fraction, indicating that this procedure can solubilize GST protein. However, GST-VINK and GST-V1N were observed as insoluble in the pellet fraction. These data suggest that GST-VINK and GST-V1N may be only partially solubilized with this protocol (Figure 7.2B).

In order to solubilize INV recombinant proteins, the bacterial cells were lysed in STE buffer (10 mM Tris pH 8.0, 150 mM NaCl, 1mM EDTA) with 0.5% of the ionic detergent sarkosyl. Previous reports found that 0.5% sarkosyl can solubilize epilysin (MMP-28) and still maintain protease activity (Lohi *et al.*, 2001). Thus, followed their condition (Chapter 2, 2.17), the GST-VINK and GST-SBG can be solubilized. Afterwards, the recombinant proteins were purified by GST sepharose beads (Figure 7.2C). As shown in Figure 7.2C, around 50% of GST-VINK and GST-SBG recombinant proteins in cell lysates can bind to the beads, leaving 50% of the GST-tagged proteins in the flow-through fraction. This may be because a high concentration of sarkosyl can affect the binding affinity of GST fusion proteins to GST beads (Frangioni & Neel, 1993).

The reduced glutathione (20 mM) was used to elute the protein from GST beads. After elution, aliquotes of the V1N, VINK and SBG elutions were loaded into gels and the concentration was evaluated by comparing with purified BSA. All the recombinant proteins can be eluted from GST beads (Figure 7.3). Notably, 5 μl (5%)

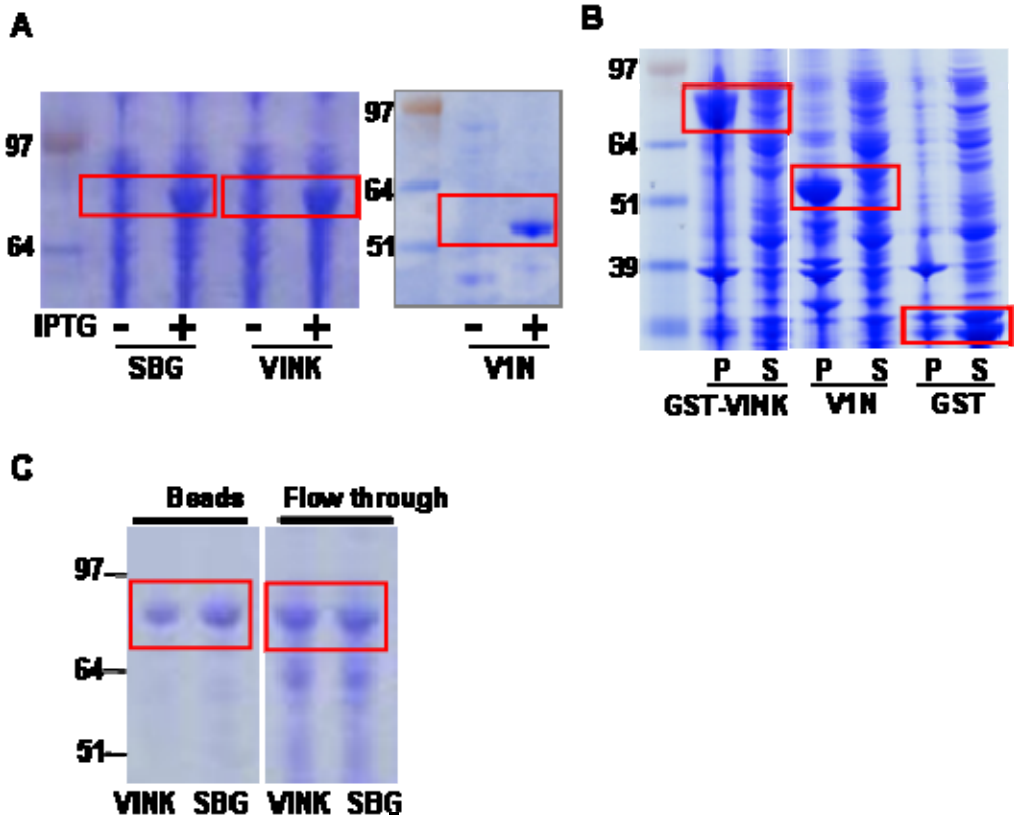

Figure 7.2 Expression of INV recombinant proteins in E. coli BL21 cells. A) Confirming protein expression after induction with IPTG. In the presence of IPTG, GST-SBG, GST-VINK and GST-V1N can be detected. The boxed areas show the expected size of the recombinant proteins. B) Determination of the solubility of INV recombinant proteins. The bacterial cells with induced of GST-VINK, GST-VIN and GST were suspended in PBS containing 0.5% TX100 (PBST). After sonication, cells were centrifuged, and divided into supernatant and pellet. Equal proportion of supernatant and pellet were resolved by electrophoresis and observed after coomassie blue staining. C) Glutathione beads (GST sepharose beads) were added to bacterial lysates to purify recombinant proteins. GST-VINK and GST-SBG recombinant protein can be solubilized in 0.5% sarcosyl and a half of the soluble protein can bind and be purified from bacterial lysates.

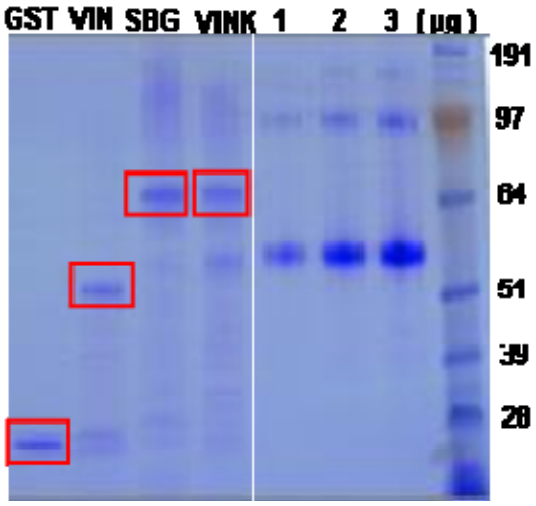

Figure 7.3 Elution of INV recombinant proteins by reduced glutathione. After purification of recombinant proteins by binding to GST sepharose beads, the INV recombinant proteins, GST-SBG and GST-VINK were eluted from beads by adding 20 mM reduced glutathione. The elution step was repeated 3 times. The concentration of the proteins was estimated using a known concentration of BSA standard.

of the eluted V1N, VINK and SBG proteins were estimated to contain 0.1 μg of protein and 0.5 μl (0.5%) of eluted GST was estimated to contain 2 μg. Eluted proteins were further used for kinase assays (Chapter 3) and zymography experiments.

7.2.2 Detection of invadolysin enzymatic activity by zymography

GST-VINK and GST-SBG revealed bands of the expected size (around 90 kDa) after purification from bacterial lysate by GST beads or after elution from GST beads (Figure 7.4A, lane group1 & 2). GST-VINK and GST-SBG were also treated with thrombin to remove the GST domain and to release the proteins from GST beads (Figure 7.4A, lane group 3).

To determine whether bacterially expressed INV displays proteolytic activity, the purified INV GST recombinant proteins (VINK and SBG) were examined by zymography SDS-PAGE followed by coomassie blue staining. Protease activity was assessed with zymogram gels containing gelatin or casein as a substrate. GST beads with bound proteins, the eluted proteins and the thrombin treated proteins (1-2 μg) were electrophoresed into zymogram gels with casein. To allow digestion, the gel was incubated in the developing buffer at 37˚C for 24 hours. Afterwards, the zymogram gel was subsequently stained with colloidal coomassie blue. If the protein has protease activity, a clear band against the dark background should be detected (Hawkes *et al*., 2001). After staining, no clear areas of digestion were observed in samples of GST-VINK and GST-SBG (Figure 7.4A, lower figure). A similar procedure was performed with gelatin zymogram gels and also showed no cleared areas in samples of the GST-VINK and GST-SBG (data not shown).

As mentioned in 7.2.1, most metalloproteases are synthesized as inactive

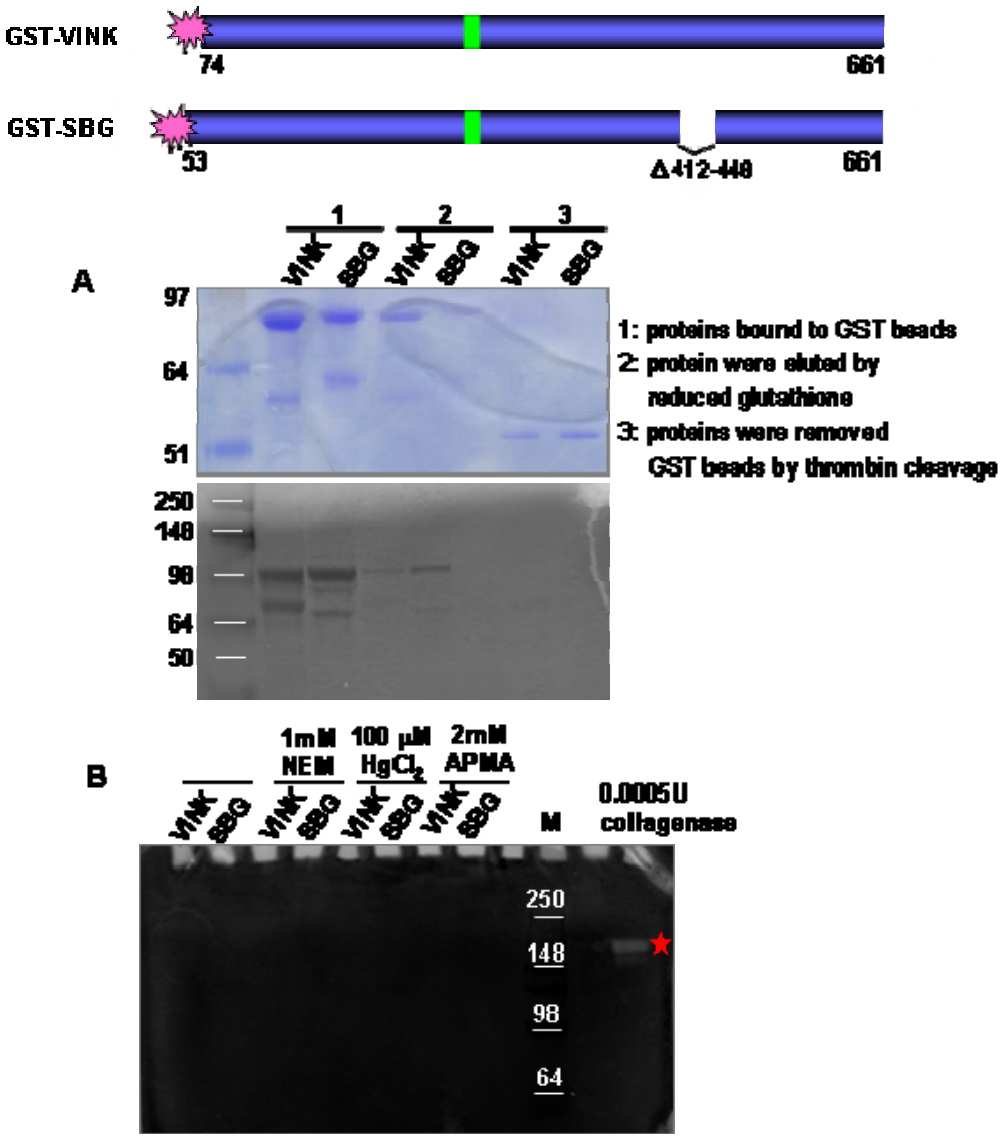

Figure 7.4 Detection of protease activity by zymography. A) GST-VINK and GST-SBG were expressed in *E. coli*. (1) Proteins were purified by binding to glutathione-sepharose beads. (2) Fusion proteins were eluted from GST sepharose beads by reduced glutathione. (3) Fusion proteins were cleaved with thrombin to remove GST. Samples from 1, 2 and 3 were then separated by electrophoresis. Next, the gel was stained with colloidal coomassie blue or analyzed by casein zymography. B) 1 μg of the eluted recombinant proteins was incubated with 1 mM NEM, 100 μM HgCl2 or 2 mM APMA at 37˚C for 2 hours and resolved by electrophoresis, followed by gelatin zymography. 0.0005U collagenase is a positive control for gelatin zymography. Red star marks the area shows activity.

precursors, where an N-terminal prodomain is important for maintaining the latency of the proteases (Khan & James, 1998). The prodomain of all MMPs contains a highly conserved cysteine residue, which is also found in GP63 (Macdonald *et al.*, 1995; Button *et al.*, 1993). Various reagents of cysteine modification were tested for their effects on activity of expressed INV. Treatment of latent proteases with compounds such as $HgCl_2$, 4-aminophenylmercuric acetate (AMPA) and N-ethylmaleimide (NEM) has been reported to disrupt the Cys-Zn complex that can mimic the cleavage of prodomain from latent protease to switch on protease activity (Macdonald *et al.*, 1995; Chen *et al.*, 1993; Loechel *et al.*, 1999).

A cysteine residue at position 64 in the N-terminus of INV may play this role. To test whether this residue affects the protease activity of INV recombinant proteins, purified GST-SBG (containing Cys 64) and GST-VINK (lacking Cys 64) were treated with cysteine modification reagents. One μg of eluted GST-VINK and GST-SBG proteins was added with either 1 mM NEM, 2 mM APMA or 100 μM $HgCl_2$ and the mixtures were incubated for 2 hours at 37˚C. Protease activity was analyzed by zymography with collagenase used as a positive control. Collagenase can digest gelatin, therefore as expected, a cleared region in the collagenase control was observed in zymography (Figure 7.4B). However, no cleared area of digestion was observed in samples of INV recombinant proteins after treatment with cysteine modification reagents (Figure 7.4B). These data suggest that 1) the protein does not act as a protease, or 2) that proteolytic activity of each construct, whether it contains prodomain or not, is inactive after the procedure of protein expression, purification, elution and Cys-Zn complex disruption.

7.2.3 Purification and zymography of INV expressed in HeLa cells

The recombinant proteins of INV (GST-VINK and GST-SBG) expressed in *E.coli* failed to show activity. Possibly, *E.coli* was unable to synthesize human INV in the proper conformation. It is also possible that the recombinant proteins remaining insoluble but purified by the strong detergent (sarkosyl) were unable to re-form the conformation required for their proteolytic activity. Bacterially expressed GP63 has been reported to lose its protease activity (Button *et al.*, 1991). When the expression system was changed to the baculovirus system, GP63 activity was detectable (Button *et al.*, 1991; Button *et al.*, 1993).

In Chapter 6, the full length INV constructs were cloned into a mammalian expression vector. INV without a tag or with a tag in region 2 of INV can be expressed in HeLa cells and detected by either INV996 antibody or a tag specific antibody (anti-HA or anti-SBP). Therefore, the pEdG-v1 (containing full length INV.v1without any tag) was transfected into HeLa cells for purification and assessment of proteolytic activity (section 6.2.7). At 24 hours after transfection, cells (3-5 x 10^6) were lysed and immunoprecipitated with INV 996 antibody or normal rabbit IgG (NRIgG). Subsequently, the protein A sepharose beads were added to absorb the immunecomplexes (the detail was described in Chapter 2, 2.25). Samples of total cell lysate, cell lysate for immunoprecipitation (lysate with the debris removed by centrifugation), lysate after immunoprecipitation by NRIgG or INV996 and the immunecomplex of NRIgG or INV996 were colleted for electrophoresis. Protein was analyzed by 4-12% SDS-PAGE and immunoblotting with the INV996 antibody. A band of 68 kDa was observed by immunoblotting (127 kDa band was a non-specific product). A similar amount of INV.v1 protein was observed in total cell lysate and cleared cell lysate for IP, suggesting that RIPA buffer can solubilize most of the construct expressed INV.v1 protein (Figure 7.5A).

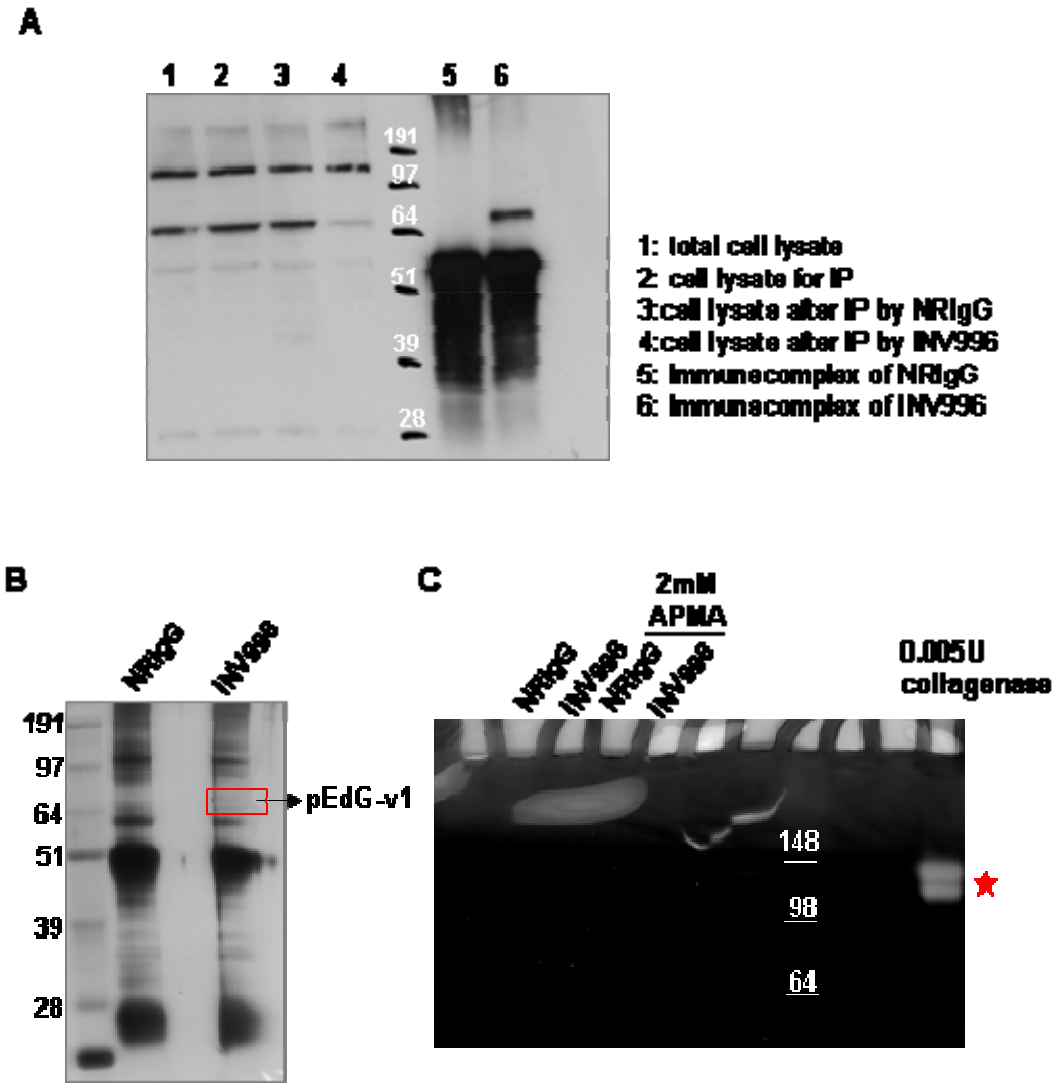

Figure 7.5 Immunoprecipitation and zymography of INV expressed in HeLa cells. A) pEdG-v1(INV.v1 with no tag) was transfected to HeLa cells. At 24 hour after transfection, cell lysates were prepared in RIPA buffer.The transfected samples were immunoprecipitated with INV 996 antibody or normal rabbit IgG (NRIgG) at 4 ˚C for 2 hour followed by protein A purification. The immunoprecipitated samples were then rsolved by electrophoresis and analyzed by immunoblotting. B) Confirming the immunecomplexed of NRIgG or INV996 by Coomassie Blue staining. C) The immunecomplexes of NRIgG or INV996 were analyzed by gelatin zymography in the presence or absence of APMA. 0.005U collagenase is a positive control for gelatin zymography. Red star marks the area shows activity.

After immunoprecipitation by INV996 antibody, the 68 kDa product in cleared lysate was decreased, whereas, a significant band of 68 kDa appeared in the immunecomplex immunoprecipitated by INV996 antibody. There was no targeted product found in the NRIgG control, suggesting that the construct expressed INV.v1 can be purified by the immunoprecipitation (Figure 7.5A). The immunoprecipitated complexes were also confirmed by coomassie blue staining (Figure 7.5B). A band of 68 kDa appeared in the INV996 immunoprecipitated complex. To determine whether the immunoprecipitated INV has metalloprotease activity, immunecomplexes from INV996 and NRIgG were treated with or without APMA (or NEM) and analyzed with by gelatin (or casein) zymogram (collagenase used as a positive control). Collagenase cleared region was observed following zymography (Figure 7.5C). However, no cleared region was observed in INV996 immunoprecipitated complexes with or without APMA treatment (Figure 7.4B). Similar procedures were performed with the other construct v1:SSBP. Unfortunately, no protease activity was detected (data not shown). This suggested that the purified of HeLa-expressed INV could be inactive or the conditions for immunoprecipitation are not compatible with the detection of protease activity.

Several buffer conditions have been tested to examine the protease activity of bacterially expressed INV and INV expressed by HeLa cells (Table 7.1). However, recombinant INV did not exhibit the proteolytic activity in any of these buffer conditions.

Table 7.1 Conditions tested for developing protease activity for INV

Bacterially expressed INV	Buffer used for washing and resuspending GST beads	Chemical for cysteine modification	Zymogram gel
GST-VINK GST-SBG (Solubilization buffer: STE buffer)	20 mM HEPES pH7.5 100 mM NaCl 1% Triton 10 mM $CaCl_2$ 1 μM $ZnCl_2$	The recombinant protein in left buffers was further treated with 100 μM $HgCl_2$, 1mM NEM or 2 mM AMPA at RT for 2 hours.	gelatin or casein
	20 mM HEPES pH7.5 100 mM NaCl 1% Triton 10 mM $CaCl_2$, 1 μM $ZnCl_2$ 1 mM DTT		
	50 mM Tris, pH7.4 100 mM NaCl 1% Triton 10 mM $CaCl_2$		
	50 mM Tris, pH7.4 100 mM NaCl 1% Triton 10 mM $CaCl_2$, 1mM DTT		
INV expressed in HeLa cells	Buffer used for washing and resuspending protein A beads		Zymogram gel
INV.v1 INV.v1SSBP (cell lysis buffer: RIPA buffer	20 mM Tris-HCl, pH7.5 150 mM NaCl 1% NP40 1 mM Na_2EDTA 1 mM EGTA	The immunecomplex in left buffer was then treated with 2 mM AMPA or 1 mM NEM at RT for 2 hours.	gelatin or casein
	20 mM Tris-HCl pH7.5, 150 mM NaCl, 1% Triton 1mM $CaCl_2$ 1mM DTT		

7.3 Discussion

There are three crucial factors affecting the results in this chapter: proper conformation of the protein, sensitivity of the detection method and specific positive controls for the assay. Although the bacterial cells can express GST-tagged INV, those recombinant proteins did not exhibit proteolytic activity. This may be because the specific post-translational modifications are necessary for their proteolytic activity. However, INV expressed in mammalian cells also did not show any protease activity by gelatin or casein zymography. It is possible that the insolubility of recombinant INV is a result of its conformation. During the process of purification (especially the solubilizing step), the conformation, as well as the proteolytic activity may have been altered. Thus, recombinant INV loses its enzymatic activity.

Possibly, zymography used in this chapter is not sensitive enough to detect the protease activity of INV. Another alternative strategy to detect protease activity is to utilize a liquid-based Quanticleave Protease Assay (Pierce or Sigma). This commercialized kit offers an extremely sensitive casein-based assay to determine protease activity in various pH and temperature profiles. This method can be tested by using purified INV proteins or the TNT system (*in vitro* transcription/translation). Both alternatives may increase the sensitivity of detection.

The most important thing is to ensure the whole experimental process is optimal for detecting the proteolytic activity. Ideally, another positive control using a metalloprotease should be used. In bacterial expression systems, MMP21, MMP28, matrilysin or MT1-MMP could be used as a positive control (Marchenko *et al.*, 2003; Lohi *et al.*, 2001; Soler *et al.*, 1995; Ho *et al.*, 1994). With an immunoprecipitation purification, other metalloprotease antibodies recognising MMP2, MMP9 and ADAM10 have been used to determine the immunoprecipitation conditions (Hall &

Erickson, 2003). Therefore, a well-known, functionally-active construct of a metalloprotease other than INV should be utilized as a control in future experiments for the procedures of protein expression and purification. With such a specific control, the protease activity of INV could be determined more reliably.

Chapter 8: Discussion

The *INV* gene encodes a conserved zinc metalloprotease of the M8 family. The loss of *INV* in homozygous mutant animals results in late larvae lethality and a range of pleiotropic phenotypes including cell cycle defects, nuclear protein accumulation and germ cell migration defects (McHugh *et al.*, 2004). In this thesis, possible mechanisms of localization and function of INV were approached. Endogenous INV is located on LDs and I showed the localization of INV to LDs during LD generation is protein kinase C dependent. In addition, the N-terminus of INV can be phosphorylated by PKC, suggesting that INV may be an *in vivo* substrate of PKC. PKC is thus a candidate for regulating INV's localization in the cellular starvation/re-feeding model. However, INV seems to have different localizations at different stages of the adipocyte differentiation process. In the early stage of differentiation, INV localized on LDs but dissociated from LDs in the late stage (mature adipocyte). The mRNA and protein levels of INV were significantly increased upon adipogenesis. This increase in INV could be blocked by inhibiting PKC and/or PI3K. This observation suggests that INV may be involved in adipogenesis and regulated by PKC/PI3K. Studying *Drosophila* loss-of-function *INV* mutants demonstrated that INV may play a role in regulating the insulin signaling pathway and subsequently affect the protein level of Lsd2, which facilitates lipid storage in *Drosophila*. Taken together, I speculate that INV plays a homeostatic role in physiology, possibly by mediating the InR/PI3K/Akt signaling pathway.

To LD or not to LD: that is the question

INV is the first metalloprotease which has been shown to localize on LDs. The

size of LDs can be increased when oleic acid was added exogenously. At the same time, an increases diameter of INV "rings" was observed. How does INV localize to LDs? Many reports have shown that the hydrophobic regions of specific proteins were implicated in targeting into LDs. Naturally occurring LD-associated proteins, such as perilipin, ADRP and TIP47 can interact with LDs through hydrophobic interactions (Garcia *et al.*, 2003; Nakamura *et al.*, 2003; Ohsaki *et al.*, 2006). Likewise, caveolin can associate with LDs via a central hydrophobic domain (Fujimoto *et al.*, 2001). Additionally, when the core protein of hepatitis C virus was expressed in cultured cells, it was found to associate with LDs via a central highly hydrophobic domain (Hope *et al*., 2002).

Does INV contain a hydrophobic region as its LD-associated companions do? Using a Kyte-Doolittle hydropathy plot to analyze the hydropobicity of INV, the only hydrophobic region of INV was identified at its C-terminus (http://gcat.davidson.edu/rakarnik/KD.html). This region was predicted to be GPI anchor site. The localization of INV to LDs might be through its GPI anchor. Recently, Gce1 (GPI-anchored phosphodiesterase) and CD73 have been reported to transiently localize to LDs via their GPI anchors (Muller *et al*., 2008; 2009). To further address the association between INV and LDs, mutating the GPI site might abrogate this targeting. It has been reported that the attachment of a GPI anchor to the plasma membrane can be interfered with by enzymatic cleavage by phosphatidylinositol-specific phospholipase C (PLC) (Lehto & Sharom, 2002). This method can be applied in future experiments.

To further address the localization and function of INV, human INV was labeled with different tags and over-expressed in human cell lines. Ectopically-expressed tagged INV localized to mitochondria. Why do endogenous INV and over-expressed

INV show different localizations? INV contains a predicted signal sequence and a predicted GPI addition site. Logically the signal sequence and the hydrophobic tail would be cleaved off and the C-terminus replaced by a GPI anchor. When a protein is synthesized via the secretory pathway, it can be delivered by vesicles to the Golgi apparatus and then be delivered to its final location. Often, the protein of interest can be highly expressed under the control of CMV promoter during transfection. If the cell can not provide efficient post-translational modification for this excess protein, altered protein conformation may cause mis-localization and/or degradation.

On the other hand, INV might have dual localizations. Post-translational modifications such as protein acylation or phosphorylation might result in different affinities to different subcellular compartments (Karniely & Pines, 2005). For example, acylation (the process of adding an acyl group to a compound) of SNAP23 leads to localization to LDs (Bostrom *et al*., 2007). Phosphorylation of CYP2B1 reduces its affinity to the ER but increases its affinity for mitochondria (Robin *et al.*, 2001). And finally, phosphorylation of caveolin is important for its redistribution to LDs (Blouin *et al.*, 2008). Therefore, it is possible that INV presents a similar case.

Immunoprecipitation of ectopically expressed HA-tagged INV from *Drosophila* heads has recently been utilized to identify potential interactors of INV. Two mitochondrially localized proteins, mitochondrial protein ATP synthase β and heat shock protein 70, were immunoprecipitated with HA-tagged INV in *Drosophila* (Francesca Di Cara, personal communication). In addition, these two proteins were also identified in LDs from embryos (Cermelli *et al.*, 2006). The relationship between INV and LD/mitochondria will be further investigated.

LDs are usually in the vicinity of other intracellular structures such as ER, mitochondria, Golgi and peroxisomes (Turro *et al.*, 2006; Bartz *et al.*, 2007).

Recently, many mitochondrial proteins have been found to localize to LDs, such as Cidea (Puri *et al*., 2008); FSP27/Cidec (Puri *et al.*, 2007) and Spartin/SPG20 (Eastman *et al.,* 2009). In addition, analysis of the sequence of ADRP has also identified a mitochondrial localization domain (Nakamura & Fujimoto, 2003). Using immunoelectron microscopy, it was found that an antibody recognizing ADRP labels not only LDs but also some adjacent membranous structures (Nakamura & Fujimoto, 2003).

Although endogenous INV localizes to LDs, relatively little information is known about the mechanisms that regulate protein targeting to LDs. In this study, targeting of INV to LDs was dependent on the activity of PKC. PKC inhibitor treatment decreased the formation of LDs in cells and caused dislocalization of INV from LDs and insoluble aggregates of INV to form. When PKC inhibitor was removed from cells, the re-localization of INV to LDs was observed, suggesting that the activity of PKC plays a crucial role in regulating INV's localization in the cellular starvation/re-feeding model.

Why does INV form aggregates in the cytosol in the presence of PKC inhibitor during re-feeding? The time course of starvation/re-feeding experiments suggested that INV can be recruited to newly synthesized LDs as they are generated (section 3.2.3). As discussed above, INV may bind to LDs via its hydrophobic GPI tail. Under condition of re-feeding, LDs would be generated and INV was recruited to LDs. Under this condition, the hydrophobic domain of INV might be exposed toward the outside to facilitate INV to bind to LD. However, in the presence of a PKC inhibitor, fewer LDs were formed in cells and INV may be forced to stay in the cytosol. Thus, the hydrophobic region of multiple INV might associate together to form intracellular aggregates (Figure 8.1). ApoB and α−synuclein have been reported to

bind to LDs through their hydrophobic regions (Ohsaki *et al.*, 2006; Cole *et al.*, 2002). It has been prospected that both ApoB and α-synuclein are likely to form aggregates via their hydrophobic domains when left free in the intracellular aqueous environment (Cole *et al.*, 2002; Segrest *et al.*, 2001). AAM-B is a putative methyltransferase and a resident protein of LDs. A N-terminal 28 amino acid hydrophobic sequence of AAM-B is necessary for targeting the protein to LD (Zehmer *et al.*, 2008). Overexpression of AAM-B lacking this sequence showed abolished targeting to LDs with the mutant protein appearing to form aggregates (Zehmer *et al.*, 2008). Thus, it is quite possible that the formation of INV aggregates is caused by the self-interaction of hydrophobic regions or by the interaction with other LDs binding proteins.

Although some LDs still existed in the presence of PKC inhibitor, LD containing INV were rarely observed (Figure 3-9A & B). It is thus possible that the phosphorylation of INV by PKC can promote the re-localization of INV to LDs. Thus, in the presence of a PKC inhibitor, INV can not be phosphorylated by PKC which might cause INV to lose its affinity to LDs. In addition, the *in vitro* PKC assay revealed that this targeting may be mediated by phosphorylating the N-terminus of INV (potentially at Ser34 or Thr269). Phosphorylation is vital for regulating activity, localization or molecular interaction of many proteins (Bartz *et al.*, 2007). In the presence of extra oleic acid or cholesterol, the recruitment of caveolin to LDs was dependent on Src and PKC activity (Blouin *et al.*, 2008; Le Lay *et al.*, 2006). Phosphatidylinositol transfer protein Nir2, implicated in maintaining the proper level of diacylglycerol in the Golgi apparatus, can either be in the Golgi apparatus or in LDs, depending on its phosphorylation state (Litvak *et al.*, 2005). Overexpression of a phospho-mimic form of Nir2 (T59E) caused Nir2 to redistribute to LDs.

Interestingly, this site is a putative PKC phosphorylation site (Livak *et al*., 2002). This suggests that INV's re-localization may also be regulated by PKC phosphorylation. To identify the exact PKC phosphorylation site of INV requires further analysis. INV might be phosphorylated at the site of Ser34 and / or Thr269 by PKC based on the NetPhosK 1.0 server's prediction. In the future, these predicted residues could be confirmed after modification by site-direct mutagenesis. Overexpressing phosphorylation mutant forms in cells could be examined for localization and effect on cells.

Figure 8.1 shows the predicted relationship between INV and LDs under different cell culture conditions. Under normal cell culture conditions, INV associates with LDs. In serum starved cells, INV is dispersed in the cytosol. In the presence of PKC inhibition during OA/FBS re-feeding, fewer LDs are present in cytosol and INV forms aggregates. The formation of the aggregates might due to the hydrophobic region of multiple INV associate together. Even though there are a few LDs remaining in the cytosol, INV does not tend to associate with these LDs. INV contains two potential PKC phosphorylation sites that might regulate the affinity between INV and LDs.

INV in adipocyte differentiation

The levels of LD binding proteins are regulated during the adipocyte differentiation process. Expression of the LD binding proteins CGI-58 and ADRP increased during adipocyte differentiation. The mRNA of Adipose triglyceride lipase (ATGL) increased at day 4 and 6 but declined at day 8 during adipogenesis, (Yamaguchi *et al.*, 2004; Zimmermann *et al.*, 2004). Since INV is a LD binding protein, the role of INV in adipogenesis is of interest. INV displays different

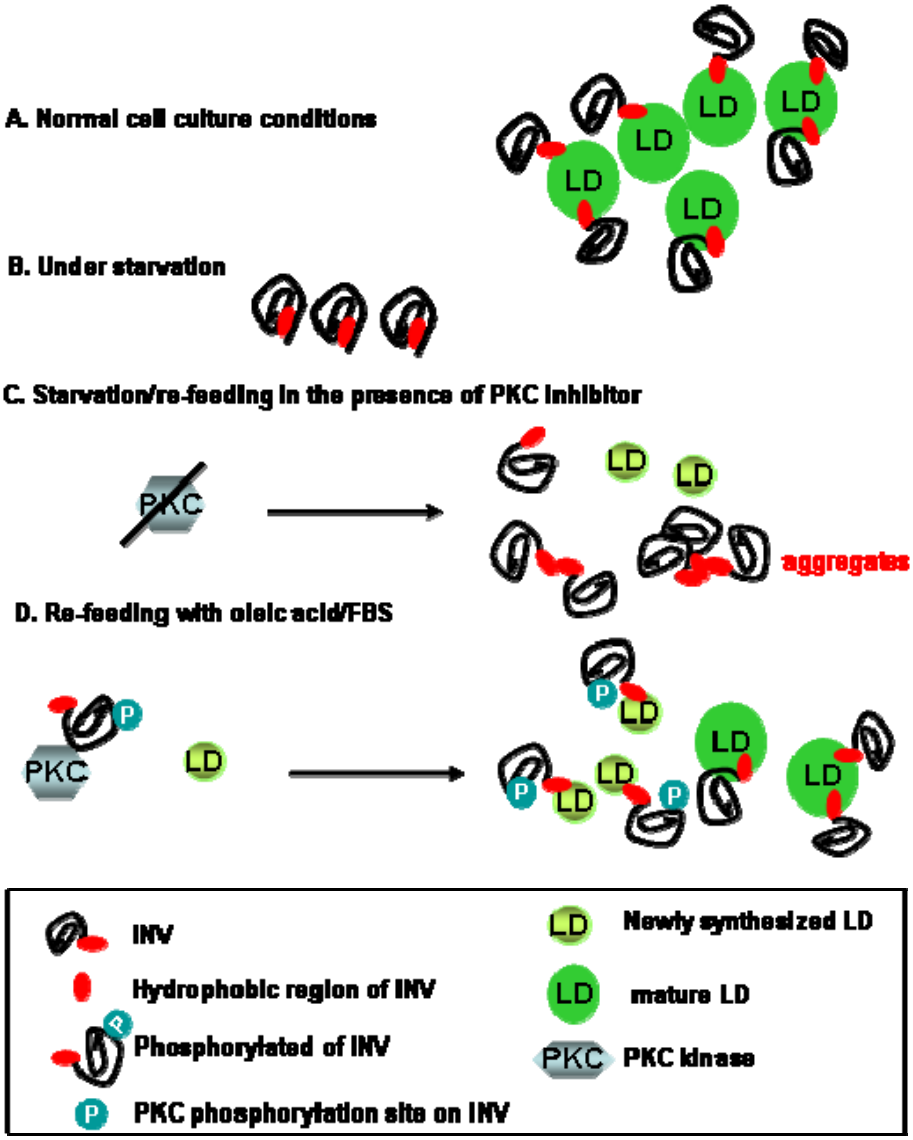

Figure 8.1 The localization mechanism of INV under starvation/re-feeding condition. A) Under normal cell culture conditions, INV associates with LDs possibly via its GPI anchor tail. B) In a serum-starved cell, the cell lacks detectable LDs and INV disperse in the cytosol. Under this condition, the hydrophobic domain of INV might be hidden rather than exposed. C) In the presence of PKC inhibitor during the re-feeding condition, the hydrophobic domain of INV might be exposed and interact with to form aggregated structures. Unphosphorylated INV might have a reduced binding affinity to LDs. D) Newly synthesized LDs are formed while re-feeding cells with oleic acid/FBS. Re-feeding induce the phosphorylation of INV and the phosphorylated INV might have elevated binding affinity to LDs, subsequently leading to the recruitment of INV to LD.

localization patterns during the differentiation process. In the early stage of differentiation (day 2 and day 4), numerous small LDs appeared and INV localized to these LDs. However, INV seemed to become diffuse in the cytosol in mature adipocytes (day 8). In the late stage of adipogenesis, several small LDs grew to more than 10 μm in diameter while the number of LDs drastically decreased. This suggests that the growth of LDs during adipocyte differentiation may be achieved by the successive fusion of LDs with one other (Nagayama *et al.*, 2007).

There was a trend that INV only binds to small LDs rather than larger ones in mature adipocyte cells (day 14 adipocyte). What is the possible role of INV on LDs in the early stages of adipogenesis? The formation of LDs in the early stage seems to be important for their further growth (Brasaemle *et al.*, 2004). INV was observed on LDs in the early stage, which suggests that INV might be recruited to LDs during LD biogenesis. An association of INV to LDs in early stage might be important for the recruitment of the other LD-associated proteins or for the maintenance of LD structure. At the later stage of adipogenesis (after day 6), the role of INV might be substituted for by other proteins. The proteins found on LDs in mature adipocytes are normally involved in lipid storage and lipolysis (Brasaemle *et al.*, 2004). Thus, I speculate that the absence of INV from the large LDs might suggest that INV is dispensable for lipid storage and/or lipolysis directly.

The existence of proteins on LDs is a dynamic scenario. After 10 minutes treatment of adipocytes with long chain fatty acids, small LDs emerge which are surrounded with TIP47 and S3-12 (Wolin *et al.*, 2006). Over the next hour of treatment, TIP47 and S3-12 still surround these small LDs, whereas, ADRP is concentrated an intermediate LDs and perilipin is concentrated on large LDs. After washing out long fatty acids, adipocytes return to their homeostatic LD architecture

and all of the LDs are encircled by perilipin (Wolin *et al.*, 2006). It would be interesting to examine INV in this type of experiment.

Although INV was not found on LDs in mature adipocyte cells, levels of mRNA and protein increased significantly during adipogenesis. Inhibition of adipogenesis by PKC and PI3K inhibitor resulted in a decrease in the levels of INV mRNA and protein. This suggests that the increase of INV during adipocyte differentiation may be dependent on the activity of PKC and PI3K. TIP47 has been reported to be functionally unrelated to adipogenesis (Yamaguchi *et al.*, 2004). Correspondingly, the level of TIP47 mRNA did not change following inhibition of PKC and PI3K. Is INV important for adipocyte differentiation? Inhibition of PKC or PI3K blocks not only adipogenesis but also the increase in INV. Is it because that inhibitor blocks adipogenesis which suppresses INV, or because the inhibitor affects INV which subsequently blocks adipocyte differentiation? In order to address these questions, the development of a depletion strategy (eg; shRNA, short-interfering RNA-mediated) knock down of INV will be necessary.

Recent studies on nuclear lamins have shed light on the role of lamin A in adipogenesis. Mutations in *LMNA* were shown to cause autosomal-dominant Emery-Dreyfuss muscular dystrophy, a disorder that affects skeletal muscle (Bonne *et al.*, 1999). A recent report has shown that the overexpression of nuclear lamin A can inhibit adipocyte differentiation (Boguslavsky *et al.*, 2006). This phenotype is associated with a decrease in the expression of PPARγ and Glut4 in 3T3-L1 cells. By contrast, a greater accumulation of intracellular lipid was found in embryonic fibroblasts lacking lamin A. The *lamin* knock-out embryonic fibroblasts also showed an increased level of phospho-Akt (Boguslavsky *et al.*, 2006). Previously the *INV* mutant in *Drosophila* was showed to have an enhanced level of nuclear envelope

proteins lamin Dm0 (B-type lamin), lamin C (A-type lamin) and otifen. INV was also shown to cleave lamin Dm0 *in vitro*. Cleavage activity was blocked by the addition of ortho-phenanthroline, a zinc chelator (McHugh *et al*., 2004). Phylogenetic analyses have revealed that the metzincin protease motif of INV is conserved in many different Species (Cobbe *et al.*, submitted). As there appears to be only one variant of INV present in mouse (Cobbe *et al.*, submitted), it is possible that mouse INV can play a similar role in the regulation of lamin A with subsequent effects an adipocyte differentiation. Therefore, INV is a strong candidate to mediate adipogenesis by regulating the level of lamin A.

The process of adipocyte differentiation is modulated by the activity of numerous transcription factors, these transcription factors as a consequence of activation of different signaling pathways (Rosen & MacDougald, 2006). Many adipocyte-specific genes, including the perilipin gene, are regulated by PPARγ, an essential transcription factor for adipogenesis (Rosen & Spiegelman, 2000). In 3T3-L1 cells, the presence of perilipin would imply that the transcription factor PPARγ has been activated, because PPARγ is a primary regulator of perilipin expression (Arimura *et al.*, 2004). The mRNA level of perilipin was dramatically increased at day 2 of adipogenesis and I demonstrated that the mRNA of INV also increase at day 2 (a grater increase was observed at day 4 of the differentiation) (Figure 4.6). This suggests that the increase of INV might be effected by PPARγ or a downstream transcription factor such as C/EBPα. In the presence of PKC and PI3K inhibitors, the level of PPARγ was decreased (Zhou *et al*., 2006; Yu *et al*., 2008). A decrease in PPARγ might be responsible for the reduced expression of INV or/and perilipin. However, to further clarify if PPARγ regulates INV expression in adipogenesis, inhibition of PPARγ by a specific inhibitor, siRNA or studies on

PPARγ null mice might help us to uncover a link between PPARγ and INV in adipocype differentiation (Rosen *et al*., 1999; Barak *et al*., 1999).

INV and insulin signaling pathway

Studying *Drosophila* loss-of-function *INV* mutants demonstrated that INV may play a role in regulating the insulin signaling pathway.

Embryonic fibroblasts lacking A-type lamin have increased phosphorylation level of Akt (Boguslavsky *et al.*, 2006). *Drosophila* INV mutant larvae exhibit increased levels of nuclear lamins (McHugh *et al.*, 2004). We have observed that the size of INV mutant larvae is smaller than that of wild type larvae at the same stage. The insulin signaling pathway is known to play a crucial role in growth and metabolism (Garofalo, 2002). The results in Chapter 5 revealed that the activity of dAkt was decreased in *INV* mutant larvae (as evidenced by a reduced level of phospho-Akt). In addition, the activity of its downstream effector molecule dS6K showed a decreased level presumed, with concomitant increase of d4E-BP transcripts. These observations suggest that INV action may be mediated by the insulin signaling pathway.

The insulin signaling pathway has been implicated in the control of fat metabolism in flies and mice. Both *S6K* and *4E-BP* mutant mice are lean and resistant to diet-induced obesity (Um *et al.*, 2004; Tsukiyama-Kohara *et al*., 2001). *4E-BP* mutant flies also show increased sensitivity to nutrient deprivation, leading to abnormal fat loss (Telema. *et al.*, 2005). Akt promotes the transcription of genes involved in lipid biosynthesis and storage pathways (Vereshchagina & Wilson, 2006; Eberle *et al.*, 2004). Activation of dAkt in *Drosophila* nurse cells results in the accumulation of Lsd2 (a homologue of perilipin) (Vereshchagina & Wilson, 200). A

decrease of phospho-Akt and reduced levels of Lsd2 protein were found in *INV* mutant larvae. Recently, Dr. Francesca Di Cara (Heck lab) performed a microarray genomic approach to identify genes whose expression changed in *INV* mutant analysis. Microarray analyses revealed an increase of *d4E-BP* and decrease of *Lsd1* (another PAT family protein in *Drosophila*). In the light of these data, I hypothesize that INV plays a homeostatic role, possibly by affecting the insulin signaling pathway.

Lsd2 mutants exhibit impaired lipid storage, thus the mutant larvae were less opaque than wild type larvae (Teixeira *et al*., 2003). The TAG (triacyglycerol) content was 27% less in the *Lsd2* mutant larvae than in wild type animals (Teixeira *et al*., 2003). Lsd2 protein levels were lower in *INV* mutant larvae, thus it is possible that the TAG level in *INV* mutant larvae might also be less than in wild type. Indeed, decreased TAG has recently been observed in *INV* mutant by TAG quantification (Edward Duca, PhD student in Heck lab).

Although the insulin signaling pathway appears to be impaired in the *INV* mutants, the precise relationship between INV and insulin signaling is still unknown. It has been demonstrated that lamin A/C can physically interact with protein phosphatase 2A (PP2A) and may modulate the function of PP2A in 3T3-L1 cells (Berlo *et al*., 2005). PP2A has been shown to dephosphorylate Akt and thereby regulate the activity of Akt in both mammals and *Drosophila* (Ugi *et al*., 2004; Vereshchagina *et al*., 2008). Since lamin Dm0 and lamin C were found to accumulate in *INV* mutant larval neuroblasts and it is possible that INV may interact with insulin signaling via the lamins. Of course, other possibilities can not be ruled out at this time. Identification of regulating and interactors of INV will be help to confirm or rrefute this hypothesis.

Overall, this PhD thesis provides a new view of INV. The data presented hint to a regulator for the localization of INV and a function that is potentially regulated by INV. The localization of INV to newly synthesized LDs is dependent on the activity of PKC. It is possible that PKC can phosphorylate INV and increase INV's affinity to newly synthesized LD, upon re-feeding (Figure 8.1).

Figure 8.2 represent the potential functions regulated by INV. According to the study on *INV* mutant larvae in *Drosophila*, levels of phospho-Akt and phospho-dS6K were decreased; while the levels of *4E-BP* mRNA were increased. In addition, the expression of Lsd2 was decreased in the *INV* mutant. These results suggest that INV might normally play a positive role in the insulin signaling pathway and subsequently regulate lipid homeostasis (through Lsd2). The insulin signaling pathway plays a central role in adipogenesis (Rosen & MacDougald, 2006). INV may regulate insulin signaling, thus it is quite possible that INV might also regulate adipocyte differentiation via this pathway. Overexpression of lamin A inhibits the accumulation of lipid, and is accompanied by a reduced expression of PPARγ (Boguslavsky *et al.*, 2006). Lamins accumulate in *INV* mutant larvae (Mchugh *et al.*, 2004). An increase of INV was observed during adipogenesis and was blocked in the presence of a PKC or PI3K inhibitor. All these data imply that INV is a strong candidate for regulation of adipocyte differentiation via lamin A and for mediating the insulin signaling pathway.

The results from this project prompted us to further analyze the physiological role of INV. More experiments need to be carried out to decipher the role of INV in both localization and function. By using the starvation/re-feeding model, a regulator of INV localization was identified. Utilization of *INV* mutant larvae in *Drosophila*

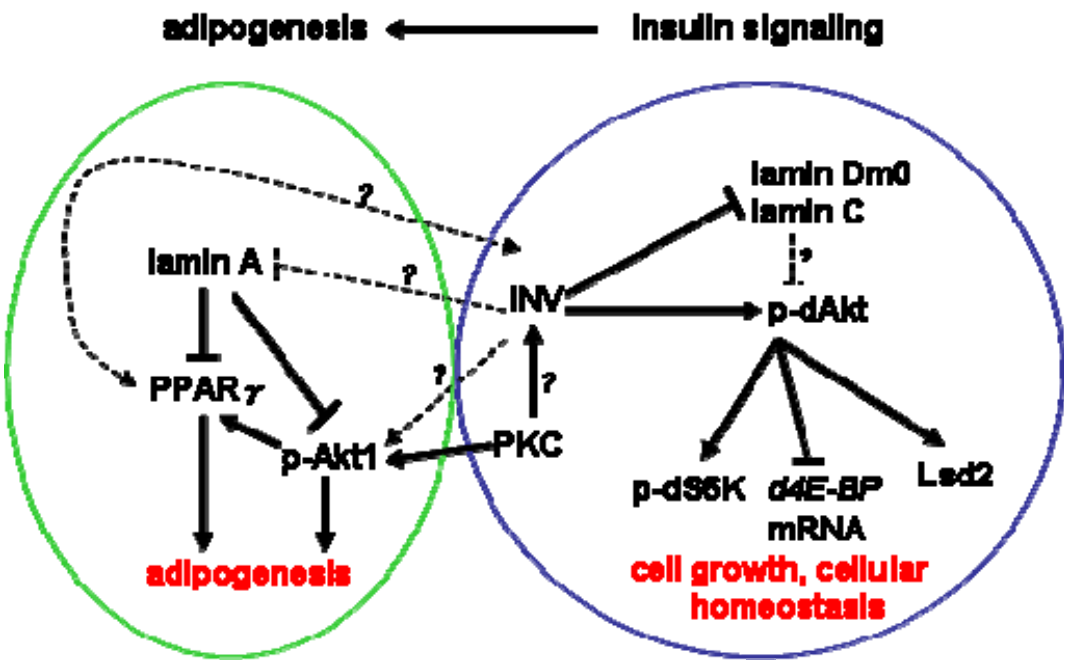

Figure 8.2 INV may regulate insulin signaling and mediate adipogenesis. Based on the study of *INV* mutants, it is possible that INV may play a promoting role in insulin signaling by activating dAkt and its downstream molecules in *Drosophila* (blue circle). In addition, INV might play a negative role in regulating the levels of lamins (*INV* mutants appeared to increase the level of lamins in neuroblasts, McHugh *et al.*, 2004). It has recently been shown that lamin A acts as an inhibitor of adipocyte differentiation, possibly by affecting PPARγ and insulin signaling (green circle, Boguslavsky *et al*., 2006). Put together, these data provide a link for INV in insulin signaling pathway and adipogenesis. INV might also promote the activity of Akt by down-regulating lamin proteins and facilitating the transcription factor, PPARγwhich subsequently promotes differentiation of adipocytes.

and the *in vitro* adipogenesis system will help us to address the likely functions of INV. As is appropriate, this thesis raises a number of provocative questions: Why does INV localize to LDs? What is the function of INV on LDs? What is the precise role of INV in adipocyte differentiation? How does INV regulate the insulin signaling pathway? It will be important to address these questions in the future.

References

Accili, D., and K.C. Arden. 2004. FoxOs at the crossroads of cellular metabolism, differentiation, and transformation. *Cell*. 117:421-6.

Accili, D., and S.I. Taylor. 1991. Targeted inactivation of the insulin receptor gene in mouse 3T3-L1 fibroblasts via homologous recombination. *Proc Natl Acad Sci U S A*. 88:4708-12.

Accioly, M.T., P. Pacheco, C.M. Maya-Monteiro, N. Carrossini, B.K. Robbs, S.S. Oliveira, C. Kaufmann, J.A. Morgado-Diaz, P.T. Bozza, and J.P. Viola. 2008. Lipid bodies are reservoirs of cyclooxygenase-2 and sites of prostaglandin-E2 synthesis in colon cancer cells. *Cancer Res*. 68:1732-40.

Aebi, U., J. Cohn, L. Buhle, and L. Gerace. 1986. The nuclear lamina is a meshwork of intermediate-type filaments. *Nature*. 323:560-4.

Agarwal, A.K., and A. Garg. 2006. Genetic basis of lipodystrophies and management of metabolic complications. *Annu Rev Med*. 57:297-311.

Akimoto, N., T. Sato, C. Iwata, M. Koshizuka, F. Shibata, A. Nagai, M. Sumida, and A. Ito. 2005. Expression of perilipin A on the surface of lipid droplets increases along with the differentiation of hamster sebocytes in vivo and in vitro. *J Invest Dermatol*. 124:1127-33.

Alexander, C.M., S. Selvarajan, J. Mudgett, and Z. Werb. 2001. Stromelysin-1 regulates adipogenesis during mammary gland involution. *J Cell Biol*. 152:693-703.

Andersson, L., P. Bostrom, J. Ericson, M. Rutberg, B. Magnusson, D. Marchesan, M. Ruiz, L. Asp, P. Huang, M.A. Frohman, J. Boren, and S.O. Olofsson. 2006. PLD1 and ERK2 regulate cytosolic lipid droplet formation. *J Cell Sci*. 119:2246-57.

Arimura, N., T. Horiba, M. Imagawa, M. Shimizu, and R. Sato. 2004. The peroxisome proliferator-activated receptor gamma regulates expression of the perilipin gene in adipocytes. *J Biol Chem*. 279:10070-6.

Arquier, N., and P. Leopold. 2007. Fly foie gras: modeling fatty liver in Drosophila. *Cell Metab*. 5:83-5.

Baker, K.D., and C.S. Thummel. 2007. Diabetic larvae and obese flies-emerging studies of metabolism in Drosophila. *Cell Metab*. 6:257-66.

Bakowska, J.C., R. Jenkins, J. Pendleton, and C. Blackstone. 2005. The Troyer syndrome (SPG20) protein spartin interacts with Eps15. *Biochem Biophys Res Commun*. 334:1042-8.

Baldassarre, M., A. Pompeo, G. Beznoussenko, C. Castaldi, S. Cortellino, M.A. McNiven, A. Luini, and R. Buccione. 2003. Dynamin participates in focal extracellular matrix degradation by invasive cells. *Mol Biol Cell*. 14:1074-84.

Barak, Y., M.C. Nelson, E.S. Ong, Y.Z. Jones, P. Ruiz-Lozano, K.R. Chien, A. Koder, and R.M. Evans. 1999. PPAR gamma is required for placental, cardiac, and adipose tissue development. *Mol Cell*. 4:585-95.

Barbero, P., L. Bittova, and S.R. Pfeffer. 2002. Visualization of Rab9-mediated vesicle transport from endosomes to the trans-Golgi in living cells. *J Cell Biol*. 156:511-8.

Bartz, R., J.K. Zehmer, M. Zhu, Y. Chen, G. Serrero, Y. Zhao, and P. Liu. 2007. Dynamic activity of lipid droplets: protein phosphorylation and GTP-mediated protein translocation. *J Proteome Res*. 6:3256-65.

Baudry, A., Z.Z. Yang, and B.A. Hemmings. 2006. PKBalpha is required for adipose differentiation of mouse embryonic fibroblasts. *J Cell Sci*. 119:889-97.

Belham, C., S. Wu, and J. Avruch. 1999. Intracellular signalling: PDK1--a kinase at the hub of things. *Curr Biol*. 9:R93-6.

Beller, M., D. Riedel, L. Jansch, G. Dieterich, J. Wehland, H. Jackle, and R.P. Kuhnlein. 2006. Characterization of the Drosophila lipid droplet subproteome. *Mol Cell Proteomics*. 5:1082-94.

Black, R.A., C.T. Rauch, C.J. Kozlosky, J.J. Peschon, J.L. Slack, M.F. Wolfson, B.J. Castner,

K.L. Stocking, P. Reddy, S. Srinivasan, N. Nelson, N. Boiani, K.A. Schooley, M. Gerhart, R. Davis, J.N. Fitzner, R.S. Johnson, R.J. Paxton, C.J. March, and D.P. Cerretti. 1997. A metalloproteinase disintegrin that releases tumour-necrosis factor-alpha from cells. *Nature*. 385:729-33.

Blouin, C.M., S. Le Lay, F. Lasnier, I. Dugail, and E. Hajduch. 2008. Regulated association of caveolins to lipid droplets during differentiation of 3T3-L1 adipocytes. *Biochem Biophys Res Commun*. 376:331-5.

Boguslavsky, R.L., C.L. Stewart, and H.J. Worman. 2006. Nuclear lamin A inhibits adipocyte differentiation: implications for Dunnigan-type familial partial lipodystrophy. *Hum Mol Genet*. 15:653-63.

Bonne, G., M.R. Di Barletta, S. Varnous, H.M. Becane, E.H. Hammouda, L. Merlini, F. Muntoni, C.R. Greenberg, F. Gary, J.A. Urtizberea, D. Duboc, M. Fardeau, D. Toniolo, and K. Schwartz. 1999. Mutations in the gene encoding lamin A/C cause autosomal dominant Emery-Dreifuss muscular dystrophy. *Nat Genet*. 21:285-8.

Bossie, C.A., and M.M. Sanders. 1993. A cDNA from Drosophila melanogaster encodes a lamin C-like intermediate filament protein. *J Cell Sci*. 104 (Pt 4):1263-72.

Bostrom, P., L. Andersson, M. Rutberg, J. Perman, U. Lidberg, B.R. Johansson, J. Fernandez-Rodriguez, J. Ericson, T. Nilsson, J. Boren, and S.O. Olofsson. 2007. SNARE proteins mediate fusion between cytosolic lipid droplets and are implicated in insulin sensitivity. *Nat Cell Biol*. 9:1286-93.

Bouloumie, A., C. Sengenes, G. Portolan, J. Galitzky, and M. Lafontan. 2001. Adipocyte produces matrix metalloproteinases 2 and 9: involvement in adipose differentiation. *Diabetes*. 50:2080-6.

Bouvier, J., P. Schneider, and R. Etges. 1995. Leishmanolysin: surface metalloproteinase of Leishmania. *Methods Enzymol*. 248:614-33.

Brasaemle, D.L., T. Barber, A.R. Kimmel, and C. Londos. 1997. Post-translational regulation of perilipin expression. Stabilization by stored intracellular neutral lipids. *J Biol Chem*. 272:9378-87.

Brasaemle, D.L., T. Barber, N.E. Wolins, G. Serrero, E.J. Blanchette-Mackie, and C. Londos. 1997. Adipose differentiation-related protein is an ubiquitously expressed lipid storage droplet-associated protein. *J Lipid Res*. 38:2249-63.

Brasaemle, D.L., G. Dolios, L. Shapiro, and R. Wang. 2004. Proteomic analysis of proteins associated with lipid droplets of basal and lipolytically stimulated 3T3-L1 adipocytes. *J Biol Chem*. 279:46835-42.

Brasaemle, D.L., and N.E. Wolins. 2006. Isolation of lipid droplets from cells by density gradient centrifugation. *Curr Protoc Cell Biol*. Chapter 3:Unit 3 15.

Brazil, D.P., Z.Z. Yang, and B.A. Hemmings. 2004. Advances in protein kinase B signalling: AKTion on multiple fronts. *Trends Biochem Sci*. 29:233-42.

Breitkreutz, D., L. Braiman-Wiksman, N. Daum, M.F. Denning, and T. Tennenbaum. 2007. Protein kinase C family: on the crossroads of cell signaling in skin and tumor epithelium. *J Cancer Res Clin Oncol*. 133:793-808.

Britton, J.S., W.K. Lockwood, L. Li, S.M. Cohen, and B.A. Edgar. 2002. Drosophila's insulin/PI3-kinase pathway coordinates cellular metabolism with nutritional conditions. *Dev Cell*. 2:239-49.

Brogiolo, W., H. Stocker, T. Ikeya, F. Rintelen, R. Fernandez, and E. Hafen. 2001. An evolutionarily conserved function of the Drosophila insulin receptor and insulin-like peptides in growth control. *Curr Biol*. 11:213-21.

Brown, D.A. 2001. Lipid droplets: proteins floating on a pool of fat. *Curr Biol*. 11:R446-9.

Brown, L.M., H.L. Fox, S.A. Hazen, K.F. LaNoue, S.R. Rannels, and C.J. Lynch. 1997. Role of the matrixin MMP-2 in multicellular organization of adipocytes cultured in basement membrane components. *Am J Physiol*. 272:C937-49.

Buccione, R., J.D. Orth, and M.A. McNiven. 2004. Foot and mouth: podosomes, invadopodia and circular dorsal ruffles. *Nat Rev Mol Cell Biol*. 5:647-57.

Buch, S., C. Melcher, M. Bauer, J. Katzenberger, and M.J. Pankratz. 2008. Opposing effects of dietary protein and sugar regulate a transcriptional target of Drosophila insulin-like

peptide signaling. *Cell Metab*. 7:321-32.
Burgering, B.M. 2008. A brief introduction to FOXOlogy. *Oncogene*. 27:2258-62.
Burgering, B.M., and G.J. Kops. 2002. Cell cycle and death control: long live Forkheads. *Trends Biochem Sci*. 27:352-60.
Burgess, A., J.C. Labbe, S. Vigneron, N. Bonneaud, J.M. Strub, A. Van Dorsselaer, T. Lorca, and A. Castro. 2008. Chfr interacts and colocalizes with TCTP to the mitotic spindle. *Oncogene*.
Button, L.L., and W.R. McMaster. 1988. Molecular cloning of the major surface antigen of leishmania. *J Exp Med*. 167:724-9.
Button, L.L., N.E. Reiner, and W.R. McMaster. 1991. Modification of GP63 genes from diverse species of Leishmania for expression of recombinant protein at high levels in Escherichia coli. *Mol Biochem Parasitol*. 44:213-24.
Button, L.L., G. Wilson, C.R. Astell, and W.R. McMaster. 1993. Recombinant Leishmania surface glycoprotein GP63 is secreted in the baculovirus expression system as a latent metalloproteinase. *Gene*. 134:75-81.
Canavoso, L.E., Z.E. Jouni, K.J. Karnas, J.E. Pennington, and M.A. Wells. 2001. Fat metabolism in insects. *Annu Rev Nutr*. 21:23-46.
Caunt, C.J., C.A. Rivers, B.L. Conway-Campbell, M.R. Norman, and C.A. McArdle. 2008. Epidermal growth factor receptor and protein kinase C signaling to ERK2: spatiotemporal regulation of ERK2 by dual specificity phosphatases. *J Biol Chem*. 283:6241-52.
Cavallo, D., D. Rudy, A. Mohammadi, J. Macri, and K. Adeli. 1999. Studies on degradative mechanisms mediating post-translational fragmentation of apolipoprotein B and the generation of the 70-kDa fragment. *J Biol Chem*. 274:23135-43.
Cermelli, S., Y. Guo, S.P. Gross, and M.A. Welte. 2006. The lipid-droplet proteome reveals that droplets are a protein-storage depot. *Curr Biol*. 16:1783-95.
Chanderbhan, R., B.J. Noland, T.J. Scallen, and G.V. Vahouny. 1982. Sterol carrier protein2. Delivery of cholesterol from adrenal lipid droplets to mitochondria for pregnenolone synthesis. *J Biol Chem*. 257:8928-34.
Chang, B.H., L. Li, A. Paul, S. Taniguchi, V. Nannegari, W.C. Heird, and L. Chan. 2006. Protection against fatty liver but normal adipogenesis in mice lacking adipose differentiation-related protein. *Mol Cell Biol*. 26:1063-76.
Chang, C., and Z. Werb. 2001. The many faces of metalloproteases: cell growth, invasion, angiogenesis and metastasis. *Trends Cell Biol*. 11:S37-43.
Chavey, C., B. Mari, M.N. Monthouel, S. Bonnafous, P. Anglard, E. Van Obberghen, and S. Tartare-Deckert. 2003. Matrix metalloproteinases are differentially expressed in adipose tissue during obesity and modulate adipocyte differentiation. *J Biol Chem*. 278:11888-96.
Chen, J.S., A.S. Greenberg, and S.M. Wang. 2002. Oleic acid-induced PKC isozyme translocation in RAW 264.7 macrophages. *J Cell Biochem*. 86:784-91.
Chen, L.C., M.E. Noelken, and H. Nagase. 1993. Disruption of the cysteine-75 and zinc ion coordination is not sufficient to activate the precursor of human matrix metalloproteinase 3 (stromelysin 1). *Biochemistry*. 32:10289-95.
Chen, Z., K. Guo, S.Y. Toh, Z. Zhou, and P. Li. 2000. Mitochondria localization and dimerization are required for CIDE-B to induce apoptosis. *J Biol Chem*. 275:22619-22.
Cho, S.Y., E.S. Shin, P.J. Park, D.W. Shin, H.K. Chang, D. Kim, H.H. Lee, J.H. Lee, S.H. Kim, M.J. Song, I.S. Chang, O.S. Lee, and T.R. Lee. 2007. Identification of mouse Prp19p as a lipid droplet-associated protein and its possible involvement in the biogenesis of lipid droplets. *J Biol Chem*. 282:2456-65.
Christoffersen, C.T., H. Tornqvist, C.J. Vlahos, D. Bucchini, J. Jami, P. De Meyts, and R.L. Joshi. 1998. Insulin and insulin-like growth factor-I receptor mediated differentiation of 3T3-F442A cells into adipocytes: effect of PI 3-kinase inhibition. *Biochem Biophys Res Commun*. 246:426-30.
Ciechanover, A., and A.L. Schwartz. 1998. The ubiquitin-proteasome pathway: the

complexity and myriad functions of proteins death. *Proc Natl Acad Sci U S A*. 95:2727-30.
Cinti, S., S. Eberbach, M. Castellucci, and D. Accili. 1998. Lack of insulin receptors affects the formation of white adipose tissue in mice. A morphometric and ultrastructural analysis. *Diabetologia*. 41:171-7.
Clarke, S.L., C.E. Robinson, and J.M. Gimble. 1997. CAAT/enhancer binding proteins directly modulate transcription from the peroxisome proliferator-activated receptor gamma 2 promoter. *Biochem Biophys Res Commun*. 240:99-103.
Cobb, M.H., and E.J. Goldsmith. 1995. How MAP kinases are regulated. *J Biol Chem*. 270:14843-6.
Cohen, A.W., T.P. Combs, P.E. Scherer, and M.P. Lisanti. 2003. Role of caveolin and caveolae in insulin signaling and diabetes. *Am J Physiol Endocrinol Metab*. 285:E1151-60.
Cole, N.B., D.D. Murphy, T. Grider, S. Rueter, D. Brasaemle, and R.L. Nussbaum. 2002. Lipid droplet binding and oligomerization properties of the Parkinson's disease protein alpha-synuclein. *J Biol Chem*. 277:6344-52.
Colombani, J., S. Raisin, S. Pantalacci, T. Radimerski, J. Montagne, and P. Leopold. 2003. A nutrient sensor mechanism controls Drosophila growth. *Cell*. 114:739-49.
Cross, D.A., D.R. Alessi, P. Cohen, M. Andjelkovich, and B.A. Hemmings. 1995. Inhibition of glycogen synthase kinase-3 by insulin mediated by protein kinase B. *Nature*. 378:785-9.
Dahl, K.N., S.M. Kahn, K.L. Wilson, and D.E. Discher. 2004. The nuclear envelope lamina network has elasticity and a compressibility limit suggestive of a molecular shock absorber. *J Cell Sci*. 117:4779-86.
Dalen, K.T., T. Dahl, E. Holter, B. Arntsen, C. Londos, C. Sztalryd, and H.I. Nebb. 2007. LSDP5 is a PAT protein specifically expressed in fatty acid oxidizing tissues. *Biochim Biophys Acta*. 1771:210-27.
Dalen, K.T., K. Schoonjans, S.M. Ulven, M.S. Weedon-Fekjaer, T.G. Bentzen, H. Koutnikova, J. Auwerx, and H.I. Nebb. 2004. Adipose tissue expression of the lipid droplet-associating proteins S3-12 and perilipin is controlled by peroxisome proliferator-activated receptor-gamma. *Diabetes*. 53:1243-52.
Darlington, G.J., S.E. Ross, and O.A. MacDougald. 1998. The role of C/EBP genes in adipocyte differentiation. *J Biol Chem*. 273:30057-60.
Davis, R.A. 1999. Cell and molecular biology of the assembly and secretion of apolipoprotein B-containing lipoproteins by the liver. *Biochim Biophys Acta*. 1440:1-31.
Dememes, D., and E. Scarfone. 1992. Fodrin immunocytochemical localization in the striated organelles of the rat vestibular hair cells. *Hear Res*. 61:155-60.
Demontis, F., and N. Perrimon. 2009. Integration of Insulin receptor/Foxo signaling and dMyc activity during muscle growth regulates body size in Drosophila. *Development*. 136:983-93.
Downward, J. 1998. Mechanisms and consequences of activation of protein kinase B/Akt. *Curr Opin Cell Biol*. 10:262-7.
Eastman, S.W., M. Yassaee, and P.D. Bieniasz. 2009. A role for ubiquitin ligases and Spartin/SPG20 in lipid droplet turnover. *J Cell Biol*. 184:881-94.
Eberle, D., B. Hegarty, P. Bossard, P. Ferre, and F. Foufelle. 2004. SREBP transcription factors: master regulators of lipid homeostasis. *Biochimie*. 86:839-48.
Elberg, G., J.M. Gimble, and S.Y. Tsai. 2000. Modulation of the murine peroxisome proliferator-activated receptor gamma 2 promoter activity by CCAAT/enhancer-binding proteins. *J Biol Chem*. 275:27815-22.
Etges, R. 1992. Identification of a surface metalloproteinase on 13 species of Leishmania isolated from humans, Crithidia fasciculata, and Herpetomonas samuelpessoai. *Acta Trop*. 50:205-17.
Feve, B. 2005. Adipogenesis: cellular and molecular aspects. *Best Pract Res Clin Endocrinol Metab*. 19:483-99.
Fingar, D.C., and J. Blenis. 2004. Target of rapamycin (TOR): an integrator of nutrient and

growth factor signals and coordinator of cell growth and cell cycle progression. *Oncogene*. 23:3151-71.
Fisher, D.Z., N. Chaudhary, and G. Blobel. 1986. cDNA sequencing of nuclear lamins A and C reveals primary and secondary structural homology to intermediate filament proteins. *Proc Natl Acad Sci U S A*. 83:6450-4.
Fisher, E., H. Scharnagl, M.M. Hoffmann, K. Kusterer, D. Wittmann, H. Wieland, W. Gross, and W. Marz. 1999. Mutations in the apolipoprotein (apo) B-100 receptor-binding region: detection of apo B-100 (Arg3500-->Trp) associated with two new haplotypes and evidence that apo B-100 (Glu3405-->Gln) diminishes receptor-mediated uptake of LDL. *Clin Chem*. 45:1026-38.
Fitzsimons, H.L., R.J. Bland, and M.J. During. 2002. Promoters and regulatory elements that improve adeno-associated virus transgene expression in the brain. *Methods*. 28:227-36.
Fleming, I., S.J. MacKenzie, R.G. Vernon, N.G. Anderson, M.D. Houslay, and E. Kilgour. 1998. Protein kinase C isoforms play differential roles in the regulation of adipocyte differentiation. *Biochem J*. 333 (Pt 3):719-27.
Frame, S., and P. Cohen. 2001. GSK3 takes centre stage more than 20 years after its discovery. *Biochem J*. 359:1-16.
Frame, S., P. Cohen, and R.M. Biondi. 2001. A common phosphate binding site explains the unique substrate specificity of GSK3 and its inactivation by phosphorylation. *Mol Cell*. 7:1321-7.
Frangioni, J.V., and B.G. Neel. 1993. Solubilization and purification of enzymatically active glutathione S-transferase (pGEX) fusion proteins. *Anal Biochem*. 210:179-87.
Fujimoto, T., H. Kogo, K. Ishiguro, K. Tauchi, and R. Nomura. 2001. Caveolin-2 is targeted to lipid droplets, a new "membrane domain" in the cell. *J Cell Biol*. 152:1079-85.
Fujimoto, T., and Y. Ohsaki. 2006. Proteasomal and autophagic pathways converge on lipid droplets. *Autophagy*. 2:299-301.
Fujimoto, T., Y. Ohsaki, J. Cheng, M. Suzuki, and Y. Shinohara. 2008. Lipid droplets: a classic organelle with new outfits. *Histochem Cell Biol*. 130:263-79.
Fujimoto, Y., H. Itabe, J. Sakai, M. Makita, J. Noda, M. Mori, Y. Higashi, S. Kojima, and T. Takano. 2004. Identification of major proteins in the lipid droplet-enriched fraction isolated from the human hepatocyte cell line HuH7. *Biochim Biophys Acta*. 1644:47-59.
Gant, T.M., and K.L. Wilson. 1997. Nuclear assembly. *Annu Rev Cell Dev Biol*. 13:669-95.
Gao, J., and G. Serrero. 1999. Adipose differentiation related protein (ADRP) expressed in transfected COS-7 cells selectively stimulates long chain fatty acid uptake. *J Biol Chem*. 274:16825-30.
Gao, J., H. Ye, and G. Serrero. 2000. Stimulation of adipose differentiation related protein (ADRP) expression in adipocyte precursors by long-chain fatty acids. *J Cell Physiol*. 182:297-302.
Garcia, A., A. Sekowski, V. Subramanian, and D.L. Brasaemle. 2003. The central domain is required to target and anchor perilipin A to lipid droplets. *J Biol Chem*. 278:625-35.
Garofalo, R.S. 2002. Genetic analysis of insulin signaling in Drosophila. *Trends Endocrinol Metab*. 13:156-62.
Garofalo, R.S., S.J. Orena, K. Rafidi, A.J. Torchia, J.L. Stock, A.L. Hildebrandt, T. Coskran, S.C. Black, D.J. Brees, J.R. Wicks, J.D. McNeish, and K.G. Coleman. 2003. Severe diabetes, age-dependent loss of adipose tissue, and mild growth deficiency in mice lacking Akt2/PKB beta. *J Clin Invest*. 112:197-208.
Gatti, M., and B.S. Baker. 1989. Genes controlling essential cell-cycle functions in Drosophila melanogaster. *Genes Dev*. 3:438-53.
Gershman, B., O. Puig, L. Hang, R.M. Peitzsch, M. Tatar, and R.S. Garofalo. 2007. High-resolution dynamics of the transcriptional response to nutrition in Drosophila: a key role for dFOXO. *Physiol Genomics*. 29:24-34.
Giasson, B.I., J.E. Duda, M.S. Forman, V.M. Lee, and J.Q. Trojanowski. 2001. Prominent perikaryal expression of alpha- and beta-synuclein in neurons of dorsal root ganglion

and in medullary neurons. *Exp Neurol*. 172:354-62.
Gingras, A.C., S.P. Gygi, B. Raught, R.D. Polakiewicz, R.T. Abraham, M.F. Hoekstra, R. Aebersold, and N. Sonenberg. 1999. Regulation of 4E-BP1 phosphorylation: a novel two-step mechanism. *Genes Dev*. 13:1422-37.
Gingras, A.C., B. Raught, and N. Sonenberg. 1999. eIF4 initiation factors: effectors of mRNA recruitment to ribosomes and regulators of translation. *Annu Rev Biochem*. 68:913-63.
Giot, L., J.S. Bader, C. Brouwer, A. Chaudhuri, B. Kuang, Y. Li, Y.L. Hao, C.E. Ooi, B. Godwin, E. Vitols, G. Vijayadamodar, P. Pochart, H. Machineni, M. Welsh, Y. Kong, B. Zerhusen, R. Malcolm, Z. Varrone, A. Collis, M. Minto, S. Burgess, L. McDaniel, E. Stimpson, F. Spriggs, J. Williams, K. Neurath, N. Ioime, M. Agee, E. Voss, K. Furtak, R. Renzulli, N. Aanensen, S. Carrolla, E. Bickelhaupt, Y. Lazovatsky, A. DaSilva, J. Zhong, C.A. Stanyon, R.L. Finley, Jr., K.P. White, M. Braverman, T. Jarvie, S. Gold, M. Leach, J. Knight, R.A. Shimkets, M.P. McKenna, J. Chant, and J.M. Rothberg. 2003. A protein interaction map of Drosophila melanogaster. *Science*. 302:1727-36.
Girard, J., D. Perdereau, F. Foufelle, C. Prip-Buus, and P. Ferre. 1994. Regulation of lipogenic enzyme gene expression by nutrients and hormones. *FASEB J*. 8:36-42.
Glauser, D.A., and W. Schlegel. 2007. The emerging role of FOXO transcription factors in pancreatic beta cells. *J Endocrinol*. 193:195-207.
Goetze, S., F. Eilers, A. Bungenstock, U. Kintscher, P. Stawowy, F. Blaschke, K. Graf, R.E. Law, E. Fleck, and M. Grafe. 2002. PPAR activators inhibit endothelial cell migration by targeting Akt. *Biochem Biophys Res Commun*. 293:1431-7.
Gomis-Ruth, F.X. 2003. Structural aspects of the metzincin clan of metalloendopeptidases. *Mol Biotechnol*. 24:157-202.
Grams, F., R. Huber, L.F. Kress, L. Moroder, and W. Bode. 1993. Activation of snake venom metalloproteinases by a cysteine switch-like mechanism. *FEBS Lett*. 335:76-80.
Gray, S., M.W. Feinberg, S. Hull, C.T. Kuo, M. Watanabe, S. Sen-Banerjee, A. DePina, R. Haspel, and M.K. Jain. 2002. The Kruppel-like factor KLF15 regulates the insulin-sensitive glucose transporter GLUT4. *J Biol Chem*. 277:34322-8.
Green, H., and O. Kehinde. 1974. Sublines of mouse 3T3 cells that accumulate lipid. *Cell* 1:113-116
Green, H., and O. Kehinde. 1975. An established preadipose cell line and its differentiation in culture. II. Factors affecting the adipose conversion. *Cell*. 5:19-27.
Green, H., and O. Kehinde. 1976. Spontaneous heritable changes leading to increased adipose conversion in 3T3 cells. *Cell*. 7:105-13.
Green, H., and O. Kehinde. 1979. Formation of normally differentiated subcutaneous fat pads by an established preadipose cell line. *J Cell Physiol*. 101:169-71.
Grewal, S.S. 2009. Insulin/TOR signaling in growth and homeostasis: a view from the fly world. *Int J Biochem Cell Biol*. 41:1006-10.
Gronke, S., M. Beller, S. Fellert, H. Ramakrishnan, H. Jackle, and R.P. Kuhnlein. 2003. Control of fat storage by a Drosophila PAT domain protein. *Curr Biol*. 13:603-6.
Gronke, S., A. Mildner, S. Fellert, N. Tennagels, S. Petry, G. Muller, H. Jackle, and R.P. Kuhnlein. 2005. Brummer lipase is an evolutionary conserved fat storage regulator in Drosophila. *Cell Metab*. 1:323-30.
Gross, J., and C.M. Lapiere. 1962. Collagenolytic activity in amphibian tissues: a tissue culture assay. *Proc Natl Acad Sci U S A*. 48:1014-22.
Gruenbaum, Y., Y. Landesman, B. Drees, J.W. Bare, H. Saumweber, M.R. Paddy, J.W. Sedat, D.E. Smith, B.M. Benton, and P.A. Fisher. 1988. Drosophila nuclear lamin precursor Dm0 is translated from either of two developmentally regulated mRNA species apparently encoded by a single gene. *J Cell Biol*. 106:585-96.
Gruenbaum, Y., K.L. Wilson, A. Harel, M. Goldberg, and M. Cohen. 2000. Review: nuclear lamins--structural proteins with fundamental functions. *J Struct Biol*. 129:313-23.
Guertin, D.A., K.V. Guntur, G.W. Bell, C.C. Thoreen, and D.M. Sabatini. 2006. Functional genomics identifies TOR-regulated genes that control growth and division. *Curr Biol*. 16:958-70.

Gunjan, A., J. Paik, and A. Verreault. 2005. Regulation of histone synthesis and nucleosome assembly. *Biochimie*. 87:625-35.
Gunjan, A., and A. Verreault. 2003. A Rad53 kinase-dependent surveillance mechanism that regulates histone protein levels in S. cerevisiae. *Cell*. 115:537-49.
Guo, Y., K.R. Cordes, R.V. Farese, Jr., and T.C. Walther. 2009. Lipid droplets at a glance. *J Cell Sci*. 122:749-52.
Gutierrez, E., D. Wiggins, B. Fielding, and A.P. Gould. 2007. Specialized hepatocyte-like cells regulate Drosophila lipid metabolism. *Nature*. 445:275-80.
Hafen, E. 2004. Interplay between growth factor and nutrient signaling: lessons from Drosophila TOR. *Curr Top Microbiol Immunol*. 279:153-67.
Hafen, E., and H. Stocker. 2003. How are the sizes of cells, organs, and bodies controlled? *PLoS Biol*. 1:E86.
Hall, R.J., and C.A. Erickson. 2003. ADAM 10: an active metalloprotease expressed during avian epithelial morphogenesis. *Dev Biol*. 256:146-59.
Hawkes, S.P., H. Li, and G.T. Taniguchi. 2001. Zymography and reverse zymography for detecting MMPs, and TIMPs. *Methods Mol Biol*. 151:399-410.
Hay, N., and N. Sonenberg. 2004. Upstream and downstream of mTOR. *Genes Dev*. 18:1926-45.
Hennig, K.M., J. Colombani, and T.P. Neufeld. 2006. TOR coordinates bulk and targeted endocytosis in the Drosophila melanogaster fat body to regulate cell growth. *J Cell Biol*. 173:963-74.
Ho, T.F., M.W. Qoronfleh, R.C. Wahl, T.A. Pulvino, K.J. Vavra, J. Falvo, T.M. Banks, P.G. Brake, and R.B. Ciccarelli. 1994. Gene expression, purification and characterization of recombinant human neutrophil collagenase. *Gene*. 146:297-301.
Holm, C. 2003. Molecular mechanisms regulating hormone-sensitive lipase and lipolysis. *Biochem Soc Trans*. 31:1120-4.
Hooper, N.M. 1994. Families of zinc metalloproteases. *FEBS Lett*. 354:1-6.
Hope, R.G., D.J. Murphy, and J. McLauchlan. 2002. The domains required to direct core proteins of hepatitis C virus and GB virus-B to lipid droplets share common features with plant oleosin proteins. *J Biol Chem*. 277:4261-70.
Imamura, M., T. Inoguchi, S. Ikuyama, S. Taniguchi, K. Kobayashi, N. Nakashima, and H. Nawata. 2002. ADRP stimulates lipid accumulation and lipid droplet formation in murine fibroblasts. *Am J Physiol Endocrinol Metab*. 283:E775-83.
Imanishi, Y., V. Gerke, and K. Palczewski. 2004. Retinosomes: new insights into intracellular managing of hydrophobic substances in lipid bodies. *J Cell Biol*. 166:447-53.
Inoki, K., Y. Li, T. Zhu, J. Wu, and K.L. Guan. 2002. TSC2 is phosphorylated and inhibited by Akt and suppresses mTOR signalling. *Nat Cell Biol*. 4:648-57.
Jiang, Z.Y., Q.L. Zhou, K.A. Coleman, M. Chouinard, Q. Boese, and M.P. Czech. 2003. Insulin signaling through Akt/protein kinase B analyzed by small interfering RNA-mediated gene silencing. *Proc Natl Acad Sci U S A*. 100:7569-74.
Juhasz, G., B. Erdi, M. Sass, and T.P. Neufeld. 2007. Atg7-dependent autophagy promotes neuronal health, stress tolerance, and longevity but is dispensable for metamorphosis in Drosophila. *Genes Dev*. 21:3061-6.
Kadereit, B., P. Kumar, W.J. Wang, D. Miranda, E.L. Snapp, N. Severina, I. Torregroza, T. Evans, and D.L. Silver. 2008. Evolutionarily conserved gene family important for fat storage. *Proc Natl Acad Sci U S A*. 105:94-9.
Kajita, M., Y. Itoh, T. Chiba, H. Mori, A. Okada, H. Kinoh, and M. Seiki. 2001. Membrane-type 1 matrix metalloproteinase cleaves CD44 and promotes cell migration. *J Cell Biol*. 153:893-904.
Karniely, S., and O. Pines. 2005. Single translation--dual destination: mechanisms of dual protein targeting in eukaryotes. *EMBO Rep*. 6:420-5.
Khan, A.R., and M.N. James. 1998. Molecular mechanisms for the conversion of zymogens to active proteolytic enzymes. *Protein Sci*. 7:815-36.
Kim, J.B., P. Sarraf, M. Wright, K.M. Yao, E. Mueller, G. Solanes, B.B. Lowell, and B.M. Spiegelman. 1998. Nutritional and insulin regulation of fatty acid synthetase and

leptin gene expression through ADD1/SREBP1. *J Clin Invest*. 101:1-9.
Kim, J.E., and J. Chen. 2004. regulation of peroxisome proliferator-activated receptor-gamma activity by mammalian target of rapamycin and amino acids in adipogenesis. *Diabetes*. 53:2748-56.
Klausner, R.D., J.G. Donaldson, and J. Lippincott-Schwartz. 1992. Brefeldin A: insights into the control of membrane traffic and organelle structure. *J Cell Biol*. 116:1071-80.
Kohyama-Koganeya, A., Y.J. Kim, M. Miura, and Y. Hirabayashi. 2008. A Drosophila orphan G protein-coupled receptor BOSS functions as a glucose-responding receptor: loss of boss causes abnormal energy metabolism. *Proc Natl Acad Sci U S A*. 105:15328-33.
Kops, G.J., and B.M. Burgering. 1999. Forkhead transcription factors: new insights into protein kinase B (c-akt) signaling. *J Mol Med*. 77:656-65.
Koshikawa, N., G. Giannelli, V. Cirulli, K. Miyazaki, and V. Quaranta. 2000. Role of cell surface metalloprotease MT1-MMP in epithelial cell migration over laminin-5. *J Cell Biol*. 148:615-24.
Kuerschner, L., C. Moessinger, and C. Thiele. 2008. Imaging of lipid biosynthesis: how a neutral lipid enters lipid droplets. *Traffic*. 9:338-52.
Kumar, Y., J. Cocchiaro, and R.H. Valdivia. 2006. The obligate intracellular pathogen Chlamydia trachomatis targets host lipid droplets. *Curr Biol*. 16:1646-51.
Kunwar, P.S., D.E. Siekhaus, and R. Lehmann. 2006. In vivo migration: a germ cell perspective. *Annu Rev Cell Dev Biol*. 22:237-65.
Lawrence, J.C., T.A. Lin, L.P. McMahon, and K.M. Choi. 2004. Modulation of the protein kinase activity of mTOR. *Curr Top Microbiol Immunol*. 279:199-213.
Le Lay, S., E. Hajduch, M.R. Lindsay, X. Le Liepvre, C. Thiele, P. Ferre, R.G. Parton, T. Kurzchalia, K. Simons, and I. Dugail. 2006. Cholesterol-induced caveolin targeting to lipid droplets in adipocytes: a role for caveolar endocytosis. *Traffic*. 7:549-61.
Leevers, S.J., D. Weinkove, L.K. MacDougall, E. Hafen, and M.D. Waterfield. 1996. The Drosophila phosphoinositide 3-kinase Dp110 promotes cell growth. *EMBO J*. 15:6584-94.
Lefevre, C., F. Jobard, F. Caux, B. Bouadjar, A. Karaduman, R. Heilig, H. Lakhdar, A. Wollenberg, J.L. Verret, J. Weissenbach, M. Ozguc, M. Lathrop, J.F. Prud'homme, and J. Fischer. 2001. Mutations in CGI-58, the gene encoding a new protein of the esterase/lipase/thioesterase subfamily, in Chanarin-Dorfman syndrome. *Am J Hum Genet*. 69:1002-12.
Leevers, S.J. and Hafen, E. 2004. Growth regulation by insulin and TOR signaling in *Drosophila*. In: M.N. Hall, M. Raff and G. Thomas, Editors, *Cell Growth: Control of Cell Size*, Cold Spring Harbor Laboratory Press, Cold Spring Harbor, NY. pp. 167–192.
Lehto, M.T., and F.J. Sharom. 2002. PI-specific phospholipase C cleavage of a reconstituted GPI-anchored protein: modulation by the lipid bilayer. *Biochemistry*. 41:1398-408.
Lian, T., and R.J. Ho. 1997. Cholera toxin B-mediated targeting of lipid vesicles containing ganglioside GM1 to mucosal epithelial cells. *Pharm Res*. 14:1309-15.
Limb, G.A., K. Matter, G. Murphy, A.D. Cambrey, P.N. Bishop, G.E. Morris, and P.T. Khaw. 2005. Matrix metalloproteinase-1 associates with intracellular organelles and confers resistance to lamin A/C degradation during apoptosis. *Am J Pathol*. 166:1555-63.
Listenberger, L.L., and D.A. Brown. 2008. Lipid droplets. *Curr Biol*. 18:R237-8.
Littman, E.D., S. Pitchumoni, M.R. Garfinkel, and E.C. Opara. 2000. Role of protein kinase C isoenzymes in fatty acid stimulation of insulin secretion. *Pancreas*. 20:256-63.
Litvak, V., N. Dahan, S. Ramachandran, H. Sabanay, and S. Lev. 2005. Maintenance of the diacylglycerol level in the Golgi apparatus by the Nir2 protein is critical for Golgi secretory function. *Nat Cell Biol*. 7:225-34.
Litvak, V., Y.D. Shaul, M. Shulewitz, R. Amarilio, S. Carmon, and S. Lev. 2002. Targeting of Nir2 to lipid droplets is regulated by a specific threonine residue within its PI-transfer domain. *Curr Biol*. 12:1513-8.
Liu, P., Y. Ying, Y. Zhao, D.I. Mundy, M. Zhu, and R.G. Anderson. 2004. Chinese hamster

ovary K2 cell lipid droplets appear to be metabolic organelles involved in membrane traffic. *J Biol Chem*. 279:3787-92.
Lizcano, J.M., and D.R. Alessi. 2002. The insulin signalling pathway. *Curr Biol*. 12:R236-8.
Loechel, F., M.T. Overgaard, C. Oxvig, R. Albrechtsen, and U.M. Wewer. 1999. Regulation of human ADAM 12 protease by the prodomain. Evidence for a functional cysteine switch. *J Biol Chem*. 274:13427-33.
Lohi, J., C.L. Wilson, J.D. Roby, and W.C. Parks. 2001. Epilysin, a novel human matrix metalloproteinase (MMP-28) expressed in testis and keratinocytes and in response to injury. *J Biol Chem*. 276:10134-44.
Londos, C., D.L. Brasaemle, C.J. Schultz, J.P. Segrest, and A.R. Kimmel. 1999. Perilipins, ADRP, and other proteins that associate with intracellular neutral lipid droplets in animal cells. *Semin Cell Dev Biol*. 10:51-8.
Londos, C., J. Gruia-Gray, D.L. Brasaemle, C.M. Rondinone, T. Takeda, N.K. Dwyer, T. Barber, A.R. Kimmel, and E.J. Blanchette-Mackie. 1996. Perilipin: possible roles in structure and metabolism of intracellular neutral lipids in adipocytes and steroidogenic cells. *Int J Obes Relat Metab Disord*. 20 Suppl 3:S97-101.
Lu, J., F. Rashid, and P.C. Byrne. 2006. The hereditary spastic paraplegia protein spartin localises to mitochondria. *J Neurochem*. 98:1908-19.
Lu, X., J. Gruia-Gray, N.G. Copeland, D.J. Gilbert, N.A. Jenkins, C. Londos, and A.R. Kimmel. 2001. The murine perilipin gene: the lipid droplet-associated perilipins derive from tissue-specific, mRNA splice variants and define a gene family of ancient origin. *Mamm Genome*. 12:741-9.
Luo, H.R., H. Hattori, M.A. Hossain, L. Hester, Y. Huang, W. Lee-Kwon, M. Donowitz, E. Nagata, and S.H. Snyder. 2003. Akt as a mediator of cell death. *Proc Natl Acad Sci U S A*. 100:11712-7.
Luong, N., C.R. Davies, R.J. Wessells, S.M. Graham, M.T. King, R. Veech, R. Bodmer, and S.M. Oldham. 2006. Activated FOXO-mediated insulin resistance is blocked by reduction of TOR activity. *Cell Metab*. 4:133-42.
Macdonald, M.H., C.J. Morrison, and W.R. McMaster. 1995. Analysis of the active site and activation mechanism of the Leishmania surface metalloproteinase GP63. *Biochim Biophys Acta*. 1253:199-207.
Mahajan, K.N., and B.S. Mitchell. 2003. Role of human Pso4 in mammalian DNA repair and association with terminal deoxynucleotidyl transferase. *Proc Natl Acad Sci U S A*. 100:10746-51.
Maines, M.D. 2007. Biliverdin reductase: PKC interaction at the cross-talk of MAPK and PI3K signaling pathways. *Antioxid Redox Signal*. 9:2187-95.
Mancia, F., and L. Shapiro. 2005. ADAM and Eph: how Ephrin-signaling cells become detached. *Cell*. 123:185-7.
Manning, B.D., A.R. Tee, M.N. Logsdon, J. Blenis, and L.C. Cantley. 2002. Identification of the tuberous sclerosis complex-2 tumor suppressor gene product tuberin as a target of the phosphoinositide 3-kinase/akt pathway. *Mol Cell*. 10:151-62.
Marchenko, G.N., N.D. Marchenko, and A.Y. Strongin. 2003. The structure and regulation of the human and mouse matrix metalloproteinase-21 gene and protein. *Biochem J*. 372:503-15.
Martin, D.E., and M.N. Hall. 2005. The expanding TOR signaling network. *Curr Opin Cell Biol*. 17:158-66.
Martin, D.E., T. Powers, and M.N. Hall. 2006. Regulation of ribosome biogenesis: where is TOR? *Cell Metab*. 4:259-60.
Martin, S., and R.G. Parton. 2005. Caveolin, cholesterol, and lipid bodies. *Semin Cell Dev Biol*. 16:163-74.
Martin, S., and R.G. Parton. 2006. Lipid droplets: a unified view of a dynamic organelle. *Nat Rev Mol Cell Biol*. 7:373-8.
McGwire, B.S., and K.P. Chang. 1996. Posttranslational regulation of a Leishmania HEXXH metalloprotease (gp63). The effects of site-specific mutagenesis of catalytic, zinc binding, N-glycosylation, and glycosyl phosphatidylinositol addition sites on

N-terminal end cleavage, intracellular stability, and extracellular exit. *J Biol Chem*. 271:7903-9.
McGwire, B.S., K.P. Chang, and D.M. Engman. 2003. Migration through the extracellular matrix by the parasitic protozoan Leishmania is enhanced by surface metalloprotease gp63. *Infect Immun*. 71:1008-10.
McHugh, B., S.A. Krause, B. Yu, A.M. Deans, S. Heasman, P. McLaughlin, and M.M. Heck. 2004. Invadolysin: a novel, conserved metalloprotease links mitotic structural rearrangements with cell migration. *J Cell Biol*. 167:673-86.
McKeon, F.D., M.W. Kirschner, and D. Caput. 1986. Homologies in both primary and secondary structure between nuclear envelope and intermediate filament proteins. *Nature*. 319:463-8.
Merzlyak, E.M., J. Goedhart, D. Shcherbo, M.E. Bulina, A.S. Shcheglov, A.F. Fradkov, A. Gaintzeva, K.A. Lukyanov, S. Lukyanov, T.W. Gadella, and D.M. Chudakov. 2007. Bright monomeric red fluorescent protein with an extended fluorescence lifetime. *Nat Methods*. 4:555-7.
Minshall, R.D., C. Tiruppathi, S.M. Vogel, W.D. Niles, A. Gilchrist, H.E. Hamm, and A.B. Malik. 2000. Endothelial cell-surface gp60 activates vesicle formation and trafficking via G(i)-coupled Src kinase signaling pathway. *J Cell Biol*. 150:1057-70.
Mishra-Gorur, K., M.D. Rand, B. Perez-Villamil, and S. Artavanis-Tsakonas. 2002. Down-regulation of Delta by proteolytic processing. *J Cell Biol*. 159:313-24.
Miura, S., J.W. Gan, J. Brzostowski, M.J. Parisi, C.J. Schultz, C. Londos, B. Oliver, and A.R. Kimmel. 2002. Functional conservation for lipid storage droplet association among Perilipin, ADRP, and TIP47 (PAT)-related proteins in mammals, Drosophila, and Dictyostelium. *J Biol Chem*. 277:32253-7.
Miyanari, Y., K. Atsuzawa, N. Usuda, K. Watashi, T. Hishiki, M. Zayas, R. Bartenschlager, T. Wakita, M. Hijikata, and K. Shimotohno. 2007. The lipid droplet is an important organelle for hepatitis C virus production. *Nat Cell Biol*. 9:1089-97.
Mori, T., H. Sakaue, H. Iguchi, H. Gomi, Y. Okada, Y. Takashima, K. Nakamura, T. Nakamura, T. Yamauchi, N. Kubota, T. Kadowaki, Y. Matsuki, W. Ogawa, R. Hiramatsu, and M. Kasuga. 2005. Role of Kruppel-like factor 15 (KLF15) in transcriptional regulation of adipogenesis. *J Biol Chem*. 280:12867-75.
Muller, G., C. Jung, J. Straub, S. Wied, and W. Kramer. 2009. Induced release of membrane vesicles from rat adipocytes containing glycosylphosphatidylinositol-anchored microdomain and lipid droplet signalling proteins. *Cell Signal*. 21:324-38.
Muller, G., S. Wied, J. Straub, and C. Jung. 2008. Coordinated regulation of esterification and lipolysis by palmitate, H2O2 and the anti-diabetic sulfonylurea drug, glimepiride, in rat adipocytes. *Eur J Pharmacol*. 597:6-18.
Murphy, D.J., and J. Vance. 1999. Mechanisms of lipid-body formation. *Trends Biochem Sci*. 24:109-15.
Murphy, G. 2008. The ADAMs: signalling scissors in the tumour microenvironment. *Nat Rev Cancer*. 8:929-41.
Nagai, S., C. Shimizu, M. Umetsu, S. Taniguchi, M. Endo, H. Miyoshi, N. Yoshioka, M. Kubo, and T. Koike. 2004. Identification of a functional peroxisome proliferator-activated receptor responsive element within the murine perilipin gene. *Endocrinology*. 145:2346-56.
Nakae, J., W.H. Biggs, 3rd, T. Kitamura, W.K. Cavenee, C.V. Wright, K.C. Arden, and D. Accili. 2002. Regulation of insulin action and pancreatic beta-cell function by mutated alleles of the gene encoding forkhead transcription factor Foxo1. *Nat Genet*. 32:245-53.
Nakae, J., T. Kitamura, Y. Kitamura, W.H. Biggs, 3rd, K.C. Arden, and D. Accili. 2003. The forkhead transcription factor Foxo1 regulates adipocyte differentiation. *Dev Cell*. 4:119-29.
Nakamura, N., and T. Fujimoto. 2003. Adipose differentiation-related protein has two independent domains for targeting to lipid droplets. *Biochem Biophys Res Commun*. 306:333-8.

Nakanishi, H., K.A. Brewer, and J.H. Exton. 1993. Activation of the zeta isozyme of protein kinase C by phosphatidylinositol 3,4,5-trisphosphate. *J Biol Chem*. 268:13-6.
Nakatsukasa, K., and J.L. Brodsky. 2008. The recognition and retrotranslocation of misfolded proteins from the endoplasmic reticulum. *Traffic*. 9:861-70.
Nanbu-Wakao, R., Y. Fujitani, Y. Masuho, M. Muramatu, and H. Wakao. 2000. Prolactin enhances CCAAT enhancer-binding protein-beta (C/EBP beta) and peroxisome proliferator-activated receptor gamma (PPAR gamma) messenger RNA expression and stimulates adipogenic conversion of NIH-3T3 cells. *Mol Endocrinol*. 14:307-16.
Naslavsky, N., J. Rahajeng, D. Rapaport, M. Horowitz, and S. Caplan. 2007. EHD1 regulates cholesterol homeostasis and lipid droplet storage. *Biochem Biophys Res Commun*. 357:792-9.
Newton, A.C. 2009. Lipid activation of protein kinases. *J Lipid Res*. 50 Suppl:S266-71.
Noe, V., B. Fingleton, K. Jacobs, H.C. Crawford, S. Vermeulen, W. Steelant, E. Bruyneel, L.M. Matrisian, and M. Mareel. 2001. Release of an invasion promoter E-cadherin fragment by matrilysin and stromelysin-1. *J Cell Sci*. 114:111-118.
Novikoff, A.B., P.M. Novikoff, O.M. Rosen, and C.S. Rubin. 1980. Organelle relationships in cultured 3T3-L1 preadipocytes. *J Cell Biol*. 87:180-96.
Ohsaki, Y., J. Cheng, A. Fujita, T. Tokumoto, and T. Fujimoto. 2006. Cytoplasmic lipid droplets are sites of convergence of proteasomal and autophagic degradation of apolipoprotein B. *Mol Biol Cell*. 17:2674-83.
Ohsaki, Y., T. Maeda, M. Maeda, K. Tauchi-Sato, and T. Fujimoto. 2006. Recruitment of TIP47 to lipid droplets is controlled by the putative hydrophobic cleft. *Biochem Biophys Res Commun*. 347:279-87.
Olofsson, S.O., P. Bostrom, L. Andersson, M. Rutberg, M. Levin, J. Perman, and J. Boren. 2008. Triglyceride containing lipid droplets and lipid droplet-associated proteins. *Curr Opin Lipidol*. 19:441-7.
Orlandi, P.A., and P.H. Fishman. 1998. Filipin-dependent inhibition of cholera toxin: evidence for toxin internalization and activation through caveolae-like domains. *J Cell Biol*. 141:905-15.
Ozeki, S., J. Cheng, K. Tauchi-Sato, N. Hatano, H. Taniguchi, and T. Fujimoto. 2005. Rab18 localizes to lipid droplets and induces their close apposition to the endoplasmic reticulum-derived membrane. *J Cell Sci*. 118:2601-11.
Page-McCaw, A., A.J. Ewald, and Z. Werb. 2007. Matrix metalloproteinases and the regulation of tissue remodelling. *Nat Rev Mol Cell Biol*. 8:221-33.
Palanker, L., J.M. Tennessen, G. Lam, and C.S. Thummel. 2009. Drosophila HNF4 regulates lipid mobilization and beta-oxidation. *Cell Metab*. 9:228-39.
Palanker, L., J.M. Tennessen, G. Lam, and C.S. Thummel. 2009. Drosophila HNF4 regulates lipid mobilization and beta-oxidation. *Cell Metab*. 9:228-39.
Palanker, L., J.M. Tennessen, G. Lam, and C.S. Thummel. 2009. Drosophila HNF4 regulates lipid mobilization and beta-oxidation. *Cell Metab*. 9:228-39.
Parton, R.G., M. Hanzal-Bayer, and J.F. Hancock. 2006. Biogenesis of caveolae: a structural model for caveolin-induced domain formation. *J Cell Sci*. 119:787-96.
Patel, H., H. Cross, C. Proukakis, R. Hershberger, P. Bork, F.D. Ciccarelli, M.A. Patton, V.A. McKusick, and A.H. Crosby. 2002. SPG20 is mutated in Troyer syndrome, an hereditary spastic paraplegia. *Nat Genet*. 31:347-8.
Peng, X.D., P.Z. Xu, M.L. Chen, A. Hahn-Windgassen, J. Skeen, J. Jacobs, D. Sundararajan, W.S. Chen, S.E. Crawford, K.G. Coleman, and N. Hay. 2003. Dwarfism, impaired skin development, skeletal muscle atrophy, delayed bone development, and impeded adipogenesis in mice lacking Akt1 and Akt2. *Genes Dev*. 17:1352-65.
Peschon, J.J., J.L. Slack, P. Reddy, K.L. Stocking, S.W. Sunnarborg, D.C. Lee, W.E. Russell, B.J. Castner, R.S. Johnson, J.N. Fitzner, R.W. Boyce, N. Nelson, C.J. Kozlosky, M.F. Wolfson, C.T. Rauch, D.P. Cerretti, R.J. Paxton, C.J. March, and R.A. Black. 1998. An essential role for ectodomain shedding in mammalian development. *Science*. 282:1281-4.
Pol, A., R. Luetterforst, M. Lindsay, S. Heino, E. Ikonen, and R.G. Parton. 2001. A caveolin

dominant negative mutant associates with lipid bodies and induces intracellular cholesterol imbalance. *J Cell Biol*. 152:1057-70.
Pol, A., S. Martin, M.A. Fernandez, C. Ferguson, A. Carozzi, R. Luetterforst, C. Enrich, and R.G. Parton. 2004. Dynamic and regulated association of caveolin with lipid bodies: modulation of lipid body motility and function by a dominant negative mutant. *Mol Biol Cell*. 15:99-110.
Polak, P., and M.N. Hall. 2009. mTOR and the control of whole body metabolism. *Curr Opin Cell Biol*.
Pollard, T. D., and W. C. Earnshaw. 2007. Cell Biology. SAUNDER, An imprint of Elsevier Science, Philadelphia, United States of America.
Potter, C.J., L.G. Pedraza, and T. Xu. 2002. Akt regulates growth by directly phosphorylating Tsc2. *Nat Cell Biol*. 4:658-65.
Prusty, D., B.H. Park, K.E. Davis, and S.R. Farmer. 2002. Activation of MEK/ERK signaling promotes adipogenesis by enhancing peroxisome proliferator-activated receptor gamma (PPARgamma) and C/EBPalpha gene expression during the differentiation of 3T3-L1 preadipocytes. *J Biol Chem*. 277:46226-32.
Puig, O., and R. Tjian. 2006. Nutrient availability and growth: regulation of insulin signaling by dFOXO/FOXO1. *Cell Cycle*. 5:503-5.
Puri, V., S. Konda, S. Ranjit, M. Aouadi, A. Chawla, M. Chouinard, A. Chakladar, and M.P. Czech. 2007. Fat-specific protein 27, a novel lipid droplet protein that enhances triglyceride storage. *J Biol Chem*. 282:34213-8.
Puri, V., S. Ranjit, S. Konda, S.M. Nicoloro, J. Straubhaar, A. Chawla, M. Chouinard, C. Lin, A. Burkart, S. Corvera, R.A. Perugini, and M.P. Czech. 2008. Cidea is associated with lipid droplets and insulin sensitivity in humans. *Proc Natl Acad Sci U S A*. 105:7833-8.
Rappoport, J.Z., and S.M. Simon. 2003. Real-time analysis of clathrin-mediated endocytosis during cell migration. *J Cell Sci*. 116:847-55.
Rawlings, N.D., and A.J. Barrett. 1995. Evolutionary families of metallopeptidases. *Methods Enzymol*. 248:183-228.
Rawlings, N.D., F.R. Morton, and A.J. Barrett. 2006. MEROPS: the peptidase database. *Nucleic Acids Res*. 34:D270-2.
Robenek, H., O. Hofnagel, I. Buers, M.J. Robenek, D. Troyer, and N.J. Severs. 2006. Adipophilin-enriched domains in the ER membrane are sites of lipid droplet biogenesis. *J Cell Sci*. 119:4215-24.
Robin, M.A., H.K. Anandatheerthavarada, J.K. Fang, M. Cudic, L. Otvos, and N.G. Avadhani. 2001. Mitochondrial targeted cytochrome P450 2E1 (P450 MT5) contains an intact N terminus and requires mitochondrial specific electron transfer proteins for activity. *J Biol Chem*. 276:24680-9.
Rosen, E.D., and O.A. MacDougald. 2006. Adipocyte differentiation from the inside out. *Nat Rev Mol Cell Biol*. 7:885-96.
Rosen, E.D., P. Sarraf, A.E. Troy, G. Bradwin, K. Moore, D.S. Milstone, B.M. Spiegelman, and R.M. Mortensen. 1999. PPAR gamma is required for the differentiation of adipose tissue in vivo and in vitro. *Mol Cell*. 4:611-7.
Rosen, E.D., and B.M. Spiegelman. 2000. Molecular regulation of adipogenesis. *Annu Rev Cell Dev Biol*. 16:145-71.
Rosen, E.D., and B.M. Spiegelman. 2000. Peroxisome proliferator-activated receptor gamma ligands and atherosclerosis: ending the heartache. *J Clin Invest*. 106:629-31.
Ross, S.E., R.L. Erickson, N. Hemati, and O.A. MacDougald. 1999. Glycogen synthase kinase 3 is an insulin-regulated C/EBPalpha kinase. *Mol Cell Biol*. 19:8433-41.
Rulifson, E.J., S.K. Kim, and R. Nusse. 2002. Ablation of insulin-producing neurons in flies: growth and diabetic phenotypes. *Science*. 296:1118-20.
Russell, D.G., and H. Wilhelm. 1986. The involvement of the major surface glycoprotein (gp63) of Leishmania promastigotes in attachment to macrophages. *J Immunol*. 136:2613-20.
Rusten, T.E., K. Lindmo, G. Juhasz, M. Sass, P.O. Seglen, A. Brech, and H. Stenmark. 2004. Programmed autophagy in the Drosophila fat body is induced by ecdysone through

regulation of the PI3K pathway. *Dev Cell*. 7:179-92.
Sakata, N., T.E. Phillips, and J.L. Dixon. 2001. Distribution, transport, and degradation of apolipoprotein B-100 in HepG2 cells. *J Lipid Res*. 42:1947-58.
Sakaue, H., W. Ogawa, M. Matsumoto, S. Kuroda, M. Takata, T. Sugimoto, B.M. Spiegelman, and M. Kasuga. 1998. Posttranscriptional control of adipocyte differentiation through activation of phosphoinositide 3-kinase. *J Biol Chem*. 273:28945-52.
Sampson, S.R., and D.R. Cooper. 2006. Specific protein kinase C isoforms as transducers and modulators of insulin signaling. *Mol Genet Metab*. 89:32-47.
Sano, H., S. Kane, E. Sano, C.P. Miinea, J.M. Asara, W.S. Lane, C.W. Garner, and G.E. Lienhard. 2003. Insulin-stimulated phosphorylation of a Rab GTPase-activating protein regulates GLUT4 translocation. *J Biol Chem*. 278:14599-602.
Santos, A.C., and R. Lehmann. 2004. Germ cell specification and migration in Drosophila and beyond. *Curr Biol*. 14:R578-89.
Sato, S., M. Fukasawa, Y. Yamakawa, T. Natsume, T. Suzuki, I. Shoji, H. Aizaki, T. Miyamura, and M. Nishijima. 2006. Proteomic profiling of lipid droplet proteins in hepatoma cell lines expressing hepatitis C virus core protein. *J Biochem*. 139:921-30.
Saucedo, L.J., and B.A. Edgar. 2002. Why size matters: altering cell size. *Curr Opin Genet Dev*. 12:565-71.
Scherzer, C.R., R.V. Jensen, S.R. Gullans, and M.B. Feany. 2003. Gene expression changes presage neurodegeneration in a Drosophila model of Parkinson's disease. *Hum Mol Genet*. 12:2457-66.
Schlagenhauf, E., R. Etges, and P. Metcalf. 1998. The crystal structure of the Leishmania major surface proteinase leishmanolysin (gp63). *Structure*. 6:1035-46.
Schwarz, E.J., M.J. Reginato, D. Shao, S.L. Krakow, and M.A. Lazar. 1997. Retinoic acid blocks adipogenesis by inhibiting C/EBPbeta-mediated transcription. *Mol Cell Biol*. 17:1552-61.
Scott, R.C., G. Juhasz, and T.P. Neufeld. 2007. Direct induction of autophagy by Atg1 inhibits cell growth and induces apoptotic cell death. *Curr Biol*. 17:1-11.
Scott, R.C., O. Schuldiner, and T.P. Neufeld. 2004. Role and regulation of starvation-induced autophagy in the Drosophila fat body. *Dev Cell*. 7:167-78.
Segrest, J.P., M.K. Jones, H. De Loof, and N. Dashti. 2001. Structure of apolipoprotein B-100 in low density lipoproteins. *J Lipid Res*. 42:1346-67.
Senft, A.P., T.R. Korfhagen, J.A. Whitsett, S.D. Shapiro, and A.M. LeVine. 2005. Surfactant protein-D regulates soluble CD14 through matrix metalloproteinase-12. *J Immunol*. 174:4953-9.
Sharma, D.K., J.C. Brown, A. Choudhury, T.E. Peterson, E. Holicky, D.L. Marks, R. Simari, R.G. Parton, and R.E. Pagano. 2004. Selective stimulation of caveolar endocytosis by glycosphingolipids and cholesterol. *Mol Biol Cell*. 15:3114-22.
Shearn, A., T. Rice, A. Garen, and W. Gehring. 1971. Imaginal disc abnormalities in lethal mutants of Drosophila. *Proc Natl Acad Sci U S A*. 68:2594-8.
Six, E., D. Ndiaye, Y. Laabi, C. Brou, N. Gupta-Rossi, A. Israel, and F. Logeat. 2003. The Notch ligand Delta1 is sequentially cleaved by an ADAM protease and gamma-secretase. *Proc Natl Acad Sci U S A*. 100:7638-43.
Smart, E.J., Y.S. Ying, and R.G. Anderson. 1995. Hormonal regulation of caveolae internalization. *J Cell Biol*. 131:929-38.
Smirnova, E., E.B. Goldberg, K.S. Makarova, L. Lin, W.J. Brown, and C.L. Jackson. 2006. ATGL has a key role in lipid droplet/adiposome degradation in mammalian cells. *EMBO Rep*. 7:106-13.
Smith, P.J., L.S. Wise, R. Berkowitz, C. Wan, and C.S. Rubin. 1988. Insulin-like growth factor-I is an essential regulator of the differentiation of 3T3-L1 adipocytes. *J Biol Chem*. 263:9402-8.
Soler, D., T. Nomizu, W.E. Brown, Y. Shibata, and D.S. Auld. 1995. Matrilysin: expression, purification, and characterization. *J Protein Chem*. 14:511-20.
Soulard, A., and M.N. Hall. 2007. SnapShot: mTOR signaling. *Cell*. 129:434.
Steinberg, S.F. 2008. Structural basis of protein kinase C isoform function. *Physiol Rev*.

88:1341-78.
Student, A.K., R.Y. Hsu, and M.D. Lane. 1980. Induction of fatty acid synthetase synthesis in differentiating 3T3-L1 preadipocytes. *J Biol Chem*. 255:4745-50.
Sturgill, T.W., and M.N. Hall. 2007. Holding back TOR advances mitosis. *Nat Cell Biol*. 9:1221-2.
Stuurman, N., S. Heins, and U. Aebi. 1998. Nuclear lamins: their structure, assembly, and interactions. *J Struct Biol*. 122:42-66.
Su, C.L., C. Sztalryd, J.A. Contreras, C. Holm, A.R. Kimmel, and C. Londos. 2003. Mutational analysis of the hormone-sensitive lipase translocation reaction in adipocytes. *J Biol Chem*. 278:43615-9.
Subramanian, V., A. Rothenberg, C. Gomez, A.W. Cohen, A. Garcia, S. Bhattacharyya, L. Shapiro, G. Dolios, R. Wang, M.P. Lisanti, and D.L. Brasaemle. 2004. Perilipin A mediates the reversible binding of CGI-58 to lipid droplets in 3T3-L1 adipocytes. *J Biol Chem*. 279:42062-71.
Sztalryd, C., G. Xu, H. Dorward, J.T. Tansey, J.A. Contreras, A.R. Kimmel, and C. Londos. 2003. Perilipin A is essential for the translocation of hormone-sensitive lipase during lipolytic activation. *J Cell Biol*. 161:1093-103.
Taguchi, A., and M.F. White. 2008. Insulin-like signaling, nutrient homeostasis, and life span. *Annu Rev Physiol*. 70:191-212.
Tamori, Y., J. Masugi, N. Nishino, and M. Kasuga. 2002. Role of peroxisome proliferator-activated receptor-gamma in maintenance of the characteristics of mature 3T3-L1 adipocytes. *Diabetes*. 51:2045-55.
Tanaka, T., N. Yoshida, T. Kishimoto, and S. Akira. 1997. Defective adipocyte differentiation in mice lacking the C/EBPbeta and/or C/EBPdelta gene. *EMBO J*. 16:7432-43.
Taniguchi, C.M., B. Emanuelli, and C.R. Kahn. 2006. Critical nodes in signalling pathways: insights into insulin action. *Nat Rev Mol Cell Biol*. 7:85-96.
Tee, A.R., and J. Blenis. 2005. mTOR, translational control and human disease. *Semin Cell Dev Biol*. 16:29-37.
Teixeira, L., C. Rabouille, P. Rorth, A. Ephrussi, and N.F. Vanzo. 2003. Drosophila Perilipin/ADRP homologue Lsd2 regulates lipid metabolism. *Mech Dev*. 120:1071-81.
Teleman, A.A., Y.W. Chen, and S.M. Cohen. 2005. 4E-BP functions as a metabolic brake used under stress conditions but not during normal growth. *Genes Dev*. 19:1844-8.
Teleman, A.A., Y.W. Chen, and S.M. Cohen. 2005. Drosophila Melted modulates FOXO and TOR activity. *Dev Cell*. 9:271-81.
Teleman, A.A., V. Hietakangas, A.C. Sayadian, and S.M. Cohen. 2008. Nutritional control of protein biosynthetic capacity by insulin via Myc in Drosophila. *Cell Metab*. 7:21-32.
Tettweiler, G., M. Miron, M. Jenkins, N. Sonenberg, and P.F. Lasko. 2005. Starvation and oxidative stress resistance in Drosophila are mediated through the eIF4E-binding protein, d4E-BP. *Genes Dev*. 19:1840-3.
Thiele, C., and J. Spandl. 2008. Cell biology of lipid droplets. *Curr Opin Cell Biol*. 20:378-85.
Tisi, R., F. Belotti, C. Paiardi, F. Brunetti, and E. Martegani. 2008. The budding yeast RasGEF Cdc25 reveals an unexpected nuclear localization. *Biochim Biophys Acta*. 1783:2363-74.
Toker, A., and L.C. Cantley. 1997. Signalling through the lipid products of phosphoinositide-3-OH kinase. *Nature*. 387:673-6.
Toker, A., M. Meyer, K.K. Reddy, J.R. Falck, R. Aneja, S. Aneja, A. Parra, D.J. Burns, L.M. Ballas, and L.C. Cantley. 1994. Activation of protein kinase C family members by the novel polyphosphoinositides PtdIns-3,4-P2 and PtdIns-3,4,5-P3. *J Biol Chem*. 269:32358-67.
Toker, A., and A.C. Newton. 2000. Akt/protein kinase B is regulated by autophosphorylation at the hypothetical PDK-2 site. *J Biol Chem*. 275:8271-4.
Tomiyama, K., H. Nakata, H. Sasa, S. Arimura, E. Nishio, and Y. Watanabe. 1995. Wortmannin, a specific phosphatidylinositol 3-kinase inhibitor, inhibits adipocytic differentiation of 3T3-L1 cells. *Biochem Biophys Res Commun*. 212:263-9.
Tontonoz, P., E. Hu, and B.M. Spiegelman. 1994. Stimulation of adipogenesis in fibroblasts

by PPAR gamma 2, a lipid-activated transcription factor. *Cell*. 79:1147-56.
Tontonoz, P., and B.M. Spiegelman. 2008. Fat and beyond: the diverse biology of PPARgamma. *Annu Rev Biochem*. 77:289-312.
Tseng, Y.H., K.M. Kriauciunas, E. Kokkotou, and C.R. Kahn. 2004. Differential roles of insulin receptor substrates in brown adipocyte differentiation. *Mol Cell Biol*. 24:1918-29.
Tsukiyama-Kohara, K., F. Poulin, M. Kohara, C.T. DeMaria, A. Cheng, Z. Wu, A.C. Gingras, A. Katsume, M. Elchebly, B.M. Spiegelman, M.E. Harper, M.L. Tremblay, and N. Sonenberg. 2001. Adipose tissue reduction in mice lacking the translational inhibitor 4E-BP1. *Nat Med*. 7:1128-32.
Turro, S., M. Ingelmo-Torres, J.M. Estanyol, F. Tebar, M.A. Fernandez, C.V. Albor, K. Gaus, T. Grewal, C. Enrich, and A. Pol. 2006. Identification and characterization of associated with lipid droplet protein 1: A novel membrane-associated protein that resides on hepatic lipid droplets. *Traffic*. 7:1254-69.
Ugi, S., T. Imamura, H. Maegawa, K. Egawa, T. Yoshizaki, K. Shi, T. Obata, Y. Ebina, A. Kashiwagi, and J.M. Olefsky. 2004. Protein phosphatase 2A negatively regulates insulin's metabolic signaling pathway by inhibiting Akt (protein kinase B) activity in 3T3-L1 adipocytes. *Mol Cell Biol*. 24:8778-89.
Um, S.H., F. Frigerio, M. Watanabe, F. Picard, M. Joaquin, M. Sticker, S. Fumagalli, P.R. Allegrini, S.C. Kozma, J. Auwerx, and G. Thomas. 2004. Absence of S6K1 protects against age- and diet-induced obesity while enhancing insulin sensitivity. *Nature*. 431:200-5.
Umlauf, E., E. Csaszar, M. Moertelmaier, G.J. Schuetz, R.G. Parton, and R. Prohaska. 2004. Association of stomatin with lipid bodies. *J Biol Chem*. 279:23699-709.
Van Berlo, J.H., J.W. Voncken, N. Kubben, J.L. Broers, R. Duisters, R.E. van Leeuwen, H.J. Crijns, F.C. Ramaekers, C.J. Hutchison, and Y.M. Pinto. 2005. A-type lamins are essential for TGF-beta1 induced PP2A to dephosphorylate transcription factors. *Hum Mol Genet*. 14:2839-49.
Van Obberghen, E., V. Baron, L. Delahaye, B. Emanuelli, N. Filippa, S. Giorgetti-Peraldi, P. Lebrun, I. Mothe-Satney, P. Peraldi, S. Rocchi, D. Sawka-Verhelle, S. Tartare-Deckert, and J. Giudicelli. 2001. Surfing the insulin signaling web. *Eur J Clin Invest*. 31:966-77.
Van Wart, H.E., and H. Birkedal-Hansen. 1990. The cysteine switch: a principle of regulation of metalloproteinase activity with potential applicability to the entire matrix metalloproteinase gene family. *Proc Natl Acad Sci U S A*. 87:5578-82.
Verdu, J., M.A. Buratovich, E.L. Wilder, and M.J. Birnbaum. 1999. Cell-autonomous regulation of cell and organ growth in Drosophila by Akt/PKB. *Nat Cell Biol*. 1:500-6.
Vereshchagina, N., M.C. Ramel, E. Bitoun, and C. Wilson. 2008. The protein phosphatase PP2A-B' subunit Widerborst is a negative regulator of cytoplasmic activated Akt and lipid metabolism in Drosophila. *J Cell Sci*. 121:3383-92.
Vereshchagina, N., and C. Wilson. 2006. Cytoplasmic activated protein kinase Akt regulates lipid-droplet accumulation in Drosophila nurse cells. *Development*. 133:4731-5.
Wan, H.C., R.C. Melo, Z. Jin, A.M. Dvorak, and P.F. Weller. 2007. Roles and origins of leukocyte lipid bodies: proteomic and ultrastructural studies. *FASEB J*. 21:167-78.
Wang, H., D. Gilham, and R. Lehner. 2007. Proteomic and lipid characterization of apolipoprotein B-free luminal lipid droplets from mouse liver microsomes: implications for very low density lipoprotein assembly. *J Biol Chem*. 282:33218-26.
Wasserman, Z.R. 2005. Making a new turn in matrix metalloprotease inhibition. *Chem Biol*. 12:143-4.
Webb, J.L., B. Ravikumar, J. Atkins, J.N. Skepper, and D.C. Rubinsztein. 2003. Alpha-Synuclein is degraded by both autophagy and the proteasome. *J Biol Chem*. 278:25009-13.
Weinkove, D., T.P. Neufeld, T. Twardzik, M.D. Waterfield, and S.J. Leevers. 1999. Regulation of imaginal disc cell size, cell number and organ size by Drosophila class I(A) phosphoinositide 3-kinase and its adaptor. *Curr Biol*. 9:1019-29.
Weller, P.F., S.W. Ryeom, S.T. Picard, S.J. Ackerman, and A.M. Dvorak. 1991. Cytoplasmic

lipid bodies of neutrophils: formation induced by cis-unsaturated fatty acids and mediated by protein kinase C. *J Cell Biol*. 113:137-46.
Welte, M.A. 2007. Proteins under new management: lipid droplets deliver. *Trends Cell Biol*. 17:363-9.
Welte, M.A., S. Cermelli, J. Griner, A. Viera, Y. Guo, D.H. Kim, J.G. Gindhart, and S.P. Gross. 2005. Regulation of lipid-droplet transport by the perilipin homolog LSD2. *Curr Biol*. 15:1266-75.
Wilkinson, K.D. 1999. Ubiquitin-dependent signaling: the role of ubiquitination in the response of cells to their environment. *J Nutr*. 129:1933-6.
Wilkinson, K.D. 2000. Ubiquitination and deubiquitination: targeting of proteins for degradation by the proteasome. *Semin Cell Dev Biol*. 11:141-8.
Wittwer, F., M. Jaquenoud, W. Brogiolo, M. Zarske, P. Wustemann, R. Fernandez, H. Stocker, M.P. Wymann, and E. Hafen. 2005. Susi, a negative regulator of Drosophila PI3-kinase. *Dev Cell*. 8:817-27.
Wolins, N.E., B.K. Quaynor, J.R. Skinner, A. Tzekov, M.A. Croce, M.C. Gropler, V. Varma, A. Yao-Borengasser, N. Rasouli, P.A. Kern, B.N. Finck, and P.E. Bickel. 2006. OXPAT/PAT-1 is a PPAR-induced lipid droplet protein that promotes fatty acid utilization. *Diabetes*. 55:3418-28.
Wolins, N.E., B. Rubin, and D.L. Brasaemle. 2001. TIP47 associates with lipid droplets. *J Biol Chem*. 276:5101-8.
Wolins, N.E., J.R. Skinner, M.J. Schoenfish, A. Tzekov, K.G. Bensch, and P.E. Bickel. 2003. Adipocyte protein S3-12 coats nascent lipid droplets. *J Biol Chem*. 278:37713-21.
Wu, C.C., K.E. Howell, M.C. Neville, J.R. Yates, 3rd, and J.L. McManaman. 2000. Proteomics reveal a link between the endoplasmic reticulum and lipid secretory mechanisms in mammary epithelial cells. *Electrophoresis*. 21:3470-82.
Wu, Q., and M.R. Brown. 2006. Signaling and function of insulin-like peptides in insects. *Annu Rev Entomol*. 51:1-24.
Wu, Z., Y. Xie, N.L. Bucher, and S.R. Farmer. 1995. Conditional ectopic expression of C/EBP beta in NIH-3T3 cells induces PPAR gamma and stimulates adipogenesis. *Genes Dev*. 9:2350-63.
Xia, X., and G. Serrero. 1999. Inhibition of adipose differentiation by phosphatidylinositol 3-kinase inhibitors. *J Cell Physiol*. 178:9-16.
Xu, G., C. Sztalryd, X. Lu, J.T. Tansey, J. Gan, H. Dorward, A.R. Kimmel, and C. Londos. 2005. Post-translational regulation of adipose differentiation-related protein by the ubiquitin/proteasome pathway. *J Biol Chem*. 280:42841-7.
Yamaguchi, T., S. Matsushita, K. Motojima, F. Hirose, and T. Osumi. 2006. MLDP, a novel PAT family protein localized to lipid droplets and enriched in the heart, is regulated by peroxisome proliferator-activated receptor alpha. *J Biol Chem*. 281:14232-40.
Yamaguchi, T., N. Omatsu, S. Matsushita, and T. Osumi. 2004. CGI-58 interacts with perilipin and is localized to lipid droplets. Possible involvement of CGI-58 mislocalization in Chanarin-Dorfman syndrome. *J Biol Chem*. 279:30490-7.
Yamaguchi, T., N. Omatsu, E. Morimoto, H. Nakashima, K. Ueno, T. Tanaka, K. Satouchi, F. Hirose, and T. Osumi. 2007. CGI-58 facilitates lipolysis on lipid droplets but is not involved in the vesiculation of lipid droplets caused by hormonal stimulation. *J Lipid Res*. 48:1078-89.
Yang, D.M., M.V. Rogers, and F.Y. Liew. 1991. Identification and characterization of host-protective T-cell epitopes of a major surface glycoprotein (gp63) from Leishmania major. *Immunology*. 72:3-9.
Yang, Q., K. Inoki, E. Kim, and K.L. Guan. 2006. TSC1/TSC2 and Rheb have different effects on TORC1 and TORC2 activity. *Proc Natl Acad Sci U S A*. 103:6811-6.
Yao, C., J.E. Donelson, and M.E. Wilson. 2003. The major surface protease (MSP or GP63) of Leishmania sp. Biosynthesis, regulation of expression, and function. *Mol Biochem Parasitol*. 132:1-16.
Yeh, W.C., Z. Cao, M. Classon, and S.L. McKnight. 1995. Cascade regulation of terminal adipocyte differentiation by three members of the C/EBP family of leucine zipper

proteins. *Genes Dev*. 9:168-81.
Yen, C.L., and R.V. Farese, Jr. 2006. Fat breakdown: a function for CGI-58 (ABHD5) provides a new piece of the puzzle. *Cell Metab*. 3:305-7.
Yu, W., Z. Chen, J. Zhang, L. Zhang, H. Ke, L. Huang, Y. Peng, X. Zhang, S. Li, B.T. Lahn, and A.P. Xiang. 2008. Critical role of phosphoinositide 3-kinase cascade in adipogenesis of human mesenchymal stem cells. *Mol Cell Biochem*. 310:11-8.
Zehmer, J.K., R. Bartz, P. Liu, and R.G. Anderson. 2008. Identification of a novel N-terminal hydrophobic sequence that targets proteins to lipid droplets. *J Cell Sci*. 121:1852-60.
Zhang, H., J.P. Stallock, J.C. Ng, C. Reinhard, and T.P. Neufeld. 2000. Regulation of cellular growth by the Drosophila target of rapamycin dTOR. *Genes Dev*. 14:2712-24.
Zhang, Y., L. Yin, and F.B. Hillgartner. 2003. SREBP-1 integrates the actions of thyroid hormone, insulin, cAMP, and medium-chain fatty acids on ACCalpha transcription in hepatocytes. *J Lipid Res*. 44:356-68.
Zhou, Y., D. Wang, F. Li, J. Shi, and J. Song. 2006. Different roles of protein kinase C-betaI and -delta in the regulation of adipocyte differentiation. *Int J Biochem Cell Biol*. 38:2151-63.
Zhou, Z., S. Yon Toh, Z. Chen, K. Guo, C.P. Ng, S. Ponniah, S.C. Lin, W. Hong, and P. Li. 2003. Cidea-deficient mice have lean phenotype and are resistant to obesity. *Nat Genet*. 35:49-56.
Zimmermann, R., J.G. Strauss, G. Haemmerle, G. Schoiswohl, R. Birner-Gruenberger, M. Riederer, A. Lass, G. Neuberger, F. Eisenhaber, A. Hermetter, and R. Zechner. 2004. Fat mobilization in adipose tissue is promoted by adipose triglyceride lipase. *Science*. 306:1383-6.
Zinke, I., C.S. Schutz, J.D. Katzenberger, M. Bauer, and M.J. Pankratz. 2002. Nutrient control of gene expression in Drosophila: microarray analysis of starvation and sugar-dependent response. *EMBO J*. 21:6162-73.